Universidade de Aveiro Departamento de Química
2017

Raquel Sofia de Oliveira Nunes da Silva

Phthalocyanine–sulfonamide conjugates - synthesis and biological activity

Conjugados de ftalocianina–sulfonamida - síntese e atividade biológica

Universidade de Aveiro
2017

Departamento de Química

Raquel Sofia de Oliveira Nunes da Silva

Phthalocyanine–sulfonamide conjugates - synthesis and biological activity

Conjugados de ftalocianina–sulfonamida - síntese e atividade biológica

Tese apresentada à Universidade de Aveiro para cumprimento dos requisitos necessários à obtenção do grau de Doutor em Química, realizada sob a orientação científica do Professor Doutor Augusto Costa Tomé, Professor Associado com Agregação do Departamento de Química da Universidade de Aveiro e sob a co-orientação científica da Professora Doutora Maria Ângela Sousa Dias Alves Cunha, Professora Auxiliar do Departamento de Biologia da Universidade de Aveiro.

Apoio financeiro da Unidade de Investigação QOPNA (FCT UID/QUI/00062/2013).

Apoio financeiro da Unidade de Investigação CESAM - Centre for Environmental and Marine Studies (FCT UID/AMB/50017/2013).

“The most exciting phrase to hear in science, the one that heralds new discoveries, is not ‘Eureka’ but ‘That’s funny...’”

Isaac Asimov

À memória de minha mãe

o júri

Presidente

Doutora Maria Hermínia Deulonder Correia Amado Laurel

Professora Catedrática da Universidade de Aveiro

Doutor Rui Ferreira Alves Moreira

Professor Catedrático da Universidade de Lisboa

Doutor João Paulo Costa Tomé

Professor Associado da Universidade de Lisboa

Doutora Maria Adelaide de Pinho Almeida

Professora Auxiliar com Agregação da Universidade de Aveiro

Doutora Rosa Cristina Simões Fernandes

Investigadora Auxiliar da Universidade de Coimbra

Doutor Augusto Costa Tomé

Professor Associado com Agregação da Universidade de Aveiro

agradecimentos

Aproveito com muito gosto a oportunidade de agradecer a todos que me ajudaram e apoiaram ao longo deste percurso.

Em primeiro lugar, ao Professor Doutor Augusto Tomé e à Professora Doutora Ângela Cunha, orientadores deste trabalho de Doutoramento, um obrigado não só pela oportunidade de realizar este trabalho, excelente orientação e conhecimentos partilhados, mas também pela amizade que prevaleceu ao longo destes anos.

I would like to thank to Doctor Jon Golding from the Health Sciences, Faculty of Science, Technology, Engineering & Mathematics, The Open University, Milton Keynes (UK) for the friendly way he received me in his laboratory in Milton Keynes.

I thank to Doctor Alexandre McRobert, University College of London, London (UK), for the pertinent suggestions on the photodynamic therapy studies.

À Professora Doutora Rita Ferreira e Professora Doutora Luísa Helguero, do Departamento de Química, e à Professora Doutora Etelvina Figueira, do Departamento de Biologia da Universidade de Aveiro, pela pronta disponibilidade em ajudar nos ensaios enzimáticos.

Ao Professor Doutor Artur Silva, à Professora Doutora Amparo Faustino e à Professora Doutora Maria da Graça Neves, do Departamento de Química da Universidade de Aveiro, um obrigada pela pronta ajuda e disponibilidade prestada.

À Professora Doutora Adelaide Almeida um agradecimento pela cedência do luminómetro para os testes de inativação fotodinâmica em *E. coli* bioluminescente.

Ao Dr. Hilário Tavares um agradecimento pela pronta disponibilidade em obter espetros de RMN 'o mais bonitos possível'. À Doutora Mónica Válega pela simpatia constante e pela pronta disponibilidade em arranjar tudo o que fosse preciso.

A todos os meus colegas de laboratório obrigada não só aos 'das porfirinas' mas também aos 'alunos do Professor Artur' pela disponibilidade, amizade e companheirismo que marcaram o dia-a-dia no laboratório. Em especial, um agradecimento ao 'Gang da marmita' pelas gargalhadas ao almoço que me deram ânimo para continuar o resto das tardes. Ao Doutor Leandro Lourenço pela ajuda nos primeiros passos neste trabalho. Também um obrigado às 'meninas da Biologia' por toda a simpatia e ajuda.

agradecimentos

Um grande agradecimento ao meu pai e irmã Mónica que sempre acreditaram em mim. Um agradecimento também ao Renato Ribeiro pela amizade de irmão. A toda a minha família e amigos um obrigado por estarem lá sempre e partilharem comigo todos os momentos.

Ao Daniel um muito obrigada por tudo…

Agradeço também à Fundação para a Ciência e Tecnologia pela bolsa de Doutoramento (SFRH/BD/87598/2012) e à Sociedade Europeia de Fotobiologia pelos subsídios para participação em congressos, curso em fotobiologia e estágio no estrangeiro.

palavras-chave ftalocianina, sulfonamida, terapia fotodinâmica, inativação fotodinâmica de microrganismos, anidrase carbónica, cancro.

resumo

O uso inapropriado de antibióticos no tratamento de doenças infeciosas tem levado a um aumento da resistência de diversos microrganismos patogénicos, o que apresenta atualmente um problema de saúde pública e tem motivado a procura de estratégias alternativas para o controlo destes microrganismos. Por outro lado, a procura de novas moléculas ou novas combinações de moléculas para o combate ao cancro é um assunto em constante desenvolvimento.

Na presente dissertação descreve-se o trabalho desenvolvido para a obtenção de conjugados de ftalocianina–sulfonamida e a avaliação da atividade dos novos compostos como fotossensibilizadores. Os conjugados foram idealizados com o intuito de promover um possível efeito sinérgico das suas unidades constituintes, nomeadamente propriedades antitumorais e/ou antimicrobianas. Para tal, desenvolveram-se métodos de síntese de sulfonamidas e de conjugados de ftalocianina–sulfonamida. Algumas das ftalocianinas obtidas foram testadas como fotossensibilizadores na eliminação fotodinâmica de células tumorais e de bactérias, utilizando-se as linhas celulares de carcinoma de células escamosas orais (HSC3) e de queratinócitos orais (HaCaT), e as bactérias *Escherichia coli* (Gram-negativo) *Staphylococcus aureus* (Gram-positivo) como modelos biológicos. Os resultados destes estudos revelaram que as ftalocianinas estudadas são muito promissoras como fotossensibilizadores para a inativação fotodinâmica de células tumorais e de microrganismos. Por outro lado, foi também desenvolvido um ensaio enzimático para avaliar a atividade dos novos compostos como inativadores da enzima anidrase carbónica, em particular a isoforma IX que se encontra sobre-expressa em células tumorais e é bem conhecida como reguladora do pH em processos de hipoxia e acidose metabólica.

Este estudo vem dar mais um passo no conhecimento científico das ftalocianinas e evidencia o potencial das ftalocianinas sulfonadas na perspetiva do controlo de infeções e da tumorogénese.

keywords phthalocyanine, sulfonamide, photodynamic therapy, photodynamic inactivation of microorganisms, carbonic anhydrase, cancer.

abstract

The inappropriate use of antibiotics in the treatment of infections has led to an increase in the resistance of several pathogenic microorganisms, which represents a major public health issue and triggered the search for novel antimicrobial drugs. On the other hand, the search for new molecules or new combinations of molecules for the fight against cancer is a subject in constant development.

The present dissertation describes the work developed to obtain phthalocyanine–sulfonamide conjugates and the biological evaluation of these compounds as photosensitizers. These conjugates were designed to explore their antimicrobial and/or antitumor properties.

Methods for the synthesis of sulfonamides and phthalocyanine–sulfonamide conjugates were developed. Some of the phthalocyanines obtained were tested as photosensitizers for the photodynamic inactivation of tumor cells and bacteria. HSC3 oral squamous cell carcinoma, HaCaT 'normal' keratinocytes, and the bacteria *Escherichia coli* (Gram-negative) and *Staphylococcus aureus* (Gram-positive) were used as biological models.

The phthalocyanines studied proved to be very promising to be considered in future studies in the perspective of the photodynamic inactivation of tumor cells and microorganisms. On the other hand, an enzymatic assay was also developed to evaluate the activity of the compounds obtained as inactivators of the enzyme carbonic anhydrase, in particular the IX isoform that is overexpressed in tumor cells and is well-known as pH regulator in processes of hypoxia and metabolic acidosis.

This study represents a contribution to the application of phthalocyanines, and in particular sulfonated phthalocyanines, in the control of infections and tumorigenesis.

Table of Contents

Table of figures

Table of schemes

Table of tables

Abbreviations

δ	Chemical shift
λ	Wavelength
AIDS	Acquired immune deficiency syndrome
ALA	5-Aminolevulinic acid
AlC_4Pc	Tetrasubstituted carboxy aluminum phthalocyanine
AZT	Azidothymidine
CA	Carbonic anhydrase
CA-RP	Carbonic anhydrase-related protein
CDK	Cyclin-dependent kinase
CFU	Colony forming units
CuAAC	Cu(I)-catalyzed alkyne–azide cycloaddition
d	Doublet
dd	Double doublet
DBU	1,8-Diazabicyclo(5.4.0)undec-7-ene
DHB	2,5-Dihydroxybenzoic acid
DHFR	Dihydrofolate reductase
DHPS	Dihydropteroate synthase
DHPP	6-Pyrophosphomethyl-7,8-dihydropterin
DHPPP	6-Hydroxymethyl-7,8-dihydropterin pyrophosphate
DLD-1	Cancer cell lines – human colon
DMEM	Dulbecco's Modified Eagle's Medium
DMF	Dimethylformamide
DMAE	2-(Dimethylamino)ethanol
DMSO	Dimethyl sulfoxide
DPBF	1,3-Diphenylisobenzofuran
dsDNA	Double-stranded DNA
EA	Elemental analysis
EDTA	Ethylenediaminetetraacetic acid
Equiv.	Equivalents
ESI	Electrospray ionization
FAB	Fast atom bombardment

FD	Field desorption
FDA	Food and Drug Administration
FDG	2-deoxy-2-[^{18}F]fluoro-D-glucose
GTP	Guanosine triphosphate
HBSS	Hank's salt
Hp	Hematoporphyrin
Hpd	Hematoporphyrin derivative
HIV-1	Human Immunodeficiency Virus 1
HPLC	High-performance liquid chromatography
HPPH	2-[1-Hexyloxyethyl]-2-devinyl pyropheophorbide-a
IR	Infrared
ISC	Inter-system crossing
IUPAC	International Union of Pure and Applied Chemistry
J	Coupling constant
LDL	Low density lipoproteins
m	Multiplet
mABS	Monoclonal antibodies
MALDI	Matrix-assisted desorption ionization
MCR	Multicomponent reaction
MFC	Microbial fuel cell
MMP	Matrix metalloproteinase
MPc	Metallophthalocyanine
MRI	Magnetic resonance imaging
MS	Mass spectrometry
m/z	Mass-to-charge ratio
NCS	*N*-Chlorosuccinimide
NIR	Near-infrared
NLT	Non-linear transmission
NMR	Nuclear magnetic resonance
$^1O_2$	Singlet oxygen
*p*ABA	*p*-Aminobenzoic acid
PBS	Phosphate-buffered saline
Pc	Phthalocyanine

PCI	Photochemical internalization
PDI	Photodynamic inactivation of microorganisms
PDT	Photodynamic therapy
PET	Positron emission tomography
Pht	Phthalonitrile
PLGA	Poly(lactic-coglycolic) acid
PLGA-NPs	Poly(D,L-lactic-co-glycolic acid)-nanoparticles
ppm	Part per million
PS	Photosensitizer
PVP	Polyvinylpyrrolidone
Por	Porphyrin
R_f	Retention factor
RLU	Bioluminescence in relative light units
ROS	Reactive oxygen species
s	Singlet
s	Spin quantum number
SA	Sulfonamide
S_0	Singlet state
S_1	Singlet state of lowest energy short-living state
S_n	Singlet state of excited state
t	Triplet
T	Triplet state
T_1	Triplet state of lowest energy
T_n	Triplet state of excited state
TPP	*meso*-Tetraphenylporphyrin
TBAB	Tris[(1-benzyl-1*H*-1,2,3-triazol-4-yl)methyl]amine
TCT	2,4,6-Trichloro[1,3,5]triazine
THF	Tetrahydrofuran
TLC	Thin-layer chromatography
TMS	Tetramethylsilane
TSA	Tryptic soy agar
TSB	Tryptic soy broth
UV	Ultraviolet

Vis	Visible
ZnPc	Zinc phthalocyanine

Chapter 1 Introduction

During the last decades photodynamic therapy (PDT) emerged as a promising and reliable technique for the treatment of different diseases, among which several forms of cancer. Its first application was the inactivation of tumor cells, but it has revealed much more relevance than initially thought. Nowadays, it is used in the clinical treatment of different oncological diseases as well as in the treatment of ocular diseases, atherosclerosis, and dermatological pathologies. Furthermore, particularizations of the technique have been developed, such as photochemical internalization (PCI) and photodynamic inactivation of microorganisms (PDI) (bacteria, fungi and virus) in living tissues, surgical equipment, surfaces and environmental matrices.[1] In recent years, PDT has become a subject of intense investigation, making this technique still an interesting topic nowadays.

Phthalocyanines (Pcs) are a class of tetrapyrrolic macrocycles of synthetic origin analogous to porphyrins (Pors). The latter were the first tetrapyrrolic macrocycles used as photosensitizers (PSs) in PDT. During the development of PDT and PDI different PSs have been studied. Pcs emerged as promising candidates due to their exceptional physico-chemical properties. In this sense, new and more effective Pc-based PSs have been developed for many applications extend beyond photodynamic therapy. They can be found in many materials science fields, surpassing Pors in a number of applications, making them one of the most highly studied macrocycle and coordination compounds.[2]

This chapter intends to provide an overview on basic knowledge on Pcs.

Due to the low solubility in common organic solvents, several functionalizations and metallations of Pcs have been studied in order to attain the most interesting properties, namely selectivity, transport across biological membranes, solubility in biological fluids, singlet oxygen production, as well as clearance after photoinactivation.[3] Photobiological and photochemical properties of PSs must be very well-known for the proper functioning of this technique. Furthermore, it is also important to understand PDT and PDI main differences and similarities.

During the last decades sulfonamides (SAs) have been used mainly as antimicrobials. However, they have also been successfully tested for other clinical purposes such as thiazide diuretics, loop diuretics, anti-arrhythmic agents, non-nucleotide reverse transcriptase inhibitors, non-peptidic vasopressin V1a receptor

antagonists, and Human Immunodeficiency Virus 1 (HIV-1) protease inhibitors. Compounds containing SAs moieties can be found in pharmaceutical formulations for the treatment of inflammatory bowel disease (e.g. Sulsalazine®), in anticonvulsants (e.g. Sultiame®), in PDE5 inhibitor (Viagra®), and in COX-2 inhibitor (Celecoxib®).[4]

As antimicrobial, SAs were initially used in the treatment of a variety of bacterial infections by inhibiting the enzyme dihydropteroate synthase (DHPS) in the folic acid pathway.[4] However, the rapid development of resistance to SAs and the discovery of more potent drugs have limited their clinical use. Beyond that, SAs continue to be used in several clinical situations.

In order to overcome resistance to antibiotics, observed not only for SAs but also to other antibiotics, efficient strategies to control microbial infections have been developed. One of them is PDI, which has proved to be effective in the inactivation of several pathogenic microorganisms, including multi-resistant bacteria, fungi and virus.

Recently, SAs have been studied as antitumoral drugs. There are several targets for SAs with antitumoral activity, but the majority of the studies are concerned around the inhibitory effect of carbonic anhydrases (CAs) IX and XII and regulation of cell cycle at the G1 phase through inhibition of cyclin-dependent kinases (CDKs).

Taking advantage of SAs potentialities as antitumor and antimicrobial agents and Pcs as PSs, the general objective of this work is to explore the additive effects between these two families of compounds. By coupling SA moieties to Pcs we expect to achieve more effective PSs. For that, a new group of PSs with a Pc backbone were designed, synthesized and tested in different bacterial models and in tumor cells, in order to gain knowledge on the biological pathways underlying the effects in target cells.

1.1 Thesis outline

This document was written in order to guide the reader along the different disciplines that this work is based upon. The basic components in which this work relays on are divided over the different experimental chapters. Since Pcs are transversal to the different works, as already mentioned, they will be addressed in this first chapter.

In chapter 2, the study focused on the synthesis and optimization of new *N*-acyl Pc–SA conjugates is described. For that, an overview of click reactions and, in particular, sulfo-click reactions is made. Following, the synthesis of new Pc–SA

conjugates is described in chapter 3. In this third chapter not only the study of the synthesis of neutral Pc–SA conjugates is described, but also the synthesis of cationizable conjugates. Likewise, the encapsulation of neutral Pc–SA conjugates is presented. The synthetic strategies to obtain SAs are detailed.

In chapter 4, the PDT of tumor cells using some neutral Pc–SA conjugates and the respective PVP-encapsulated conjugates is evaluated. For that, HSC3 oral squamous cell carcinoma and HaCaT 'normal' keratinocytes were used as cellular models. In addition, the properties of these neutral Pc–SA conjugates as inhibitors of the enzyme carbonic anhydrase (CA) were also accessed. The rationality on the use of the CA as a PDT target is explained as an introduction.

The evaluation of neutral Pc–SA conjugates as PSs at 10 and 20 μM is addressed in chapter 5. The results obtained in the PDI of *Escherichia coli* and *Staphylococcus aureus* under white and red light, with neutral Pc–SA conjugates and the same compounds encapsulated in polyvinylpyrrolidone (PVP) micelles are discussed. In this chapter, basic concepts of PDI and biological functions of SAs are explained.

1.2 Phthalocyanines

Tetrapyrrolic macrocycles, such as heme and chlorophylls, are important in Nature, playing vital roles in biological systems responsible for oxygen transport, cell growth, light transformation into useful energy in plants, electron transfer chains in mitochondria and prokaryote cells, and in protective responses to oxidative damage. Pcs are synthetic tetrapyrrolic macrocycles that, while having a similar structure to natural Pors, are not found in Nature.[3,5–7]

Pcs have four basic isoindole units connected through *aza* bridges, presenting an eighteen π-electrons aromatic cloud delocalized over an arrangement of alternated carbon and nitrogen atoms (Figure 1.1).[3,8]

The word Pc is derived from the Greek terms for cyanine (dark blue) and naphtha (rock oil) and also from the phthalic acids, which were the first precursors used for the synthesis of these macrocycles. Professor Reginald P. Linstead, from the Imperial College of Science and Technology, was the first to use the term "phthalocyanine", between 1933 and 1934.[8–10] The first X-ray structure was

investigated by J. Monteath Robertson in the 1930's at the Davy Faraday Research of the Institution Laboratory Royal.[8,10,11]

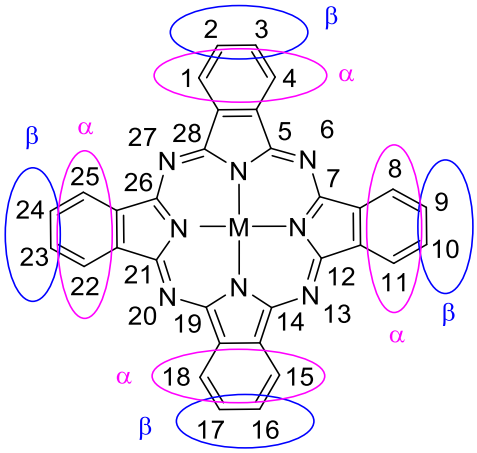

Figure 1.1: Structure and numeration of phthalocyanines. M is representing two protons or a metal ion.

Metal-free and metallated Pc derivatives have recently attracted an increasing interest not only for the preparation of new dyes and pigments, but also as building blocks for the design of novel molecular materials, due to their outstanding electronic and optical properties.[12] Furthermore, efficient singlet oxygen production, high stability in relation to temperature and light, desirable spectroscopic features and low dark toxicity, make Pcs currently one of the most potent and promising PSs for application in PDT and PDI.[8,10]

Pcs have been applied in a wide range of fields of medicinal[3] and materials[10,13] sciences. They are applied in the treatment of cancer[14–17] and photodynamic inactivation of pathogenic bacteria,[18] virus[19] and fungi,[20] as well as in bone marrow purging, age-related macular degeneration,[21] atherosclerosis,[22–24] theranostics,[25] anti-oxidants,[26] tumor imaging,[27–29] catalysis,[30] chemical sensors,[31–33] information storage and colorful liquid crystal systems, photovoltaic cells, semiconductors, non-linear transmission (NLT)[34–36] and conductive polymers.[8,10,11] On the other hand, the very low solubility of unsubstituted Pcs in common organic solvents and aqueous media has been the main limitation for their biological application.[6]

1.2.1 Historical background

The first Pc was discovered accidentally in 1907 by Braun and Tcheriac,[37] South Metropolitan Gas Company in London, during the chemical conversion of 1,2-disubstituted benzene derivatives, in which they observed the formation of a small amount of an insoluble blue-green byproduct during the preparation of 2-cyanobenzamide (Scheme 1.1).[38]

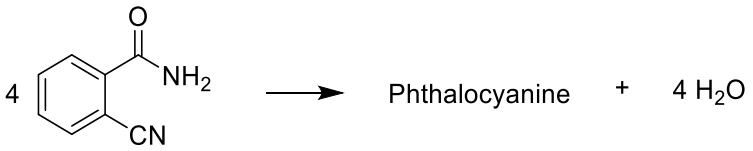

Scheme 1.1: Accidental synthesis of Pcs.[37]

Twenty years later, Diesbach and von der Weid, University of Fribourg, Germany, prepared, for the first time, a copper Pc in 23% yield by reacting 1,2-dibromobenzene with copper(I) cyanide in refluxing pyridine (Scheme 1.2).[3,8,10,39]

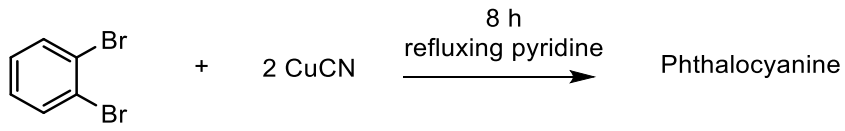

Scheme 1.2: Reaction performed by Diesbach and von der Weid.

Diesbach and von der Weid tried to characterize this compound without success. Therefore, the credit of the discovery of these compounds was given to Scotish and Dyes Ltd., when in 1928, during the industrial preparation of phthalimide from phthalic anhydride, an impurity was formed. The production of this blue-green impurity resulted from the exposure of the phthalimide to the outer layer of the iron reactor. Normally, such impurity simply would be discarded. However, this accidental discovery occurred in a dye company (Scottish Dyes, Ltd., Grangemout, Scotland) and the blue-green product attracted immediate their interest. This dye company performed some initial studies revealing that the iron-containing byproduct was exceptionally stable and insoluble in the majority of the common organic solvents, acquiring potential applications as pigment. The first patent was issued to Dandridge, Drescher, and Thomas of Scottish Dyes Ltd., in 1929.[8,10,11]

Pcs also turn out to have moderate cost of manufacture, good stability, tinctorial properties, and light absorption in the visible region of the spectrum. After 1938, several

companies like du Pont Company and Standard Ultramarine & Color Company started to produce copper Pc. Nowadays, there are a large number of companies all over the world producing Pcs and researchers have addressed themselves to the synthesis of substituted Pcs and determination of the physical and chemical properties of compounds.[8,10,11]

Still, the evolution of Pcs chemistry has not only been aimed at finding synthetic strategies that provide increasingly sophisticated Pcs systems, but also similar structures. Pc analogues (Figure 1.2) have also been studied and it is possible to find a different variations of the basic structure of the Pc macrocycle.[10,39]

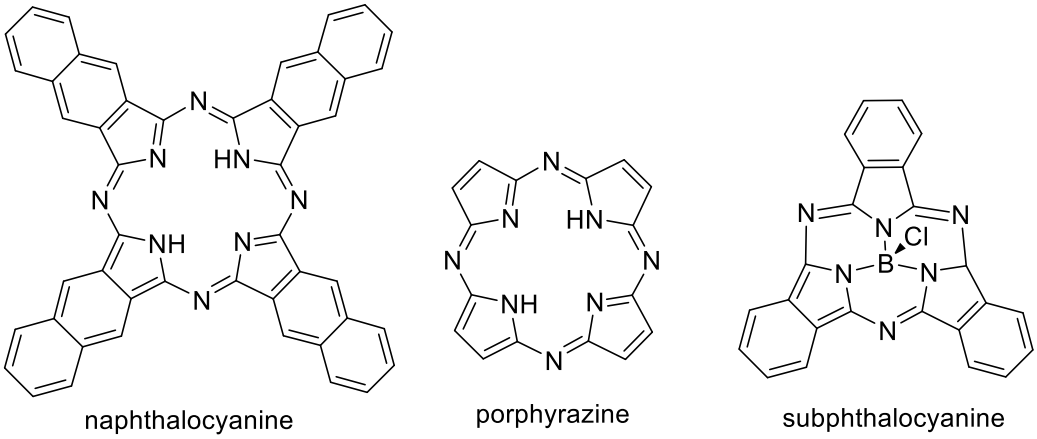

Figure 1.2: Analogues of phthalocyanine.

1.2.2 Molecular structure and numeration

According to the International Union of Pure and Applied Chemistry (IUPAC) numbering, the only atoms that cannot be numbered are the fusion carbons between the pyrrole ring and the benzene ring. Often the positions of the inner and outer carbons of the benzene rings are called alpha (α) and beta (β), respectively (Figure 1.1).

In the center of metal-free Pcs there are two hydrogen atoms which can be replaced by metal ions. Metallated Pcs are usually called metallophthalocyanines (MPcs) (Figure 1.1). Also, the sixteen peripheral hydrogen atoms in the four benzene rings can be replaced by different groups or even halogens.[40,41]

1.2.3 Physical and chemical properties

Although the chemical and physical properties of Pcs can be easily modulated, they are very stable due to an extended network of conjugated electrons. This stable

electronic configuration makes this macrocycle unable to undergo many reactions than redox or substitution reaction, in which electrons or hydrogen atoms are exchanged respectively by suitable oxidizing/reducing agents or electrophilic/nucleophilic reagents. Additionally, other reactions like ring opening or additions are very rare because they would certainly lead to a disruption of the Pc skeleton. Yet, in some cases, reactions like acid-base or transformation of the metal ion M (Figure 1.1), do not alter the aromatic character of Pcs and can be used in metallated derivatives.[8,10]

An important disadvantage of Pcs, especially for biological applications, is the extreme insolubility of their unsubstituted derivatives. The extreme hydrophobicity of the aromatic core and planarity of the molecules lead to stacking which results in highly stable crystal structures with high molecular lattice energies. These characteristics result in Pc aggregation. Aggregation is generally viewed as an association of molecules in solutions. In the case of Pcs aggregation is usually depicted as a coplanar association of rings progressing from monomer to dimer and higher order complexes, driven by non-bonded attractive interactions. This leads to a perturbation of the Pc electronic structure, which is undesirable in some applications that take advantage of the optical or catalytic properties. Besides, separation, electronic spectra and characterization are also negatively affected.[10] Even so, there are some techniques to diminish this aggregation tendency. The synthesis of axially substituted Pcs represent one of the most effective strategies, by not only diminishing aggregation but also by promoting solubility of the peripherally unsubstituted Pc compounds. Additionally, it is known that aggregation of Pcs may vary with solvent, addition of neutral disaggregating agents, presence of electrolytes, varying pH, and within micelles forming surfactants.[8,10,11]

Pcs have been extensively studied as second-generation PSs for PDT.[42–45] Due to the four additional peripheral benzene rings, they have absorptions at higher wavelengths compared with Pors, in the red visible region, allowing a deeper light penetration into tissues.

In addition, the metal ions of Pcs also influence their photophysical properties. Commonly, Pcs containing a closed shell and diamagnetic metal centre, such as Zn^{2+}, Al^{3+}, and Ga^{3+} have higher triplet state quantum yields and longer lifetime.[46]

1.2.3.1 Aromaticity

As already mentioned, Pcs are molecules whose planar aromatic character is provided by eighteen π-electrons delocalized over an alternate arrangement of atoms of carbon and nitrogen, obeying the Huckel's rule.[10] This unique electronic delocalization confers excellent electronic properties to the molecules. One of such properties is the high absorption capacity in the near-ultraviolet (UV) regions of the visible electromagnetic spectrum, similarly to Pors. However, in Pcs, the absorption bands of greater intensity are located in the visible range.[3]

1.2.3.2 Solubility

The major disadvantage of these compounds is their insolubility in water (aqueous media) and in most organic solvents. Unsubstituted Pcs only dissolve in solvents of high boiling point, such as quinoline, chlorobenzene or 1-chloronaphthalene, due to the natural tendency of the molecules to stack (π–π stacking). The only effective solvent is sulfuric acid at concentrations greater than 8 M, by inducing solubility *via* protonation of the *aza* nitrogens, thus modifying the properties of the macrocycle and severely limiting the applications of these solutions. For instance, protonation of the *aza* nitrogens causes a strong bathochromic shift of up to 80–120 nm in the Q band. However, physical, chemical, and electronic properties of Pcs can also be fine-tuned *via* the addition of suitable substituents and functional groups, which can enhance the solubility of these compounds.[3]

However, in some applications, insolubility of unsubstituted Pcs is essential. That is the case of the use of Pcs as dyes for textiles, paints and inks, in which, contrary to what is observed for biological applications, insolubility of these compounds is crucial for theirs application as dyes, along with Pcs glue-green intense colors.

1.2.3.3 Absorption spectra of phthalocyanines

All Pc compounds absorb light on both sides of the blue-green region of the visible light spectrum. The extensively conjugated aromatic chromophoric system of Pcs generates intense bands in their absorption spectra. The spectrum of the metal-free Pc differs from the metal-containing ones. MPcs UV-Visible (Vis) spectra show a strong Q band while metal-free Pcs UV-Vis spectra show two Q bands. Q band split is

due to less symmetry of metal-free Pcs in relation to MPcs. In Figure 1.3 it is possible to observe differences in the absorption range of a metal-free Pcs and MPcs.[47]

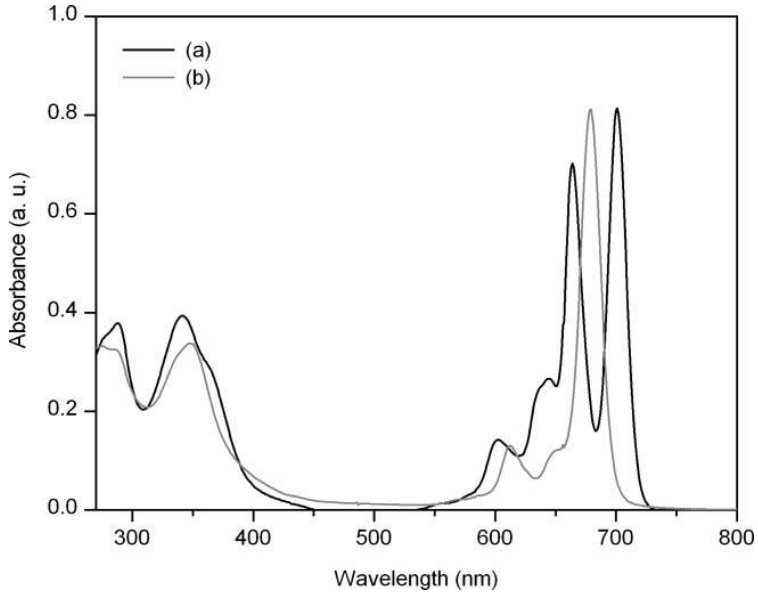

Figure 1.3: Absorption spectra of metal-free phthalocyanines (a) and metallophthalocyanines (b).[48]

The strongest absorption band(s) (Q band(s)) in most Pcs lies in the visible region at wavelengths between (620–700 nm), while the weaker band (Soret or B band) is near 350 nm. The Q band(s) (red light region) is (are) responsible for the characteristic blue-green color of Pcs. The position of the absorption bands in Pc are affected by axial substitution, peripheral and non-peripheral substitution, solvent, aggregation, and extension of the conjugation.[10] This effect is more pronounced in the Q band(s).[49]

1.2.4 Synthesis of phthalocyanines

Depending on the precursors used, Pcs can be synthetized by several methods. Pcs can be obtained *via* a metal-templated cyclotetramerization reaction from aromatic *ortho*-dicarboxylic derivatives like phthalic acids, Phts, phthalic anhydrides, phthalimides, diiminoisoindolines and *o*-cyanobenzamides (Figure 1.4). In Scheme 1.3 some reactions examples by which Pcs can be obtained are described.

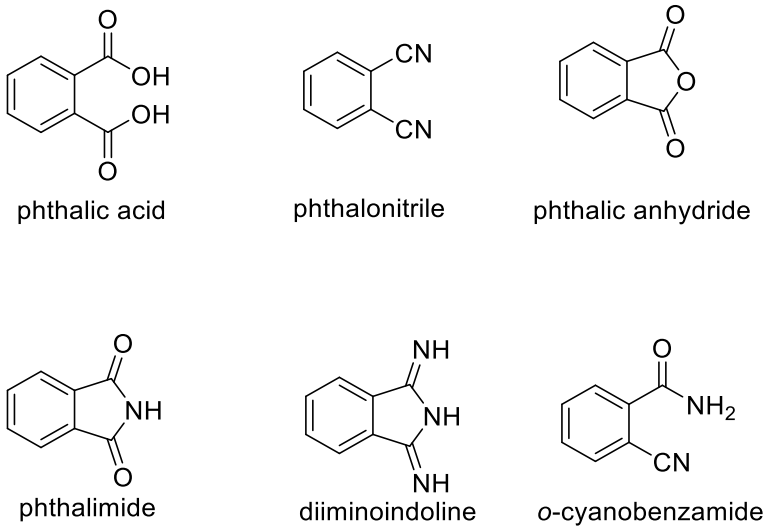

Figure 1.4: Precursors of phthalocyanines.

The most used Pc precursors are Phts because of their capacity to render good yields and higher purity. There are a large number of commercially available substituted Phts bearing diverse functional groups. Others can be synthesized by different classical methods from inexpensive commercial available starting materials.[8,10]

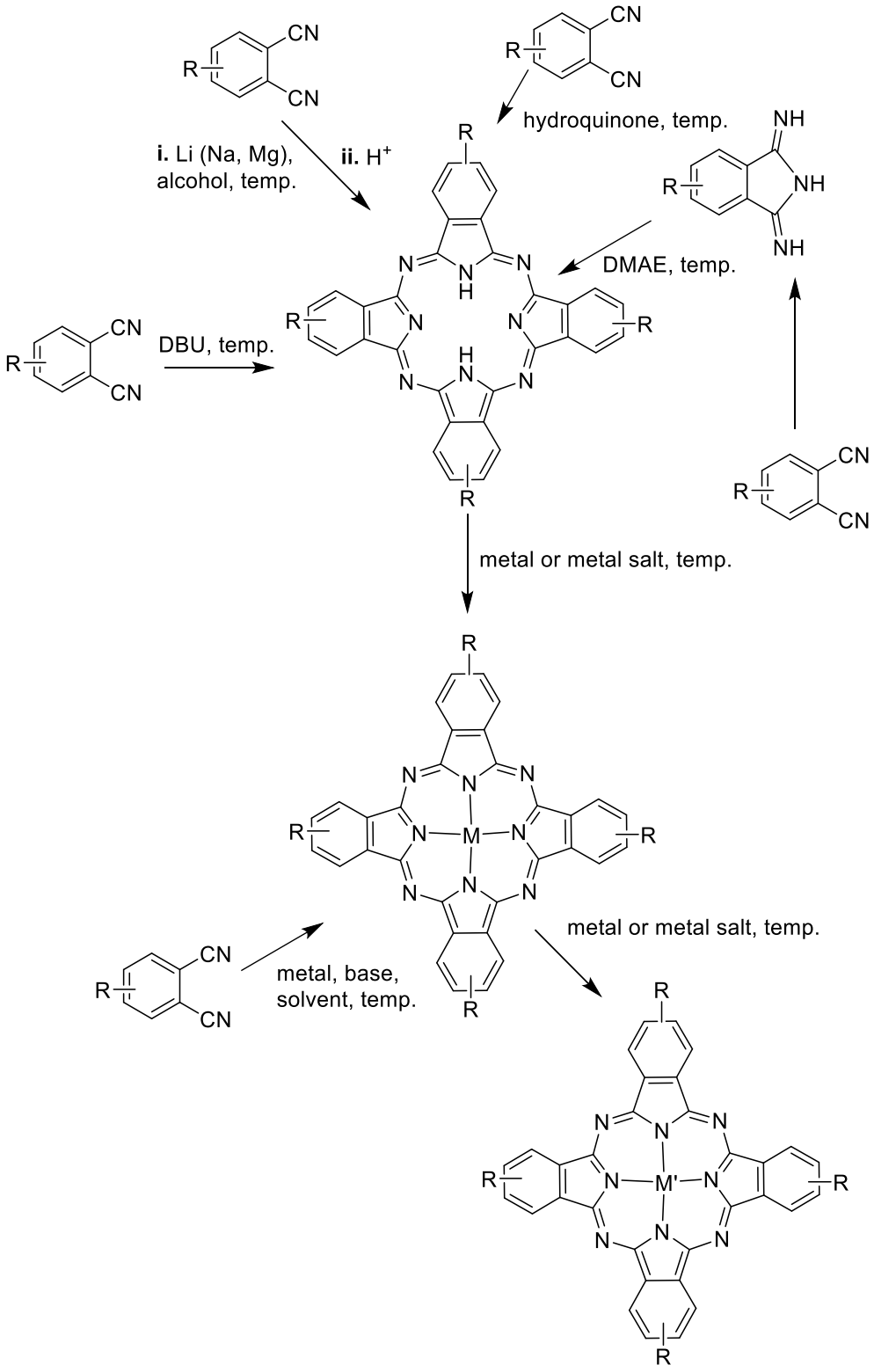

Scheme 1.3: Examples of the possible strategies for the synthesis of metal-free phthalocyanines and metallophthalocyanines.

The fine-tuning of the properties of a Pc can be accomplished by one of two basic methods: in the first one, the substitution takes place directly on the pre-existing Pc; in the second method the substitution takes place in precursors of Pcs, leading to far cleaner reactions in terms of degree of substitution. The second method, by modulation of the precursors of Pcs, is the most used one. Through this method, a more precise modulation can be made, leading to a mono- or even to an octa-substituted Pc in the positions 2, 3, 9, 10, 16, 17, 23 and 24. In spite the fact that the potential sites for Pc substitution are well-known, these methods can lead to a formation of constitutional isomers (Figure 1.5), which are very difficult to separate. This was only accomplished for very specific Pcs using specially designed high-performance liquid chromatography (HPLC) columns.[8,10]

Nucleophilic aromatic substitution is by far the most used reactions employed in the modification of substituted Phts. This reaction is successful when appropriate leaving groups are present in the Pht, due to the electron-withdrawing capacity of the dinitrile functionality. Many leaving groups have been used on substituted Pht synthesis. The most used and with best results leaving group for nucleophilic aromatic substitution reactions is NO_2. Nevertheless, there are other leaving groups used in this type of reaction. Although the order of leaving group ability depends on the nature of the nucleophile employed during the reactions. The approximate order of leaving group ability is F > NO_2 > OTs > Cl, Br, I.[8–11,40]

The majority of the work around Phts as precursor of Pcs has been carried out using the NO_2 group of both 3- and 4-nitrophthalonitrile as the leaving group and an alcohol as the nucleophile. Thiols and amines can also be used as nucleophiles. Usually this reaction is carried out in a dry polar aprotic solvent, such as dimethyl sulfoxide (DMSO) or dimethylformamide (DMF), using sodium or potassium carbonate as a base. In some cases, the dry potassium carbonate is added portionwise over time. Moreover, there are other solvents which can be used, such as dioxane, *N*-methyl-2-pyrrolidone and *N,N*-dimethylacetamide. Despite the fact that 3-nitro- and 4-nitrophthalonitrile are known to react with ammonia and primary and secondary amines to give the corresponding aryl amines, the number of works where these nucleophiles are used is small.[8,9,50] From the few compounds synthesized by this reaction, 4-(phenothiazin-10-yl)phthalonitrile can be highlighted, as well as a series of heteroarylphthlalonitriles,

where heterocyclic *N*-nucleophiles were used like benzotriazole, 3,5-diphenyl-1,2,4-triazole, phthalazine and 4-quinazolinone (Figure 1.6).[8–10,21]

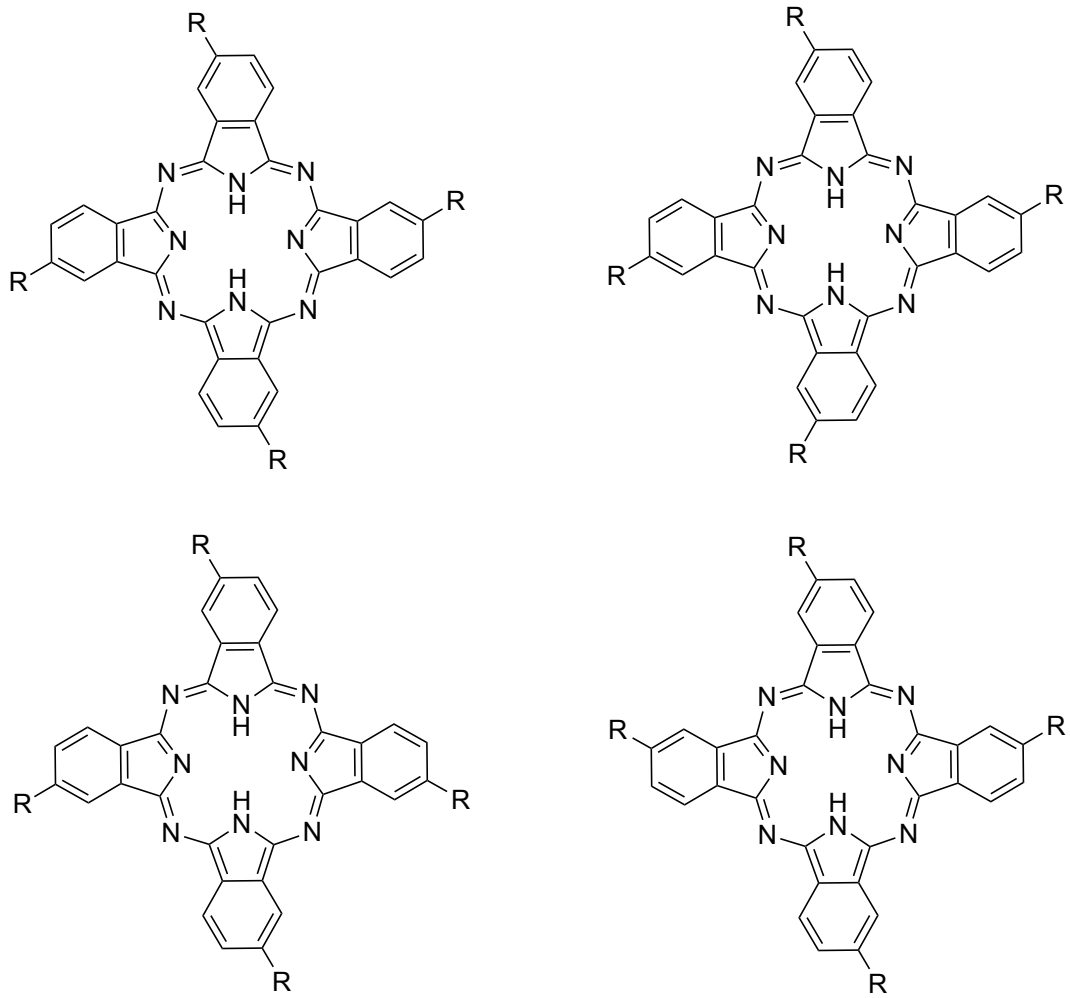

Figure 1.5: Constitutional isomers for a tetrasubstituted phthalocyanine.

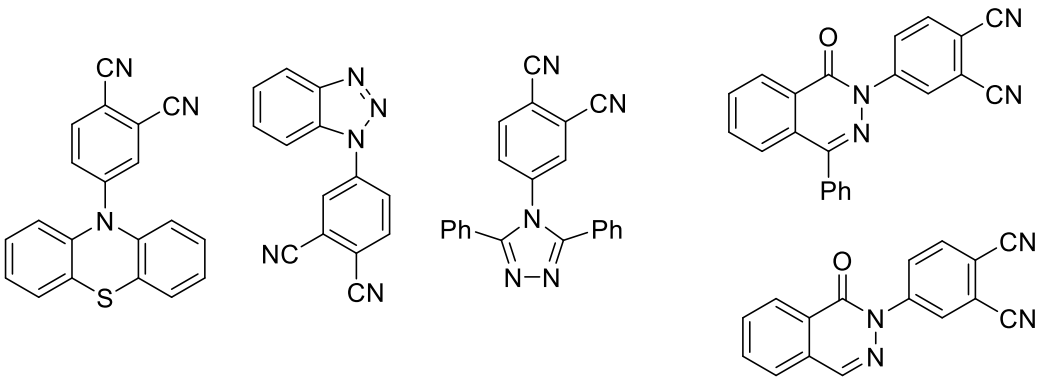

Figure 1.6: Phthalonitriles with amine groups.

The most used conditions to obtain substituted Pcs *via* Phts consists on the reaction of one or two different Phts (that can previously be modified with the insertion of the desired substituents) in an alcohol, such as 2-dimethylaminoethanol (DMAE) or penta-1-ol in the presence of a metal ion (Li^{+}, Mg^{2+}, Al^{3+} or Zn^{2+}). In some cases, a base catalyst such as 1,8-diazabicyclo(5.4.0)undec-7-ene (DBU) is required. Free-metal Pcs can be obtained by the treatment of LiPcs or MgPcs with trifluoroacetic acid and temperature, or by reaction of one or more different Pht(s), in the presence of dioxane or with ammonia in DMAE.[8–10] The statistical condensation of two different Phts leads to the formation of six different substituted Pcs (not including constitutional isomers) (Figure 1.7).[8,10] When only one type of precursor is used in the reaction it can be obtained a mixture of constitutional isomers. In some cases, such as for di-, tri- or tetrasubstituted Phts, only one product is obtained.

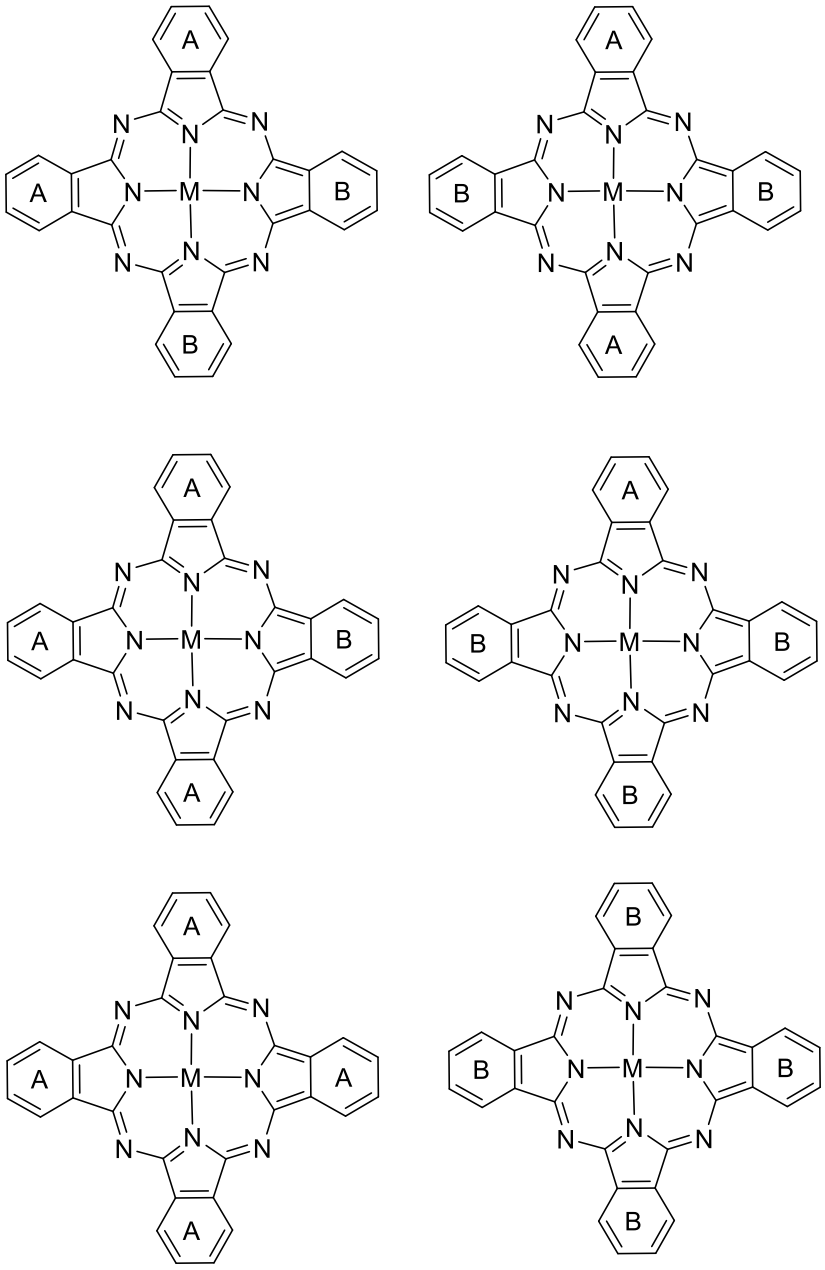

Figure 1.7: During a mixed condensation reaction of two different substituted precursors can be formed six different phthalocyanines. **A** and **B** represent two different substituted isoindoline units.

The specificities of cyclotetramerisation are still far from being fully understood. Nevertheless, there is a possible mechanism for the formation of Pcs (Scheme 1.4). Commonly, cyclotetramerisation reactions are highly exothermic and occur under harsh conditions. Thus, it is difficult to access Pc synthesis mechanism because the classical techniques for mechanistic elucidation cannot be applied readily. The mechanistic

option most accepted is based on isolated intermediates in Pc synthesis. All synthetic routes studied use an alcohol as solvent.

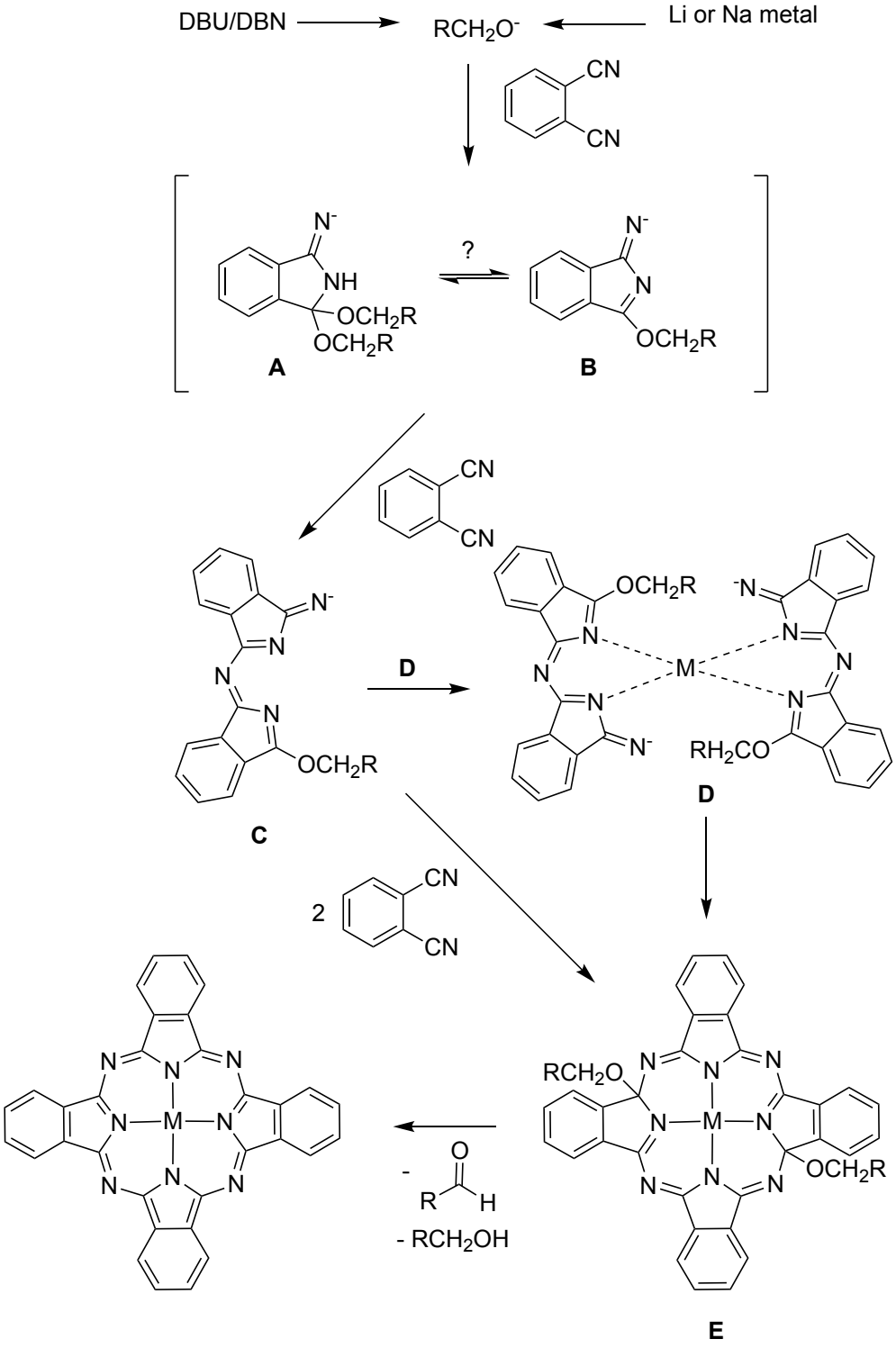

Scheme 1.4: Intermediates involved in the formation of phthalocyanine.

This reaction of cyclotetramerization is believed to involve a polymerization of the precursors, followed by coordination with the central atom leading to cyclization.

This process starts by the formation of the alkoxide due to the presence of an alcohol and the metal ion. The study of cyclotetramerization of Pht in the presence of metal ions such as Li^+ or Na^+ resulted in isolation of **A** and **B**. It is believed that solvents such as methanol and ethanol favor the formation of structure **A**, whereas larger alcohols are related with the formation of the structure **B**. Furthermore, it is probable that both structures are intermediates in Pc formation using pentan-1-ol as solvent at reflux. The intermediate **C** was obtained when 4-nitrophthalonitrile and lithium methoxide are reacted in methanol at 116 ºC. Intermediate **D**, which it is not more than two **C** units coordinated with a metal, was isolated when the reaction was carried out with $NiCl_2$ and diiminoisoindoline in pentan-1-ol under reflux. Heating complex **D** gave NiPc with pentan-1-ol and pentanal release, giving rise to the Pc, throw complex **E**, which were isolated and characterized by single crystal X-ray crystallography.[10]

In some cases, due to the presence of halogens or leaving groups in the precursors, a synthesis *via* alkoxide mediator, it is not recommended. Under these, the cyclotetramerization reaction is usually carried out at higher temperatures in a high boiling solvent, such as chlorobenzene, quinoline, nitrobenzene, or 1-chloronaphthalene can be used to obtain the desired Pcs. These methodologies can also be used when high reaction temperature is required to achieve the desired Pcs.

1.2.5 Separation and purification of phthalocyanines

The most used Pc separation method is chromatography. Due to strong tendency of Pcs to aggregate in solution, every chromatographic technique must be carefully used to prevent contamination with previous and forward compounds and consequently obtain pure fractions of Pcs. The aggregation phenomenon can be surpassed by using diluted solutions, addition of coordination solvents and by heating the eluent. Likewise, gel permeation chromatography can be used to separate Pcs from small precursors and byproducts, since this technique separate the compounds based on molecular exclusion.[10]

Taking advantage of remarkable stability of Pcs and some of its unsubstituted metal derivatives, they can be purified by sublimation at temperatures up to 600 ºC in vacuum. This method is used to obtain ultra-pure materials. Another method of purification relying on the stability of Pcs is reprecipitation from concentrated sulfuric

acid into water or ice. However, it cannot be applied to substituted derivatives that can undergo hydrolysis or sulfonation.[10]

1.2.6 Characterization of phthalonitriles and phthalocyanines

Pcs are usually characterized by the classical methods such as elemental analysis (EA), infrared (IR), and UV-Vis spectroscopy. A particular and very important analysis is the position of the Q-band in the UV-Vis spectrum. This analysis allows the visualization and procurement of useful information of the influence of insertion of substituents on the Pc periphery and the insertion of central metal ions.[10]

What is more, some structures of Pcs have been solved by single crystal X-ray, which is another important characterization method along with nuclear magnetic resonance (NMR). NMR is a useful technique for soluble derivatives since the analysis by this technique requires the solution of the desired compound in a deuterated organic solvent. However, Pcs are poorly soluble in many organic solvents and tend to aggregate in solution leading, frequently, to broad signals. Thus, good results are highly dependent on the choice of the solvent and on the use of low concentrations and high temperature. The chemical shift is strongly influenced by aggregation, which also has a direct relation with the concentration. This deviation can undergo a chemical variation up to 2 ppm. The electronic structure of the Pc ring creates a strong induced current and, consequently, a very intense anisotropic effect. Thereby, the protons directly linked to the ring are quite unprotected, and theirs resonances will occur at very high chemical shift values, in the region typical for aromatic protons. On the other hand, the inner hydrogens are rather protected, and as a result will have negative chemical shift values, appearing on the right of the tetramethylsilane (TMS) signal.[10]

Finally, mass spectrometry (MS) is also a commonly used technique for the structural characterization of Pcs, especially by matrix-assisted laser desorption ionization (MALDI).[10]

1.2.7 Applications

Since their accidental discovery in the beginning of the twentieth century, Pcs have been extensively studied in many fields. The first application as dyes for textiles, paints and inks was due to the dark green-blue color. Interesting physicochemical properties triggered the application in a wide range of techniques and processes like

catalysts for oxidation reactions, lubrication greases, molecular electronic devices and optical materials.[2]

Guilherme Amaral and co-workers[26] evaluated the possible anti-oxidant capacities of four MPcs and one metal-free Pc. The tests were carried out in lipid peroxidation assay. With this strategy, Amaral *et al.*[26] were able to confirm, by the juxtaposition to a non-induced control, the capacity of these Pcs to protect from sodium nitroprusside-induced oxidative damage to supernatant from the homogenized liver, brain and kidney of mice. They were also able to observe that MPcs have a better anti-oxidant capacity than metal-free Pcs. In this work it was observed that the approximate order of decreasing efficiency was MgPc, CuPc, FePc, ZnPc and, as the least efficient, metal-freePc.

It is known that cationic Pcs form complexes with nucleic acids. The binding of positively charged oligonucleotide substituted Pcs with single- and double-stranded DNA (dsDNA) was investigated and it was shown that these Pcs interact with nucleic acids through an outside binding mode. These Pcs were investigated ultimately aiming at potential applications as nucleic acid molecular probes because only few molecules are available to image DNA.[51,52] In addition, anionic Pcs have also been shown to interact with DNA, although not directly. As an example, some anionic Pcs are known to efficiently inhibit telomerase activity, even in the presence of excess dsDNA, due to their selective binding to telomere G-quadruplex.[53] G-quadruplex is a four-stranded structure formed by guanine-rich sequences in which anionic compounds can selectively bind such as anionic Pcs. Yaku *et al.*[53] reported for the first time the utilization of anionic Pcs comprising four sulfonic groups that bound telomere G-quadruplex with high selectivity, inhibiting telomerase activity.

Another application of Pcs is the utilization of this macrocycle as cathode catalyst for oxygen reduction in microbial fuel cells (MFCs). MFCs are devices that use bacteria as the catalysts to oxidize organic and inorganic matter and generate current. Electrons produced by the bacteria from these substrates are transferred to the anode and flow to the cathode linked by a conductive material containing resistor.[54] The development of oxygen reduction catalysts for fuel cells has been increasing and an efforts have been made to develop inexpensive non-noble metal electrocatalysts. Pcs and metalloPors have emerged as an important alternative for the substitution of platinum and other related oxygen reducing precious metals as cathode catalyst in fuel

cells.[54–58] In this context, Yuan *et al.*[56] investigated the utilization of amino-functionalized multi-walled carbon nanotube-supported iron Pc as a catalyst for the oxygen reduction in an air-cathode single-chambered MFC. These nanotube-supported iron Pcs proved to be efficient for reducing conversion and showed maximum power density of 601 mWm^{-2}.

Recently, Pcs have been used as PSs in PDT and PDI. Examples of these applications, along with their basic concepts, will be addressed in the following chapters.

1.3 Aim

Considering the photosensitizing potential of Pcs to be used in the photodynamic inactivation of Gram-negative, Gram-positive and tumor cells, and the antibacterial and antitumor activity of SAs, the aim of this work is to obtain Pc–SA conjugates to be used as antimicrobial and antitumor compounds. The presence of SA moieties will give higher specificity to photosensitization due to specific selectivity to the folic acid pathway and to antitumor targets such as CA. It will increase the efficiency and specificity of the photodynamic therapy and reducing any toxic effects on non-target tissues. Examples of PSs, such as Pors coupled to the SAs are documented in the literature.[59] For some of these PSs, the photodynamic effect was proven.[60] Similarly, there is also information on the synthesis of sulfonated Pcs,[61,62] but, as far as we are aware of, there is no reports on the utilization of Pc–SA conjugates as PSs. Thus, the synthesis of Pc–SA conjugates with antimicrobial and/or antitumor activity addresses a gap in scientific knowledge and will provide a scientific platform for application of sulfonated Pcs as a new tool in the control of tumorigenesis and infection diseases, including those caused by multiresistant microorganisms. For that, it was projected to develop new methods for the synthesis of Pc–*N*-acyl-SA conjugates and Pc–SA conjugates; and evaluate the biological activity of the synthesized compounds in bacteria and tumor cells.

This work will be a contribution to circumvent microbial resistance to antibiotics which is observed worldwide. Moreover, it will also be an asset in developing interesting strategies against oncological diseases, particularly by increasing the selectivity of the compounds used in PDT.

Chapter 2 Synthesis of phthalocyanine–*N*-acyl-sulfonamide conjugates

Look carefully to Nature and you will find that nucleic acids, proteins and polysaccharides are condensed polymers of small subunits (blocks) linked together by carbon–heteroatom bonds. In Nature there is an almost perfect biosynthesis efficiency involving reactions that occur in quantitative yields, few/no byproducts or side-reactions and are, in the majority of the cases, stereoselective.[63] For instance, Nature links small molecules *via* carbon–heteroatom bonding in order to synthesize essential molecules for life like polypeptides, polysaccharides, or polynucleotides.[64] From this idea, and ever since initial publications of Sharpless and co-workers,[65] the area of click chemistry has turned into a field with exponential growth.[66] One important click reaction is the sulfo-click reaction, a variation of the Cu(I)-catalyzed alkyne–azide cycloaddition (CuAAC).

With this information in mind, we decided to study the applicability of the sulfo-click reaction[67–70] in the construction of new PSs bearing *N*-acyl SA moieties. In this chapter it is described how it was carried out and the results obtained.

2.1 Introduction

Using new synthetic methods, as the principle of click chemistry, introduced by Sharpless and co-workers in 2001,[65] new SA derivatives have been developed. Click chemistry involves chemical reactions that generate substances quickly in smooth reaction conditions and in high yield, by the addition of small blocks. This principle has aroused great interest, particularly in the synthesis of *N*-acyl SAs. Its applications are found in large aspects of drug discovery, combinatorial chemistry and target-template chemistry, drug delivery nanosystems, polymers and nanoparticle surface modification, and in proteomics and DNA research, using bioconjugation reactions.[66]

The prime example of a click reaction, and the most studied, is the CuAAC. It has found applications in a wide variety of research areas, including materials science, polymer chemistry, and pharmaceutical science. This reaction is regioselective, forming only 1,4-disubstituted 1,2,3-triazoles, and can be performed at room temperature.[66] Beyond that, it produces the desired product in high yields and is faster than the uncatalyzed reaction. Another important aspect of the success of this reaction, related to

materials science and biotechnology, is that the starting azides and terminal alkynes are exceptionally stable and can be introduced in a wide range of macromolecules.[71]

There are a few classes of chemical transformations that have click characteristics. In Figure 2.1 some examples of each class of click reactions are schematized.

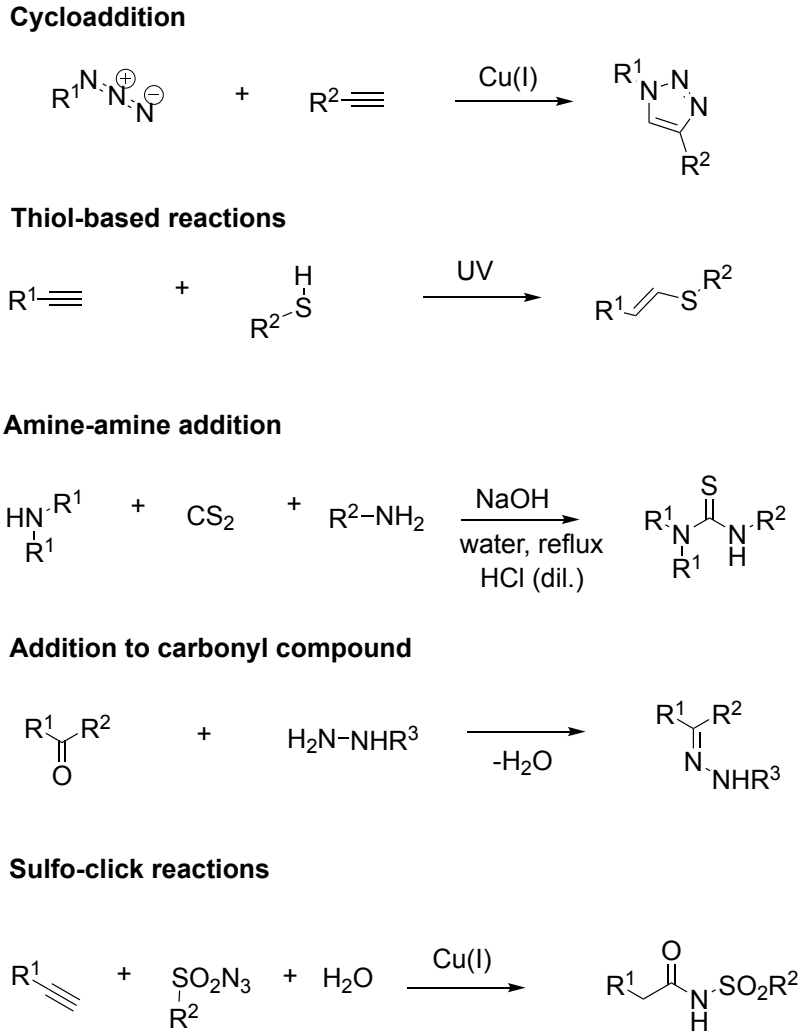

Figure 2.1: Examples of chemical reactions that fall within the framework of click chemistry.

This category of reactions turns out to be an important tool in medical and materials science (especially in polymer material design[72]) by their versatility. This is especially important in living systems, because a critical aspect of any strategy of labelling a target biomolecule inside a living cell or organism by a chemical reaction is that the reaction must be chemoselective, and in particular bioorthogonal.[66]

As already referred, the sulfo-click reactions are a type of click reactions that lead to SAs. SAs, have interesting properties for application in medicine and veterinary.[4,73,74]

Sulfo-click chemistry takes advantage of the combination of more than two components, falling in the category of a multicomponent reaction (MCR). Since it also requires Cu(I) as catalyst, it can be considered a variation of the CuAAC. Chang and co-workers,[69,75] from a modified Staudiger reaction of azides with phosphines, has drawn a new synthetic pathway in which sulfonylazides react with terminal alkynes in the presence of catalytic amounts of CuI and a base, to give rise to *N*-acyl SAs (Scheme 2.1).[70] This reaction is completely regioselective, occurs under very mild conditions and the products are obtained in high yields. Thereafter, they found that the best yields and shorter reaction times are obtained by using water as solvent, making this type of reaction surprisingly adequate for biological applications.[69,75] The mechanism for this reaction is not yet fully identified, but there are some results pointing that this type of reaction develops a common ketenimide intermediate generated from the Cu-mediated intermolecular cycloaddition between azide and alkyne.[69,75,76]

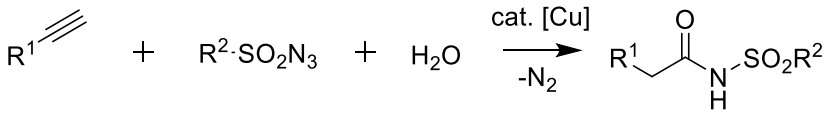

Scheme 2.1: Sulfo-click reaction.

Although a detailed understanding of the mechanism of this reaction will require additional studies, Cassidy *et al.*[67] proposed a mechanism similar to the copper(I)-catalyzed triazole synthesis (Scheme 2.2). After acetylene activation by Cu catalyst, the formed (1,2,3-triazol-5-yl)copper species, which in a copper(I)-catalyzed triazole reaction normally undergoes proteolysis to release the triazole product, in this reaction, due to a strongly electron-withdrawing group at N^1, elimination of a dinitrogen molecule occurs producing a transient Cu-alkynamide compound. This complex is then protonated to give the highly reactive ketenimine which is immediately trapped by water to form the *N*-acyl SA. There is an alternative route to ketenimine production through a ring-opening pathway, resembling the Dimroth rearrangement, forming a diazoimine derivative.

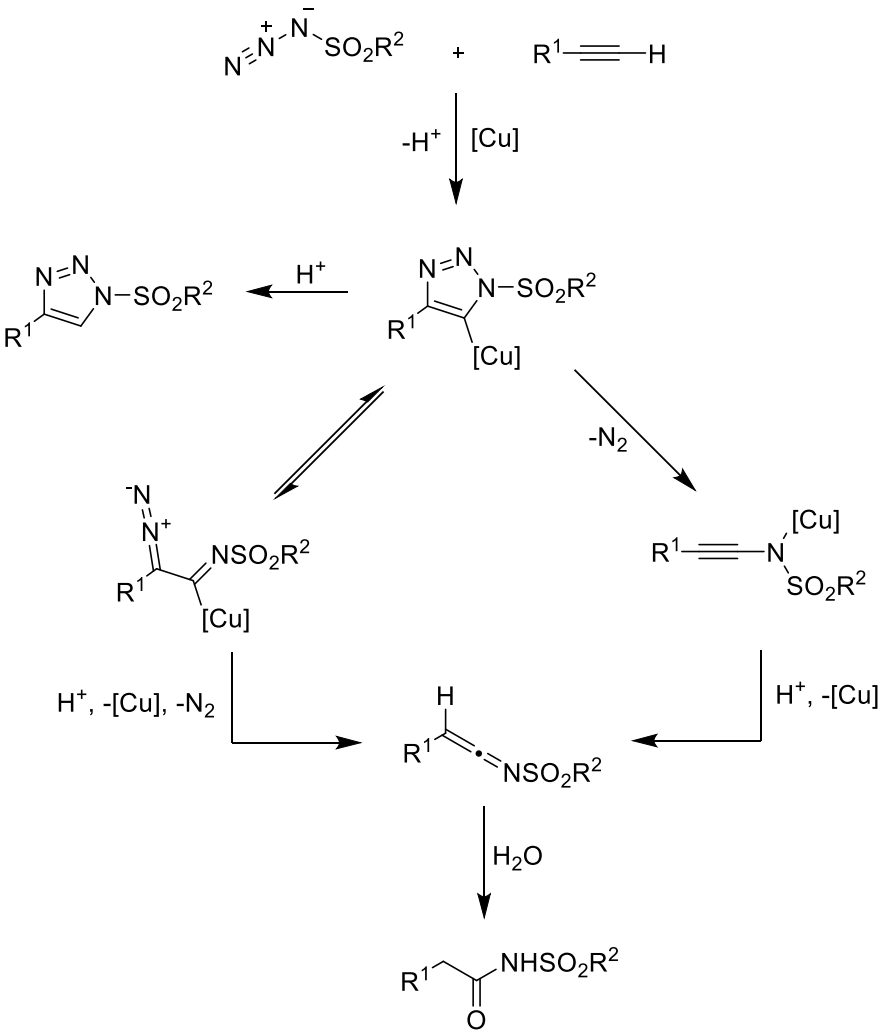

Scheme 2.2: Sulfo-click mechanism (see description in the text).[67]

2.2 Results and discussion

For the synthesis of Pc–*N*-acyl-SA conjugates, two synthetic routes can be followed as described in Figure 2.2. In the synthetic route **A** Pht–*N*-acyl-SA conjugates and Pc–*N*-acyl-SA conjugates are obtained from 4-(4-azidosulfonylphenoxy)phthalonitrile. In synthetic route **B** 4-(3-ethynylphenoxy)phthalonitrile is used as starting material. Results and details related with synthetic routes **A** and **B** will be described in sections 2.2.1 and 2.2.2, respectively.

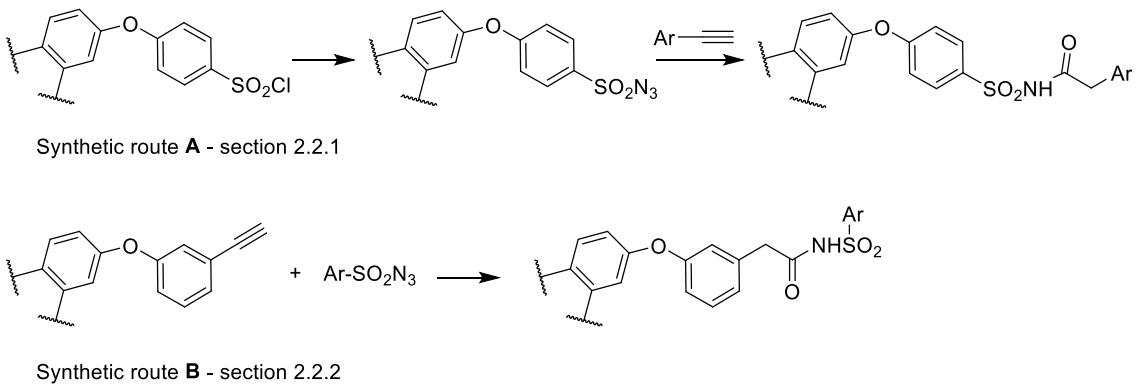

Figure 2.2: Planned synthetic routes **A** and **B**.

2.2.1 Synthetic route A - from 4-(4-azidosulfophenoxy)phthalonitrile

The first part of the work for the synthesis of Pc–*N*-acyl-SA conjugates, through synthetic route **A**, convey the synthesis of Pht–*N*-acyl-SA conjugates, taking advantage of the sulfo-click reaction, using as reagent a Pht with an azidosulfonyl group. The planned synthetic route to those compounds is described in Scheme 2.3.

Firstly, 4-phenoxyphthalonitrile (**1**) was obtained by a nucleophilic aromatic substitution of the nitro group in 4-nitrophthalonitrile by phenoxide. The reaction was carried out in DMF under basic conditions with portionwise additions of potassium carbonate in order to avoid phenol oxidation. Then, the reaction mixture was left overnight at room temperature. The consumption of the 4-nitrophthalonitrile was verified by thin-layer chromatography (TLC) and the desired product was obtained by precipitation in cold water, filtered and washed several times with water and hexane. Finally, the product was crystallized from a mixture of chloroform/hexane (77.8% yield).

Pht **1** was characterized by ^{1}H NMR, ^{13}C NMR and mass spectrometry (MS) using electrospray ionization (ESI) in positive mode. All spectra are in agreement with those described in the literature.[77–82] The crystalline structure has also already been reported.[79]

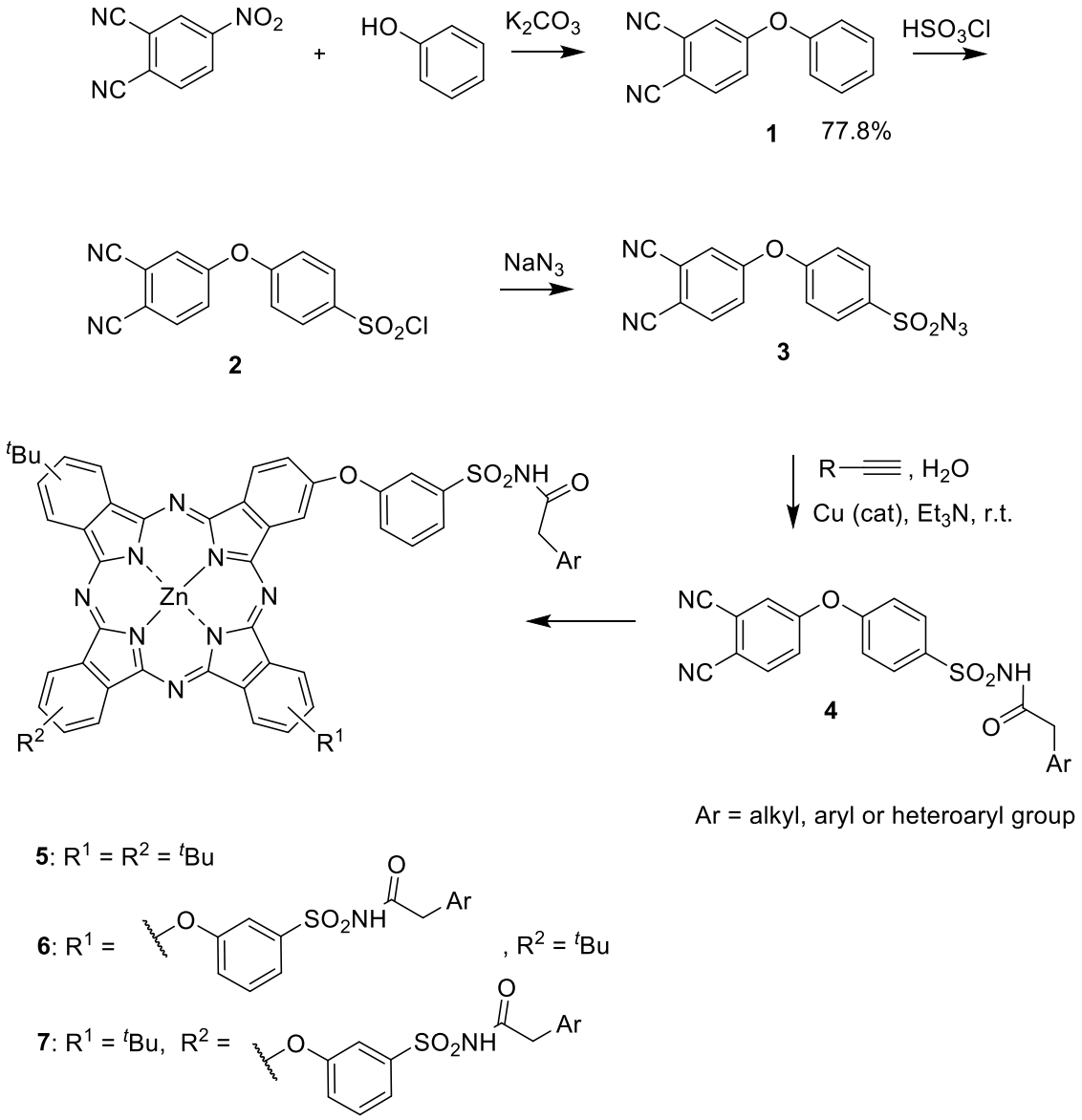

Scheme 2.3: Planned route for the synthesis of phthalocyanine–*N*-acyl-sulfonamide conjugates from 4-(4-azidosulfophenoxy)phthalonitrile (**3**).

Then, we proceeded to the synthesis of the chlorosulfonyl derivative **2** by chlorosulfonation of the phenoxy group (Scheme 2.3). This conversion proved to be quite demanding. Pht **1** reacted with an excess of chlorosulfonic acid for 45 min at 0 ºC, following the conditions described by Carvalho *et al.*[61,62] However, instead of the chlorosulfonated derivative, more than once, we obtained the product 4-(4-sulfophenoxy)phthalonitrile (**8**) (Scheme 2.4), that was confirmed by ^{1}H NMR spectrum where it showed a peak at δ 11.32 ppm, attributed to the proton of the sulfonic moiety and by ESI-MS analysis in positive mode, where we were not able to observe the isotopic pattern of the chlorine atom expected for the chlorosulfonyl derivative **2**.

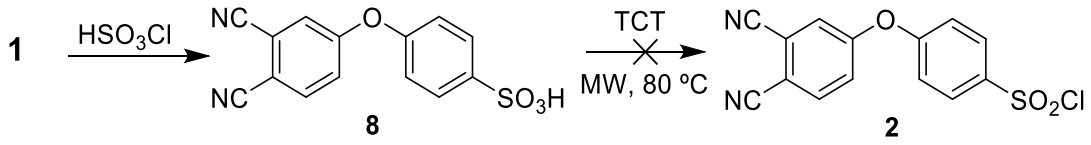

Scheme 2.4: Synthetic procedure for the conversion of **8** into the chlorosulfonyl derivative **2** with the chlorinating agent TCT.

So, in order to achieve the desired compound, we evaluated the applicability of 2,4,6-trichloro[1,3,5]triazine (TCT) as chlorinating agent of reagent **8** (Scheme 2.4). The procedure consisted in the addition of TCT to a mixture of the sulfonic acid and triethylamine, all in equimolar quantities, in acetone. The reaction was carried out under microwave irradiation in a sealed tube at 80 ºC for 20 min as described by Luca *et al.*[83] and Blotny.[84] However, with this procedure, we were also not able to verify the conversion of the sulfonic acid **8** into the corresponding chlorosulfonyl derivative **2**.

In addition, in a parallel reaction, we also verified whether we were in the presence of derivative **2** or **8**. For that, the white powder afforded from the reaction of Pht **1** with chlorosulfonic acid, was reacted with diethylamine in acetonitrile at room temperature (Scheme 2.5).[61,62] Yet, we did not afford the expected SA **9**, confirming that we were in the presence of the sulfonic acid **8**.

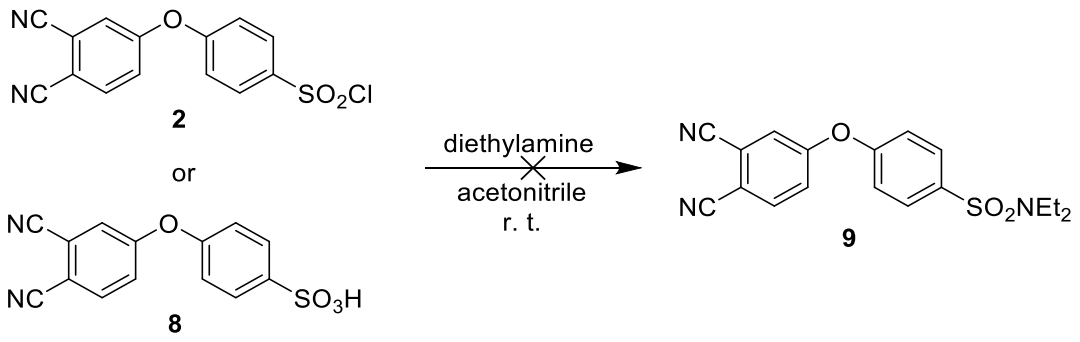

Scheme 2.5: Reaction of the white powder (from the reaction of phthalonitrile **1** and HSO_3Cl) with diethylamine.

As a parenthesis of our planned work, and to better understand the sulfo-click reaction, we decided to use the commercial chlorosulfonyl derivative **10** as a precursor to the *N*-acyl SA **12,** in a two steps procedure, as shown in Scheme 2.6.

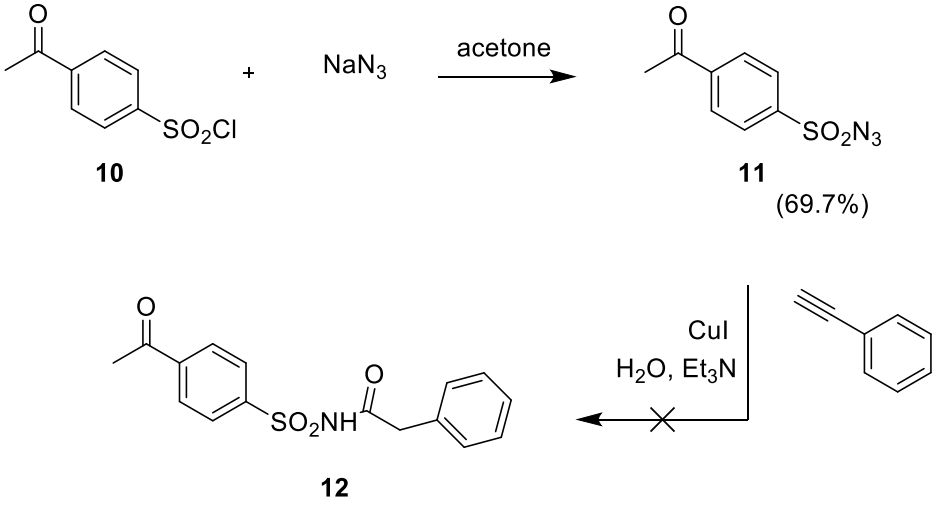

Scheme 2.6: Planned synthetic route to *N*-((4-acetylphenyl)sulfonyl)-2-phenylacetamide (**12**).

In the first step the chlorosulfonyl derivative **10** was reacted with sodium azide, in acetone at room temperature. 4-Acetylbenzenesulfonyl azide (**11**) was obtained in 69.7% yield as a white powder. The structure of **11** was confirmed by ^{1}H and ^{13}C NMR. In the ^{1}H NMR spectrum (Figure 2.3) it is possible to observe a singlet at δ 2.69 ppm, which corresponds to the protons at the acetyl group. In the aromatic region, an AB system with a peak at δ 8.05–8.09 ppm and another at δ 8.15–8.19 ppm is observed. In the ^{13}C NMR spectrum (Figure 2.4) it is possible to observe the peak corresponding to the methyl group at δ 26.95 ppm, whilst the peaks for the carbons in the *ortho* and *para*

positions appear at δ 127.85 ppm and 129.38 ppm, and at δ 141.52 ppm and 141.94 ppm the other two carbons of the aromatic ring. Finally, the peak corresponding to the carbonyl group can be observed at δ 196.26 ppm.

The ^{1}H and ^{13}C NMR spectra of azidosulfonyl derivative **11** is similar to the ones of the chlorosulfonyl **10** (data not shown), from which there is only a difference in the sulfonyl moiety. Therefore, there are no significant changes in the chemical shifts and multiplicities of the ^{1}H NMR spectrum and ^{13}C NMR spectrum of product **11** when compared to the reagent **10**. Nonetheless, reagent **10** and product **11** have quite different retention factors (R_f) in TLC plates (silica gel, CH_2Cl_2/hexane (1:1) as eluent): 0.37 for **10** and 0.21 for **11**. Additionally, in ESI-MS spectrum the molecular ion (M^+) of azidosulfonyl **11** at *m/z* 225.2 and $[M+K]^+$ ion at *m/z* 264.2 was observed, confirming the success of the conversion of chlorosulfonyl reagent **10** into the azidosulfonyl derivative **11**.

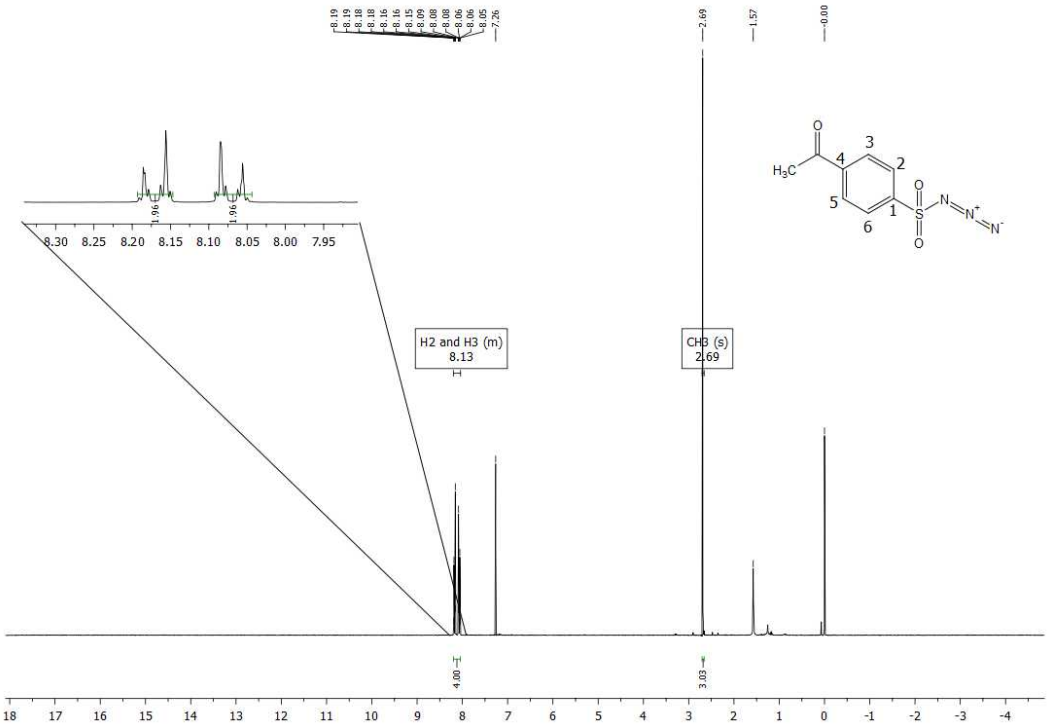

Figure 2.3: ^{1}H NMR spectrum of acetylbenzenesulfonylazide (**11**) in $CDCl_3$.

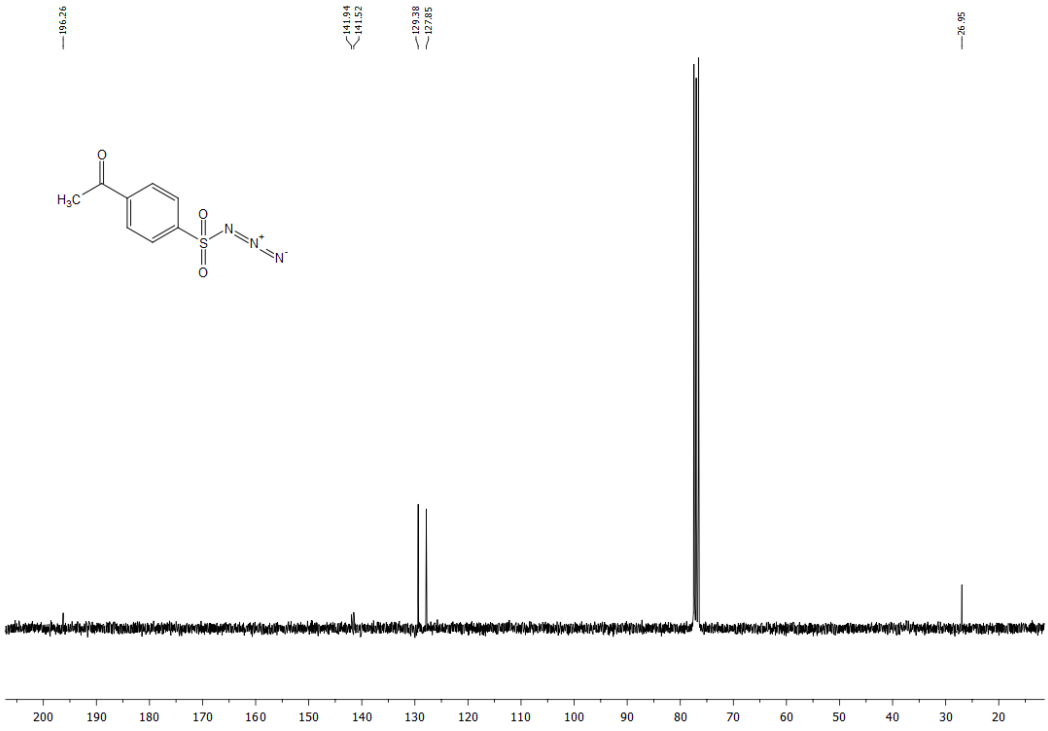

Figure 2.4: ^{13}C NMR spectrum of acetylbenzenesulfonylazide (**11**) in $CDCl_3$.

Next, in the second reaction described in Scheme 2.6, sulfonylazide derivative **11** was used as reagent in a sulfo-click reaction with ethynylbenzene and Et_3N in H_2O following the procedure described by Cho *et al.* using CuI as catalyst.[68,69] However, the *N*-acyl SA derivative was not obtained using these reaction conditions.

After analyzing the results discussed in this section (synthetic route **A**), it was decided to change the synthetic route. As already explained, in the new synthetic route (Figure 2.2 - synthetic route **B**), the synthesis of ethynylphenoxy-Phts and the corresponding ethynylphenoxy-Pcs were studied. Then, the conversion of these compounds (ethynylphenoxy-Phts and ethynylphenoxy-Pcs) into *N*-acyl SA derivatives due to a sulfo-click reaction was evaluated. In the next section, the results and details about these conversions in the synthetic route **B,** will be discussed.

At this point it is important to emphasize that all sulfo-click reactions reported in this section were carried out using CuI as catalyst. However, in the next section it is discussed the use of other Cu(I) sources in this type of reaction.

2.2.2 Synthetic route B - from 4-(3-ethynylphenoxy)phthalonitrile

In the synthetic route **B**, 4-(3-ethynylphenoxy)phthalonitrile (**13**) was used as starting material for the synthesis of *N*-acyl SA precursors of Pcs in a sulfo-click reaction. The planned synthetic route is described in Scheme 2.7. Firstly, by a nucleophilic aromatic substitution with 4-nitrophthalonitrile and 3-ethynylphenol, 4-(3-ethynylphenoxy)phthalonitrile (**13**) was obtained. Then, as described in Scheme 2.7, two pathways can be followed: Pht **13** can be used in a statistical condensation with 4-*tert*-butylphthalonitrile to obtain Pcs with ethynyl groups; or **13** can be used in a sulfo-click reaction with a sulfonylazide to obtain *N*-acyl SA **17**. Then, the latter compound can be used in a statistical condensation with other Phts to produce the corresponding Pcs **18**–**20**. In both cases the resulting compounds will be as Pc-acyl group-SA while synthetic route **A** (section 2.2.1) leads to compounds of type Pc-SA-acyl group.

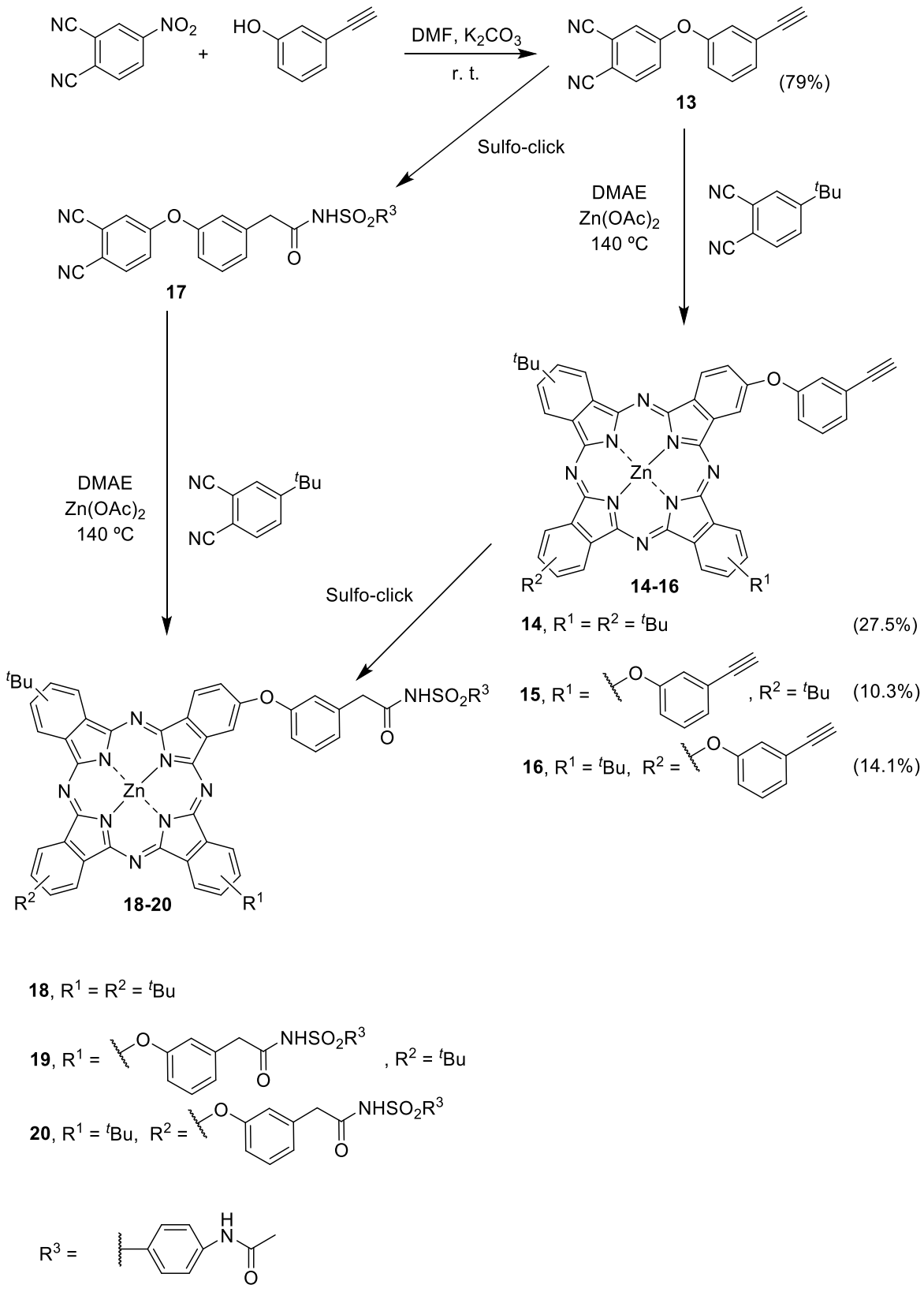

Scheme 2.7: Planned route for the synthesis of metallophthalocyanine–*N*-acyl-sulfonamide conjugates from 4-(3-ethynylphenoxy)phthalonitrile (**13**)

(synthetic route **B**).

The 4-(3-ethynylphenoxy)phthalonitrile (**13**) was obtained in 79.0% yield by a nucleophilic aromatic substitution between 4-nitrophthalonitrile and 3-ethynylphenol in DMF. The structure of the **13** was confirmed by ^{1}H NMR and MS. In the ^{1}H NMR spectrum (Figure 2.5) it is possible to observe the peak corresponding to the proton at the ethynyl group at δ 4.34 ppm. In the aromatic region, at δ 7.24–7.53 ppm the peaks of the protons in the ring bearing the ethynyl group are observed. Protons at the Pht ring appear at δ 7.86 ppm and δ 8.12 ppm. In the mass spectrum a peak at *m/z* 245.4 corresponding to the $[M+H]^{+}$ ion is observed.

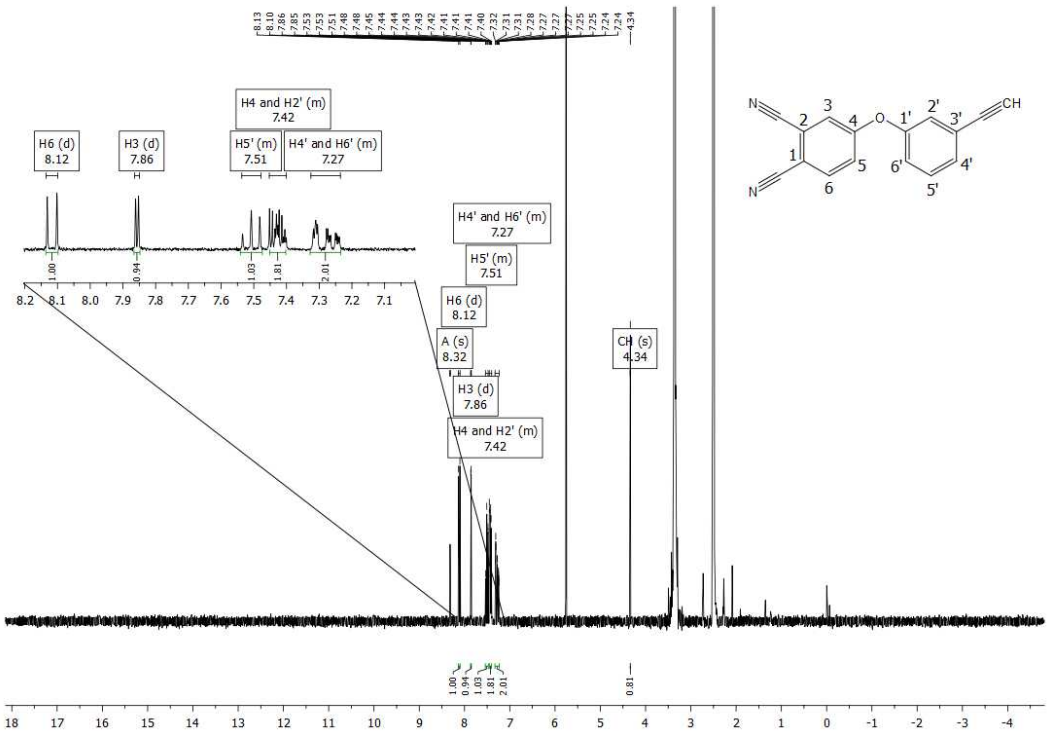

Figure 2.5: ^{1}H NMR spectrum of the 4-(3-ethynylphenoxy)phthalonitrile (**13**) in DMSO-d_6.

Pcs **14**–**16** were synthesized *via* a statistical condensation of 4-(3-ethynylphenoxy)phthalonitrile (**13**) and 4-*tert*-butylphthalonitrile in a ratio of 1:5. The statistical condensation was carried out in DMAE at 140 ºC, in the presence of zinc acetate (Scheme 2.7) obtaining three ethynylphenoxy ZnPcs (**14**–**16**) and *t*-BuZnPc. The four ZnPcs obtained were characterized by ^{1}H NMR and MS. The spectra allowed to confirm that, besides tetra(*tert*-butyl)Pc, tri(*tert*-butyl)-mono(3-ethynylphenoxy)Pc **14** and two di(*tert*-butyl)-bis(3-ethynylphenoxy)Pcs **15** and **16** were obtained (Scheme 2.7).

The ^{1}H NMR spectrum of Pc **14** illustrates all proton resonances as multiplets for the α- and β-aromatic protons of the Pc macrocycle between δ 9.30 and δ 7.93–7.37 ppm, corresponding to the 8 α-protons and 4 β-protons, respectively. Furthermore, the proton resonances of the phenoxy moiety appear in the same multiplet as the 4 β-protons. Finally, the resonance of the acetylenic proton appears at δ 4.34 as a singlet (Figure 2.6a).

Figure 2.6b illustrates, as an example, the ^{1}H NMR spectrum of Pc **16**. The protons of the Pc macrocycle appear between δ 9.31–8.80 and δ 7.80–7.44 ppm, corresponding to the 8 α-protons and 4 β-protons, respectively. At δ 7.80–7.44 ppm the resonance of the 8 protons of the phenoxy groups is also observed. The two acetylenic protons appear at δ 4.34 and 4.37 ppm as two singlets, probably due to conformational differences of the two ethynyl groups.

The photochemical and photophysical properties of Pcs **14**–**16** were also studied. Figure 2.7 shows the UV-Vis spectra of Pcs **14**–**16** in chloroform. In all studied Pcs the absorption spectrum has a broad Soret band at λ 343, 348 or 345 nm, respectively, and a Q-band at 679, 678 or 679 nm, respectively (Table 2.1). Despite the structural differences of Pcs studied, a significant difference in UV-Vis spectra is not observed. Figure 2.8 shows the fluorescence spectra of Pcs **14**–**16** upon excitation at 590 nm in chloroform. These spectra reveal maxima at 679, 677 or 674 nm, respectively, and the quantum yields found for **14** (0.04), **15** (0.07) and **16** (0.09) (Table 2.1) are higher than the quantum yield of zinc hexadecafluoroPc used as reference (0.01).[85] The emission spectra of Pcs **14**–**16** in chloroform is shown in Figure 2.8.

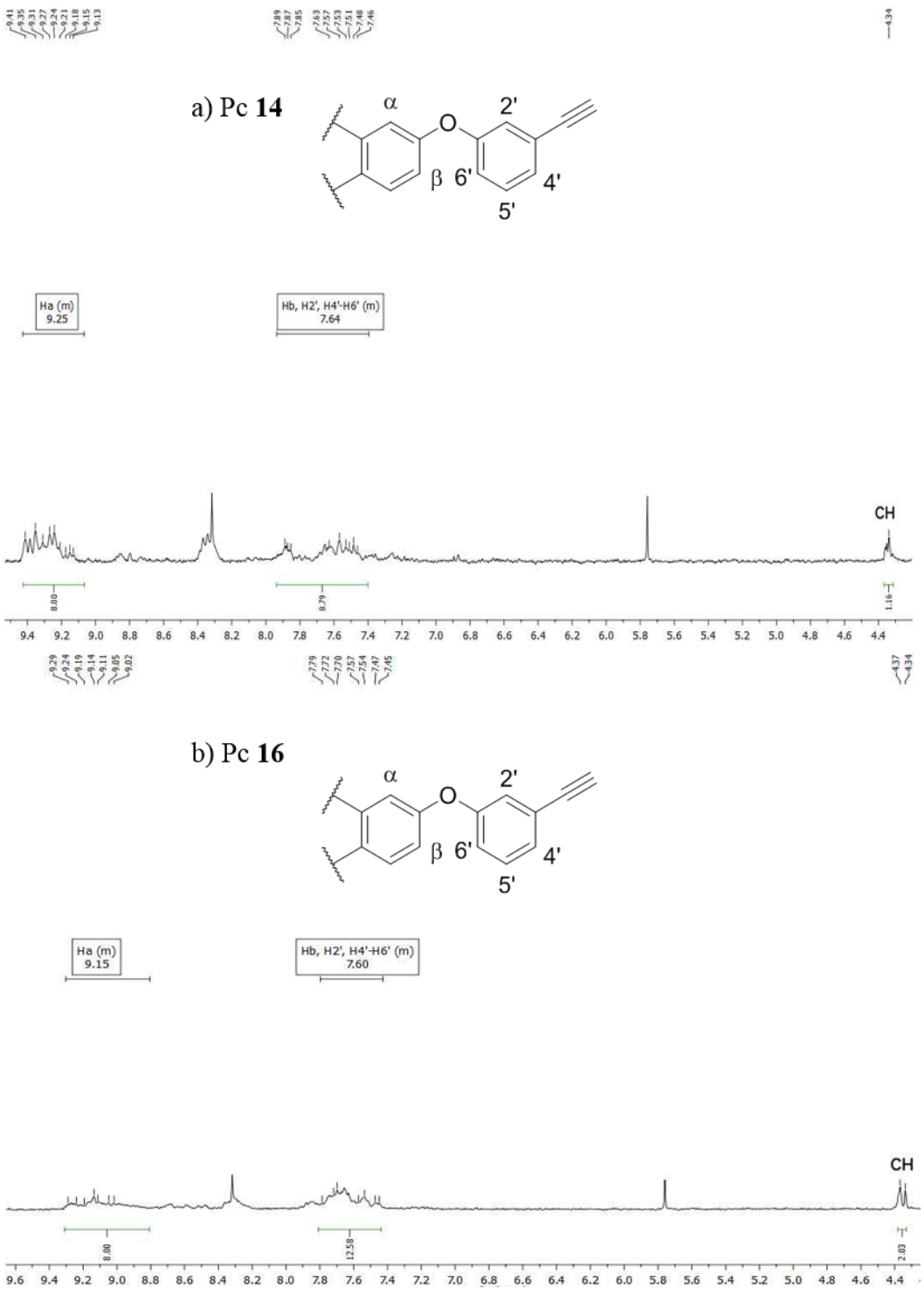

Figure 2.6: ^{1}H NMR spectra of **a)** mono-substituted Pc **14** and **b)** di-substituted Pc **16** in DMSO-d_6.

The mass spectra of the Pc derivatives show the expected molecular ions (M^{+}) at *m/z* 860.2 for Pc **14** and at *m/z* 980.2 for Pcs **15** and **16**, and thus support the proposed structures.

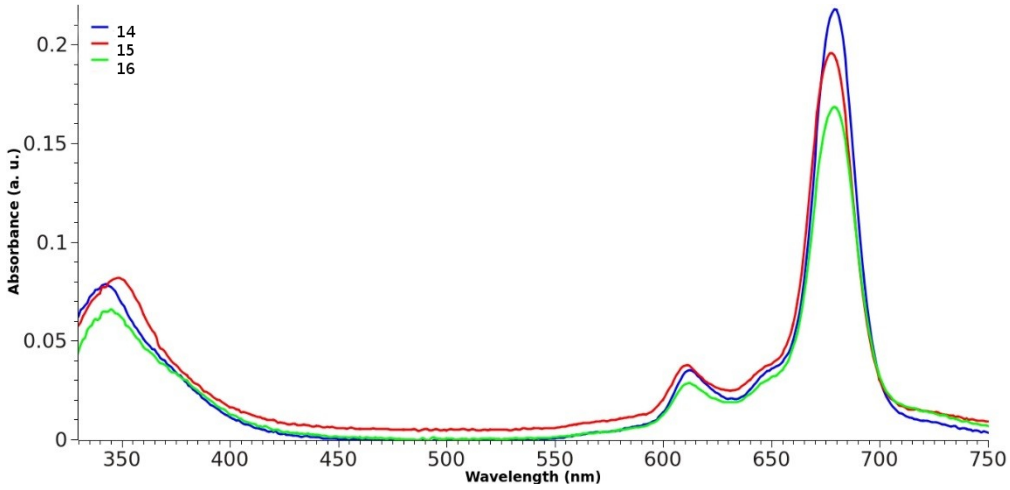

Figure 2.7: Absorption spectra of Pcs **14–16** in chloroform.

Table 2.1: Molar extinction coefficients (ε) and fluorescence quantum yields (Φ_f) for Pcs **14–16**.

Compounds	**Absorption λ_{max} (nm)**	**ε_1 ($M^{-1}cm^{-1}$)**	**ε_2 ($M^{-1}cm^{-1}$)**	**Φ_f (a.u.)**
14	343/679	1.2×10^5	4.5×10^6	0.04
15	348/678	1.2×10^5	5.1×10^6	0.07
16	345/679	1.5×10^5	5.9×10^6	0.09

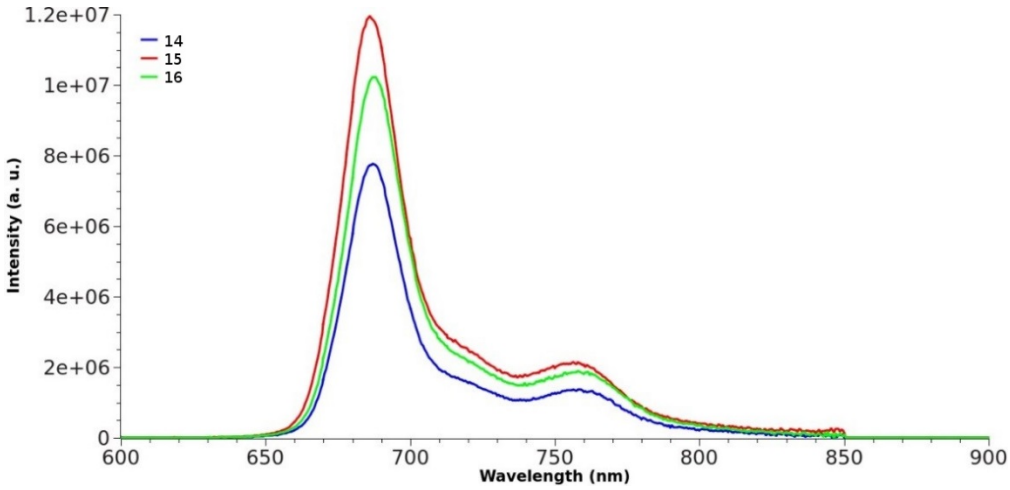

Figure 2.8: Emission spectra of Pcs **14–16** in chloroform. Excitation wavelength: 590 nm.

Then, we studied the possibility of obtaining tetrakis(3-ethynylphenoxy)Pc **21** *via* cyclotetramerization of Pht **13** in DMAE at 140 ºC in the presence of $Zn(OAc)_2$ (Scheme 2.8). With these reaction conditions the expected modification in the color of the reaction mixture from light yellow to blue-green was not observed, indicating that the Pc **21** was not formed.

Drawing our attention to recent sulfo-click reactions[67–69] in which sulfonyl azides react with terminal alkynes in the presence of catalytic amounts of copper(I), a base and water, we proceeded with the study aiming at the synthesis of Pht–*N*-acyl-SA conjugates and Pc–*N*-acyl-SA conjugates.

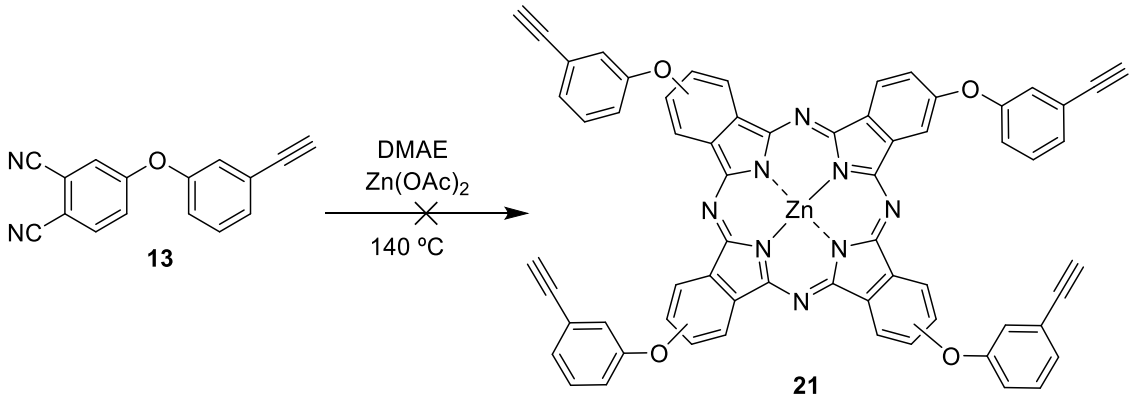

Scheme 2.8: Synthesis of tetra-2-(3-ethynylphenoxy)phthalocyanine **21**.

To this end, the reaction of 4-(3-acetylenephenoxy)phthalonitrile (**13**) with 4-acetamidobenzenesulfonyl azide (a commercial compound) was carried out in the presence of catalytic amounts of CuI and triethylamine, in water at room temperature (Scheme 2.9 - pink), following the conditions described by Cho *et al.*[68,69] From this reaction resulted a variety of products from which it was possible to isolate two pure compounds. However, their ^{1}H NMR spectra do not correspond to the desired structure. In order to verify if the products obtained result, or not, from the reaction of the sulfonyl azide with the cyano groups of the Pht, we also carried out the reaction of mono-2-(3-acetylenephenoxy)Pc with the commercial sulfonyl azide. Again several products were formed but, unfortunately, we were unable to obtain the desired Pc–*N*-acyl-SA conjugates.

In order to better understand the sulfo-click reaction we carried out the reaction of phenylacetylene with 4-acetamidobenzenesulfonyl azide under the same conditions used previously, using CuI as catalyst (Scheme 2.9 - blue), but in the presence of

sodium ascorbate and tris[(1-benzyl-1*H*-1,2,3-triazol-4-yl)methyl]amine (TBAB), and in various solvents. From all these reactions, different compounds were isolated but their structures did not correspond to the desired compounds and, in the majority of the cases, in very low yields. Thus, we concluded that the reaction conditions for these transformations would not be the most appropriate.

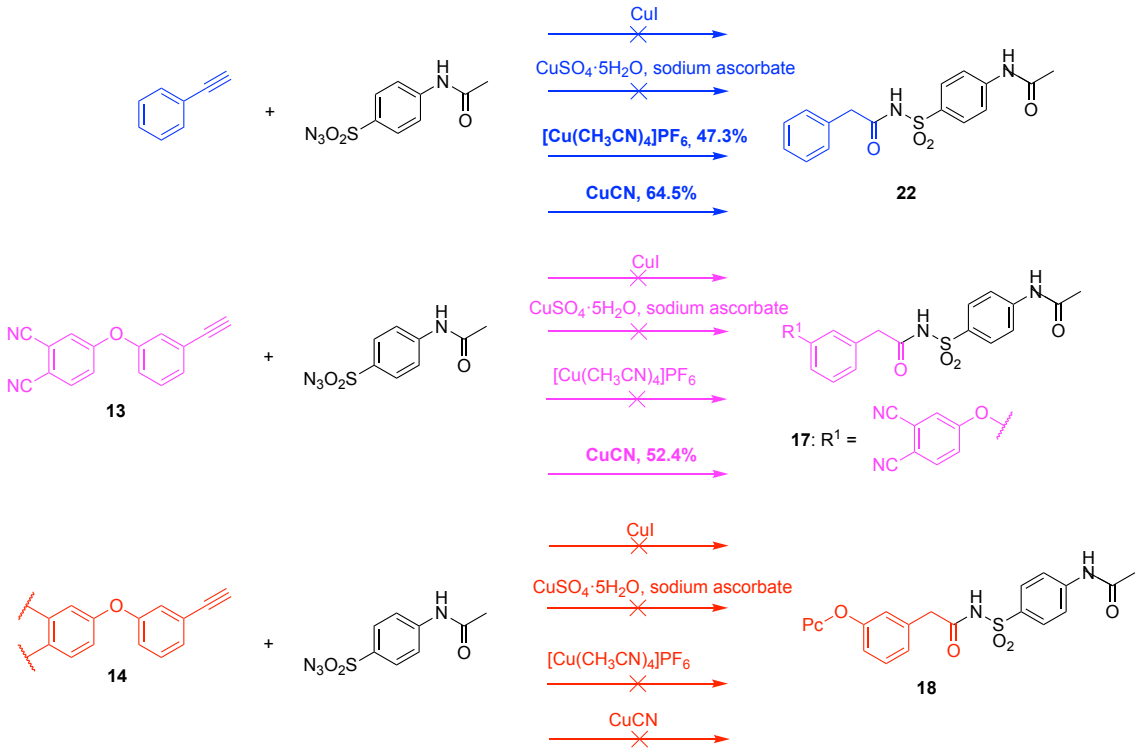

Scheme 2.9: Evaluation of different Cu(I) sources for the synthesis of *N*-acyl sulfonamide derivatives.

With these results, we decided to explore different reaction conditions and, in particular, to study the use of different Cu(I) sources.

Diverse copper(I) sources, such as CuI, CuBr, $[Cu(CH_3CN)_4]PF_6$, and $CuSO_4$/ascorbate, are reported as suitable catalysts for sulfo-click reactions. The pH value has also been described as having a pronounced effect on the outcome of these reactions: mildly basic conditions favor the conversion into *N*-acyl SAs.[67,68,86] With this in mind, we proceeded to study different catalysts and reaction conditions in order to obtain the desired *N*-acyl SAs. For that, an exploratory work was conducted using 4-acetamidobenzenesulfonyl azide and phenylacetylene as reagents and following the experimental conditions reported by Cassidy *et al.*,[67] equimolar quantities of the two reagents were stirred in tetrahydrofuran (THF)/H_2O (4:1) in the presence of

$CuSO_4 \cdot 5H_2O$ (2 mol%) and sodium ascorbate (0.1 equiv.). After 34 hours the reaction was ended but the desired *N*-acyl SA was not formed.

Following Govindaranju *et al.*[86] conditions, phenylacetylene was reacted with 4-acetamidobenzenesulfonyl azide in equimolar quantities in the presence of 2 mol% of $Cu(CH_3CN)_4PF_6$, 2 mol% of the tertiary amine TBTA, 4 mol% sodium ascorbate and 1 equiv. $NaHCO_3$ in aqueous conditions. The desired derivative was obtained in 47.3% yield. The best result was attained when CuCN was used as catalyst, as disclosed by Cho *et al.*[87] In this experiment copper(I) cyanide and 4-acetamidobenzenesulfonyl azide were poured in a boiling flask and then distilled water and ethynylbenzene were added. Finally, triethylamine was slowly added *via* syringe over one minute, at room temperature, and the reaction was then stirred while open to air for 4 hours at room temperature. From the reaction mixture a white solid was obtained in 64.5% yield. The structure of **22** was confirmed by its ^{1}H NMR spectrum, and the results are in agreement with those described in the literature.[87]

The procedure developed by Cho *et al.*[90] using CuCN as catalyst turned out to be very promising. We used these conditions to study the synthesis of *N*-acyl Pht–SAs and the results were very interesting. For that, 4-(3-ethynylphenoxy)phthalonitrile was used as starting material in a sulfo-click reaction using CuCN as catalyst. The procedure used was similar to the one described for **22** and the expected Pht **17** was obtained in 52.4% yield (Scheme 2.9 - pink). The structure was confirmed by ^{1}H NMR and MS. In the ^{1}H NMR spectrum (Figure 2.9) the peaks corresponding to methyl and methylene protons are observed, respectively, at δ 2.09 and 3.60 ppm. The signal corresponding to H4 appears at δ 6.69 ppm as a broad singlet due to the presence of H5 and H7 at *meta* distances. Protons H5 and H7 appear at δ 7.03-7.12 ppm as a multiplet. The signal of H2 appears at δ 7.32 ppm as a double doublet with coupling constants of $J = 2.5$ and 8.8 due to the presence of H1 and H3 in the vicinity. At δ 7.40 ppm appears H6 as a triplet, and a multiplet is observed at δ 7.72–7.85 ppm corresponding to H1, H8 and H9 (integrating to 5 protons). Finally, proton H3 appears at δ 8.09 ppm as a doublet. At δ 10.39 and 12.24 appear the NH groups.

Having Pht **17** in hand, we tried to convert it into Pc–*N*-acyl-SA conjugates. In that way, we attempted a statistical condensation of **17** and *t*-butylphthalonitrile in the presence of $Zn(OAc)_2$ and using DMAE as solvent at 140 ºC (Scheme 2.7). However, again, only the tetra(*t*-butyl)Pc was formed. Since Pht **17** was not recovered, the absence

of the expected Pc–*N*-acyl-SA conjugate seems to indicate that this Pht probably decomposes at the temperature required for the condensation reaction (140 ºC).

Considering the good results obtained in the sulfo-click reactions using CuCN as catalyst, as confirmed with the synthesis of compounds **17** and **22**, we decided to apply these experimental conditions to the synthesis of Pc **18** (Scheme 2.9 - red). In fact, we carried out the reaction of Pc **14** with 4-acetamidobenzenesulfonyl azide, using CuCN as catalyst. A blue-green product was isolated and its structure was studied by ^{1}H NMR and MS. In the ^{1}H NMR spectrum, it was not possible to identify, without any doubt, the peaks corresponding to the methyl and methylene groups. That is, the results from the ^{1}H NMR were inconclusive. Moreover, in MS analysis the ion or adduct corresponding to the desired compound was not found, leading us to conclude that we were not in the presence of the desired Pc.

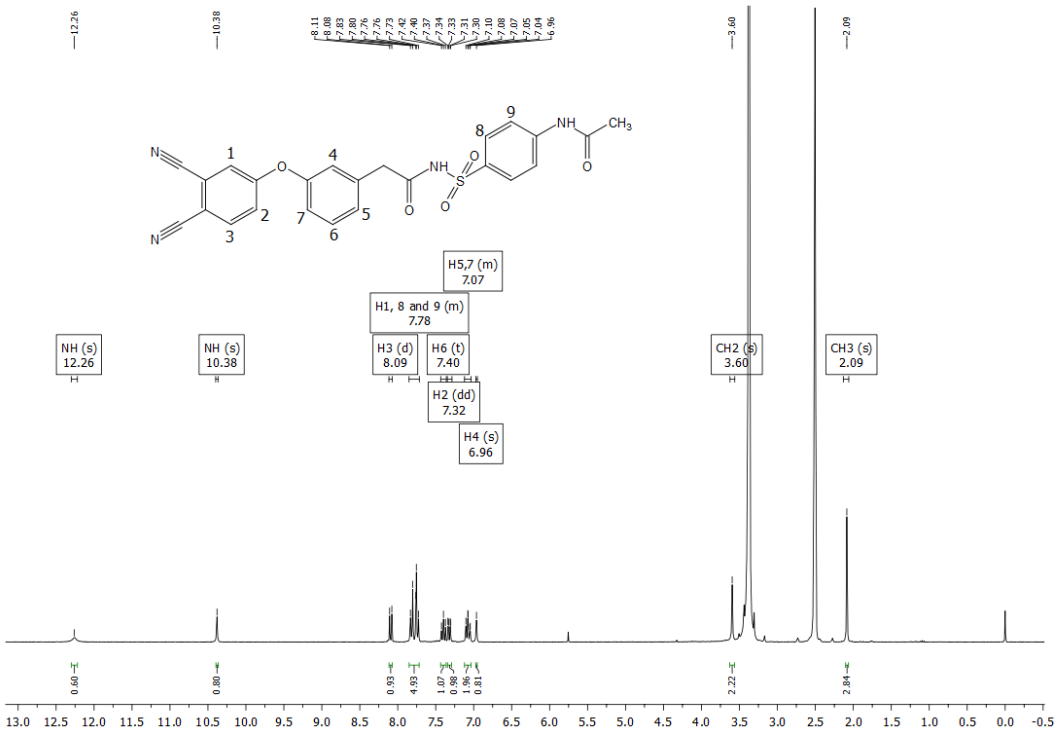

Figure 2.9: ^{1}H NMR spectrum of **17** in DMSO-d_6.

2.3 Conclusions

Taking into account the work published on sulfo-click reactions,[67–70] we were interested to verify if this type of reaction could be used to prepare Pc–*N*-acyl-SA conjugates. In order to elucidate this question, two complementary synthetic routes were drawn. Route **A** involved the synthesis of SA-Phts and their conversion into Pcs while

route **B** involved the synthesis of Pcs bearing ethynyl groups and their reaction with sulfonyl azides. Although the disappointing results, route **B** allowed to better understand the scope and limitations of the chlorosulfonation and sulfo-click reactions when used in the transformation of Phts and Pcs.

In the synthetic route **B**, we were able to synthetize, for the first time, a new Pht–*N*-acyl-SA conjugate (**17**) and also new Pcs with acetylene groups. 3-Ethynylphenoxy-Pht **13** and zinc-ethynylphenoxy-Pcs **14**–**16** bearing one or two 3-ethynylphenoxy groups and their photophysical properties, namely absorption and fluorescence spectroscopy were also studied. The structural analysis of these compounds by mass spectrometry and NMR spectroscopy was also reported. Besides, a new methodology for the synthesis of new ethynylphenoxy-Pcs was proposed and the applicability of sulfo-click reaction in Phts was demonstrated. The scope of sulfo-click reaction, in particular for Phts, was likewise disclosed.

The new Pcs **14**–**16** are versatile substrates for further structural modifications. Particularly, in a collaboration with Professor Óscar Rodrigues, from the Federal University of Santa Maria, Rio Grande do Sul - Brazil, the coupling of azidothymidine (AZT) derivatives to zinc-ethynylphenoxy-Pcs **14**–**16** is under study. AZT is a well-known antiretroviral used to prevent and treat HIV/acquired immune deficiency syndrome (AIDS) and, along with its derivatives, is also studied as an antioxidant and antitumoral drug.[88] Therefore, these new Pcs would be suitable to be studied as new PSs in the inactivation of virus and cancer cells. This is an ongoing work.

The differences between the results obtained by Eliana *et al.*[61,62] and those described in this work can be related to structural differences among mono and disubstituted Phts. In the next chapter, new synthetic approaches to overcome this limitation will be discussed.

Chapter 3 Synthesis of phthalocyanine–sulfonamide conjugates

Substitutions in the periphery of macrocycles such as Pcs with other organic groups are a commonly strategy to fine-tune the properties of these compounds for a specific application in materials or pharmaceutical sciences. In particular, in this work the aim is to synthesize Pcs to be used as potential PDT and PDI agents.

SAs stand out as an interesting class of compounds with a wide range of applications in medicine. Moreover, SAs are still a first-line approach in the treatment of several infection diseases. Still, SA resistance is well-known and the synthesis of new SAs needs to be addressed.

In this work, the synthesis of new Pc–SA conjugates was disclosed as a continuation of the work developed by Carvalho *et al.*[62] For that, new synthetic approaches to obtain SAs and new methods to afford Pc–SA conjugates were studied and are described in this chapter.

3.1 Introduction

SAs are organic basis compounds containing a group $-SO_2NR^1R^2$ used for different therapeutic purposes.[4,74,89,90] SAs with inhibitory capacity of CA have been used to disrupt the growth of tumor cells in hypoxic conditions and acidification.[73] Additionally, Owa *et al.*[90] synthesized SAs capable of regulating cell cycle at the G1 phase through inhibition of cyclin-dependent kinase (CDK). Furthermore, the antimicrobial effect of SAs is carried out as competitive antagonists of *p*-aminobenzoic acid (*p*ABA), which is a substrate of the enzyme DHPS, in the biosynthesis of folic acid. Antimicrobial SAs exhibit a broad spectrum of action, covering all groups of organisms which operate in the biosynthesis of folic acid.[4] These antimicrobials were first introduced in the 1930s and were widely used on the treatment of several infections initiated by a number of pathogenic microorganisms, including *Neisseria meningitidis* and *Pneumocystis carinii.*

Currently this class of synthetic antibiotics is still a first-line therapeutic option in human and veterinary medicine. They are commonly applied in the treatment of malaria (*Plasmodium falciparum*), toxoplasmosis (*Toxoplasma gondii*), eye infections initiated by *Staphylococcus aureus* and *Candida albicans*, urinary tract infections by

Escherichia coli, lymphogranuloma venereum by *Chlamydia trachomatis*, pulmonary infections caused by *Nocardia* and autoimmune borne diseases such as rheumatic fever, infections affected by *Streptococcus pyogenes*.[4,74,89,90]

3.1.1 Historical background

SA was the first antimicrobial drug and was responsible for the antibiotic revolution in medicine. The first commercially available antimicrobial SA was sold by the trademark Prontosil™. This prodrug was developed in 1932 by Josef Klarer and Fritz Mietzsch at the Bayer Laboratories of the IG Farben conglomerate in Germany but only several years later the physician Gerhard Domagk found the exact compound that had remarkable effects on stopping some bacterial infections in mice. Prontosil™ turned out to be a strong protective agent against infections caused by streptococci, including blood infections, childbed fever, and erysipelas, and a lesser effect on infections caused by other *cocci*.[91]

For several years in the late 1930s, the production of sulfa products was increased until the elixir sulfanilamide disaster in the fall of 1937. During this year at least 100 people were poisoned with diethylene glycol by improperly prepared sulfanilamide. In 1937 the S. E. Massengill Company, a pharmaceutical manufacturer, created a preparation of sulfanilamide using diethylene glycol as a solvent. Diethylene glycol is poisonous to humans but company's chief pharmacist and chemist was not aware of it. Since SA was the only effective antibiotic available in the years before penicillin, it continued to be used at the early years of World War II.[92,93]

Thousands of molecules with SA backbone have been created with improved formulations, greater effectiveness and less toxicity. SAs are still widely used not only as antibiotics but also, for example, as antitumor and antidiabetic agents.

3.1.2 Synthesis of sulfonamides

The oldest and most commonly used method to obtain SAs involves the synthesis of a chlorosulfonated derivative by chlorosulfonation with chlorosulfonic acid.[94,95]

The chlorosulfonic acid is a versatile reagent which is extensively used for the sulfonation or chlorosulfonation of aromatic compounds.[95] Depending on the number of equivalents (equiv.) of acid used, the products obtained may be sulfonic acids, sulfones

or sulfonyl chlorides. Generally, for the sulfonation only one molar equivalent is necessary. This type of reaction is usually conducted in an inert solvent, for example chloroform, to avoid the formation of byproducts. However, if chlorosulfonation is desired, it is necessary to use a large excess of chlorosulfonic acid over the other reagent. This reaction can be carried out in the absence or presence of an inert solvent. The optimization of reaction conditions depends on the nature of the aromatic substrate which is sulfonated or chlorosulfonated (Schemes 3.1).

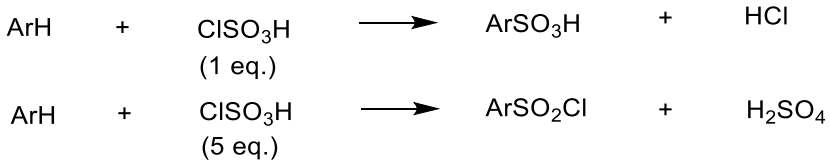

Scheme 3.1: Sulfonation and chlorosulfonation of aromatic compounds with chlorosulfonic acid.

There are few mechanistic evidences on this type of reaction. However, thermodynamic studies have shown that reactions with aromatic substrates using an equimolar amount of chlorosulfonic acid, quickly forms its sulfonated derivatives with release of hydrochloric acid. In the presence of excess reagent, sulfonated derivatives are slowly converted to the sulfonyl chloride with release of sulfuric acid. The formation of the intermediate sulfonic acid and sulfonyl chloride, under mild conditions (low temperature) using an excess of chlorosulfonic acid as solvent, may possibly be represented as shown in the Scheme 3.2.

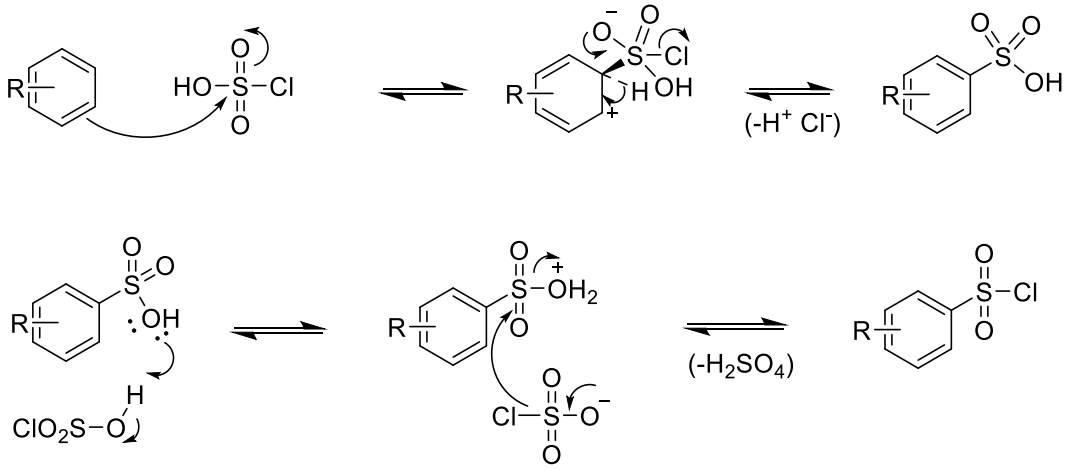

Scheme 3.2: Mechanism of the chlorosulfonation.

Over the last years, additional ways to get the sulfonyl chloride were developed. Chlorosulfonic acid may be used "alone" or in conjugation with thionyl chloride, phosphorous pentachloride (PCl_5),[96] or with phosphoryl chloride ($POCl_3$).[97] It is also possible to obtain the sulfonyl chloride by the oxidation of thiols with KNO_3-SO_2Cl_2 (2.5 equiv.) (Scheme 3.3).[98]

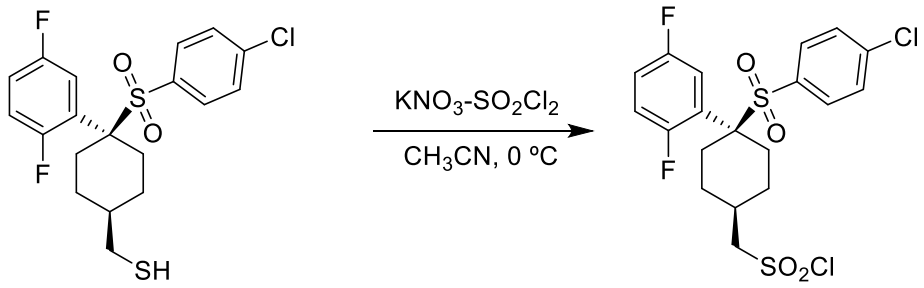

Scheme 3.3: Oxidation of thiols to sulfonyl chlorides.

In 2003[84] Blotny reported a new method for the preparation of sulfonyl chlorides that involved the treatment of a sulfonic acid or a sodium sulfonate with TCT (cyanuric chloride) in refluxing acetone under neutral conditions (Et_3N or 18-crown-6, respectively) (Scheme 3.4).

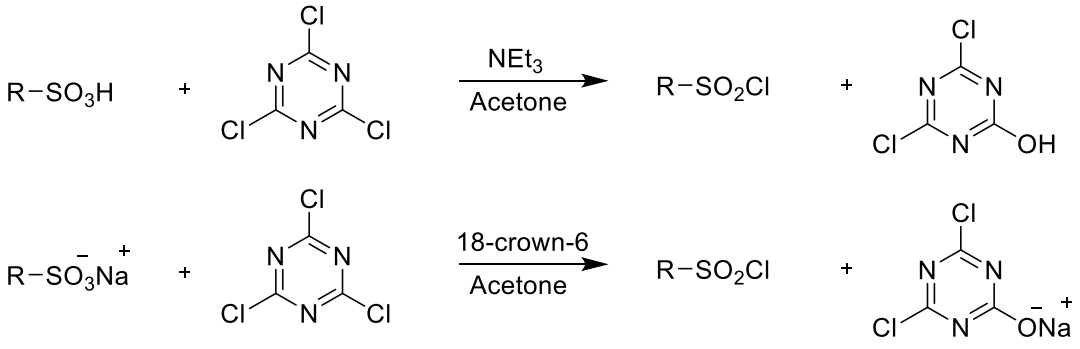

Scheme 3.4: Synthesis of sulfonyl chlorides using cyanuric chloride as chlorinating agent.

During the last years, new strategies for the synthesis of SAs have been developed. SAs are really important as building blocks of pharmaceutical and bioactive compounds. Nowadays, as already mentioned, SAs can be obtained by the conventional reaction of sulfonyl chlorides with NH_3 or amines, but can also be got by modification of the SA group, namely by catalytic cross coupling of SAs with organic halides[99–104] arylsulfinates,[105] alkyl halides and thiourea,[106,107] or alcohols.[108] Additionally, they can

be prepared by aminosulfonation of hydrocarbons,[109,110] or even by oxidation of sulfenamides,[111] diazonium salts,[112] Grignard reagents,[113] sulfinates and amines[102,114] and sulfonylazides.[115–117] They can also be obtained by transformation of heterocyclic compounds,[118,119] modification of other SAs by *N*-alkylation/arylation[99,102–104,108,120–127] and by modification at carbon atoms.[128–131] Herein, some recent examples will be described.

Concerning the utilization of thiols as precursors for SAs synthesis, in 2010 Taniguchi,[132] by a dehydrocoupling of aryl thiols with amines using copper as catalyst, produced sulfenamides and SAs. Using the system CuI-bpy (10 mol %) as a catalyst under an oxygen atmosphere in DMSO, at 60 ºC, Taniguchi was able to obtain SAs (Scheme 3.5). The substrate scope of this reaction was studied in different aryl thiols and amines. The best result was obtained when thiophenol and $^{t}BuNH_2$ were used, and by the formation of *N*-(*tert*-butyl)benzenesulfonylsulfonamide in 90% yield with trace amounts of the respective sulfenamide and sulfinamide. Additionally, using aryl thiols and amines as reagents, Huang *et al.*[133] reported the synthesis of SAs using cinnamic acid, Cu(II) as oxidant, under air condition, providing a novel and direct strategy *via* an oxygen-activated radical process. However, further studies on the mechanism must be taken in future work.

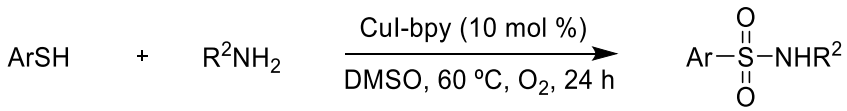

Scheme 3.5: Synthesis of sulfonamides from thiols.

Also using copper as catalyst Tang *et al.*[114] developed a method for the construction of SAs in a copper-catalyzed oxidative coupling between sodium sulfinates and amines with 1 atm O_2 or DMSO as the oxidant by *in situ* conversion of Cu(I) to Cu(II). This method proved to be efficient and robust for the synthesis of functional SAs in good yields and chemoselectivity. The reaction is carried out using $CuBr_2$ as catalyst in DMSO (Scheme 3.6). Using various amines and sodium sulfinates, under these reaction conditions, the desired SAs were obtained in good yields (61–97%). Furthermore, mono-*N*-heteroaryl SAs have been synthetized using CuI as catalyst.[102]

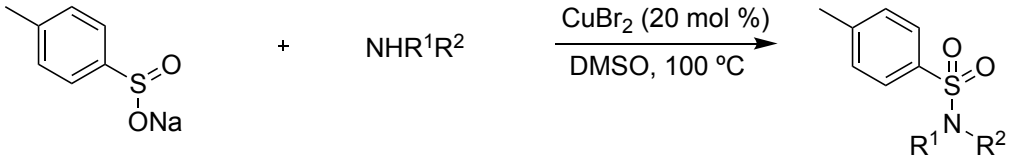

Scheme 3.6: Synthesis of sulfonamides from amines and sodium sulfinates.

In an interesting work from 2003, Burton *et al.*[124] developed an efficient microwave-promoted palladium-catalyzed coupling of aryl-chlorides with SAs. After conditions optimization for the SA coupling, the best results were obtained using $Pd_2(dba)_3$ as catalyst, and an aminophosphine ligand, in basic conditions in 1,4-dioxane (Scheme 3.7).[125] In a similar work, in order to reduce reaction temperatures and catalyst loadings was developed a Pd-catalyzed cross-coupling of methaneSA with aryl bromides and chlorides. After ligand screening, the best reaction conditions were $[Pd(Allyl)Cl]_2$, ligand *t*-BuXPhos, in basic condition, using 2-MeTHF as solvent. Also using microwave heating, in a copper(I) catalyzed system, *N*-arylation of SAs with aryl halides, in basic conditions, have been performed.[103]

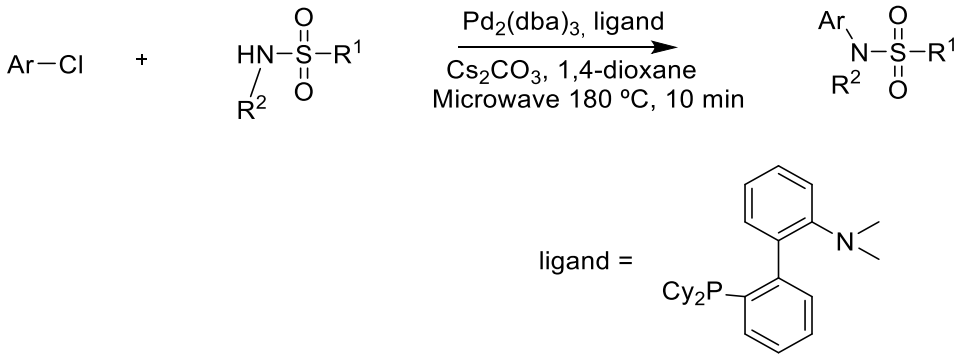

Scheme 3.7: Palladium catalyzed *N*-arylation of sulfonamides with aryl chlorides.

3.2 Results and discussion

In this section, the results of the synthesis of Pc–SA conjugates are described. For that, the synthesis of Pht–SA conjugates is firstly addressed. So, in subsection 3.2.1 is described the work developed for the synthesis of Pht–SA conjugates, from sulfonyl chlorides and from other sulfo sources. It is also addressed the synthesis of Phts with cationizable groups. Next, in subsection 3.2.2, the results obtained in the synthesis of neutral and cationic Pcs from the precursors previously obtained are discussed.

3.2.1 Synthesis of the precursors of phthalocyanine–sulfonamide conjugates

The synthetic route to achieve the desired precursors is shown in Scheme 3.8. 4-Nitrophthalonitrile and 2,4-dichlorophthalonitrile are converted to compounds **1** and **23**, respectively, *via* a nucleophilic aromatic substitution with an excess of phenol at room temperature. Phenoxy-Phts **1** and **23** were obtained in good yields as described in the literature.[61,62,77–82,134] Then, Phts **25**, **28** and **29** were synthesized as described in a previous work[61,62] and **9**, **26** and **27** were obtained by modification of the same procedure that will be described in more detail in this section.

4-Phenoxyphthalonitrile (**1**) has already been mentioned as starting material in chapter 2. For the synthesis of 4-(4-chlorosulfonylphenoxy)phthalonitrile (**2**) different synthetic strategies were tested. As described in chapter 2, we tried the chlorosulfonation with five equiv. of chlorosulfonic acid at room temperature and by using other chlorinating agents, such as TCT, but without success. In this chapter, we describe the successful conversion of 4-phenoxyphthalonitrile (**1**) into the corresponding chlorosulfonyl derivative **2**. For that, a combination of chlorosulfonic acid and thionyl chloride was used.[135] 4-Phenoxyphthalonitrile was slowly added to 5 equiv. of chlorosulfonic acid cooled in an ice bath. The addition is slow so that the temperature of the reaction mixture did not increase. The reaction mixture was stirred for 15 minutes at a temperature between 0 ºC and 5 ºC and then the temperature was allowed to rise to room temperature for more 15 minutes. After 30 minutes, thionyl chloride (2 equiv.) was added and the reaction was left for more 30 minutes at room temperature. After this time, the reaction mixture was slowly poured onto ice and the solid formed was filtered and washed with cold water. The compound was dried under vacuum at room temperature and used in the next reaction without further purification. In the following reaction the white powder obtained was dissolved in acetonitrile and the solution was cooled to 0 °C. Diethylamine was added slowly to the reaction mixture. The reaction mixture was then stirred at room temperature for 2 hours and poured into water ice. The resulting precipitate was filtered and washed with cold water. After recrystallization in CH_2Cl_2/Hexane and drying under vacuum at 60 ºC, a white powder was obtained in 78.0% yield. The structure of the desired Pht–SA conjugate **9** was confirmed by ^{1}H NMR, ^{13}C NMR and MS.

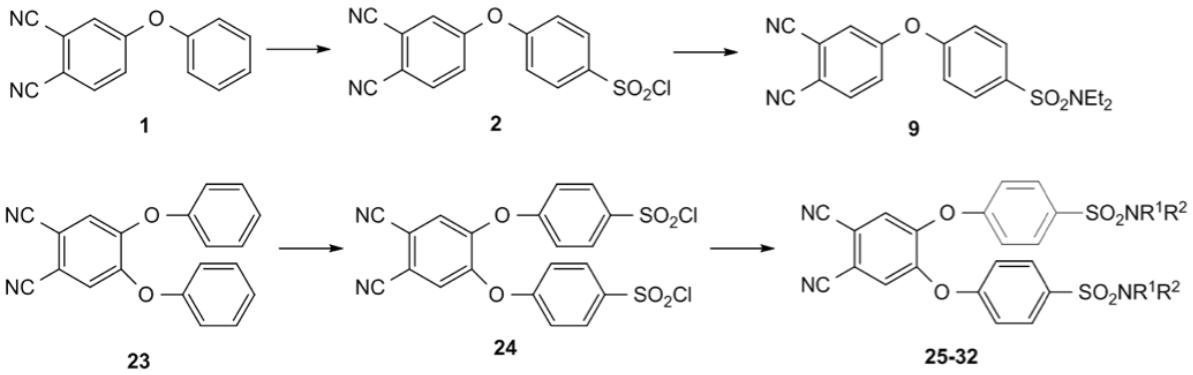

Compound	NR^1R^2
25	NEt_2
26	NH-*i*-Pr
27	NH-thiazol-2-yl
28	NH-4-$MeOC_6H_4$
29	NH-dodecyl
30	N-(*i*-$Pr)_2$
31	NH-1,2,4-triazol-3-yl
32	NH-$CH_2C_6H_4$-4-SO_2NH_2

Scheme 3.8: Systematization of the synthetic route used to obtain precursors from sulfonyl chlorides.

In ^{1}H NMR spectrum (Figure 3.1), the signals corresponding to the methyl and methylene groups are observed at δ 1.18 and 3.29 ppm. In the aromatic region the resonances of the protons 8 and 9 appear as multiplets at δ 7.18 and 7.91 ppm, respectively Finally, the signals of protons H3, H5 and H6 emerged as a combined system in which H6 appear at δ 7.38 ppm as a doublet (J = 8.7), H5 at δ 7.31 ppm as a double doublet (J = 2.4 and 8.7) and H3 at δ 7.80 ppm as a doublet (J = 2.4). The ^{13}C NMR spectrum (Figure 3.2) shows the carbons of the methyl and methylene groups at δ 14.26 and 42.19 ppm, respectively. Between δ 110.35 and 138.09 ppm are observed the peaks corresponding to the aromatic carbons, in wich at δ 114.65 and 115.04 ppm are emerged the resonances of the nitrile groups. At the ESI-MS spectrum was observed a peak at *m/z* 355.3 corresponding to the molecular ion (M^{+}).

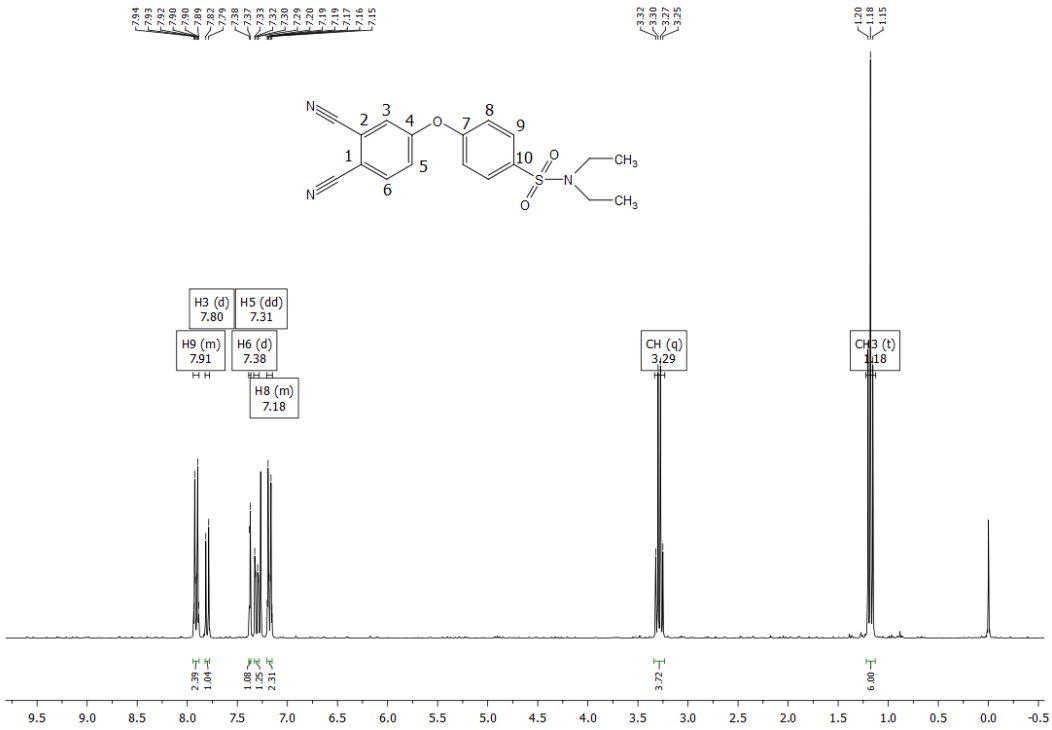

Figure 3.1: ^{1}H NMR spectrum of 4-(4-(diethylaminosulfonyl)phenoxy)phthalonitrile (**9**) in $CDCl_3$.

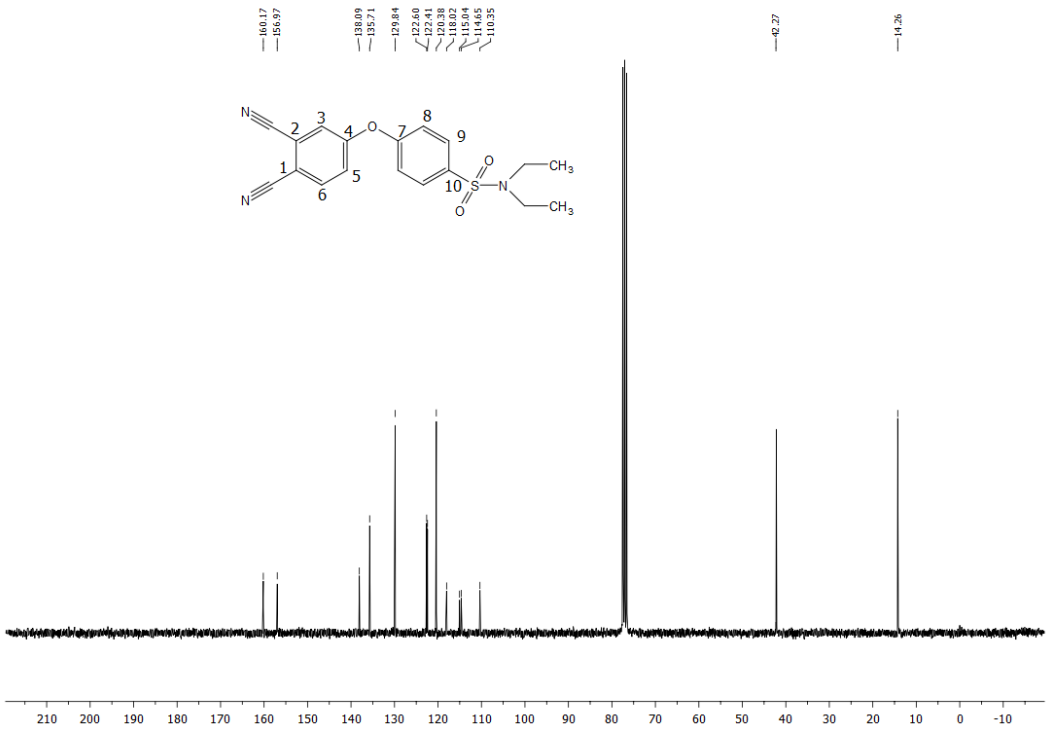

Figure 3.2: ^{13}C NMR spectrum of 4-(4-(diethylaminosulfonyl)phenoxy)phthalonitrile (**9**) in $CDCl_3$.

Then we proceeded with the synthesis of SA derivatives **26** and **27**. 4,5-Bis(isopropylaminosulfonylphenoxy)phthalonitrile (**26**) was obtained in similar conditions for compound **9**. In a boiling flask, with 4,5-bis(4-chlorosulfonylphenoxy)phthalonitrile **24**, 6 equiv. of isopropylamine were slowly added in acetone. The reaction mixture was stired for 1 hour under nitrogen atmosphere. Then, the reaction was quenched with cold water and the resulting precipitate was filtrated. After recrystallization in CH_2Cl_2/hexane a white powder was obtained in 23.0% yield.

Figure 3.3 shows the ^1H NMR spectrum of Pht **26** recorded in $CDCl_3$. The resonances of the methyl and methine groups of the isopropyl group appear as a doublet and a multiplet at δ 1.12 and 3.45-3.58 ppm respectively. The multiplets at δ 7.05 and 7.92 ppm are attributed to the resonances of protons 7 and 6, respectively. A singlet due to protons 3 is observed at δ 7.44 ppm. The ^{13}C NMR spectrum (Figure 3.4) shows two peaks in the aliphatic region corresponding to the carbon atoms of the methyl and methine groups (δ 23.89 and 46.34 ppm). At the aromatic region is present the carbons from the three aromatic rings (δ 112.77–138.45 ppm) and the carbons of the nitrile

groups emerged at δ 114.23 ppm. At ESI-MS spectrum was observed a peak at *m/z* 554.6 (M^+).

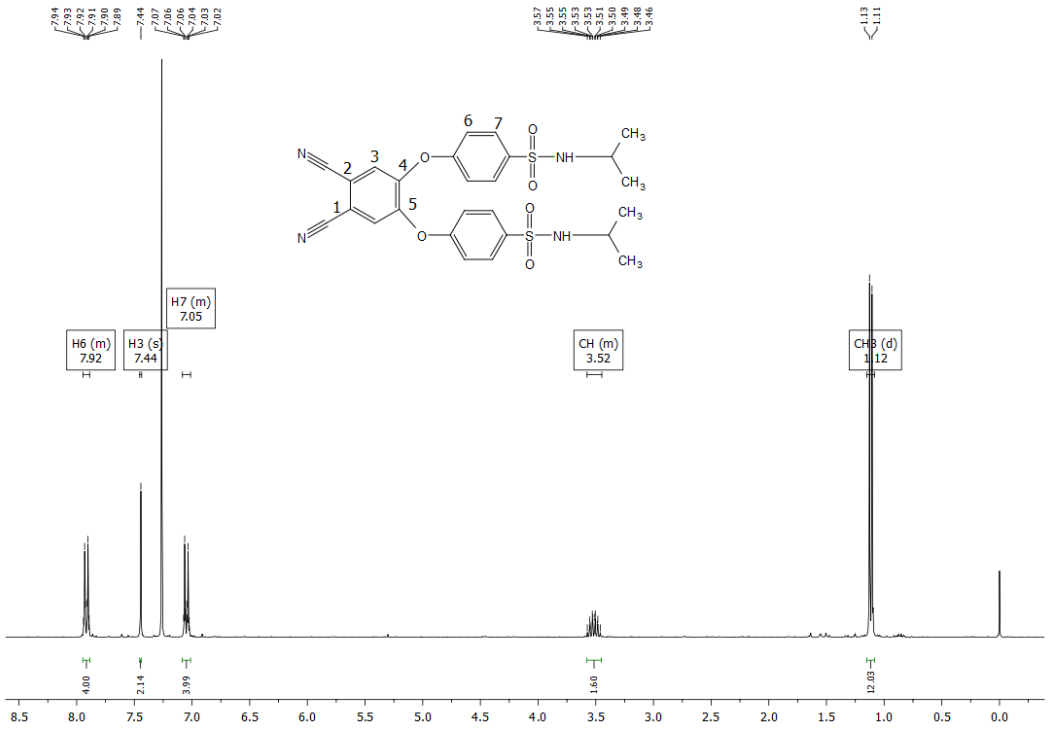

Figure 3.3: ^{1}H NMR spectrum of 4,5-bis(4-isopropylaminosulfonylphenoxy) phthalonitrile (**26**) in $CDCl_3$.

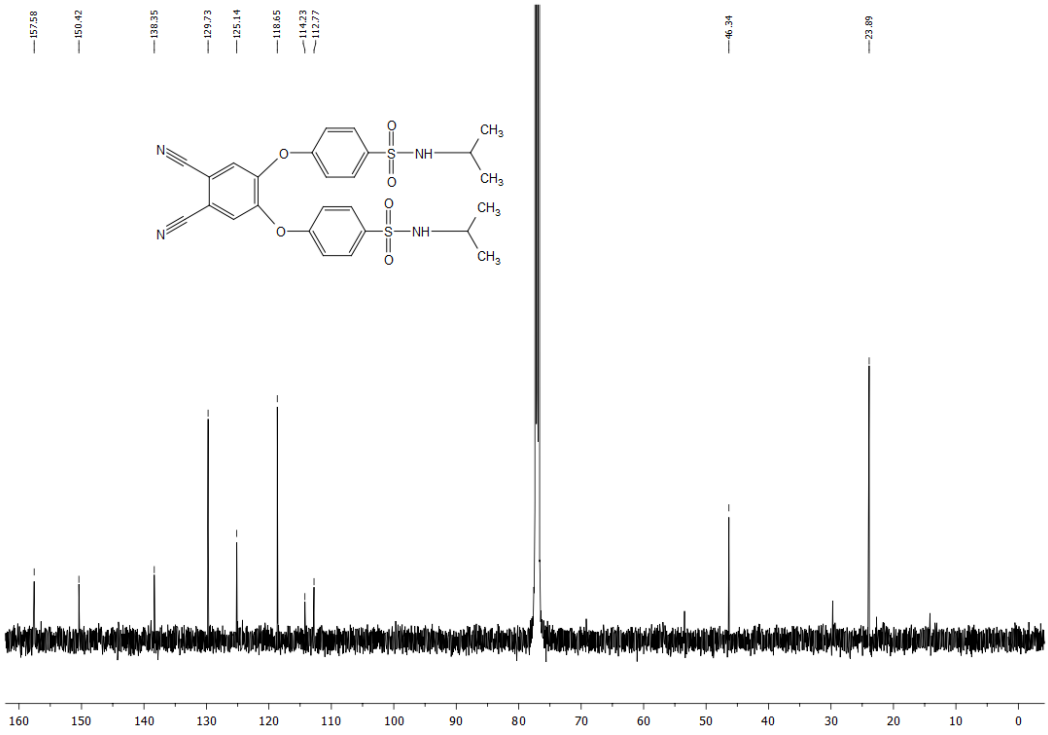

Figure 3.4. ^{13}C NMR spectrum of 4,5-bis(4-(isopropylaminosulfonyl)phenoxy) phthalonitrile (**26**) in $CDCl_3$.

For SA derivative **27** the synthesis procedure was slightly different since 2-aminothiazole is a solid. 4,5-Bis(4-chlorosulfonylphenoxy)phthalonitrile **24** reacted with 2-aminothiazole in acetonitrile in the presence of slowly added 4 eq. of triethylamine. After 2.5 hours at room temperature, under nitrogen atmosphere, water was added and the desired compound was extracted with dichloromethane and washed with water. The desired product was purified by chromatography over a silica gel column using a mixture of CH_2Cl_2/hexane (3:1) and crystallization from CH_2Cl_2/hexane. Compound **27** was obtained in 16.2% yield.

The ^1H NMR spectrum (Figure 3.5) shows two doublets δ 7.07 and 7.75 ppm corresponding to protons 10 and 11, respectively, from the thiazolyl group. Protons 6 and 7 from the phenyl ring emerged at δ 7.35 and 7.56 ppm, and protons 3 appear at δ 8.39 ppm as a singlet. The ESI-MS spectrum shows a peak at *m/z* 637.7 corresponding to the $[M+H]^+$ ion.

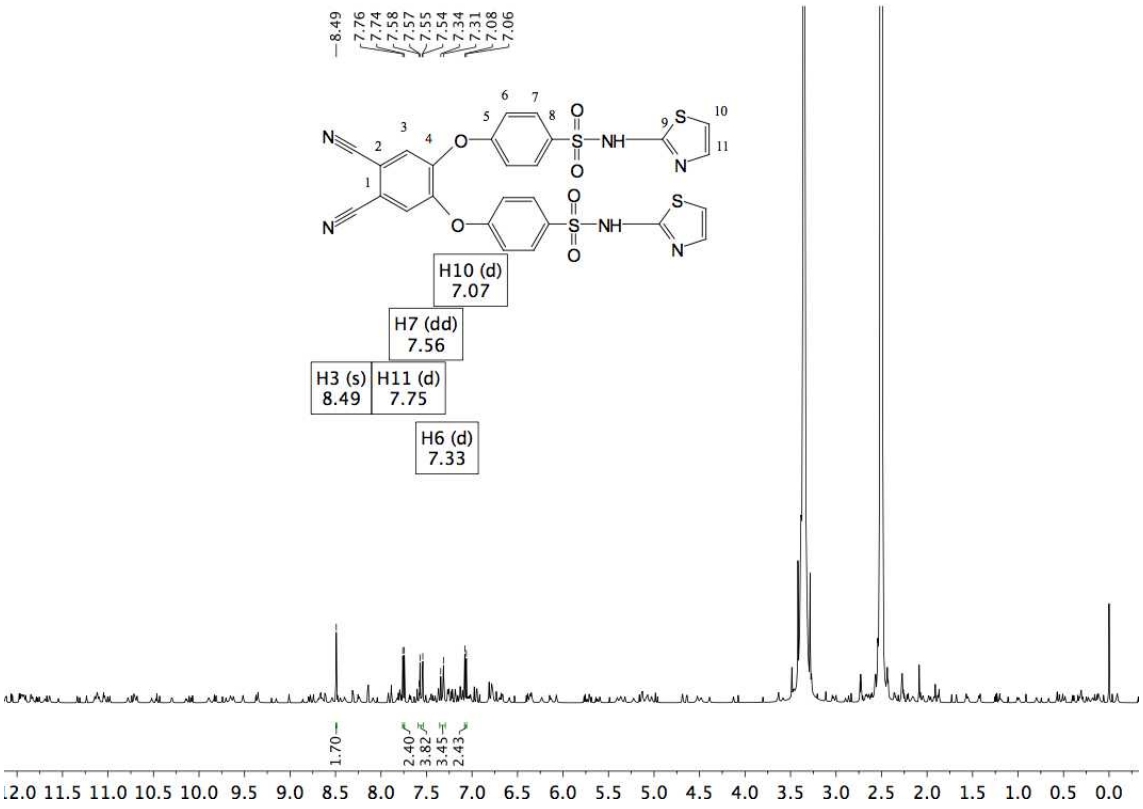

Figure 3.5: ^{1}H NMR spectrum of 4,5-bis(4-(thiazol-2-ylaminosulfonylphenoxy) phthalonitrile (**27**) in DMSO-d_6.

In addition, we also study the reaction of 4,5-bis(4-chlorosulfonylphenoxy)phthalonitrile **24** with diisopropylamine, 3-amino-1,2,4-triazole and 4-(aminomethyl)benzenesulfonamide in order to obtain Pht–SA conjugate **30**, **31** and **32**, respectively. Unfortunately, the reactions were not sucessful, probably due to low solubility of these amines in these reaction conditions or due to steric effects.

Following the procedure of Trujillo *et al.*,[136] in which 2,4-disubstituted oxazole sulfonyl chlorides are obtained by the treatment with *N*-chlorosuccinimide (NCS) in AcOH-H_2O in good yield, we studied the extension of this reaction to Phts. For that 4-(benzylthio)phthalonitrile (**33**) was obtained *via* a nucleophilic aromatic substitution with 4-nitrophthalonitrile and phenylmethanethiol at room temperature in DMF and in the presence of cesium carbonate (Scheme 3.9). The solid obtained was dried at room temperature in a desiccator. The desired Pht **33** was obtained at 86.1% yield. The ^{1}H NMR spectrum (Figure 3.6) shows the diagnostic signal of the methylene group at δ 4.25 ppm. In the aromatic region emerge a multiplet at δ 7.37–7.32 ppm corresponding to the protons of the benzyl group (H2'-H7'). Finally, at δ 7.35-7.61 it is observed the

characteristic signals of a 4-substituted Pht. The structure of the desired compound was also confirmed by ESI-MS in which it is observed a peak at *m/z* 251.1 corresponding to the $[M+H]^+$ ion.

Then, we attempted to convert compound **33** into the sulfonyl chloride **34** using NCS in AcOH-H_2O. The reaction mixture was cooled with an ice-water bath and after 10 minutes NCS (4 eq.) was slowly added in three portions. After stirring for 15 min at 0 ºC and 2 h at room temperature the reaction was stopped. After the workup and separation by column chromatography the white powder obtained was characterized by ^{1}H NMR. In the ^{1}H NMR spectrum of the isolated compound it is possible to verify the absence of signals corresponding to the benzyl group (data not shown), confirming that this group was cleaved. Finally, in order to confirm if we were in the presence of the expected sulfonyl chloride, the white powder was reacted with diethylamine (5 equiv.) in acetonitrile at room temperature. After 4 hours we were not able to observe any product in TLC so we decided to increase the temperature, firstly to 50 ºC and then to 90 ºC. No SA could be obtained from this reaction. With these results we may conclude that the reaction with NCS did not afford the sulfonyl chloride **34**.

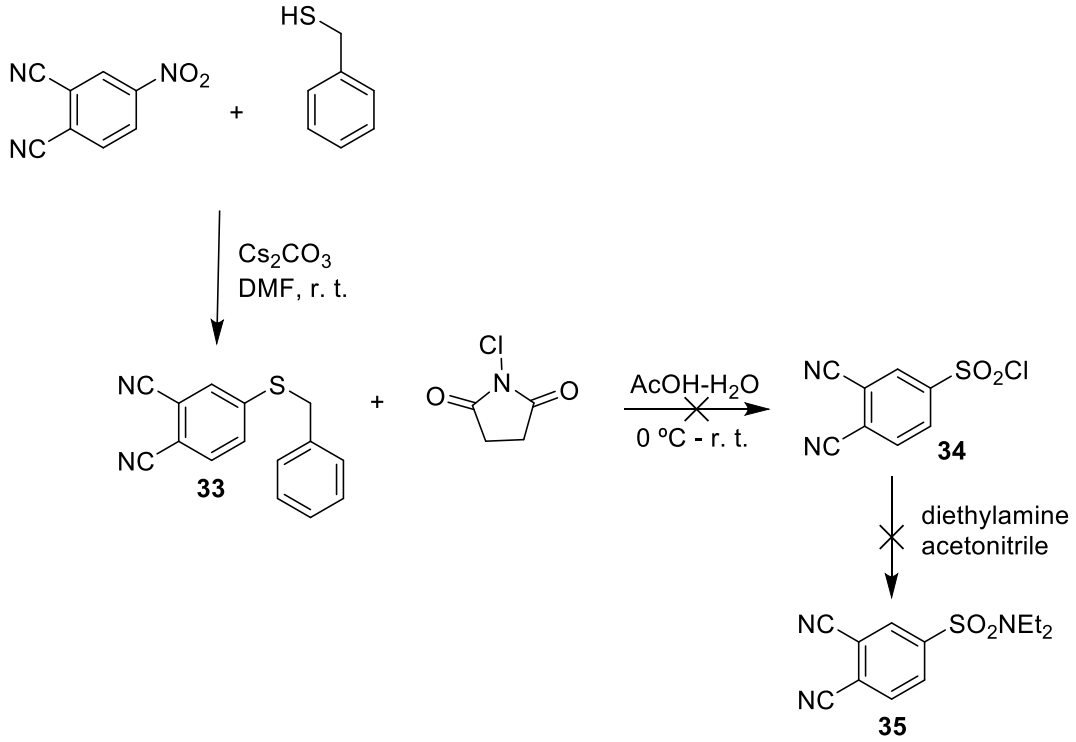

Scheme 3.9: Planned synthetic route for the synthesis of 4-(diethylaminosulfonyl) phthalonitrile (**35**).

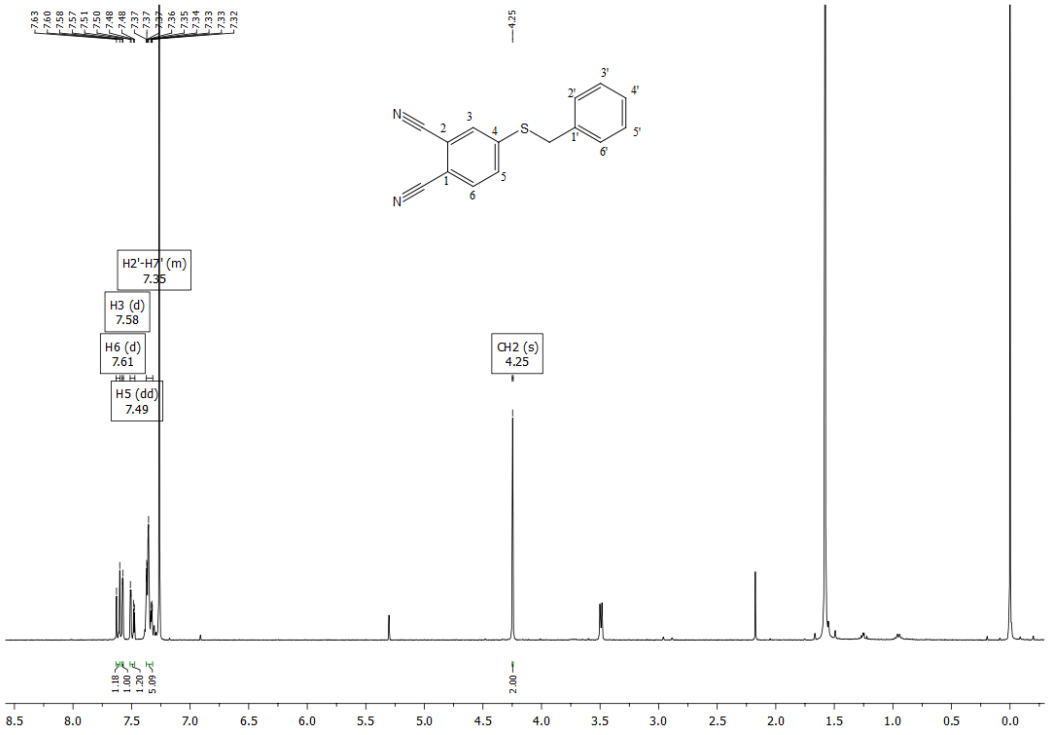

Figure 3.6: ^{1}H NMR spectrum of 4-(benzylsulfanyl)phthalonitrile (**33**) in $CDCl_3$.

Using TCT as chlorinating agent, disulfonate Pht **36** was tried to be converted into the sulfonyl chloride **24** by microwave irradiation in quick experiment. For that, compound **36** and TCT were dissolved in acetone in the presence of 2 equiv. of triethylamine and reacted in microwave at 50 W. After 20 minutes the reaction was ended with cold water. The isolated compound was the starting disulfonate Pht **36** and not to the desired sulfonyl chloride **24**, indicating that this synthetic strategy was not successful in this transformation.

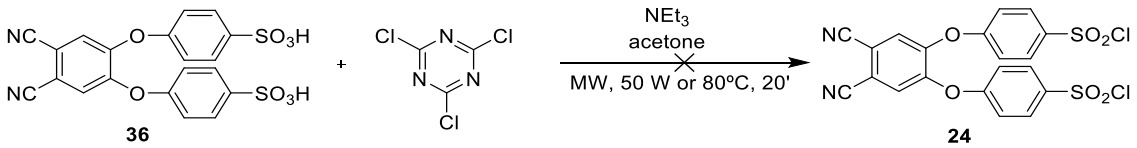

Scheme 3.10: Chlorination of disulfonate phthalonitrile **36** with TCT.

In parallel, other strategies for the synthesis of SAs, that do not use sulfonyl chlorides as intermediates, were evaluated. It was reported by Bahrami *et al.*.[137] that SAs may be synthetized in a mild and efficient way by the direct conversion of thiols into SAs in the presence of $H_2O_2/ZrCl_4$ in acetonitrile at room temperature In order to evaluate the applicability of this reaction in our compounds, in a first approach, we used simple reagents like thiophenol with *p*-toluidine (Scheme 3.11) in order to obtain *N*-(*p*-

tolyl)benzenesulfonamide **37**. We obtained SA **37** in 98.6% yield, which is in line with what is described in the literature.[137–140] ^{1}H NMR and MS spectra confirmed the structure of compound **37**. This strategy was then extended to the synthesis of a new Pht–SA conjugate, using 4-aminophthalonitrile and thiophenol but the desired compound was not obtained probably due to the presence of the cyano groups that may reduce the reactivity of the amino group.

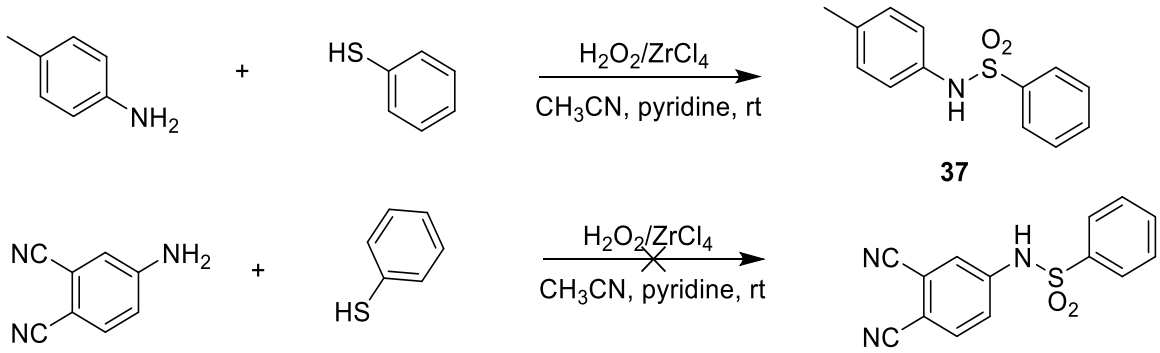

Scheme 3.11: Synthesis of *N*-(*p*-tolyl)benzenesulfonamide (**37**) and extension of the synthetic conditions to the synthesis of a new phthalonitrile–sulfonamide conjugate.

In order to obtain Pcs with SA and cationic groups, due to the cationization of Phts with amine groups, a study around the best synthetical strategy to obtain free amine groups substituted Phts, which could be cationization, was conducted. For that, we started by studying the possibility of obtaining 4,5-bis(2-(dimethylamino)etoxi)phthalonitrile (**38**) *via* a nucleophilic aromatic substitution between the commercial 4,5-dichlorophthalonitrile and 2-(dimethylamino)etanol (DMAE) in DMF, from room temperature to 90 ºC (Scheme 3.12). Various experimental condition and temperatures were tested. In lower temperatures there was no reaction and at higher temperatures it was observed a formation of green byproducts that were very difficult to separate from other colorless compounds that were obtained in very low yields. This strategy to obtain cationic Pcs *via* dimethylaminoethoxy di-substituted precursors proved not to be the most practical and straight way for this goal.

In the literature it is possible to find some work about the synthesis of Phts and Pcs with 2-(dimethylamino)ethoxy and 2-(dimethylamino)ethylsulfanyl groups.[141–147] However, in those articles the focus was on the synthesis of mono-substituted 2-(dimethylamino)ethoxy and not on the di-substituted Pht. Contrariwise, in the case of dimethylaminoethylsulfanyl substituted precursors the mono- and also di-substituted

precursors were already synthetized. To give an example, 2-(dimethylamino)ethylsulfanyl mono- and di-substituted Phts and respective Ti(IV) Pcs in the neutral and cationized form were reported by Arslanoglu *et al.*.[146] In other work, the same group[147] also describes the synthesis of 4-(2-dimethylaminoethoxy)phthalonitrile and the corresponding tetra-substituted neutral and cationic Ti(IV) Pcs.

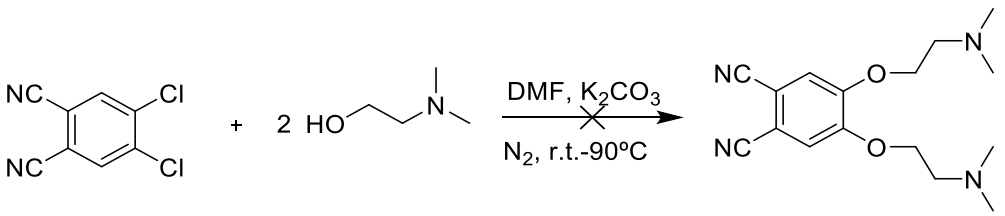

38

Scheme 3.12: Synthetic approach to obtain 4,5-bis(2-(dimethylamino)etoxy) phthalonitrile (**38**).

The strategy that proved to be viable was the utilization of Phts with pyridyl groups. Following the procedure described by Pereira *et al.*[148] we obtained 4-pyridylsulfanylphthalonitrile (**39**) and 4,5-di(4-pyridylsulfanyl)phthalonitrile (**40**) in 76.2% and 53.5% yield, respectively. These pyridyl-Phts will be used in the next section as starting materials in a statistical condensation to obtain cationizable Pc-SA conjugates.

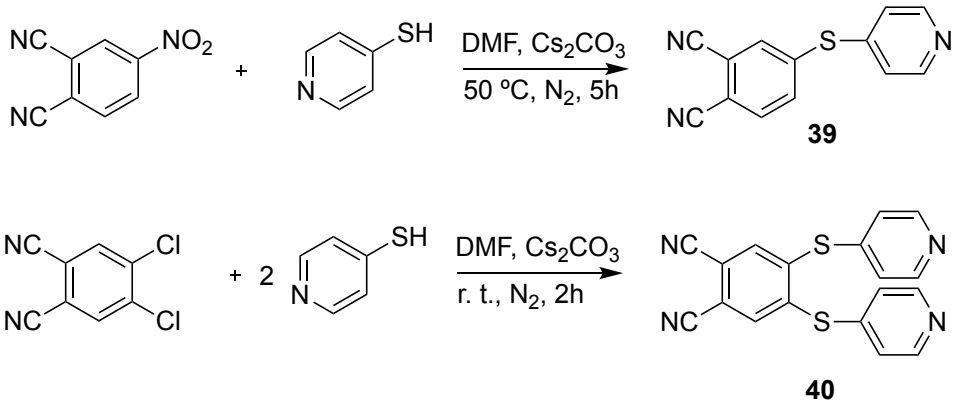

Scheme 3.13: Synthesis of 4-pyridylsulfanylphthanitrile (**39**) and 4,5-di(4-pyridylsulfanyl)phthalonitrile (**40**).

3.2.2 Synthesis of the phthalocyanine–sulfonamide conjugates

Pcs **Mg41**, **41**, **Zn41**, **Zn44** and **Zn45** were synthesized as described in previous works from our group.[61,62] Pcs **Mg42**, **Mg43**, **Mg44**, **Mg46, Mg47**, **42**–**45**, **Zn42**, **Zn43** and **Zn46** will be described here in more detail. These Pcs were obtained following the same protocol used by Carvalho *et al*.[62] Pcs **Mg42**, **Mg43** and **Mg46** were prepared by cyclotetramerization of the corresponding Phts in the presence of magnesium pentoxide. First, magnesium turnings were added to pentan-1-ol and the suspension was heated to 150 °C with reflux. After the formation of the alkoxide (overnight), octan-1-ol was added to the suspension, followed by the respective Phts **26**, **27** and **9**. Then, the reaction mixture was stirred at 160 °C overnight. After cooling to room temperature, the mixture was added to a 5:1 methanol/water mixture and the resulting Pcs **Mg42**, **Mg43** and **Mg46** were isolated by filtration. These Pcs were then converted into the respective metal-free and ZnPcs (**Zn42**, **Zn43** and **Zn46**) as described in the literature.[62] The formation of the metal-free and Zn derivatives was confirmed by UV-Vis. UV-Vis absorption spectroscopic properties of Pcs **42**, **43**, **46**, **Zn42**, **Zn43** and **Zn46** will be discussed in chapters 4 and 5.

Pcs **Mg42**, **Mg43** and **Mg46** were characterized by ^{1}H NMR and MS. Apart from the α and β protons of the Pc macrocycle, in ^{1}H NMR spectrum of **Mg42** (Figure 3.7) it is also observed the peaks corresponding to the methyl and methyne groups at δ 1.11 and 3.46 ppm, respectively, and at δ 7.02 and 7.87 ppm the peaks corresponding to the H1 and H2, respectively. As the ^{1}H NMR spectrum of

Mg43 is concerned, the characteristic peaks of thiazolyl group emerge at δ 6.98 ppm as a multiplet overlapped with the protons of the Pc macrocycle. Furthermore, the peaks at δ 7.47 and 7.71 ppm corresponding to the H1 and H2, respectively. Finally, the ^{1}H NMR spectrum of **Mg46** show unequivocally the signals corresponding to the protons of the methyl and methylene groups at δ 1.16 and 3.26 ppm, respectively, and the peaks corresponding to the H1 and H2 (δ 7.81 ppm) as a multiplet overlapped with the α protons of the Pc macrocycle. At δ7.15 ppm emerge the peak corresponding to the β protons of the Pc macrocycle. The structure of Pcs **Mg42**, **Mg43** and **Mg46** were also confirmed by MALDI-MS at positive mode in the presence of 2,5-dihydroxybenzoic acid (DHB) matrix.

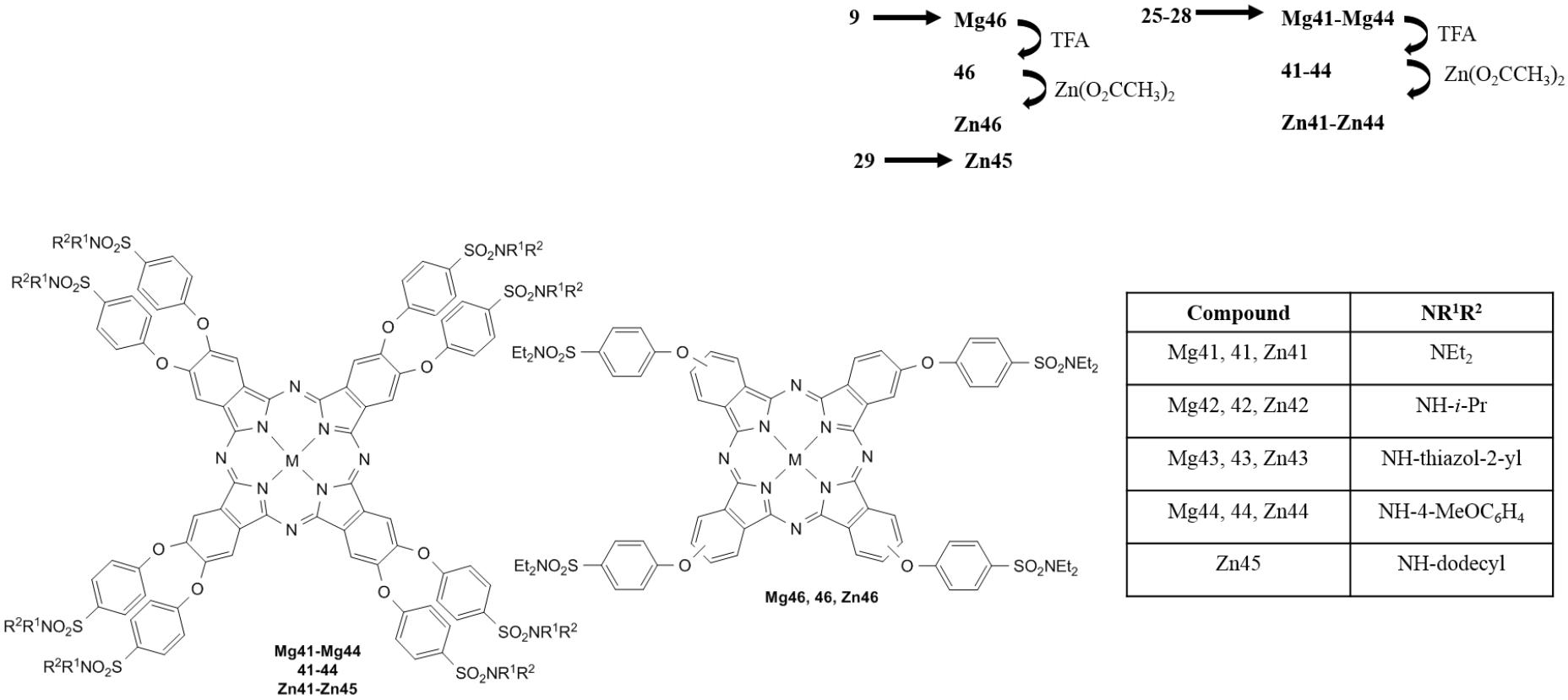

Compound	NR^1R^2
Mg41, 41, Zn41	NEt_2
Mg42, 42, Zn42	NH-*i*-Pr
Mg43, 43, Zn43	NH-thiazol-2-yl
Mg44, 44, Zn44	NH-4-$MeOC_6H_4$
Zn45	NH-dodecyl

Scheme 3.14: Systematization of the synthetic route used to phthalocyanine–sulfonamide conjugates.

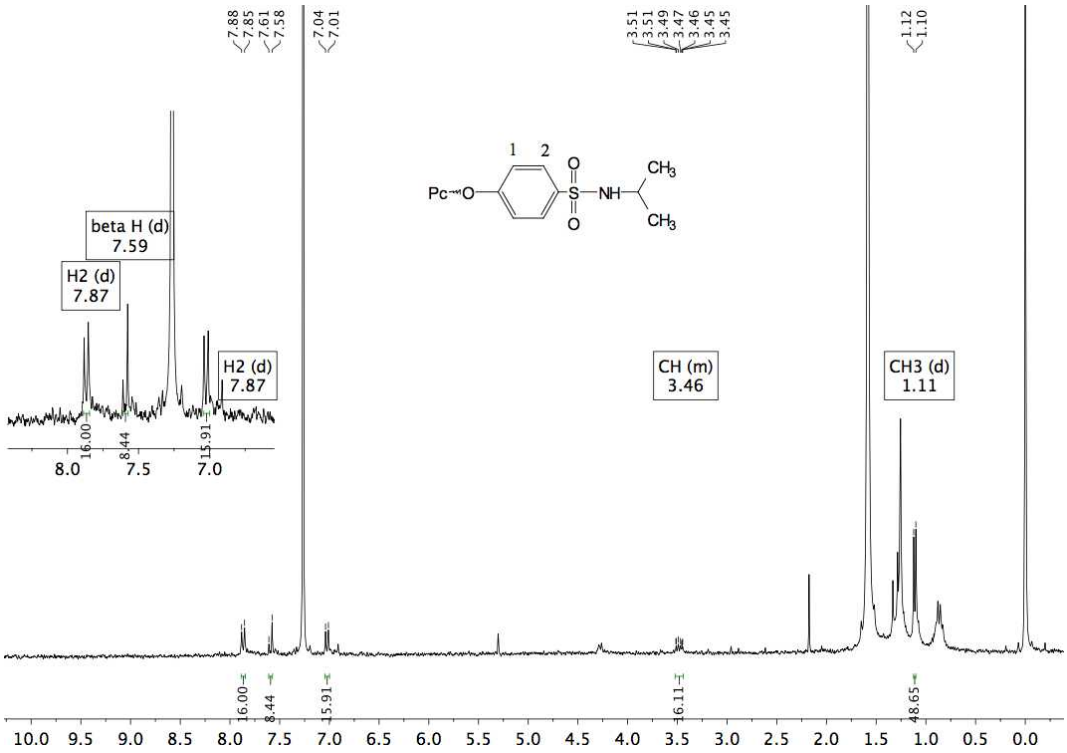

Figure 3.7: ^{1}H NMR spectrum of {2,3,9,10,16,17,23,24-[octakis(4-isopropylaminosulfonyl)phenoxy]phthalocyaninato}magnesium(II) (**Mg42**) in $CDCl_3$.

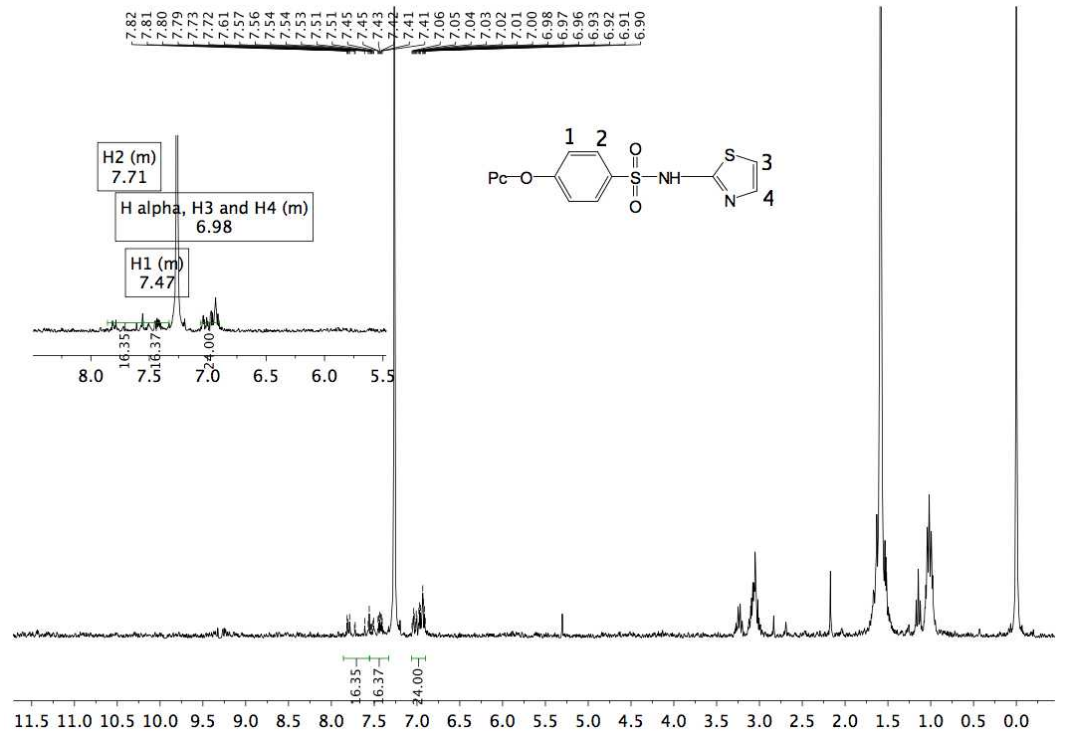

Figure 3.8: ^{1}H NMR spectrum of {2,3,9,10,16,17,23,24-[octakis(4- (thiazol-2-ylaminosulfonyl)phenoxy]phthalocyaninato}magnesium(II) (**Mg43**) in $CDCl_3$.

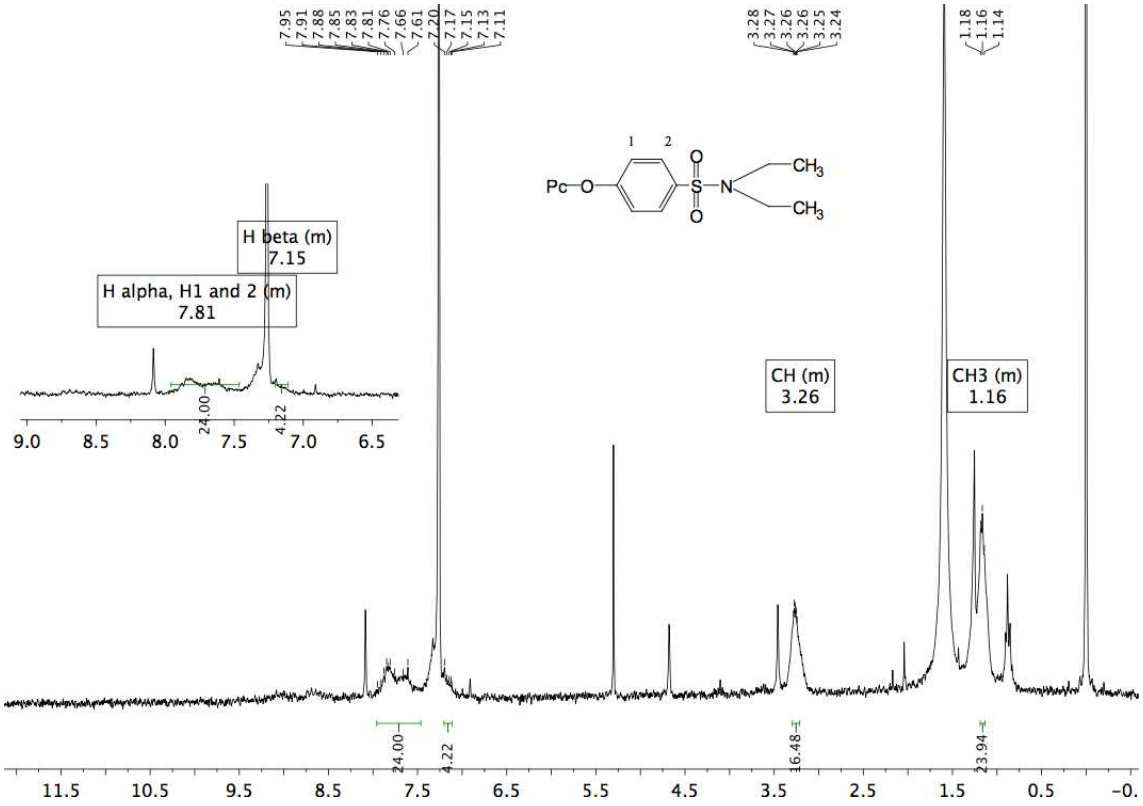

Figure 3.9: ^{1}H NMR spectrum of {2,9(10),16(17),23(24)-[tetrakis(4-diethylaminosulfonyl)phenoxy]phthalocyaninato}magnesium(II) (**Mg46**) in $CDCl_3$.

Then, we started the study of the synthesis of cationic Pc–SA conjugates. For that, we planned three synthetic routes to obtain cationizable Pcs with *N,N*-diethylaminosulfonyl groups (Figure 3.10). In the three synthetic routes, 4,5-bis(4-(*N,N*-diethylaminosulfonyl)phenoxy)phthalonitrile (**25**) was used as starting material.

In the first route (Figure 3.10 - blue), in a statistical condensation with magnesium turnings and pentan-1-ol, Pht–SA conjugate **25**, 4-pyridylsulfanylphthalonitrile (**39**) and octan-1-ol were added to the suspension after alkoxide formation. The suspension was heated to 160 °C and stirred overnight. From this reaction was obtained a mixture of Pcs as confirmed from TLC observations and from mass spectrometry analysis in which it was possible to observe the molecular ion (M^+) at *m/z* 1318.6 of **Mg47**.

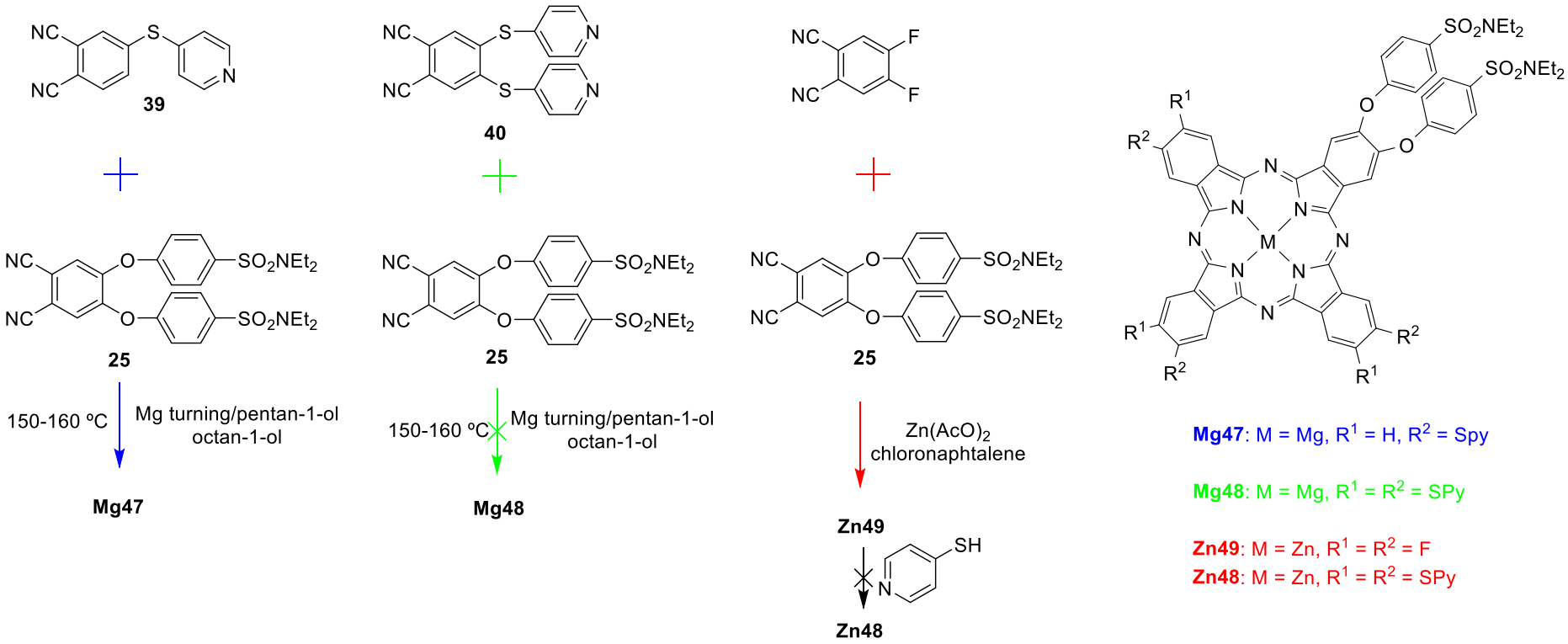

Figure 3.10: Planned route for the synthesis of cationic phthalocyanine–*N,N*-diethylaminosulfonamide conjugates.

With these results, we decided to try to obtain a pure fraction of **Mg47**. Different chromatographic procedures were tried from normal phase to reverse phase column chromatography and repeated crystallizations from water and a variety of organic solvents. The best procedure consisted on the purification in preparative TLC with normal silica gel, using CH_2Cl_2/hexane/pyridine (1:1:0.5%) as eluent. Yet, with this procedure we were not able to afford a complete pure fraction. A mixture of **Mg47** and traces of tetra thio-pyridine derivative was obtained.

Then we studied the synthesis of hexa(thio-pyridine) Pc–SA conjugates **Mg48** and **Zn48**. For the synthesis of **Mg48** - second route (Figure 3.11 - green) - Pht **25** was reacted with 4,5-di(pyridylsulfanyl)phthalonitrile (**40**) in DMF in the presence of $Zn(AcO)_2$, at 120-150 ºC. After 12 hours, the color of the reaction mixture changed from yellowish to blue-green. Still in the TLC, different spots could be observed inducing that we would be in the presence of a mixture of Pcs. After mass spectrometry analysis it was possible to conclude that, from this reaction, we only afford the octa(thio-pyridine) derivative which was not our goal.

To overcome these difficulties, we drew a synthetic route (Figure 3.11 - red) in which 4,5-difluorophthalonitrile and Pht **25** were converted in the Pc–hexafluoroSA conjugates **Zn49**. Then, after purification, this Pc would be converted, by a nucleophilic aromatic substitution, in the desired Pc–hexa(pyridylsulfanyl)-SA conjugate **Zn48**. The idea with this procedure was to reduce the polarity of the Pcs obtained making the purification of these compounds easier. For that, 4,5-difluorophthalonitrile and Pht **25** were reacted in a statistical condensation in chloronaphthalene and in the presence of $Zn(AcO)_2$. After purification the desired hexafluoroPc (**Zn49**) was obtained and its structure confirmed in ^{1}H NMR and mass spectrometry. In ^{1}H NMR spectrum is observed the protons corresponding to the methyl and methylene groups at δ 1.15 and 3.24 ppm, respectively. In the aromatic region, at δ 7.03 ppm is shown the peak corresponding to H2, at δ 7.49 ppm the peak corresponding to the α-protons and at δ 7.81 ppm the resonances for protons H3. The structure was also confirmed by MS in which the ion $[M+Na]^+$ was observed at *m/z* 1163.4.

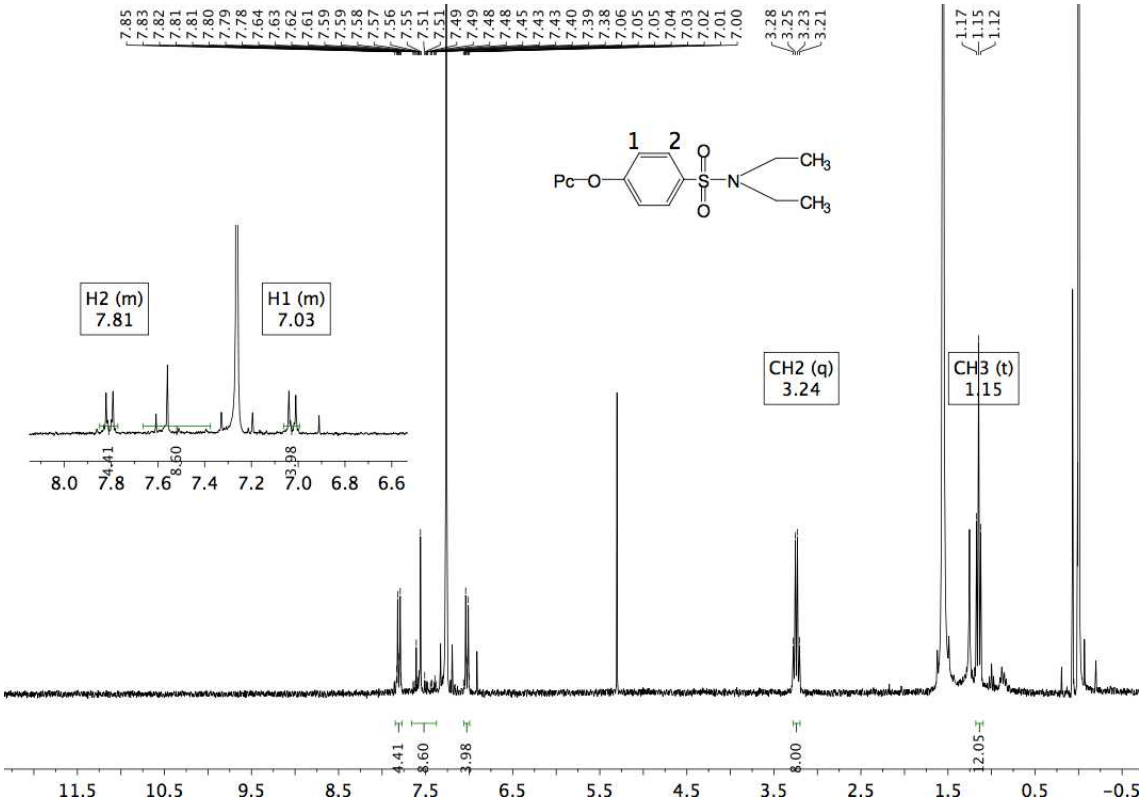

Figure 3.11: ^{1}H NMR spectrum of {9,10,16,17,23,24-[hexafluoro-2,3-bis(4-diethylaminosulfonyl)phenoxy]phthalocyaninato]zinc(II) (**Zn49**) in $CDCl_3$.

Next, we tried the reaction of **Zn49** with 4-mercaptopyridine in DMF in the presence of cesium carbonate. Different reaction temperatures were tried. The reaction was stirred from room temperature to 90 ºC. following the procedures described in the literature for the nucleophilic aromatic substitution of fluoro-Pors and fluoro-phhalocyanines.[149–152] However, no differences in the TLC were observed.

3.2.3 Encapsulation of phthalocyanine–sulfonamide conjugates in PVP micelles

Some of the conjugates obtained were chosen to be encapsulated in PVP micelles in order to be soluble in aqueous media. The encapsulation procedure is quite simple and practical. The encapsulation within the water soluble PVP was performed with Pcs **41**–**44**, **46** and **Zn41**–**Zn46** in an incubator at 50 ºC overnight, obtaining complete blue-green solutions.

3.3 Conclusions

This chapter describes the work developed for the synthesis of Pc–SA conjugates. To that end, firstly, neutral conjugates were synthesized. It was obtained new Phts mono-substituted with SO_2NEt_2 (**9**) and di-substituted with SO_2NH-isopropyl (**26**) and SO_2NH-thiazol-2-yl (**27**) that were used for the synthesis of Pc-SA conjugates. Furthermore, the synthesis of precursors for cationizable Pc-SA conjugates were also accessed.

With the synthetized Phts we were able to obtain, for the first time, the Pc-SA conjugates **Mg42**–**Mg44**, **42**–**44**, **Zn42**–**Zn43**, **Mg46**, **46** and **Zn46**. These results consisted on an upgrade of a work developed in our group in 2009.[62] Furthermore, we were also able to identify the presence of a new cationizable Pc-SA conjugate **Mg47** in a mixture of Pcs. The synthesis of cationic conjugates turned out to be very demanding but these results are very promising for future studies involving the synthesis of cationic Pc-SA conjugates.

Chapter 4 Evaluation of phthalocyanine–sulfonamide conjugates as photosensitizers in PDT and as carbonic anhydrase inhibitors

This chapter reports on the work developed in collaboration with the group of Doctor Jon Golding from the Health Sciences, Faculty of Science, Technology, Engineering & Mathematics, The Open University (UK) and Doctor Etelvina Figueira from the Biology Department, University of Aveiro. This is an ongoing work from which the most recent results will be presented.

Taking advantage of Pc outstanding properties as PSs and SAs potentialities as antitumor agents, this work had the purpose of testing the hypothesis of a additive effect between Pcs and SAs. In this sense, these two active moieties were coupled in one molecule and evaluated as PS in the inactivation of cancer cells.

Pc–SA conjugates were assessed as PSs by photophysical, photochemical and *in vitro* photobiological studies. Solubility, photostability/stability and singlet oxygen generation of these compounds were determined and their photodynamic activities were investigated on HSC3 oral squamous cell carcinoma and HaCaT 'normal' keratinocytes. Four of these compounds were encapsulated in PVP micelles and the differences on photophysical, photochemical and photobiological properties of these compounds were also accessed. In addition, the properties of these compounds as modulators of the activity of the enzyme CA were evaluated.

The Pc–SA conjugates used in this work are indicated in Scheme 4.1. In the case of compounds **Zn41**, **Zn44**, **Zn45** and **Zn46** an encapsulation in PVP micelles was performed.[153–160] The procedures involved in the synthesis of all compounds and encapsulation of the selected compounds (**Zn41(PVP)**, **Zn44(PVP)-Zn46(PVP)**) are described in chapter 3.

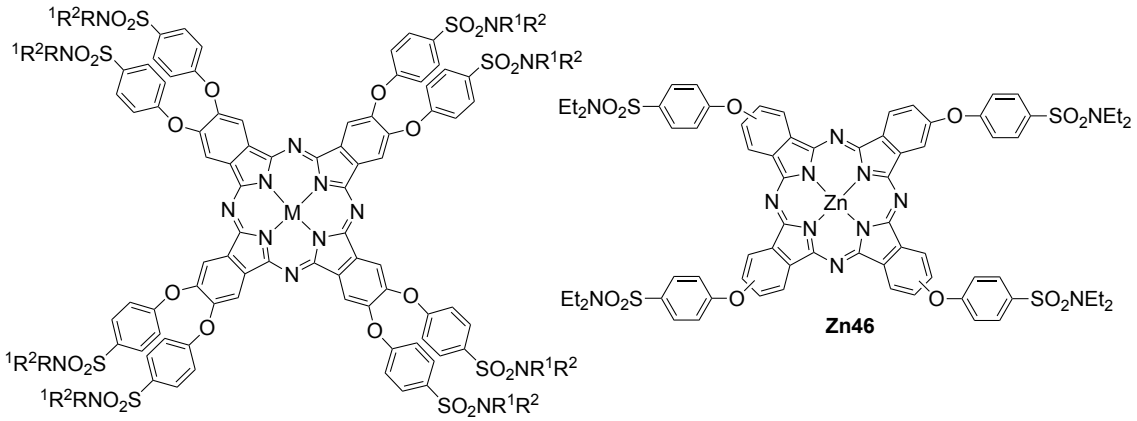

42: M = 2H, NR^1R^2 = NH(*i*-Pr)
Zn41: M = Zn, NR^1R^2 = NEt_2
Zn43: M = Zn, NR^1R^2 = NH(thiazol-2-yl)
Zn44: M = Zn, NR^1R^2 = NH(4-$MeOC_6H_4$)
Zn45: M = Zn, NR^1R^2 = NH(dodecyl)

Scheme 4.1: Structure of the phthalocyanine–sulfonamide conjugates.

From the results it was possible to confirm that Pc–SA conjugates are important compounds to be considered as photosensitizes for PDT. The PVP encapsulation turned out to be a very good approach to enhance solubility of these compounds in aqueous media and consequently increase singlet oxygen generation. Furthermore, it was also possible to highlight Pc–SA conjugate **Zn41(PVP)** as the PS with higher cytotoxicity for the lowest uptake, probably due to the selectivity to the inactivation of the enzyme CA.

4.1 Introduction

Photodynamic therapy represents a new treatment opportunity for several diseases. Although still emerging, it is already being successfully used in the treatment of malignant and non-malignant diseases. Since 1985, when some Pcs were demonstrated as efficient PSs of mammalian cells, the interest of these compounds in photobiology increased considerably.[2,161–164]

During the last decades, great attention has been paid to photodynamic therapy. One of the main challenges of this technique is the performance of the PS which should preferentially accumulate in malignant tissues relative to normal tissues, while having a good solubility in aqueous media and a also high singlet oxygen generation.[161,165–168]

The functionalization and metallation of Pcs have been studied in order to obtain compounds with better properties, such as increased solubility in biological fluids,

transport, selectivity, singlet oxygen production, as well as clearance after photoinactivation. To overcome low solubility of phthacyanines in aqueous media, several approaches have been explored. One example is the encapsulation in a drug delivering vehicle. There are several micelles encapsulation possibilities reported in literature.[153–160,169,170] One example is the encapsulation in PVP micelles that, as Pcs are concerned, it is described in the literature as reducing aggregation and consequently improving solubility in aqueous media and singlet oxygen generation yield.[169]

Furthermore, SAs have been studied as antitumor drugs. There are a variety of mechanisms by which SAs have antitumor action such as disruption of microtubule assembly, functional suppression of the transcriptional activator NF-Y, or angiogenesis (matrix metalloproteinase, MMP) inhibition.[91] But there are two that are more studied: One of them is related with the inhibition of CAs IX and XII. These enzymes are responsible for maintaining pH within viability values in cells and are known to be overexpressed in several tumours.[73] The other mechanism is the regulation of cell cycle at the G1 phase through inhibition of cyclin-dependent kinases.[90]

4.1.1 Brief historical perspective of photodynamic therapy

Going back over 4,000 years it is possible to trace the attempts to use light in the treatment of diseases.[171–173] It was firstly applied in Ancient Egyptian, Indian, and Chinese civilizations where light was used to treat various diseases including rickets, psoriasis, skin cancer and vitiligo.[174] In the late nineteenth century, first reports of contemp orary PDT appeared during the investigations led by Finsen when he found that exposure of red light can prevent the formation and discharge of smallpox pustules.[175] In addition, he also demonstrated that phototherapy could be used to successfully treat cutaneous tuberculosis, for which he won the Nobel Prize in Physiology and Medicine in 1903.[162]

Chemical sensitization of tissue by light was reported in 1900 by Raab *et al.*,[176] who discovered that a combination of acridine red and light could kill a species of *Paramecium.* In the same year, using eosin (a brominated derivative of fluorescein) orally in the treatment of epilepsy, Prime, a French neurologist, discovered that this treatment induced dermatitis in sun-exposed areas of skin,[175] leading to the first therapeutic medical application of PDT.[46]

The basic concept of photodynamic therapy was disclosed and the term 'photodynamic action' ('*photodynamische Wirkung*') was introduced in 1904 by Tappeiner and Jesionek.[46] Ten years later, a German doctor Friedrich Meyer-Betz inject himself with 200 mg of hematoporphyrin (Hp). When exposed to sunlight, adverse reactions like extreme swelling occurred and photosensitivity persisted for several months.[177] Upon these observations, Lipson and co-workers[3] prepared hematoporphyrin derivative (Hpd) by reacting Hp with acetic acid and sulfuric acid (9:1). During this reaction, apart from the formation Hp and related dehydration analogues, a completely unexpected product, was formed in about 50% yield, which was named Hpd. In the late 1960s and early 1970s Hpd starts becoming known as an important drug for diagnosis. Several groups during the 1970s, upon *in vitro* and *in vivo* studies, recognized the potential utilization of Hpd coupled to light for tumor destruction. In 1978, Dougherty *et al.*[178] reported an extensive pre-clinical study in which a series of 25 patients were treated with Hpd following photodynamic therapy showed partial or complete response in 111 of 113 tumors. These results were very important in PDT area but only in 1980 Hpd was purified and Photofrin® was partially identified as a fraction of Hpd. Hpd is a mixture of dimers and higher oligomers in which the Por units are joined by ether, ester and carbon-carbon bonds.[10] The first approval of using Photofrin® for PDT by the Food and Drug Administration (FDA) in the United States was obtained in 1995 for palliation of obstructive esophageal cancer.[175] Since Photofrin® discovery increased worldwide interest in this treatment modality took place and several other PSs have been developed and studied, some of them with Pc-base structure.[8]

Nowadays, there is a large variety of potent PSs and some of them are under investigation in clinical trials or already used in clinic.[8,165,168,171,175,179]

4.1.2 Basic components of photodynamic therapy

PDT is a 3-stage procedure which consists on the administration and distribution of a non-toxic drug - light-sensitive PS - systemically, locally, or topically to a patient bearing a lesion (first stage), which is frequently, but not always cancer, followed by an incubation period (second stage) and photodynamic inactivation by irradiation with a light of appropriate wavelength (third stage). Virtually, photodynamic inactivation can occur in any organ in the body using flexible fibrotic devices.[180] The first key step of PDT is the accumulation of the PS in malignant tissue after the administration of the PS,

which can be taken orally or introduced in the body by intravenous administration. Accumulation must be as selective as possible. The second and crucial step is singlet oxygen production after PS illumination with light of an appropriate wavelength creating a photochemical reaction called photodynamic effect. This effect, third step, results in tissue destruction. The description of the interaction with light with the PS and the generation of reactive oxygen species (ROS) including singlet oxygen is described in the modified Jablonski diagram (see section 0).[165,181,182]

In this technique, the combination of the selectivity of the PS and precise delivery of light is decisive for the success of this technique. When irradiated with light, the PS will produce singlet oxygen, damaging tumor cells, leading to death and elimination of cancer cells (Figure 4.1).[3,165] As Pcs are concerned, it is usually used red visible light (620–690 nm).[8]

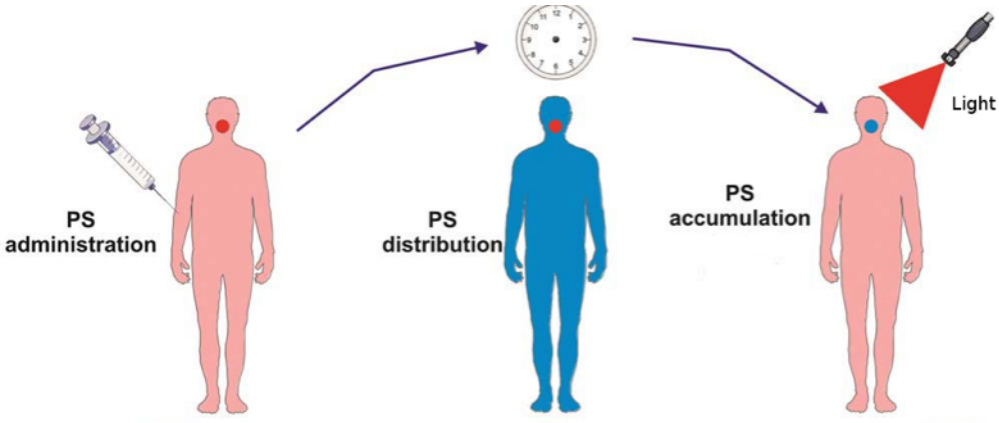

Figure 4.1: Principles of photodynamic therapy (adapted from Agostinis *et al.*).[165]

The use of PDT as cancer therapy is particularly attractive because of its potential specificity. This is due to the fact that the PS can be localized in the malignant tissue. When the light is directly focused on the lesion, the ROS that are generated during photo-sensitization result in cellular destruction in that particular region. In recent years, PDT has become a subject of intense investigation as a possible treatment modality for various forms of cancer.[165,175,179]

PDT can be a complementary treatment to chemotherapy, radiotherapy, or surgery and can be used either before or after, without compromising these therapeutic procedures. The currently used PSs do not accumulate in cell nuclei and do not present the adverse effects of chemotherapy or radiation, beyond that it is an excellent technology for the treatment of patients with skin cancers and do not present significant

changes in tissue temperature, preserving connective tissue leading to minimal fibrosis.[165]

As previously referred, one key step of PDT is the accumulation of the PS in malignant tissue which can be influenced by many factors such as hydrophobicity, pH, lymphatic drainage and lipoprotein binding. In addition, it is known that pH of interstitial fluids in malignant tumors is by tendency lower than that of normal tissues. This phenomenon is due the elevated production of lactic acid by tumor cells because of its high metabolic rates. Other factor that influences PS accumulation is lymphatic clearance that in tumors generally is poor due to underdevelopment of lymphatic system and due to lymphatic obstruction. Thus, the difference between poor lymphatic drainage of tumors and normally enhanced tumor vasculature permeability and hypervascularity are considered to be the main reasons for the accumulation of proteins and macromolecules in tumors. Serum protein binding is a phenomenon well described for several drugs. It is known that some tetrapyrrolic compounds like Pors bind to proteins, especially albumin, which is an important carrier of endogenous Por in the blood.[165,175,183]

4.1.3 Photosensitizers

PSs are compounds that when irradiated with light have the capability to absorb light in a specific wavelength and transform photons into other forms of energy.[179] PSs play a crucial role in PDT, indeed they are the crucial parameter in this technique.

The demand for new compounds with improved photo-physical and photo-biological properties has led to the development of several generations of PSs. However, there are challenges to be addressed, in particular in terms of specificity to the target and enhanced ability to be carried to the target site. Although there are a variety of natural photosensitizing compounds such as methylene blue, rose bengal, and acridine also used as PSs in PDT, the majority of the PSs are cyclic tetrapyrroles and their analogues, with enhanced photobiological properties. In this group we can highlight Pors, chlorins, bacteriochlorins, expanded Pors, and Pcs.[179]

Pors, first-generation PSs, have been successfully applied in PDT since the 1970s, in the photodynamic therapy of detection of neoplasic tissues and photodynamic inactivation of viral pathogens present in the blood plasma. In addition, already on the market there are some active principles with approval for this therapy. First-generation

PSs Photofrin® presented some disadvantages. Out of these, the prolonged skin photosensitivity, low selectivity towards the tumor tissue and the poor band of absorption (630 nm - out of red zone), stand out. Moreover, like Photofrin®, most of these PSs are mixtures because it is virtually impossible to isolate and characterize the main active compounds.[162,165,184]

In the attempt to improve the first-generation PSs, new and more effective PSs have been developed (second-generation PSs), with activity and selectivity improved in relation to those already commercially available. These molecules exhibit some differences when compared to the first-generation compounds. They differ in the intervals between administrations, in the intervals of irradiation, in the dose administered and light requirements to cause necrosis. The synthesis of these PSs has been established of the ideal characteristics for a compound to be used in PDT. Some relevant properties of an ideal PS should include:

- adequate solubility in body fluids, which affects transport and retention time;
- high selectivity for tumor tissue compared to normal tissue;
- negligible toxicity in the absence of light;
- absorption near to red visible spectrum ($\lambda > 650$nm), for better tissue penetration;
- high yield of singlet oxygen generation;
- stability upon exposure to light, since this can affect singlet oxygen quantum yield;
- simplicity of synthesis with high yields;
- purity and stability of composition;
- rapid clearance from normal tissues;
- stability and solubility in the injectable solvents (formulation);
- inducer of cell death neoplasic tissues.[184]

meso-Tetraphenylporphyrin (TPP) was the first Por to be used as second-generation It was an important improvement from Photofrin® and the first Por-based PS as a single compound. TPP has an absorption maximum of 630 nm and is an efficient generator of $^1O_2$ but has limited solubility in biological media. However, some modification of the molecule with suitable substituents, have been done in order to enhance the hydrophilicity.[179]

Apart from Pors and in particular TPP, some second-generation PSs with Por related structures were developed, such as reduced Por derivatives (chlorins, bacteriochlorins), benzoporphyrines, Pcs and naphthalocyanines. These compounds have the desirable photophysical properties. Chlorins and bacteriochlorins have absorption bands between 660–690 nm and 730 nm, respectively, and Pcs and naphthalocyanines have an intense band at 670 nm and 820 nm, respectively.[162,184] Due to the four additional peripheral benzene rings, Pcs absorb at longer wavelengths compared with other second-generation PSs. The use of PSs which absorb at longer wavelength gives rise to a higher penetration of light and consequently to an increased therapeutic effect. A recent example of a Pc-based PS used clinically is the so called Photosens®, which is a mixture of sulfonated aluminum Pcs with various degrees of sulfonation. This PS was developed in General Physics Institute in Russia. Photosens® is activated by 675 nm red light and has already been used in photodynamic therapy trials. It has also been tried on age-related macular degeneration.[2,179,185]

Recently, third-generation PSs have been developed. Photosensitizers bearing targeting moieties or encapsulate in a drug delivery vehicle, such as nanoparticles or polymeric or lipoic micelles have been develop and a huge improvement of photodynamic properties have been observed.[186]

Some clinically used PSs are summarized in Table 4.1. When compared with Photofrin®, Pcs have high molar-extinction coefficient ($e = \sim 10^5$) and red-shift absorption maximum around 680 nm. Furthermore, Pcs are excellent singlet oxygen generators and when chelated with a metal ion such as zinc or aluminum singlet oxygen efficiently increases to nearly 100%. So, metal complexes of Pcs became very interesting for PDT.[2]

Table 4.1: Clinically used photosensitizers.[179]

Photosensitizer	Structure	Wavelength (nm)	Cancer types
Porfimer sodium (HPD) (Photofrin®)	Porphyrin	630	Lung, esophagus, bile duct, bladder, brain, ovarian
5-aminolevulinic acid (ALA)	Porphyrin precursor	635	Skin, bladder, brain, esophagus
ALA esters	Porphyrin percursor	635	Skin, bladder
Temoporfin (Foscan®)	Chlorin	652	Head and neck, lung, brain, skin, bile duct
Verteporfin	Chlorin	690	Ophthalmic, pancreatic, skin
HPPH	Chlorin	665	Head and neck, esophagus, lung
SnEt2 (Purlytin®)	Chlorin	660	Skin, breast
Talaporfin	Chlorin	660	Liver, colon, brain
Ce6-PVP (Fotolon®), Ce6 derivatives	Chlorin	660	Nasopharyngeal, sarcoma, brain
Silicon Pc (Pc4)	Phthalocyanine	675	Cutaneous T-cell lymphoma
Padoporfin (TOOKAD®)	Bacteriochlorin	762	Prostate
Motexafin lutetium (Lutex®)	Texaphyrin	732	Breast
Photosens®	Phthalocyanine	675	nd

Apart from the outstanding photophysical and photochemical properties of Pcs,[12,187] their properties can be changed through rational modification of the substituents either on the periphery of the macrocycle or at the axial positions linked to the metal center. There are several studies in which PSs are covalently attached to various molecules that have some affinity for neoplasia, to receptors expressed on specific tumors or to specific metabolic receptors. The intention is to control the localization where PS will be attached. These vehicles can be monoclonal antibodies, antibody fragments, peptides, proteins, low density lipoproteins (LDL), various carbohydrates, somatostatin, and folic acid, among others.[165]Observations that neoplasic tissues have affinity for Pcs was already reported before,[2] but was only in 1985 by Ben-Hur and Rosenthal[164] that Pcs became interesting, as PSs for PDT.

Singlet oxygen generation capacity is also affected by the tendency of Pcs to aggregate which shortens the singlet excited state lifetime and hence decreases the singlet oxygen quantum yield by dissipating energy through internal conversions.[188]Apart from the modulation of the periphery of the macrocycle with large substituents, this problem can also be circumvented by encapsulating the Pc in emulsifying agents (liposomes),[183] polymer-drug conjugates,[189] polymeric micelles[190,191] or nanoparticles.[192]

4.1.4 Light sources

The longer the wavelength the greater the penetration into living tissues. The best region for light penetration in tissues is between 600 and 1200 nm and is often called the optical therapeutic window of the tissue. Nevertheless, after 800 nm light is not appropriated to generate singlet oxygen because the energy required to initiate a photodynamic reaction is low. Therefore, the ideal light source and light wavelength choice should be based on the type of PS used and its photophysical properties (fluorescence excitation and action spectra). It should also take into account the localization, size, accessibility of the tumor, tissue characteristic and cost (Figure 4.2).[165]

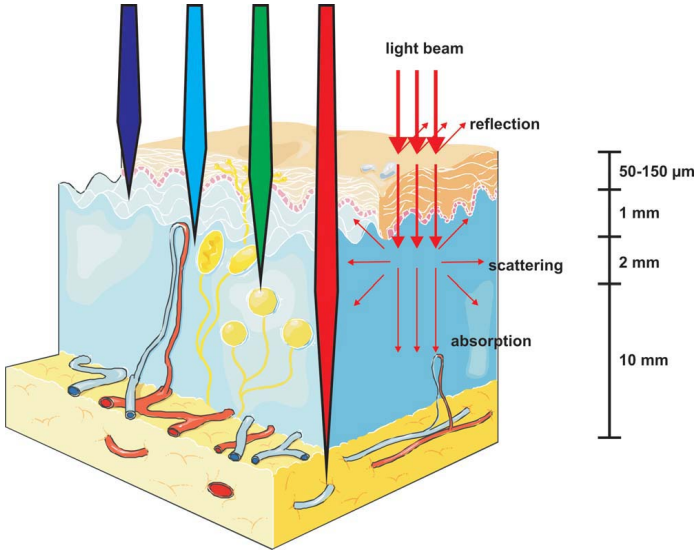

Figure 4.2: Light penetration though tissues.

4.1.5 Photophysics and photochemistry

Luminescence is the phenomena in which a substance emits light, and occurs by a transition between electronically excited states to a less energetic state. Depending on the nature of the excited state, luminescence is formally divided into two categories: fluorescence and phosphorescence. Fluorescence is the emission of light by a substance that has absorbed light or other electromagnetic radiation. This excited state is very unstable and emits excess energy as fluorescence and/or heat, returning to the ground state. When allowed, it can also occur rapidly by emission of a photon. Typically, fluorescence emission rates are 10^8 S^{-1}. Phosphorescence is the emission of light from triplet excited states, in which the electron in the excited orbital has the same spin orientation as the ground-state electron. Transitions to the ground state are forbidden and the emission rates are slower than in fluorescence. After light exposure, the phosphorescence substances glow for several minutes.

Fluorescence spectroscopy is an optical spectroscopy technique that analyses fluorescence emitted by type specimens. It involves the use of a light source, usually UV-Vis, which excites the electrons of the molecules in the sample and cause emission of light of lower energy, typically but not necessarily visible light. This optical apparatus is used to analyze PSs fluorescence and phosphorescence.[42,47]

The events experienced by a molecule since it absorbs radiation until it returns to the ground state can be illustrated in a Jablonski diagram (Figure 4.3), which

represents the energy states of a molecule and transitions between them. Aleksander Jablonski was one of the pioneers of molecular photophysics and is regarded as the father of fluorescence spectroscopy. Jablonski diagrams are often used as the starting point for discussing light absorption and emission.[166]

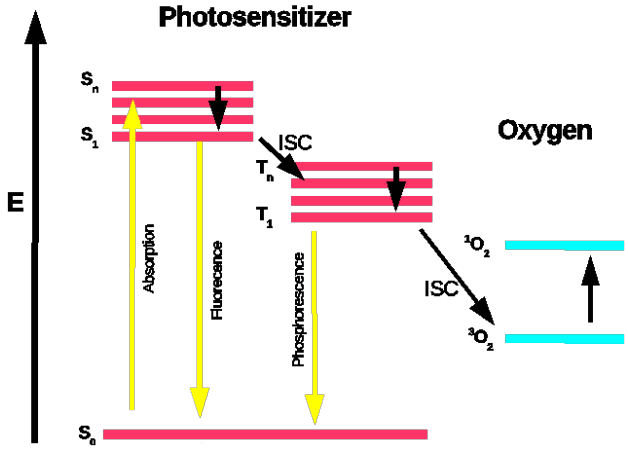

Figure 4.3: Modified Jablonski diagram.

The absorption of light of appropriate wavelengths (photons) by a population of molecules induces the passage of electrons from the ground electronic state - singlet state (S_0) - to an excited state S_n, where $n > 1$. The molecule S_n returns to the lowest energy short-lived excited state S_1 emitting energy to the outside environment, in the form of heat.[42]

From the lowest energy excited state S_1, the molecule returns to S_0 state *via* four different competitive processes. It can be by photon emission (fluorescence) or dissipating the absorbed energy to the environment by heat. This type of energy is non-radiative. A third route is described when the excited molecules pass some energy to another molecule located in the vicinity through collisions or energy transfer; and finally, the excitation can proceed by transient passage due to the passage of energy from the S_1 state to an excited triplet state of lowest energy T_1. This phenomenon is referred as inter-system crossing (ISC).[42,47]

Then, the energy is transferred from the triplet state T_1 to the ground state S_0. This is driven by three similar ways to the state transition from S_1 to S_0, which may occur throw emission of a photon (phosphorescence), by non-radiative energy

dissipation (heat), and may also occur, by energy transfer to a close molecule (collision) or to a short distance molecule.[42]

A chromophore (part of the molecule or functional group which is responsible for color) which emits photons is called a fluorophore. Many are not necessarily fluorescent chromophores. In this case, the absorbed energy is dissipated to the environment as thermal energy, energy of collision with the molecules of the solvent and also by energy transferred to other molecules. For example, the heme group absorbs energy but it is not fluorescent. The lack of fluorescence results from the total energy transfer from the Por to the metal ring.[42]

The ground state of an oxygen molecule can be described as a triplet in which two higher-energy electrons are unpaired and each occupies a degenerate orbital. When an oxygen molecule is excited the two highest energy electrons pass to be located in a single orbital, getting paired. An oxygen molecule in this state is called singlet oxygen, whose state is the highest energy and is therefore less stable.[42,47]

The triplet or singlet designations are the result of the spin quantum number (s). An electron rotates around itself with a movement quantified by a spin quantum number. The singlet and triplet states depend on this number. According to the Pauli Exclusion Principle, two electrons in a same defined orbital may not have the same quantum numbers including spin quantum number. Two spins are assigned to an electron, + 1/2 and – 1/2. Thus, two electrons must have opposite spin to belong to the same orbital.[42]

The multiplicity (m) of that two electron states is defined by $m = 2|s1+s2|+1$, and refers to the number of possible states with the same energy. When the spins are antiparallel ($m = 1$), we have the singlet state (S). When the spins are parallel ($m = 3$), we have the triplet state (T).Most molecules are in the singlet state. Oxygen is in the triplet state and, when excited, passes to a singlet excited state. In triplet oxygen state there are in total three possible spin orientations for the two higher-energy electrons. While in singlet oxygen there is only one possible spin orientation.[47]

The rotation speed of an electron around its axis is very small compared with the speed of light. Thus, the magnetic contribution to the absorption can be neglected compared to the contribution of the magnetic field. During absorption, electronic transition results from the interaction between the electrons and the electric field generated by radiation. For this reason, during absorption, there is no change in the

number of electron spin. This way, only the transitions $S_0 \rightarrow S_n$ are possible and transitions $S_0 \rightarrow T_n$ are forbidden.[42]

In many organic molecules, the internal conversion from the higher excited state to the lowest energy state occurs much faster than the decay of the lowest energy excited state to the ground state. Thus, fluorescence takes place mainly from the excited state to the lowest energy state, even if the initial molecule has an excited state of higher energy.[42]

The photosensitization by a tetrapyrrolic compound, like Pc, is a photodynamic reaction in which oxygen is required for the reaction. This process may follow by a type I or type II mechanism. In both mechanisms, there is a generation of a long-lived triplet state. In a type I mechanism the PS in a triplet state undergoes a primary reaction with a target biomolecule in its vicinity, leading to an hydrogen atom abstraction or an electron transfer process which results in the formation of a radical. This radical will react with molecular oxygen to produce multiple oxidized products, usually called as ROS, such as superoxide, hydroperoxyl and hydroxyl radicals and hydrogen peroxide. In a type II mechanism, the excited Pc triplet state directly interacts with molecular oxygen. In this interaction, the electronically excited singlet state oxygen ($^1O_2$) is formed *via* energy transfer. Singlet oxygen will react with an electron-rich region of biomolecules to produce oxidized species.[42] It is generally accepted that the type II photodynamic mechanism prevails during the process and that the singlet oxygen is the most important cytotoxic species. However, the type I mechanism may become more significant in environments with low oxygen concentration. Probably there are many cases in which the two processes act accordingly. But more important than all this, is that both mechanisms trigger oxidative reactions that induce cell death and lead to a higher tumor destruction.[42,166]

4.1.6 Biological mechanisms of photodynamic therapy

It is now known that photodynamic treatment can go through three different mechanisms:[29] direct tumor cell destruction, vascular destruction, and recruitment of an antitumor immune response. These three mechanisms are not independent and can influence each other.

As direct damage and cell death is concerned, ROS generated during PDT can kill tumor cells directly. By PDT, the elimination of tumor cells can occur by at least

two types of cell death processes: necrosis or apoptosis.[3,30,31] Necrosis is a violent and immediate form of degeneration that results from extensive cellular damage. It is characterized by the release of intra-cellular contents into the extracellular compartment resulting from the destruction of organelles and disruption of the plasma membrane. Apoptosis is a mechanism in which genetically programmed death of old or damaged cells occurs. It involves a common sequence of morphological and biochemical changes, including condensation of chromatin and formation of apoptotic bodies.[166]

The viability of a tumor depends on the amount of nutrients supplied by blood vessels. In this sense, vessels around the tumor are very important. There are a number of reports of PDT that can induce damage to tumor microvasculature leading to post-PDT tumor hypoxia/anoxia and nutrient deficiency, which is lethal to the tumor.[166] This mechanism by which tumor microvasculature is damaged includes vascular occlusion, vessel constriction/collapse, macromolecular leakage, leukocyte adhesion, blood flow stasis, and thrombus formation.[193]

PDT can also trigger inflammatory and immune responses, by photodynamically induced changes in the plasma membrane and membrane organelles, which can activate multiple signal transduction pathways. This includes the activation of a variety of protein kinase signalling cascades leading to an inflammatory or immune response and, ultimately, to cell death.[161,193] In the late 1980s and early 1990s several studies have reported the infiltration of lymphocytes, leukocytes, and macrophages into PDT-treated tissue which indicates an activation of the immune response.[180,194] The initiated inflammatory response can have differences in the nature and intensity between normal and cancerous tissues that may be an additional contribute to the selectivity of PDT.[29]

Mitochondria, plasma membranes, lysosomes and nuclei have been proposed as subcellular structures targets of the photodynamic effect. Additionally, it has also been reported that photodynamic treatment can also result in, direct or indirectly, DNA damage. In the case of Photofrin®, it is believed that the major mechanism of tumor necrosis is due to damage of tumor vasculature that leads to blood stasis and consequently starving the tumor of oxygen and nutrients. Furthermore, it is believed that in the initial phase after irradiation, the plasma membranes and the membranes of mitochondria and lysosomes start to disintegrate. After this phase, there is a continuous depletion of the ATP pool with drastic consequences for all energy-consuming process. Joining to this, the membrane breakdown can cause rapid liberation of phospholipids,

such as arachidonic acid, leading to the release of vasoactive and inflammatory mediators like thromboxanes, prostaglandins and leukotrienes. All these inflammatory mediators initiate an acute inflammatory process with massive edema and vascular damage. This vascular damage leads to a local hypoxia and initiation of a necrotic process by nutrient deprivation. In response to this hemorrhage, platelets aggregation and adhesion to damaged tissue is activated and are released IL-1β, IL-2 and TNF-α increasing the pathological effect of the eicosanoids. However, other mechanisms of tumor necrosis have also been proposed like direct cell killing and apoptosis.[161,165,166,172,184]

It is believed that PSs, with high partition coefficients (increased hydrophobicity), are more likely to accumulate in malignant tissue by preventing drugs from entering or continuing on blood circulation, and it is important for membrane penetration. Lipophilicity has proven to be a very important molecular descriptor and is often well correlated with bio-activity of chemical entities. On the other hand, hydrophilicity is vital for a proper PS distribution in biological fluids, thus a proper balance between hydrophobicity and hydrophilicity is important.[162,167,179]

4.1.7 Applications of phthalocyanines in PDT

In medicals sciences, the major utilization of Pcs is as PSs in PDT to inhibit/eliminate cancer cells. There are several examples of such applications.[195–197] In a study by Fadel *et al.*,[43] nanoparticles formulated from the biodegradable copolymer poly(lactic-coglycolic) acid (PLGA) containing zinc phthalocyanine (ZnPc) were investigated as a drug delivery systems to enhance tissue uptake, permeation, and targeting for photodynamic therapy. These nanoparticles were prepared with different sonication time in order to study the effect on nanoparticle shape, encapsulation and size distribution, *in vitro* release, and *in vivo* photodynamic efficiency in tumor-bearing mice. This study revealed that tumor-bearing mice injected with Pc nanoparticles exhibited significantly smaller mean tumor volume, delay tumor growth and enhanced survival, compared with the control group and with the group injected with free ZnPc during the time course of the experiment. This was attributed to the increase of the solubility and dissolution rate, allowing sustained drug release.[43] One year later, Maduray *et al.*[44] performed *in vitro* toxicity testing of zinc tetrasulfoPcs in fibroblast and keratinocyte cells for the treatment of melanoma cancer by photodynamic therapy.

With this *in vitro* study, they were able to show that ZnTSPc mediated photodynamic therapy (50 μg/ml) with a light dose of 4.5 J/cm^2, represented and effective therapeutic option for melanoma, by selectively destroying melanoma cells *via* apoptosis with low killing effects on healthy normal skin cells. In the same year, Lim and coworkers[45] used an indocyanine green PS with 785 nm LED light to treat cancer from oral region. With this methodology Lim *et al.* were able to conclude that focused and increased depth of penetration due to longer wavelength are not required to an effective treatment. These results will be important to enhance the treatment of one of the most difficult cancers due to its late diagnoses.

In 2012, tetrasubstituted carboxy aluminum phthalocyanines (AlC_4Pc) were covalently encapsulated in silica shells and used as PSs in magnetic resonance imaging and photodynamic therapy of liver cancer cells. The nanoparticles obtained showed uniformity in size, stability against PS leaching, and also showed high efficient in photogenerating cytotoxic singlet oxygen under near-infra-red light.[55] Also in 2012, using the same Pc, Manono *et al.*[15] determined the subcellular localization of ZnTSPc and its effect on two cancer cell lines - human colon (DLD-1) and lung (A549) carcinoma cells. ZnTSPc was activated at a wavelength of 680 nm with 5 J/cm^2 and subcellular localization was determined by fluorescence microscopy. Alongside, toxicity of PS alone and combination of light was determined by cell morphology, viability, proliferation and cytotoxicity. With this procedure cell death was induced in both cell lines. PS was localized in vital organelles such mitochondria and lysosomes. A collaboration involving the University of Aveiro, the Universidad Autonoma de Madrid, Memorial Sloan-Kettering Cancer Centre in New York and the University of Erlanger, in Germany,[198] glycoPcs were tested as PSs for triggering mitotic catastrophe and apoptosis in cancer cells. In this study, the photodynamic-effect of three symmetric and asymmetric Pcs with *D*-galactose on HeLa carcinoma cells was analyzed. This work revealed that asymmetric glycoPc with the sugar in only one side of the Pc is very efficient and selective, producing higher photo-cytotoxicity on cancer cells than in nonmalignat HaCaT, probably due to its amphiphilic character. The other example is the utilization in PDT and magnetic resonance imaging (MRI) in cancer cells of Lanthanide-doped up conversion nanoparticles with a AlC_4Pc. *In vitro* studies indicated that these nanoparticles could effectively kill cancer cells upon near-infrared (NIR) irradiation (700-1000 nm), which affords deep light penetration, low auto-fluorescence

and photo-damage, and reduced light scattering. Furthermore, the nanoparticles also demonstrated good MRI contrast, both in aqueous solution and inside cells. The third work from 2012 was carried out by Korbelik *et al.*[199] in which it was developed a poly(D,L-lactic-co-glycolic acid)-nanoparticles (PLGA-NPs) preparation of hypocrellin-based derivative SL052. In collaboration with Quest PharmaThech Inc., Edmonton, AB, Canada, Korbelik used this new formulation in preclinical and clinical tests in photodynamic therapy. The nano formulation encapsulating SL052 into biodegradable polymer PLGA was developed using single-emulsion solvent evaporation technique and characterized in terms of particle size and loading of the photosensitizing agent.

An interesting field of PDT is the utilization of antibodies coupled with Pcs which has been study in newer years. To give an example, in 2011, Stuchinskaya *et al.*[16] developed and studied the utilization of anti-HER2 monoclonal antibodies-Pc-polyethylene glycol-gold nanoparticle to target photodynamic therapy of breast cancer cells. The nanoparticle conjugates showed low aggregation, and under irradiation with visible red light efficiently produced cytotoxic singlet oxygen. Cellular experiments demonstrated that the nanoparticle conjugates selectively target breast cancer cells that over-express the HER2 epidermal growth factor cell surface receptor, and that they are effective photodynamic therapy agents. However, the large size of monoclonal antibodies (mAbs) hinders tissue penetration and lowers cellular uptake when used *in vivo* has been created some concern. Furthermore, the attachment of PSs to mAbs may also reduce the antigenic specificity of the mAbs. As a result, smaller antibody fragments have been used as alternative carriers. An alternative strategy involves the utilization of peptides with appropriate sequences which can specifically bind to different surface markers of cancer cells and tumor vasculatures. This biding is achieved by the formation of a triazole by a click reaction.[17]

Photodynamic therapy has been showing promising results in the treatment of atherosclerosis acting on vascular walls. Recent experiments in animal samples provided a solid evidence for successful use of photodynamic therapy for preventing and reducing the intimal hyperplasia.[22–24] Borshch *et al.* in 2012[23] used a silicon Pc and a commercial phthalocyaninic PS (Photosens - sodium salt of sulfonated hydroxyalumino) on the treatment of atherosclerosis by inducing the apoptosis of the cellular population of atherosclerotic plaques. Heckenkamp *et al.*[24] using as PS

chloroaluminum sulfonated Pc, achieved an inhibition of intimal hyperplasia, with better results in comparison to the treatment with γ-irradiation. The same research group, using the same PS, designed a study to test the hypothesis that PDT alters the vascular wall matrix thereby inhibiting invasive cell migration, and as such, provides an important barrier mechanism to favorably alter the vascular injury response. With this protocol, Heckenkamp and colleagues were able to observe a 52% reduction of invasive SMCs and a reduction up to 59% in fibroblast migration, but not significant effects on the secretion of matrix metalloproteinases. Additionally, PDT induced collagen matrix changes, including cross-linking, which resulted in resistance to protease digestion, and led to a durable 45% reduction in pepsin digestion susceptibility of treated arteries and inhibition of periadventitial cell migration into the media.[22]

Also using a sulfonated MPc, Ranyuk *et al.*[28] labelled a series of ZnPcSn with ^{64}Cu in good yields. Tumor-bearing mice were injected with the ^{64}Cu-labeled products and subjected to 3 hours dynamic positron emission tomography (PET). The [^{64}Cu]$CuPcS_n$ complexes demonstrate to be suitable for PET imaging, allowing the rapid generation of preliminary biodistribution data with only a few animals. However, only some Pcs with amphiphilic groups like [^{64}Cu]$CuPcS_2$ and [^{64}Cu]$CuPcC_6$ showed biodistribution patterns and highest tumor-to-back-ground rations. In another study, hexyn-1-yl-trisulfophthalocyanine ($ZnPcS_3C_6$) and hexyn-1-yl-trisulfobenzo-mononaphthalo-porphyrazine ($ZnNPS_3C_6$) were also used as testing PS for PET. Cauchon *et al.*[27] combined PET with the constant infusion of 2-deoxy-2-[^{18}F]fluoro-D-glucose (FDG) as a tracer to monitor in real-time transient metabolic chances resulting from photodynamic therapy in animals bearing a tumor.

4.1.8 Sulfonamides as antitumoral agents

The antitumoral activity of SAs is, in general, associated with arrestment of activity CDKs in the regulation of the cell cycle[200,201] and inhibition of CA in tumor membrane.[73]

The inhibition of growth of human cancer cells in culture by direct action of specific SA CA inhibitors was first reported by Chegwidden and Spencer,[202] who drew attention to their therapeutic potential in the treatment of cancer. This work demonstrated that potent CA inhibitors such as acetazolamide, methazolamide and

ethoxzolamide, strongly inhibit the growth of human lymphoma cells with GI_{50} values of 0.5 μM for ethoxzolamide and 0.25 mM for acetazolamide.

CAs (also known as carbonate dehydratases) are a class of ubiquitous metallo-enzymes that catalyze the reversible hydration of carbon dioxide to the bicarbonate ion (Scheme 4.2).[203] This reaction is the basis for the regulation of acid–base balance in organisms.[204,205] Fifteen different CA isoforms have been identified in humans (Table 4.2 and Figure 4.4), and these proteins are also present in prokaryotes and eukaryotes.[206]

$$CO_2 + H_2O \xrightarrow{CA} H_2CO_3$$

Scheme 4.2: Reaction catalyzed by the enzyme carbonic anhydrase.

CAs are involved in crucial physiological processes related with respiration and transport of CO_2 between metabolizing tissues and the lungs. The primary function of the enzyme in animals is in the interconversion of carbon dioxide and bicarbonate to maintain acid-base balance in blood and other tissues, a reversible reaction that occurs relatively slowly in the absence of a catalyst. CA is also related with pH homeostasis, bone resorption, calcification, production of body fluids, gluconeogenesis, lipogenesis, electrolyte secretion in a variety of tissues/organs, biosynthetic ureagenesis and tumorigenicity.[207–209] CA-related proteins (CA-RP VIII, CA-RP X and CA-RP XI) are acatalytic forms due to the default of one or more histidine residues which are essential for the binding of the zinc ion in the active site.[207] The zinc ion, essential for catalysis, is coordinated by the imidazole rings of 3 histidine residues, His94, His96, and His119. CA XV is the most recent discover isoenzyme that is absent in humans and monkeys but is expressed in a number of other species.[203,209] Recently, CA IX closed association with tumors was revealed and CA XII were found to be overexpressed in renal carcinoma.[203]

Hypoxia is key feature in many tumors. An inadequate supply of oxygen is a crucial pathophysiological consequence of structurally and functionally disturbed microcirculation and deteriorated oxygen diffusion processes. It seems that tumor hypoxia is strongly associated with tumor propagation, malignant progression, and resistance to chemotherapy and radiotherapy. In a hypoxia environment there is an overexpression of CA IX. CA IX expression is strongly increased in many types of tumors.[209]

CAs are encoded by four evolutionarily unrelated gene families: α-CAs (in vertebrates, bacteria, algae and cytoplasm of green plants), β-CAs (predominantly in bacteria, algae and chloroplasts), γ-CAs (in archaea and some bacteria), δ-CAs (were found in marine diatoms), ζ-CAs (exclusively found in bacteria in few chemolithotrophs and marine cyanobacteria), and, finally, η-CAs (in organisms of the genus *Plasmodium*). In plants, CA helps raise the concentration of CO_2 and it is crucial in photosynthesis.[206,210–218] In fact, CA inhibitors reserved special attention to fight infection caused by microorganisms such as protozoa, fungi or bacteria.[209]

Two main classes of CA inhibitors are known: metal-complexing anions and unsubstituted SAs and their bioisosteres such as sulfamates and sulfamides compounds. CA inhibition by aromatic and heterocyclic SAs has been exploited clinically for half a century in the treatment of glaucoma, epilepsy, congestive heart failure, mountain sickness, gastric and duodenal ulcers and diuretic agents. From this class can be highlighted acetazolamide, methazolamide and ethoxzolamide. In particular acetazolamide is a well-known strong inhibitor of several CA isoforms and it is a potential modulator of anticancer therapies due of increase of hypoxia of intra-tumoral environment ensued after CA inhibition.[207,219–223]

An interesting example of the application of SAs as antitumoral agents was reported in 2017 by Jung *et al.*[224]. In that work, the additive effect of a SA (acetazolamide) and a BODIPY PS was evaluated. The conjugate was designed to take advantage of the two active subunits: the acetazolamide ligand to provide both CA IX inhibition and efficient tumor targeting, and a BODIPY moiety to serve both a singlet oxygen-producing PS and to allow fluorescence-based tracking of cellular uptake and distribution by combining the benefits of anti-angiogenesis therapy with PDT. In the *in vitro* studies with Human breast cancer cells (MDA-MB-231 cells) it was observed an accumulation of the conjugate in mitochondria of cancer cells that overexpress CA IX and the highest singlet oxygen generation was achieved at 660 nm. *In vivo* studies in xenograft mouse models revealed notable tumor suppression. Furthermore, a parallel gene expression study showed a decrease of various angiogenesis factors.

Table 4.2: CA isoforms and sub-cellular location.[207]

Isozyme	Sub-cellular location	Tissue location
CA I	Cytosol	Red blood cell and GI tract
CA II	Cytosol	Almost ubiquitous
CA III	Cytosol	8% of soluble protein in Type I muscle
CA IV	Membrane-bound	GI tract, kidney, endothelium
CA V	Mitochondria	Liver
CA VI	Secreted to saliva	Saliva and breast milk
CA VII	Cytosol	Widely distributed
CA-RP VIII	Probably cytosolic	nd[a]
CA IX	Membrane-bound	Normal GI tract, several cancers
CA-RP X	nd[a]	nd[a]
CA-RP XI	Membrane-bound	nd[a]
CA XII	Membrane bound	Kidney, certain cancers
CA XIII	Cytosol	Widely distributed
CA XIV	Membrane-bound	Kidney, heart, skeletal muscle, brain
CA XV	Membrane-bound	Not expressed in human tissues

[a]nd: not determined

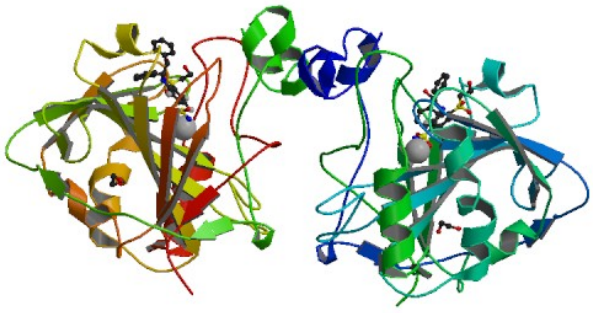

Figure 4.4: Crystal structure of catalytic domain of human carbonic anhydrase isozyme XII with inhibitor.[225]

4.2 Results

In this work we studied the applicability of Pc–SA conjugates and Pc–SA conjugates encapsulated in PVP micelles as PSs in PDT. Firstly, photophysical and photochemical parameters were accessed (subsections 4.2.1, 4.2.2 and 4.2.3). Then, an *in vitro* test was performed in Doctor Jon Golding laboratory (subsections 4.2.4 and 4.2.5). Finally, by an adaptation of Doctor Etelvina Figueiras procedure around the determination of CA activity an enzymatic assay was conduct (subsection 4.2.6). Herein will be presented the results obtained.

4.2.1 UV-Vis absorption spectroscopic properties

The electronic absorption of compounds **42**, **Zn41(PVP)**, **Zn43**, **Zn44**, **Zn44(PVP)**, **Zn45(PVP)** and **Zn46** was recorded at increasing concentrations (1, 3, 6, 9 and 12 μM) in DMSO or phenol red-free Dulbecco's Modified Eagle's Medium (DMEM) to determine if the Pc–SA conjugates and corresponding Pc–SA conjugates encapsulated in PVP micelles, at this concentration range, followed the Beer-Lambert law. The spectra of Pcs **42**, **Zn43**, **Zn44** and **Zn46** in DMSO (Figure 4.5) display B bands around 350-370 nm, vibronic band around 610-620 nm and Q-bands around 660-720 nm. For Pcs **Zn43**, **Zn44** and **Zn46** the intense, single and narrow Q band is typical of monomeric metallated Pcs. On the other hand, the spectrum of Pc **42** shows two Q bands, typical of metal-free Pcs.[226] The graphics obtained from the plotting of the Q band intensity *versus* Pc concentration in DMSO show a linear regression for all Pcs under study, indicating that no significant aggregation occurred in DMSO.

In contrast to the well-defined absorbance spectra in DMSO, the spectra of the Pcs in DMEM + 0.08% DMSO show a broadened Q band with much lower absorbance when compared with the spectra in DMSO at equivalent concentration. This suggests that these Pcs aggregate in DMEM + 0.08% DMSO media (data not shown), as had been previously observed.[169] Nonetheless, the absorbance values at the studied concentration range (1, 3, 6, 9 and 12 μM), at fixed wavelengths, gave almost straight line graphs obeying the Beer-Lambert law, suggesting that a proportion of each compound remained as a monomer in DMEM + 0.08% DMSO, in agreement with Liang *et al.*.[169]

Figure 4.6 represents the spectra in DMEM of the Pc–SA conjugates encapsulated in PVP micelles **Zn41(PVP)**, **Zn44(PVP)**–**Zn46(PVP)**. Except for **Zn45(PVP)**, the values of absorbance obtained at a fixed wavelength, at the concentration range under study, in the line graph obey the Beer-Lambert law, suggesting that in DMEM, no significant aggregation occurred. This is due to the presence of the long alkyl chains that hamper solubilisation in DMEM, forming a turbid solution (observed by naked eye). As a control, PVP UV-Vis spectrum was also obtained confirming, as expected, that it does not absorb in the wavelength recorded.

4.2.2 Fluorescence spectroscopic properties

Fluorescence spectra of all Pc–SA conjugates and Pc–SA conjugates encapsulated in PVP micelles under study were recorded at 15 μM in phenol red-free DMEM + 0.08% DMSO for Pc–SA conjugates and in water and phenol red-free DMEM for encapsulated compounds, at excitation wavelength of 610 nm (Figure 4.7).

4.2.3 Singlet oxygen generation

The ability of these PSs to generate singlet oxygen was qualitatively evaluated following the photo-oxidation of 1,3-diphenylisobenzofuran (DPBF) when irradiated with light at a fluence rate of 9 mW/cm (Table 4.3). The generation of singlet oxygen was recorded in three different solvents: DMF, phenol red-free DMEM + 0.08% DMSO and phenol red-free DMEM for the Pc–SA conjugates encapsulated in PVP micelles. The reactions were followed spectrophotometrically by observing the decrease of the absorption peak of DPBF at 415 nm as a function of irradiation time.

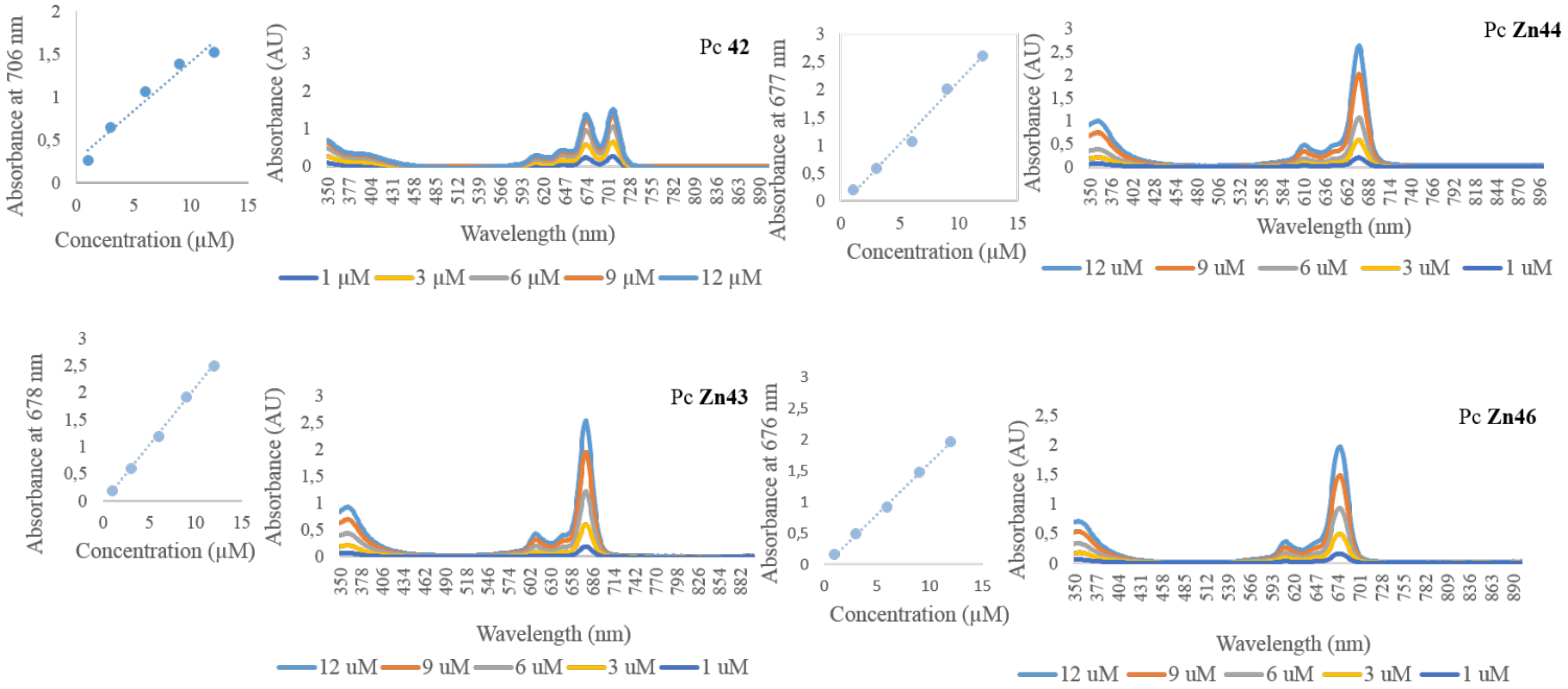

Figure 4.5: UV-Vis spectra of compounds **42**, **Zn43**, **Zn44** and **Zn46** in DMSO at different concentrations. The linear regression graphics plotted the Q-band absorbance versus the concentrations in DMSO.

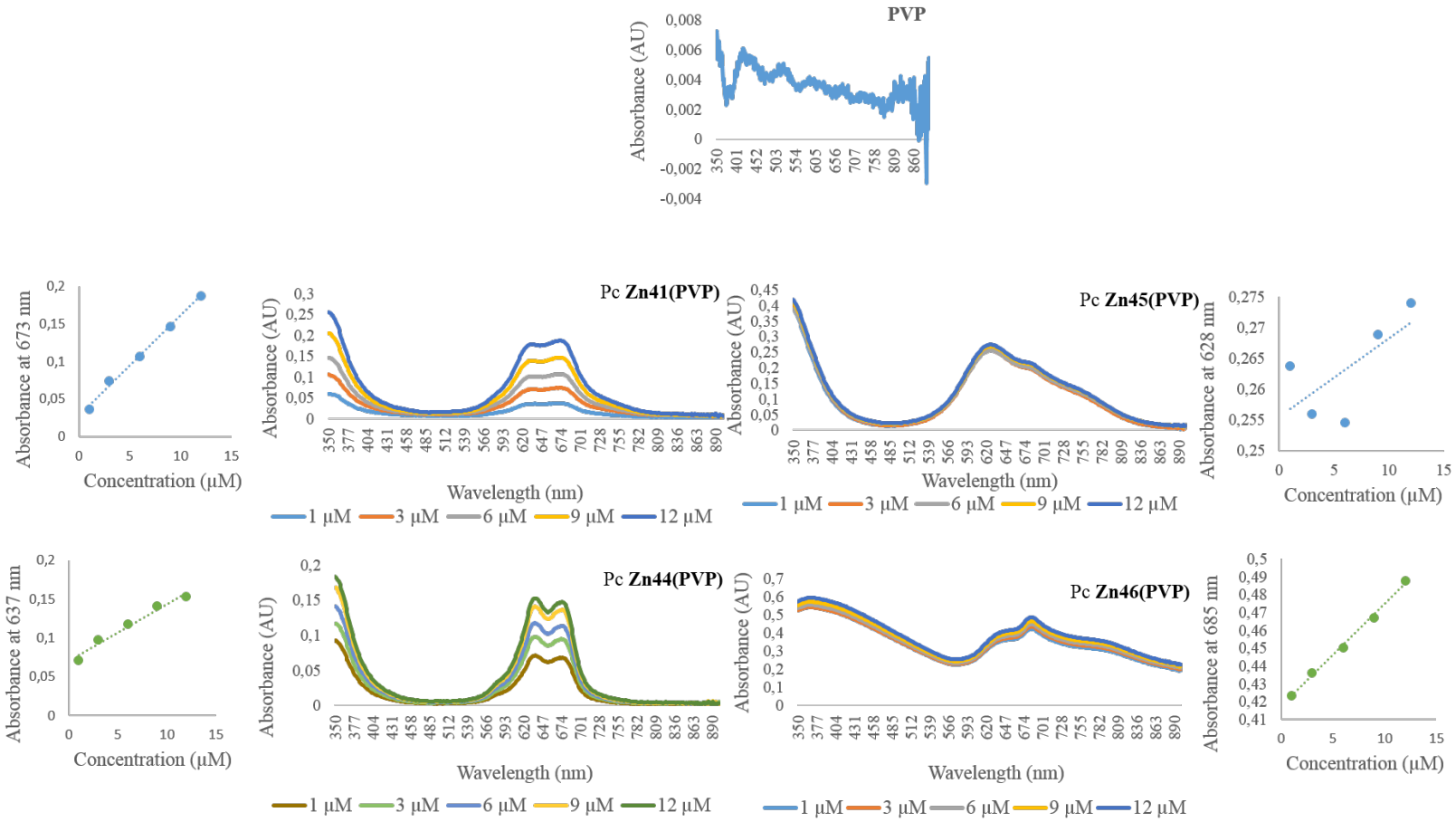

Figure 4.6: UV-Vis spectra of PVP and compounds **Zn41(PVP)**, **Zn44(PVP)**–**Zn46(PVP)** in DMEM at different concentrations. The linear regression graphics plotted the Q-band absorbance versus the concentrations in DMEM.

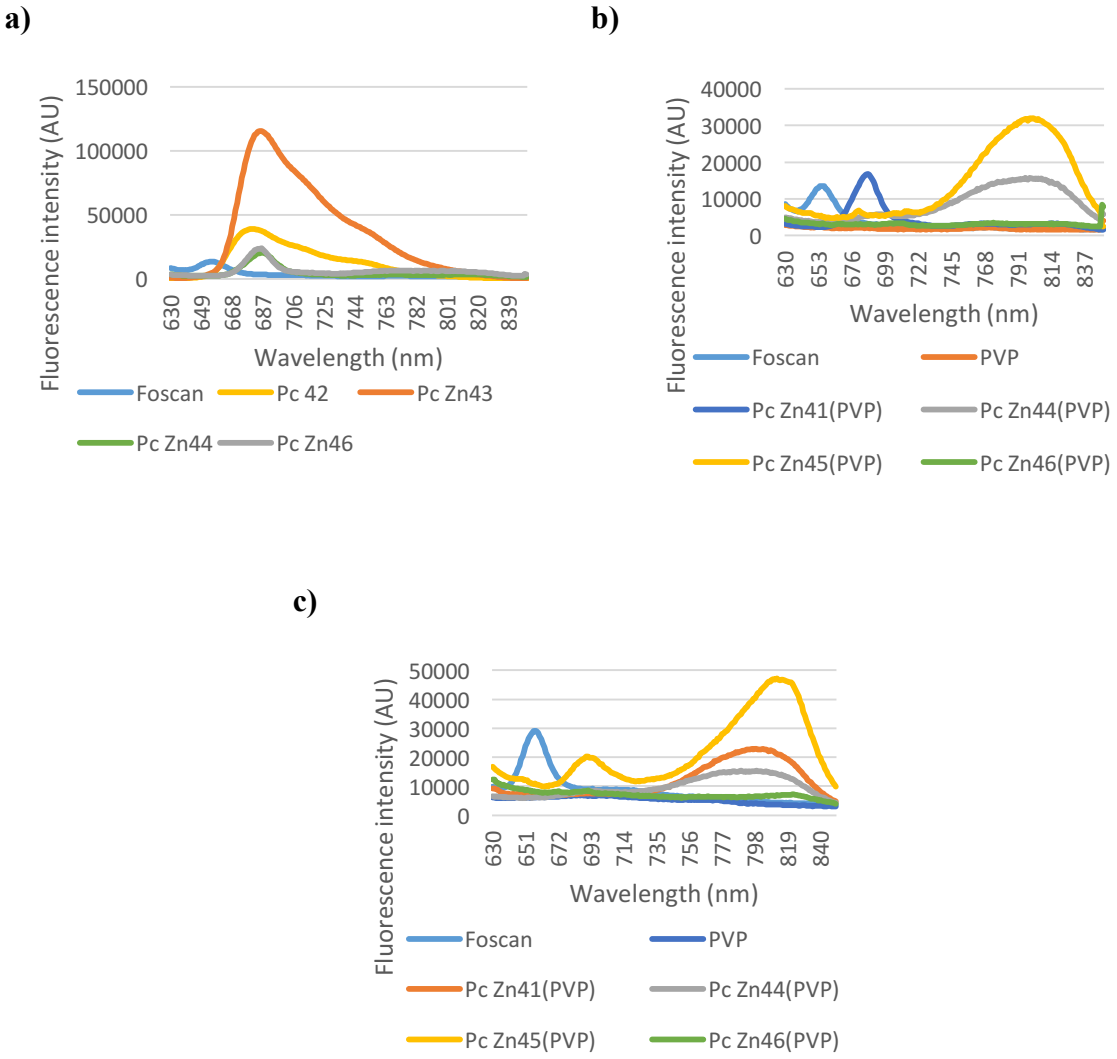

Figure 4.7: Fluorescence spectra in a) DMEM, b) DMEM + 0.08% DMSO, c) water of the Pc–SA conjugates under study (exc.: 610 nm).

The results confirm that all compounds are good singlet oxygen generators, causing a decay of DPBF absorption higher than 90% after 7 minutes of irradiation (Table 4.3). The decay caused by Pc–SA conjugate **42** is higher than for the other Pcs. For phenol red-free DMEM + 0.08% DMSO and DMEM + PVP, as was already described by Liang *et al.*[169] and also observed in the results obtained in the photodynamic inactivation of microorganisms (see chapter 5), it is possible to observe that there is a large enhancement on the efficiency of singlet oxygen production after encapsulation in of Pc–SA conjugates **Zn41(PVP)**, **Zn44(PVP)–Zn46(PVP),** when compared with singlet oxygen generation by the Pcs in phenol red-free + 0.08% DMSO.

Table 4.3: Photooxidation of DPBF by singlet oxygen generated by the Pc–SA conjugates and Pc–SA conjugates encapsulated in PVP micelles.

Sample		**PVP**	**42**	**Zn41**	**Zn43**	**Zn44**	**Zn45**	**Zn46**
DPBF decay (%) (after 7 minutes of irradiation)	**DMF**	nd[a]	99.6	94.8	98.9	99.4	99.0	93.5
	DMEM + 0.08% DMSO	nd[a]	4.0	7.1	0.3	3.1	1.8	3.5
	DMEM + PVP	4.0	nd[a]	68.8	nd	79.9	61.1	73.7

[a]not determined in the encapsulated conjugate

4.2.4 Cellular uptake and accumulation of PSs

Conjugates **42**, **Zn43**, **Zn44**, **Zn46**, **Zn41(PVP)** and **Zn44(PVP)–Zn46(PVP)** were used as PSs in PDT of HSC3 oral squamous cell carcinoma and HaCaT 'normal' keratinocytes, as cellular models (Figures 4.8 and 4.9). The cellular uptake and accumulation of the PSs were assessed after 1, 2 and 4 hours on HSC3 and HaCaT cells. The second-generation PS Foscan was used as a positive control. Foscan was kindly provided from Doctor Alexandre McRobert, University College of London, London.

Comparing the Pc–SA conjugates uptake on the two cell models, a similar pattern can be found. Conjugates **Zn44** and Pc **Zn46** are clearly the PSs with the highest cellular uptake, for both cell lines.

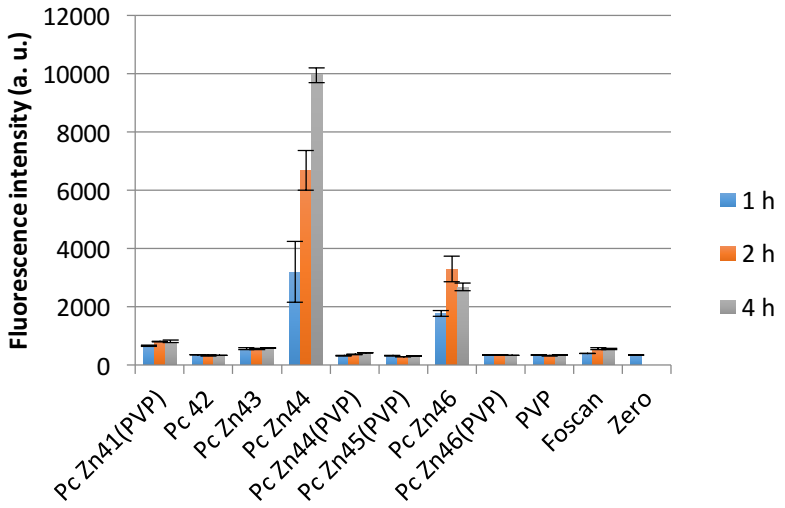

Figure 4.8 Cellular uptake of Pc–SA conjugates **42**, **Zn43**, **Zn44**, **Zn46**, **Zn41(PVP)**, **Zn44(PVP)–Zn46(PVP)** at 1, 2 and 4 hours in HaCaT cells.

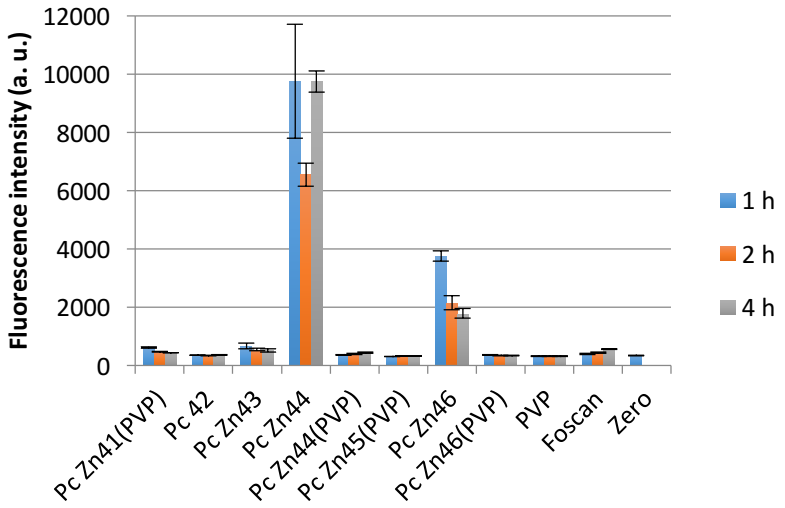

Figure 4.9 Cellular uptake of Pc–SA conjugates **42**, **Zn43**, **Zn44**, **Zn46**, **Zn41(PVP)**, **Zn44(PVP)–Zn46(PVP)** at 1, 2 and 4 hours in HSC3 cells.

4.2.5 Cytotoxicity studies

The effect of the Pc–SA conjugates **42**, **Zn43**, **Zn44**, **Zn46**, **Zn41(PVP)**, **Zn44(PVP)–Zn46(PVP)** on HSC3 and HaCaT cells viability and cell number in the absence of light (dark toxicity - DT) and after PDT treatment (phototoxicity - PDT) were investigated and compared with Foscan. In this section, cells were loaded for 2 h with 0, 3, 10 and 15 μM with the selected PSs.

4.2.5.1 Morphology

After light exposure, microscopic observations of the cell cultures were made. Cell viability was quantified by microscopic observations of the cells under test and controls. A simple, quantitative and preliminary scale was developed in which cell detachment and change in morphology was taking in count. The scale consists on: no toxic (there are no differences in cell detachment or cell morphology when compared to controls), slight toxic (there are some differences on cell detachment when compared to controls), toxic (there are differences in cell detachment and cell morphology when compared to controls) and very toxic (there are unmistakable and sharp differences in cell detachment and cell morphology).

Microscope observations showed that only conjugate **42** produce slight dark toxicity in HaCaT cells in the highest concentration (data not shown). The results of the PDT assays show that only the highest concentration produced toxicity on the two cell models. At the concentration 3 μM, none of the PSs under study produced any obvious dark toxicity.

For Pc–SA conjugates **Zn41(PVP)**, **42**, **Zn43**, **Zn44** and **Zn44(PVP),** light exposure induced toxicity at the highest concentration of PS. A slight toxicity was also observed at 10 μM concentration for Pcs **Zn44(PVP)** and **Zn46(PVP)**. No dark toxicity was observed on HSC3 cells (data not shown). Under light conditions, at the highest PS concentrations, all Pcs under study were cytotoxic and Pcs **Zn43** and **Zn44** were very toxic. At 10 μM Pcs **42**, **Zn43**, **Zn44**, **Zn44(PVP)**–**Zn46(PVP)** also caused cytotoxic effects. Microscope observations of both cell models in the presence of PVP under dark and light condition were also performed but no toxic effects were detected.

With these results it is possible to highlight Pc–SA conjugates **Zn44** and **Zn45(PVP)** as phototoxically selective for HSC3 cells.

4.2.5.2 Cell viability

Cell viability was quantified by MTS assay and the results were expressed as a percentage of the total cell population (Figures 4.10-4.12).

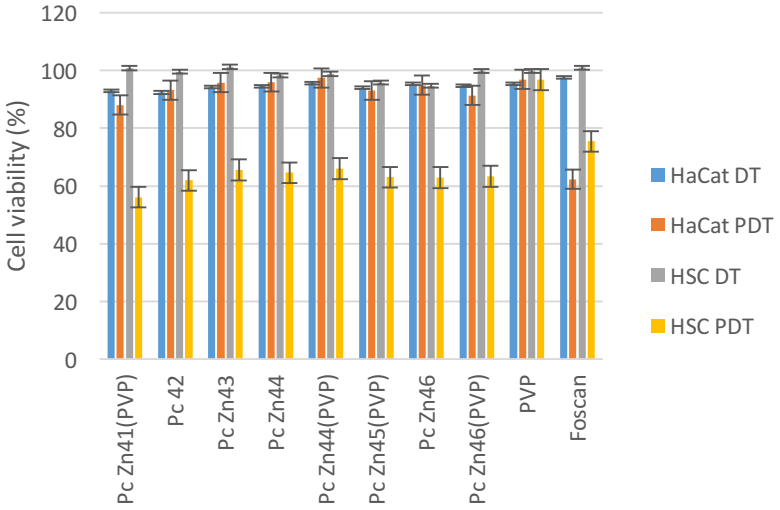

Figure 4.10: Dark toxicity and phototoxicity effect of Pc–SA conjugates **42**, **Zn43**, **Zn44**, **Zn46**, **Zn41(PVP)**, **Zn44(PVP)–Zn46(PVP)** and **PVP**, and the positive control **Foscan** on HSC3 and HaCaT cells viability at 3 μM concentration.

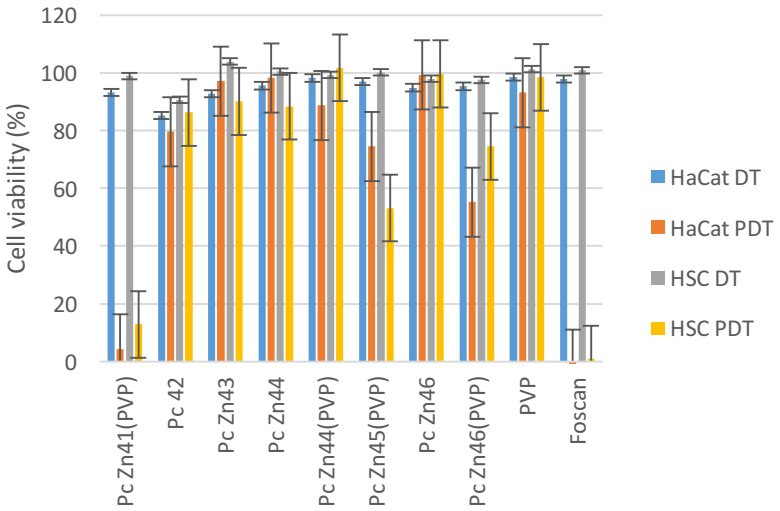

Figure 4.11: Dark toxicity and phototoxicity effect of Pc–SA conjugates **42**, **Zn43**, **Zn44**, **Zn46**, **Zn41(PVP)**, **Zn44(PVP)–Zn46(PVP)** and **PVP**, and the positive control **Foscan** on HSC3 and HaCaT cells viability at 10 μM concentration.

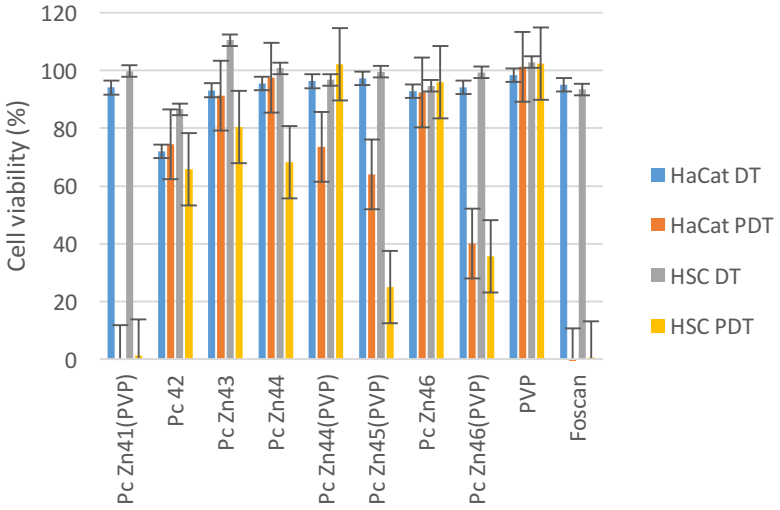

Figure 4.12: Dark toxicity and phototoxicity effect of Pc–SA conjugates **42**, **Zn43**, **Zn44**, **Zn46**, **Zn41(PVP)**, **Zn44(PVP)–Zn46(PVP)** and **PVP**, and the positive control **Foscan** on HSC3 and HaCaT cells viability at 15 μM concentration.

In the dark, the treatment of HSC and HaCaT cells with 3, 10 and 15 μM of the Pc–SA conjugates under study did not affect cell viability over a period of 2 hours duration, compared with no Pc control in the dark. Under white light, at 3 μM concentration, it is not observed for all Pc–SA conjugates under study large differences when compared with the dark for HaCaT cells, suggesting that there is a cytotoxic selectivity at this concentration for HSC3 cells. At 10 and 15 μM **Zn41(PVP)** was highlight as very cytotoxic for both cells under study. Pc–SA conjugates **Zn45(PVP)** and **Zn46(PVP)** also caused a decrease in cells viability.

4.2.6 Carbonic anhydrase assay

In the presence of encapsulated Pc–SA conjugate **Zn41(PVP)**, a lower pH variation was observed when compared with standard activity control (Figure 4.13), meaning that it is taking place a decrease of CA activity. So, with this result is suggested that **Zn41(PVP)** is working as an inhibitor of this enzyme. On the other hand, the higher CA activity (indicated by the higher value of ΔpH) was observed for conjugate **Zn45(PVP)**.

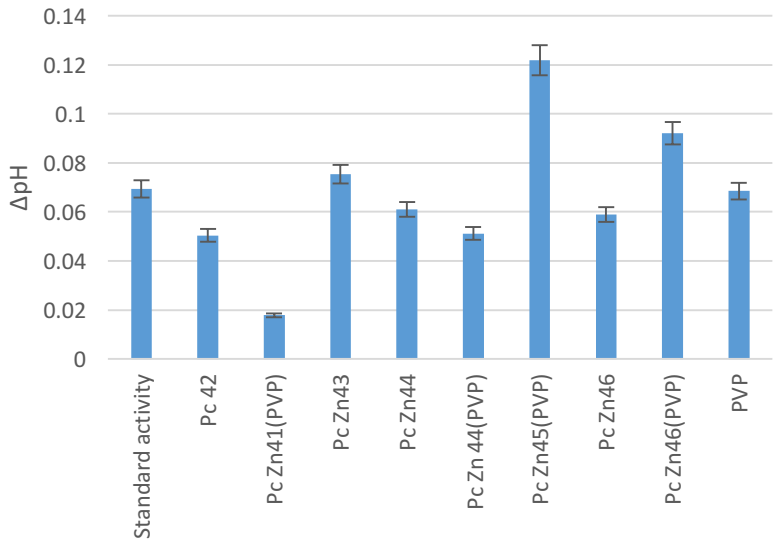

Figure 4.13: Carbonic anhydrase assay results for Pc–SA conjugates **42**, **Zn43**, **Zn44**, **Zn46**, **Zn41(PVP)**, **Zn44(PVP)–Zn46(PVP)** and **PVP** at 15 μM concentration. Results are shown as the ΔpH for the same red cells extract total protein quantity.

4.3 Discussion

PSs with SAs have been recently tested.[227–229] For this work, Pc–SA conjugates were developed and their photophysical properties and possible applications were evaluated.[61,62] The aim of this study was to evaluate the PDT efficiency of these compounds (**42**, **Zn43**, **Zn44**, **Zn46**, **Zn41(PVP)**, **Zn44(PVP)–Zn46(PVP)**) using HSC3 oral squamous cell carcinoma and HaCaT 'normal' keratinocytes as cell models. Furthermore, we also intended to evaluate the activity of these compounds, in particular the SA moiety, as modulators of CA activity.

Aggregation of Pcs in aqueous media is well-known in Pc chemistry.[3] Photosensitization efficiency of Pcs changes dramatically as a result of aggregation. Therefore it is important to evaluate the aggregation behaviour of the Pcs under study. Aggregation have been examined in DMSO, phenol red-free DMEM + 0.08% DMSO and phenol red-free DMEM. As expected, the best aggregation results were obtained for PVP-encapsulated Pc–SA conjugates in DMEM, in which an effective decrease on aggregation is observed. This decrease in the aggregation can be due to a monomerization state of the Pcs molecules increasing the solubility in aqueous medium (DMEM). This phenomenon have already been observed in other studies.[169]

Furthermore, an increase in singlet oxygen generation was also observed, due to the better homogenization of the solution.

In the *in vitro* assay, using equimolar concentrations (3, 10 and 15 μM) of each compound and standardized illumination conditions (10 J/cm^2 halogen white light), it was evident that **Zn41(PVP)** was the most cytotoxic to HSC3 oral squamous cell carcinoma and HaCaT 'normal' keratinocytes. These results are in line with the ones obtained for the well-known PS (positive control) Foscan, especially for the PS concentration of 15 μM. Furthermore, this conjugate (**Zn41(PVP)**) was the PS that showed the lowest uptake values. For the same concentration and time light exposure, **Zn41(PVP)** was the PSs that shown the highest cytotoxicity for the lowest uptake, resulting in the most effective PS under study.

For the CA assay, the compounds under study were compared with a standard activity which was obtained by the exposure of the enzyme lysate with the subtract (CO_2) without the presence of any compound. From this study Pc **Zn41(PVP)** was highlighted as the compound that caused lowest differences in pH and therefore the one with higher capability to reduce the activity of the enzyme CA.

In addition, it was also possible to highlight PVP-encapsulated conjugate **Zn45(PVP)** as the compound that caused the higher difference in pH. Since we obtained for **Zn45(PVP)** a high variation in PVP. These results suggest that **Zn45(PVP)** as CA activator properties.

From these results, conjugate **Zn41(PVP)** showed the higher cytotoxicity effect for the lowest uptake, probably due to the additive effect of the photodynamic effect of the Pc and the inactivation effect of the enzyme CA by the SA present in this compound.

4.4 Conclusions

This study highlights, for the first time, the potential of Pc–SA conjugates as PSs for PDT. It was also possible to evaluate the difference in aggregation, and consequently singlet oxygen production, of some of these compounds without PVP and encapsulated in PVP micelles in phenol red-free DMEM. **Zn41(PVP)** was the conjugate with the highest cytotoxicity effect for HSC3 oral squamous cell carcinoma and HaCaT 'normal' keratinocytes. This result can be explained by the capacity of this compound,

through the SA moiety, to inactivate the enzyme CA as shown in the enzymatic assay conducted in this study.

As already mentioned, this is an ongoing work in collaboration with the group of Doctor Jon Golding from the Health Sciences, Faculty of Science, Technology, Engineering & Mathematics, The Open University, Milton Keynes, and Doctor Etelvina Figueira from the Biology Department, University of Aveiro. The relation between PDT efficacy and CA inhibition is still being studied. After these final experiments, these results will be integrated in an article that will be submitted for publication.

This work opens a new window for further work in the future. New SA moieties can be study in order to better adjust SA structure–inactivation effect in CA activity. Furthermore, different Pcs properties and drug delivering vehicles can be explored.

Chapter 5 Photodynamic inactivation of Gram-negative and Gram-positive bacteria with phthalocyanine–sulfonamide conjugates

SAs are frequently used as antimicrobials[230–232] acting by inhibition of the enzyme DHPS in the folic acid pathway. Antimicrobial SAs exhibit a broad spectrum of action, covering all organisms that have to synthetize *de novo* folic acid through the folate biosynthetic pathway.[4] This biosynthetic pathway is present in plants, fungi, certain protists, most bacteria and, crucially, it is absent in mammals,[4] which makes the folate pathway attractive as an antimicrobial drug target. In recent years SAs have also been tested as inhibitors and activators of different enzymes in different biological systems.[90,233–247]

Considering that unsubstituted Pcs are generally not soluble in water and in most organic solvents, several strategies to overcome this disadvantage have been developed, such as the fine-tuning *via* the addition of suitable substituents, which can enhance the solubility[3]. As an alternative, Pcs can be encapsulated in drug delivery vehicles like polymeric micelles, conjugated polymer nanoparticles or inorganic nanoparticles. Water-soluble PVP micelles are one of these types of drug vehicles that have been successfully used in many studies.[153–155,157–159,169,248]

Considering the potential of Pcs as PSs and SAs as antimicrobial molecules, with this work we intended to use Pc–SA conjugates, either in solution or encapsulated in PVP micelles, as PSs for photodynamic antimicrobial therapy, taking advantage of the additive effect of the two components of the PS molecule and of the encapsulation system.

The efficiency of Pc–SA conjugates in the photodynamic inactivation of Gram-negative (*Escherichia coli*) and Gram-positive (*Staphylococcus aureus*) bacteria was evaluated. Zinc Pc–SA conjugates with simpler structures (*N*,*N*-diethylsulfonamide, *N*-isopropylsulfonamide, methoxylsulfonamide) caused stronger inactivation than Pcs with heterocyclic structures (thiazol-2-ylsulfonamide) or long chains (dodecylsulfonamide), in both bacteria. Furthermore, the encapsulation within PVP polymeric micelles, used as drug delivery vehicles, enhanced the inactivation efficiency. As already discussed, the results show that encapsulated Pc–SA conjugates are a promising class of PSs to be used in photodynamic antimicrobial therapy.

The compounds used in this work are described in Scheme 5.1. The synthesis of these compounds and encapsulation in PVP micelles are described in chapter 3.

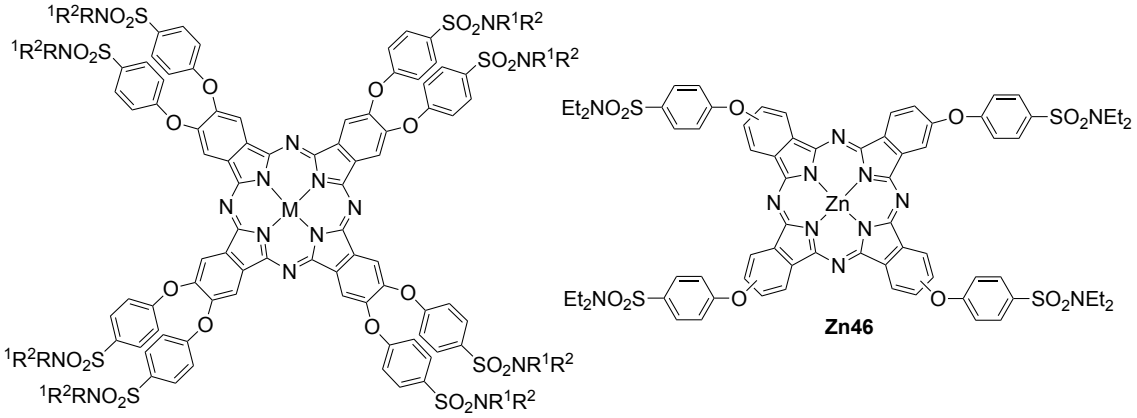

41: M = 2H, NR^1R^2 = NEt_2
42: M = 2H, NR^1R^2 = NH(*i*-Pr)
44: M = 2H, NR^1R^2 = NH(4-$MeOC_6H_4$)
Zn41: M = Zn, NR^1R^2 = NEt_2
Zn42: M = Zn, NR^1R^2 = NH(*i*-Pr)
Zn43: M = Zn, NR^1R^2 = NH-thiazol-2-yl
Zn44: M = Zn, NR^1R^2 = NH(4-$MeOC_6H_4$)
Zn45: M = Zn, NR^1R^2 = NH-dodecyl

Scheme 5.1: Photosensitizer used in this study

5.1 Introduction

PDI has been studied during the last decade as an approach for the inactivation of pathogenic microorganisms, in order to circumvent the problem of drug resistance.[18]

The first observation of photo-toxicity against microorganisms was in 1900 when Oskar Raab observed that the toxicity of acridine hydrochloride against *Paramecium caudatum* was dependent on the amount of light.[176] In addition, his teacher Hv Tappeiner also reported that the toxic effects in the presence of light are not due to heat, and after further experiments, light was excluded as the main influence factor.[46] Additional investigations demonstrated that oxygen is the crucial molecule in the inactivation of bacteria because the antibacterial activity of fluorescent dyes against the facultative anaerobic species *Proteus vulgaris* could not be demonstrated in the absence of oxygen.[249]

Since the discovery of antibiotics, in the middle of the last century, antimicrobial photodynamic therapy was put aside. However, after the worldwide rise in antibiotic resistance, PDI re-emerged as alternative to these drugs.

In order to follow the process of photodynamic inactivation of bacterial pathogens, different methods were developed. The more conventional methods

frequently involve *in vivo* animal sacrifice, removal of the infected tissue, homogenization, serial dilution, plating and colony counting. *In vitro*, the studied organism is cultured in liquid media, after irradiation an aliquot is planted in solid media, and the colonies are counted. Colony-counting method is still commonly used nowadays. Bioluminescence-based methods have emerged has reliable, fast, sensitive, and effective options. These methods only allow the detection of active or viable cells and do not need administration of substrates to obtain light emission.[250,251]

Bioluminescence consists on the process of visible light emission by living organisms through the intervention of an enzyme catalyst. With this method, an indirect assessment of cell viability is made by the measurement of the intensity of bioluminescence. This method is usually used to monitor PDI.[250–255]

The resistance of Gram-negative bacteria to photosensitization by macrocyclic dyes as Pors or Pcs is still an important challenge to antibacterial PDI. In 1880, Christian Gram classified bacteria as Gram-positive or Gram-negative, due to their different staining on Gram staining. The difference in staining is due to structural differences on bacteria outer cell membrane of the wall (Figure 5.1a). Gram-positive bacterial cell is thicker (15-80 nm) than the Gram-negative ones. The first one contains up to 100 peptidoglycan layers and a small quantity of lipids or proteins. Gram-positive bacteria wall presents a rather high degree of porosity. This way, several macromolecules from 30 to 57 kDa can easily diffuse to the inner plasma membrane. On the other hand, Gram-negative bacteria (Figure 5.1b) wall has an additional layer, the outer membrane, external to the peptidoglycan layer, presenting an asymmetric lipid structure composed by strongly negative charged lipopolysaccharides, phospholipids, lipoproteins and proteins. In this type of bacterial cell, only relatively hydrophilic compounds with molecular weight lower than 600-700 Da can diffuse through the porin channels. Thus, Gram-negative outer membrane is a very effective permeability barrier that confers resistance against host cellular and humoral defence factors.[76,256] Cationic PSs have provided promising results by establishing electrostatic interactions with negatively charged sites of the outer membrane. Some compounds, such as ethylenediaminetetraacetic acid (EDTA) or polymixin B nanopeptide have been used to enhance the activity of neutral or anionic PSs by altering and disorganizing the outer membrane and enhancing the penetration of PSs to inner cell compartments. The attachment of poly-*L*-lysine chains to the PS has also been tested, since this

oligopeptide is positively charged at physiological pH and dramatically increases the ability of photodynamic inactivation of Gram-negative bacteria.[257–259]

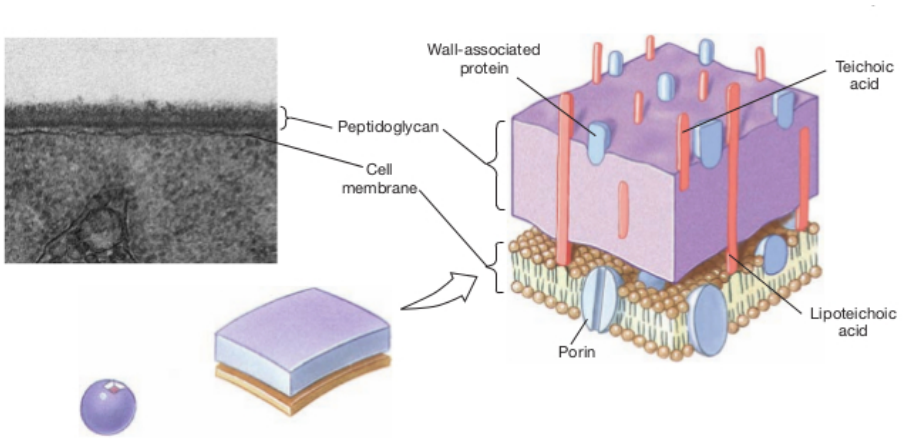

a) Gram-positive

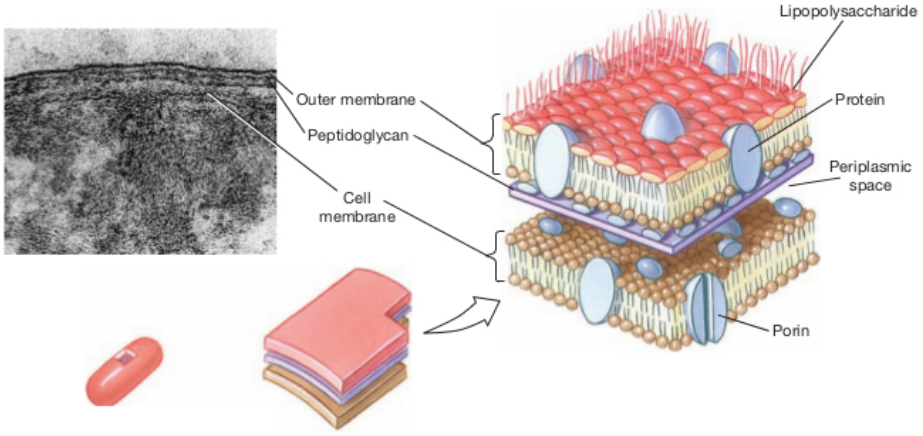

b) Gram-negative

Figure 5.1: Schematic representation of bacteria cell wall(adapted from Black *et al.*[260]).

5.1.1 Applications of microbial photodynamic inactivation

In 2009, Alves *et al.*[261] reported the effect of PS charges on the efficiency of PDI of Gram-negative and Gram-positive bacteria with cationic meso-substituted Pors. In this study, the Gram-positive model *Enterococcus faecalis* and the Gram-negative model *Escherichia coli* were used. The number of positive charges and charge distribution in Pors' structure seems to have an important influence on the PDI efficiency of both bacterial models. In that study, Alves and co-workers were also able to identify the cationic Por Tri-Py^{+}-Me-PF as the most efficient PS. In 2010,[262] the same

group used the cationic Por Tri-Py^{+}-Me-PF against *Vibrio fisheri* and recombinant bioluminescent strain of *Escherichia coli*. With this study, Tavares and coworkers showed that the PS Tri-Py^{+}-Me-PF can be a promising option for efficiently destroying Gram-negative bacteria.

Tri-Py^{+}-Me-PF was also used against non-enveloped virus (bacteriophages) with promising results.[263] Using cationic ZnPcs, Soncin *et al.*[264] achieved inactivation of both wild-type and methicillin-resistant *Staphylococcus aureus* strains. These PSs, in 0.1 μM concentration, showed to be efficient photoantimicrobial agents by causing a 4-5 log decrease in bacterial viability upon short irradiation times. Furthermore, by carefully adjusting experimental parameters to low Pc concentrations and low light doses, Soncin and co-workers were able to conclude that it is possible to inactivate these pathogens without damaging host tissues, taking human fibrosarcoma cells and keratinocytes as host models for skin and mucosa.

As already mentioned, Pcs can be substituted in order to fine-tune their properties. Concerning PDT and PDI, Pcs must be properly substituted with specific molecules with affinity to cell targets. SAs will be described in the next section as possible substituents of Pcs.

5.1.2 Sulfonamides as DHPS inhibitors

A SA moiety can be found in several groups of drugs. Still, the primary clinical application of these compounds is as antimicrobial agents.

Every single cell, whether prokaryotic or eukaryotic, requires reduced folate cofactor for the biosynthesis of a diverse range of cellular components. Tetrahydrofolate is an important carbon donor in a variety of biosynthetic processes through the formation of methionene, purines and thymine. Furthermore, tetrahydrofolate can be used as cofactor in many reactions, especially in the metabolism of amino acids and nucleic acids, and in degradative reactions as acceptor of one carbon unit. In spite of being a universal requirement, the way cells obtain folate differs between prokaryotes and eukaryotes. Unlike plants and most microorganisms, in which folate must be synthesized through the folate biosynthesis pathway, mammals possess an active transport system making them resistant to any compound that disrupts the folate pathway. This difference between mammals and microorganisms in obtaining folate is very important in the design of antimicrobial drug targets.[4]

Folate biosynthetic pathway (Scheme 5.2) consists of the transformation of guanosine triphosphate (GTP) in 7,8-dihydrofolate in six enzyme-catalyzed steps. In the first step, GTP is converted in 7,8-dihydroneopterin triphosphate by the enzyme GTP cyclohydrolase I, which forms the pterin. Next, there is a cascade of kinase, aldolase and pytophosphokinase step adding by the production of an activated pyrophosphorylated intermediate (6-pyrophosphomethyl-7,8-dihydropterin – DHPPP). In the fifth step, DHPS catalyzes the formation of a C-N bond (7,8-dihydropteroate) by joining the pterin ring moiety to *p*ABA. Finally, with addition of a *L*-glutamate moiety to 7,8-dihydropteroate, the synthesis of 7,8-dihydrofolate is completed, which will after be transformed in tetrahydrofolate by the enzyme dihydrofolate reductase (DHFR).[4]

SAs with antimicrobial effect were the first drugs which could be used systematically to selectively act on bacteria. They act as structural analogues of *p*ABA and appear to be competitive inhibitors of the enzyme DHPS. It has been shown that SAs can act as alternative substrate for DHPS effectively depleting the folate pool and in that way, inhibit cell growth. Therefore, SAs act as bacteriostatic agents, inhibiting the growth and multiplication of bacteria. Furthermore, the final enzyme of the pathway, DHFR, can be inhibited by diaminopyrimidine antibiotics. In some cases, clinical treatment uses a combination of both SA and diaminopyrimidine antibiotics. To give an example, a combination of SA and trimethoprim (a diaminopyrimidine) was used to treat urinary tract infections.[4] This combination overcame the problem of target organism resistance, although nowadays some resistance to this combined therapy has also been observed.[265]

DHPS crystalline structure has been solved from *E. coli*, *S. aureus*, and *M. tuberculosis*, and adopts a classic TIM2 barrel fold, consisting of an eight-stranded central parallel β-sheet, bounded by α-helices (Figure 5.2). DHPS structure is a ternary complex, in which analogues of pterin substrate, like SA or sulfanilamide, can bind in the active site. The active site is located at the C-terminal end of the central β-sheet.[4]

The binding site of DHPP is well identified by ligand soaking and co-crystallization studies. In his pocket, DHPP is rotated in a way that its ring system sits parallel with the axis plane of the eight-stranded beta-sheet binding with hydrophilic residues (Asp66, Asn115, Asp185 and Lys221, *E. coli* sequence numbering). On the other hand, structural information on the second substrate, *p*ABA, is more limited. It is known that *E. coli* DHPS will use SAs and sulfanilamide as substrates, forming

dihydropterinsulfonamide products.[4] The crystal structure of ternary complex of these bindings was reported by Achari *et al.*.[266]

The folate pathway is a validated target for antibacterial drugs. Recent structural information obtained specially for DHPP binding site has been important to correlate structural binding sites modifications with resistance to SAs. SA resistance mutation, in the *dhps* gene from several pathogenic organisms, has been mapped as alteration on the residues surrounding the binding sites of both substrates. In different organisms, the mutation is concentrated in Loop2, which appears to play a role in recognition of the pyrophosphate moiety in 6-hydroxymethyl-7,8-dihydropterin pyrophosphate (DHPPP). Furthermore, in bacteria like *E. coli* and *N. meningitidis* resistance mutation have been observed of a single Phe to Leu or Ile in Loop1. This alteration will not directly alter substrates binding but will indirectly influence the way substrate binds through interactions with residues in Loop2. Furthermore, alterations in positions within the Loops 4, 5 and 6 have also been associated with resistance mutations.[4]

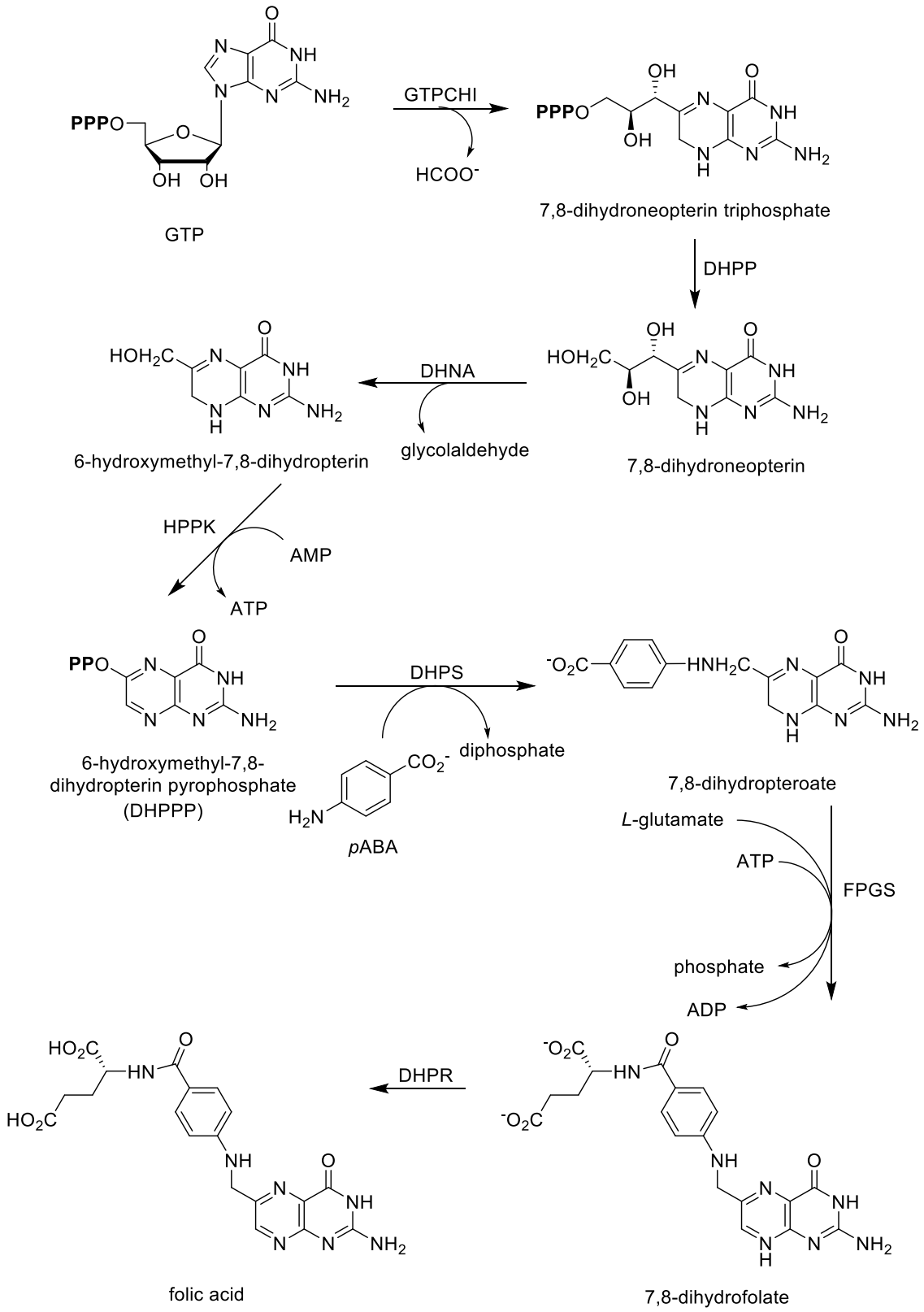

Scheme 5.2: Folic acid pathway.[4]

The SA chemical moiety is also present in other drugs that do not have antimicrobial activity. That is the case of thiazide diuretics, loop diuretics, sulfonylureas, COX-2 inhibitors, antitumoral, anti-inflammatory, among others.[4]

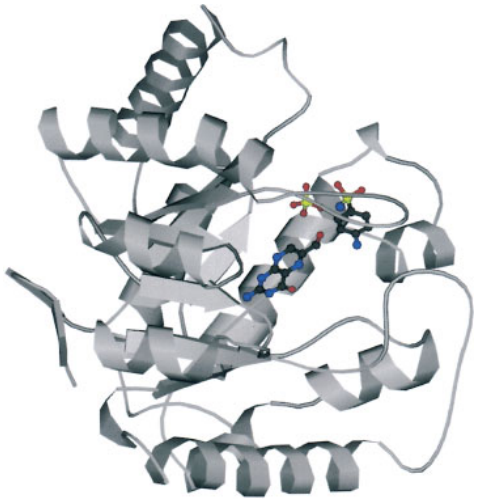

Figure 5.2: DHPS crystal structure.[4]

5.2 Results

In this work, the applicability of Pc–SA conjugates as PSs in the PDI of *E. coli* (subsection 5.2.4) and *S. aureus* (subsection 5.2.5) were evaluated under white and red light. For that, subsection 5.2.3 describes the correlation between bioluminescence and viable counts for the bioluminescent *E. coli* strain. In addition, the solubility (subsection 5.2.1), photostability and singlet oxygen generation (subsection 5.2.2) of the conjugates under studied were assessed.

5.2.1 Phthalocyanine solubility

The solubility of selected Pc–SA conjugates and the corresponding encapsulated in PVP conjugates in DMSO and phosphate-buffered saline (PBS) + 10% DMSO in the case of Pcs and PBS for Pcs(PVP), was analyzed by UV-Vis spectroscopy. The measurements were made in concentrations between 2.5 and 25 μmol/L in order to determine if the Pcs, at this concentration range, follow the Beer-Lambert law. The graphics were obtained by the plotting of the Q-band intensity versus Pc concentration in DMSO. A linear relation was observed for all zinc and metal-free Pcs under study, confirming a low aggregation of these compounds in organic solvents. In PBS + 10% DMSO the relation was not linear.

A similar approach was used to test the solubility of Pc–SA conjugates encapsulated within PVP in PBS. A linear relation was observed for all encapsulated conjugates (Figure 5.3).

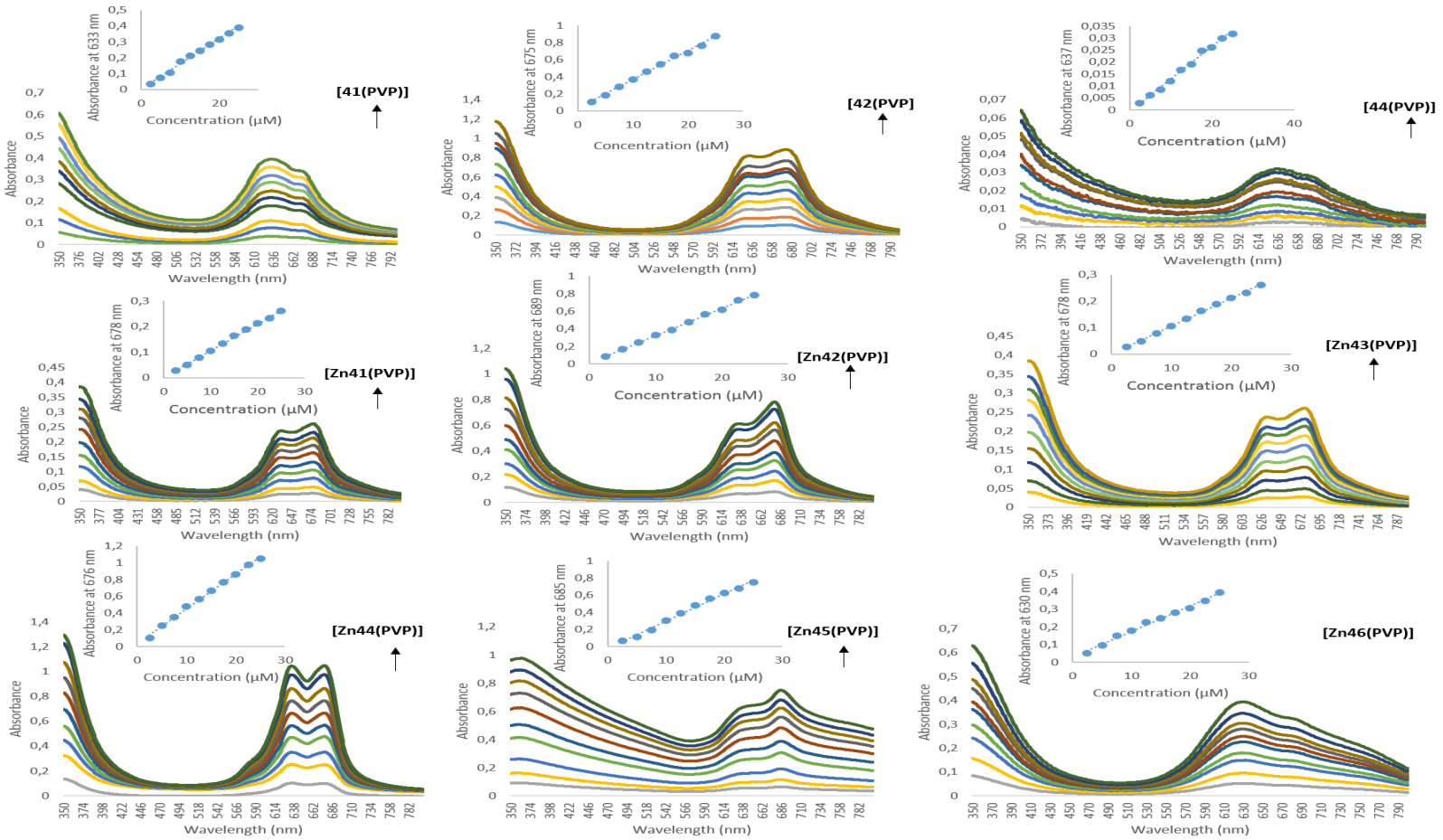

Figure 5.3: UV-Vis spectra of Pc–SA conjugates **41(PVP)**, **42(PVP)**, **44(PVP)** and **Zn41(PVP)–Zn46(PVP)** in PBS at different concentrations. The linear regression graphics plotted the Q-band absorbance versus the concentrations in PBS.

5.2.2 Photostability and singlet oxygen generation

The results of the photostability studies conducted during 30 min with a fluence rate of 150 mW/cm^2 indicated that, in aqueous media and under white and red light, none of the Pcs suffered pronounced changes in the residual absorbance (Table 5.1), and were photostable under the conditions of the experiments.

Table 5.1: Photostability and stability by Pc–SA conjugates and encapsulated Pc–SA conjugates under study. L – Light, D – Dark.

	Photostability and stability (%)								
Compound	**White**		**Red**		**Compound**	**White**		**Red**	
	L	**D**	**L**	**D**		**L**	**D**	**L**	**D**
41	71	71	98	98	**41(PVP)**	98	98	98	98
42	64	65	97	97	**42(PVP)**	95	95	96	96
44	58	58	99	99	**44(PVP)**	89	89	89	88
Zn41	58	58	96	96	**Zn41(PVP)**	94	96	98	95
Zn42	74	74	66	61	**Zn42(PVP)**	99	99	99	99
Zn43	40	45	96	96	**Zn43(PVP)**	87	88	90	95
Zn44	75	75	99	99	**Zn44(PVP)**	96	96	84	84
Zn45	68	69	89	90	**Zn45(PVP)**	65	65	78	78
Zn46	74	74	95	95	**Zn46(PVP)**	97	97	95	97

The results of the evaluation of the singlet oxygen generation by each PS, measured as the photo-oxidation of DPBF when irradiated with light at a fluence rate of 9.0 mW/cm^2, showed that they were able to generate singlet oxygen but in different ranges (Table 5.2). All Pcs in DMF showed a high generation of singlet oxygen. However, in the aqueous medium PBS + 10% DMSO there was a strong decrease of singlet oxygen generation for all Pcs under study. All encapsulated Pc–SA conjugates in

PBS showed a high generation of singlet oxygen and PVP-free samples a low generation of singlet oxygen.

Table 5.2: Relative photo-oxidation of DPBF by singlet oxygen generated by Pc–SA conjugates and encapsulated Pc–SA conjugates.

Compound	DPBF decay (%)[b]		
	DMF	PBS + 10% DMSO	PBS + PVP
PVP	nd[a]	nd[a]	nd[a]
41	92.7	0.9	68.1
42	95.9	3.5	73.7
44	92.3	4.1	58.6
Zn41	94.8	5.3	78.9
Zn42	99.6	1.0	80.1
Zn43	98.9	4.9	84.9
Zn44	99.4	4.7	77.5
Zn45	99.0	5.2	91.0
Zn46	93.5	6.2	70.5

[a]not determined, [b]after 7 minutes of irradiation.

5.2.3 Relation between bioluminescence and concentration of viable cells

A significant linear correlation between bioluminescence and viable counts for the bioluminescent *E. coli* strain was observed ($R^2 = 0.9526$) (Figure 5.4).

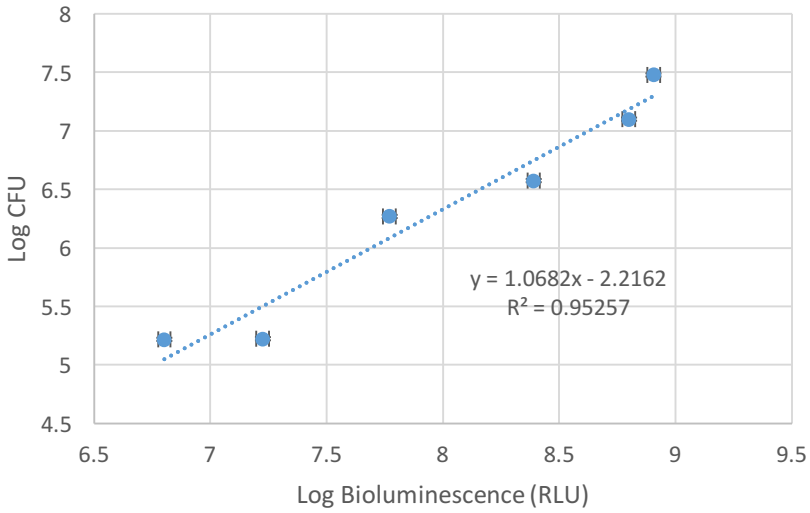

Figure 5.4: Linear correlation between the bioluminescence signal and colony counts of overnight cultures of recombinant bioluminescent *E. coli* serially diluted in PBS. Bacterial counts are expressed in colony forming units (CFU)/ml and bioluminescence in relative light units (RLU).

5.2.4 Photodynamic inactivation of *E. coli*

The results of the photodynamic inactivation experiments showed that the viability of the recombinant bioluminescent *E. coli* was neither affected by light alone (light control) nor by the direct effect of the tested PSs (dark controls).

Significant differences in the inactivation profiles obtained with the different PS were observed (Figures 5.5–5.8).

Upon irradiation with white light in presence of 10 μM of PS (Figure 5.5), **42** and **44** and **Zn41**, **Zn42**, **Zn44** and **Zn46** caused stronger inactivation (3.9, 4.0, 3.7, 3.0, 3.0 and 3.7 logs of reduction in bioluminescence emission, respectively) than **41** and **Zn43** and **Zn45** (1.5, 0.9 and 0.2 logs reduction in bioluminescence emission, respectively), after 180 min of irradiation. The differences between the controls and the test result are significant ($p < 0.05$) for all Pcs (**41**, **44**, **Zn41**–**Zn45** and **Zn46**).

Under red light (Figure 5.6), similar inactivation profiles were obtained with **42** and **44**, and **Zn41**, **Zn42**, **Zn43** and **Zn46**, that caused stronger inactivation (2.9, 2.8, 3.4, 3.7, 2.6 and 4.1 logs of reduction in bioluminescence emission, respectively) than **41** and **Zn43** and **Zn45** (1.8, 0.7 and 0.3 logs reduction in bioluminescence emission, respectively).

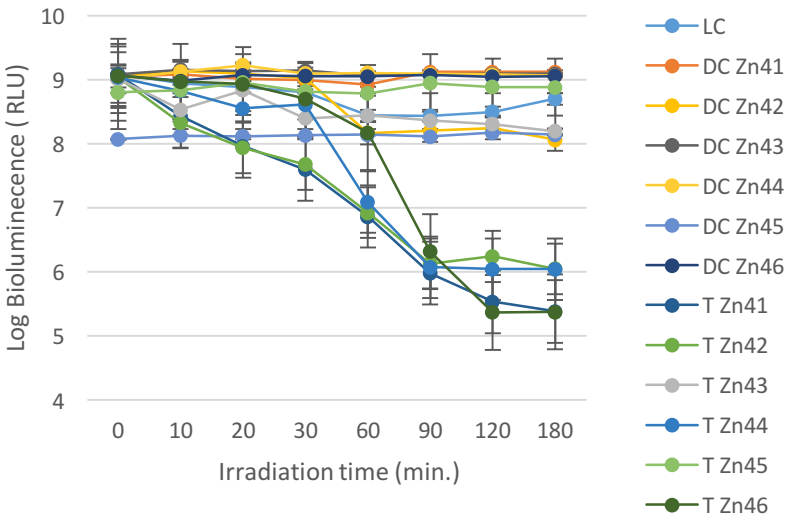

a) ZnPcs

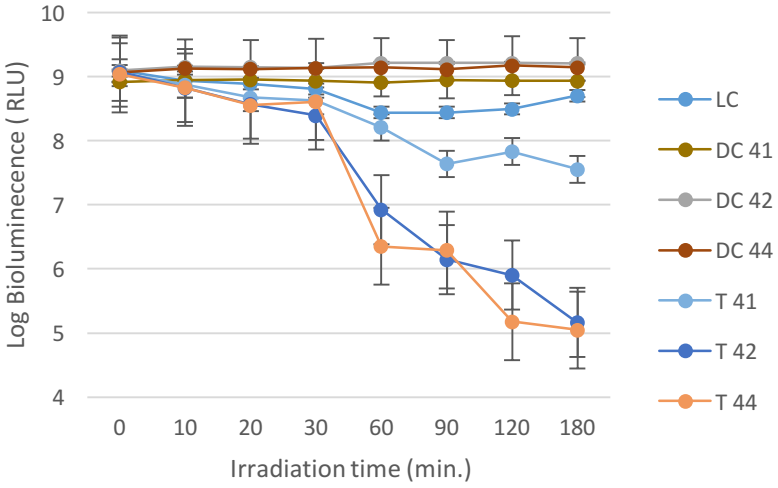

b) 2HPcs

Figure 5.5: Photodynamic inactivation of bioluminescent *E. coli* in the presence of 10 μM of a) ZnPcs and b) 2HPcs under white light (150 mW/cm^2) for 0, 15, 30, 60, 90, 120 and 180 min. Each value represents the average of three measurements in a single assay. LC – Light control; DC – Dark control; T – Test. Error bars indicate the standard deviation. Lines just combine the points. Small bars are overlapped by the symbols.

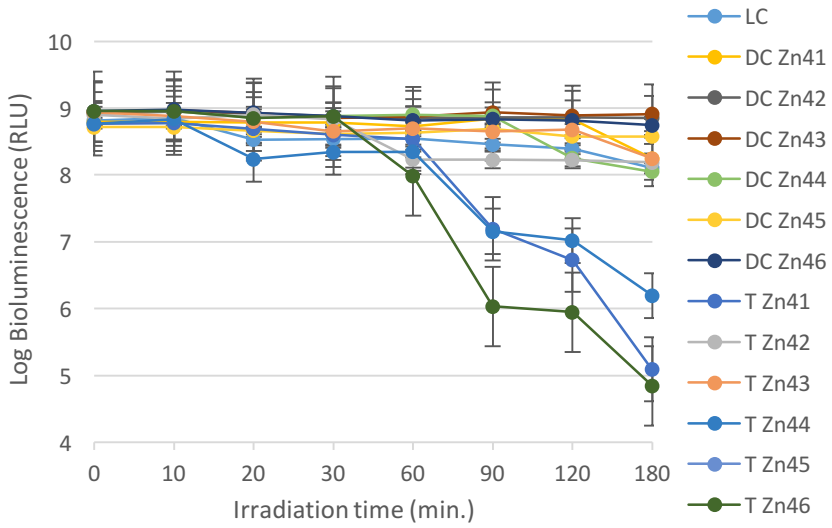

a) ZnPcs

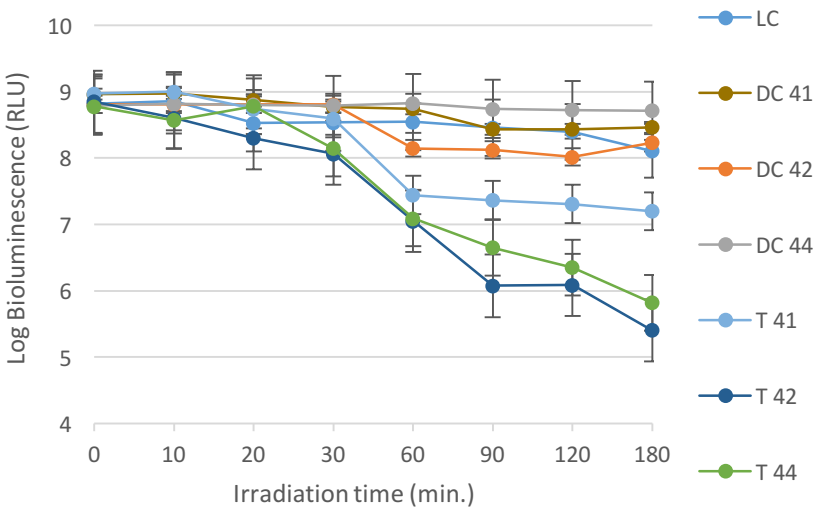

b) 2HPcs

Figure 5.6: Photodynamic inactivation of bioluminescent *E. coli* in the presence of 10 μM of a) ZnPcs and b) 2HPcs under red light (150 mW/cm^2) for 0, 15, 30, 60, 90, 120 and 180 min. Each value represents the average of three measurements in a single assay. LC – Light control; DC – Dark control; T – Test. Error bars indicate the standard deviation. Lines just combine the points. Small bars are overlapped by the symbols.

In the case of **42** and **44**, **Zn42**, **Zn43** and **Zn44** the differences between controls and test are significantly different ($p < 0.05$).

Similarly to what was observed in the concentrations of 10 μM, at 20 μM concentration, the viability of bioluminescent *E. coli* was not affected by the PS, in the dark. Table 5.3 contains a summary of the logarithmic reduction of this Gram-negative bacteria with 20 μM of each PS. Furthermore, **42** and **Zn41**, **Zn42**, **Zn44** and **Zn46** were effective against *E. coli* (Figure 5.7) causing 2.4, 3.0, 3.9, 2.9, 3.2 logs reductions, respectively, after 180 min of exposure to white light. Pcs **41** and **44**, **Zn43** and **Zn45** caused a less pronounced effect (0.0, 0.6, 0.5 and 1.1 logs reduction in bioluminescence emission, respectively). For **42**, **44** and **Zn42**–**Zn44** significant differences between controls and test ($p < 0.05$) were observed.

Table 5.3: Systematization of the results obtained in the photoinactivation of *E. coli* under white and red light at 20 μM.

Reduction (log)	**PVP**	**41**	**42**	**44**	**Zn41**	**Zn42**	**Zn43**	**Zn44**	**Zn45**	**Zn46**
White	nd[a]	0.0	2.4	0.6	3.0	3.9	0.5	2.9	1.1	3.2
White Pc(PVP)[b]	0.1	1.0	0.3	0.6	3.1	4.4	1.1	4.2	2.1	3.6
Red	nd[a]	-0.2	2.2	0.7	4.5	4.0	1.0	3.8	2.2	3.5
***R*ed Pc(PVP)[b]**	-0.5	-0.5	0.4	-0.5	1.9	4.4	-0.4	3.9	0.9	2.0

[a]not determined; [b]Pc(PVP) refers to the encapsulated Pc indicated in the first row of this table.

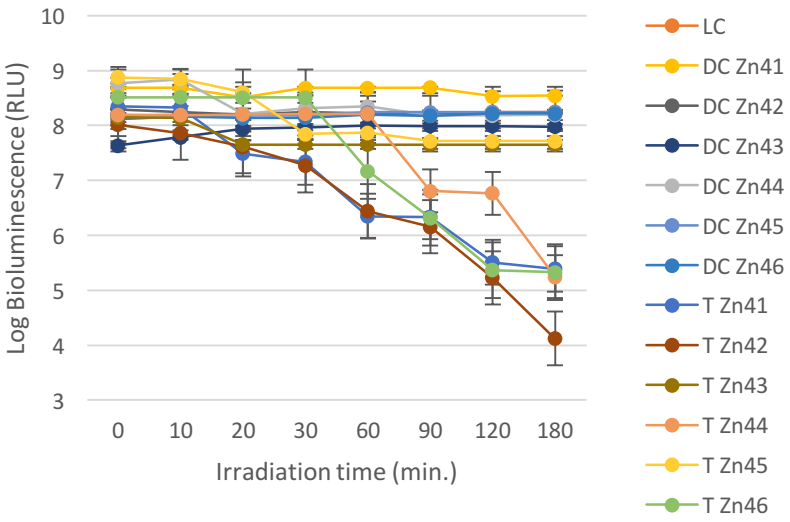

a) ZnPcs

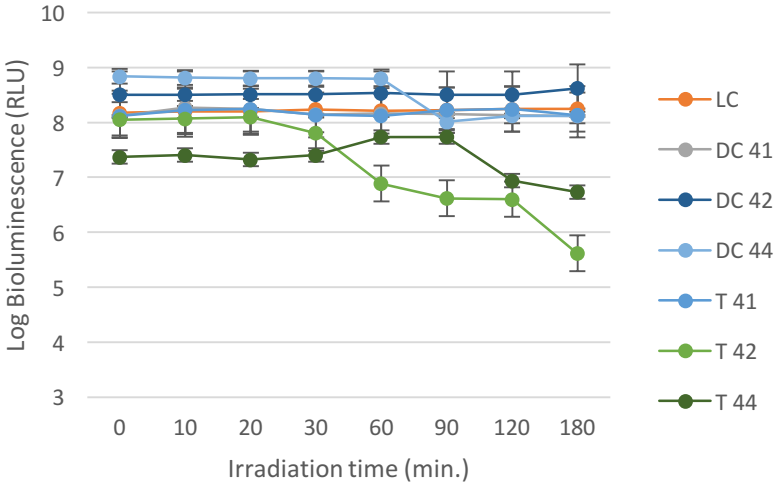

b) 2HPcs

Figure 5.7: Photodynamic inactivation of bioluminescent *E. coli* in the presence of 20 µM of a) ZnPcs and b) 2HPcs under white light (150 mW/cm^2) for 0, 15, 30, 60, 90, 120 and 180 min. Each value represents the average of three independent assays. LC – Light control; DC – Dark control; T – Test. Error bars indicate the standard deviation. Lines just combine the points. Small bars are overlapped by the symbols.

In the assays with red light (Figure 5.8), **42**, **Zn41**, **Zn42**, **Zn44**, **Zn45** and **Zn46** caused 2.2, 4.5, 4.0, 4, 3.8, 2.2 and 3.5 log reductions, respectively. **44** and **Zn43** caused log reductions of 0.7 and 1.0 respectively. Conjugate **41** failed to cause significant inactivation. For **42**, **44**, **Zn43** and **Zn45** there were significant differences for a p value < 0.05.

The results of the assays conducted with the encapsulated Pc–SA conjugates under white light at a 20 μM concentration of PS (Figure 5.9) showed that **Zn41(PVP)**, **Zn42(PVP)**, **Zn44(PVP)** and **Zn46(PVP)** were the most effective (log reductions of 3.1, 4.4, 4.2 and 3.6, respectively), while **41(PVP)**, **42(PVP)**, **44(PVP)**, **Zn42(PVP)** and **Zn45(PVP)** were less effective (1.0, 0.3, 0.6, 1.1 and 2.1 log reductions, respectively). Differences between controls and tests were significant for **44(PVP)** and **Zn41(PVP)–Zn46(PVP)**, considering a p value < 0.05.

Upon irradiation with red light (Figure 5.10), **Zn41(PVP)**, **Zn42(PVP)**, **Zn44(PVP)** and **Zn46(PVP)** caused log reductions of 1.9, 4.4, 3.9, 2.0, respectively and **Zn45(PVP)** was less effective with 0.9 log reductions. Pc–SA conjugates **41(PVP)**, **44(PVP)** and **Zn43(PVP)** failed to inactivate. For **42(PVP)**, **44(PVP)**, and for all encapsulated conjugates significant differences between controls and tests were observed ($p < 0.05$).

PVP (Pc unloaded control) caused a negligible effect either with white or red light.

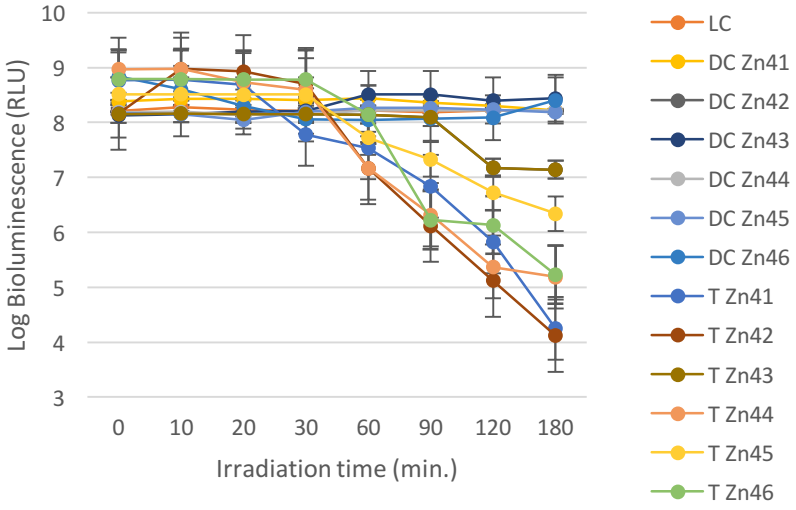

a) ZnPcs

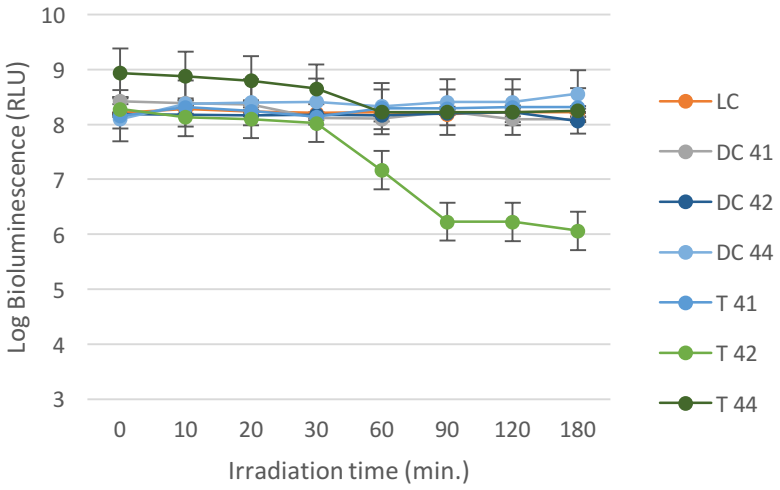

b) 2HPcs

Figure 5.8: Photodynamic inactivation of bioluminescent *E. coli* in the presence of 20 μM of a) ZnPcs and b) 2HPcs under red light (150 mW/cm^2) for 0, 15, 30, 60, 90, 120 and 180 min. Each value represents the average of three independent assays. LC – Light control; DC – Dark control; T – Test. Error bars indicate the standard deviation. Lines just combine the points. Small bars are overlapped by the symbols.

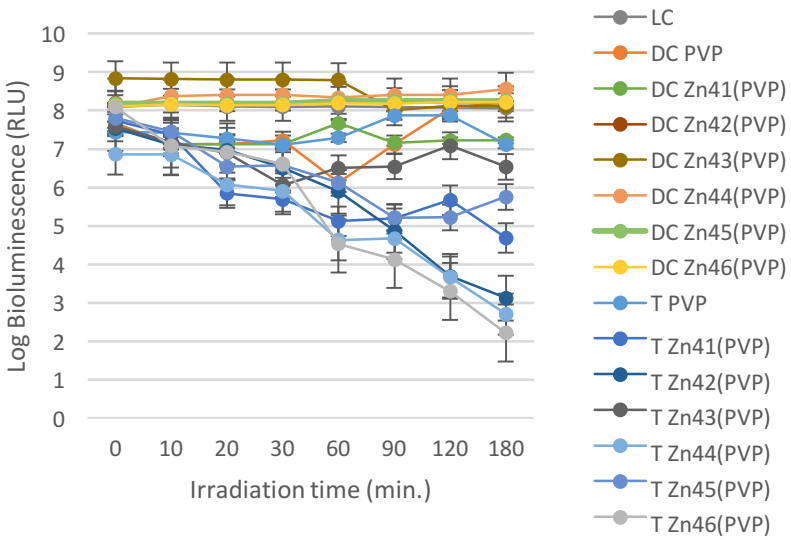

a) ZnPcs(PVP)

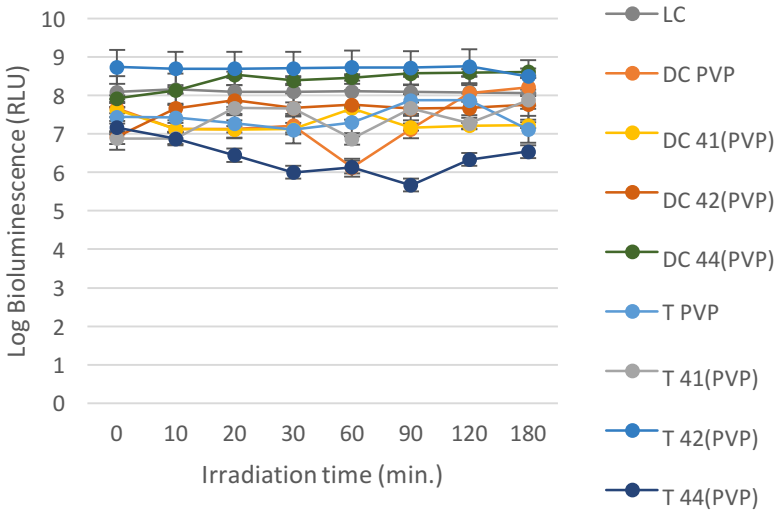

b) 2HPcs(PVP)

Figure 5.9: Photodynamic inactivation of bioluminescent *E. coli* in the presence of 20 µM of a) ZnPcs(PVP) and b) 2HPcs(PVP) under white light (150 mW/cm^2) for 0, 15, 30, 60, 90, 120 and 180 min. Each value represents the average of three independent assays. LC – Light control; DC – Dark control; T –Test. Error bars indicate the standard deviation. Lines just combine the points. Small bars are overlapped by the symbols.

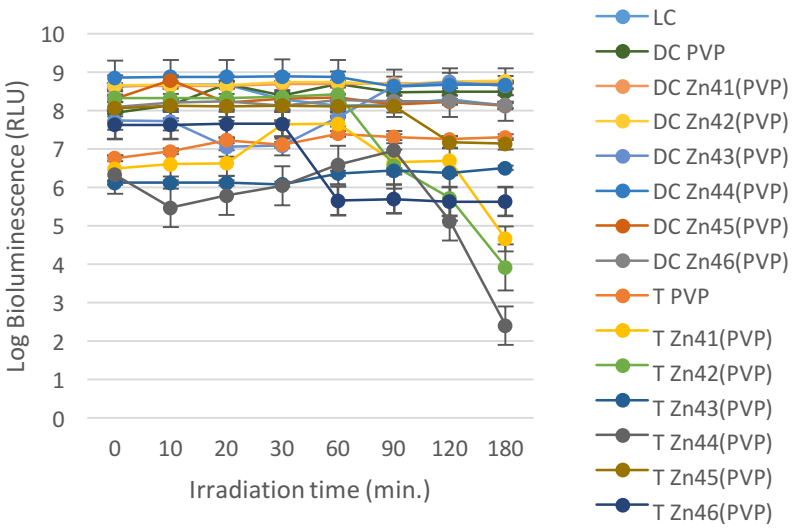

a) ZnPcs(PVP)

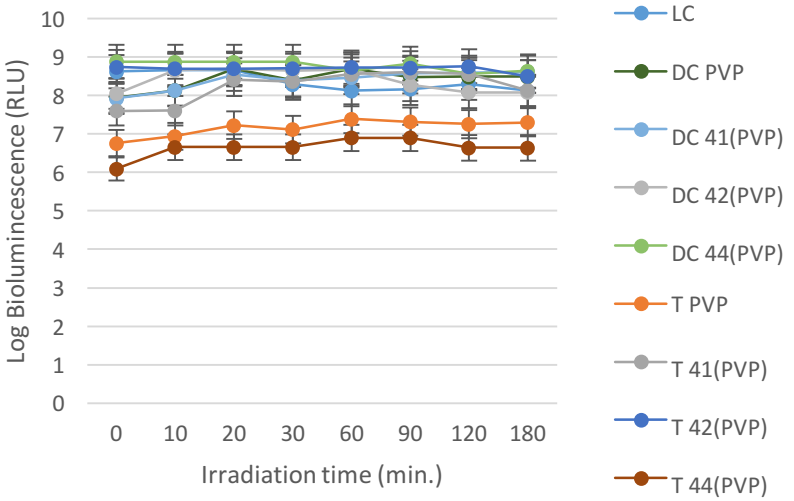

b) 2HPcs(PVP)

Figure 5.10: Photodynamic inactivation of bioluminescent *E. coli* in the presence of 20 µM of a) ZnPcs(PVP) and b) 2HPcs(PVP) under red light (150 mW/cm^2) for 0, 15, 30, 60, 90, 120 and 180 min. Each value represents the average of three independent assays. LC – Light control; DC – Dark control; T – Test. Error bars indicate the standard deviation. Lines just combine the points. Small bars are overlapped by the symbols.

5.2.5 Photodynamic inactivation of *S. aureus*

Inactivation of *S. aureus* was evaluated upon irradiation with white and red light (150 mW/cm^2) for 0, 10, 20 and 30 min, at a concentration of PS of 20 μM, using colony counts as an estimate of cell survival. Similarly to what was observed in the inactivation of bioluminescent *E. coli*, the viability of *S. aureus* was not affected by light alone (light control) nor by the direct effect of the tested PS (dark controls). Such as observed in the assays with *E. coli*, clear differences in the inactivation efficiency of the different PS were observed. The log reductions obtained in the photodynamic inactivation assays with S. aureus are summarized in Table 5.4.

Table 5.4: Systematization of the results obtained in the photoinactivation of *S. aureus* under white and red light.

Reduction (log)	**PVP**	**41**	**42**	**44**	**Zn41**	**Zn42**	**Zn43**	**Zn44**	**Zn45**	**Zn46**
White	nd[a]	4.1	2.9	2.6	7.0	7.9	2.0	6.3	4.1	6.8
White Pc(PVP)[b]	0.5	0.5	0.4	3.0	9.5	9.5	3.2	5.9	5.6	7.9
Red	nd[a]	4.0	3.0	3.3	7.0	7.5	1.0	6.8	3.8	5.1
Red Pc(PVP)[b]	0.3	5.3	3.0	4.3	9.4	9.0	3.8	7.9	4.3	7.1

[a]not determined; [b]Pc(PVP) refers to the encapsulated Pc indicated in the first row of this table.

Under white light (Figure 5.11), **Zn41**, **Zn42**, **Zn44** and **Zn46** caused significantly higher inactivation (7.0, 7.9, 6.3 and 6.8 log reductions, respectively) than **41**, **42**, **44**, **Zn43** and **Zn45** (4.1, 1.9, 2.6, 2.0 and 3.8 log reductions, respectively). The differences between controls and test groups are significant for **42**, **44** and **Zn41**–**Zn45**.

Upon irradiation with red light (Figure 5.12), **Zn41**, **Zn42**, **Zn44** and **Zn46** were more effective (7.0, 7.5, 6.8 and 5.1 log reductions, respectively) than **41**, **42**, **14**, **Zn13** and **Zn45** (4.0, 3.0, 3.3, 1.0 and 3.8, respectively). There are significant differences for **41**, **Zn44** and **Zn46**, considering a p value < 0.05, comparing to the controls.

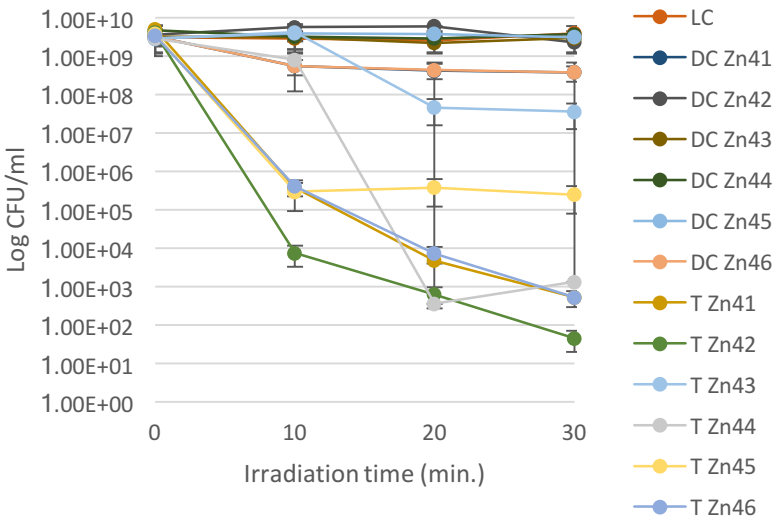

a) ZnPcs

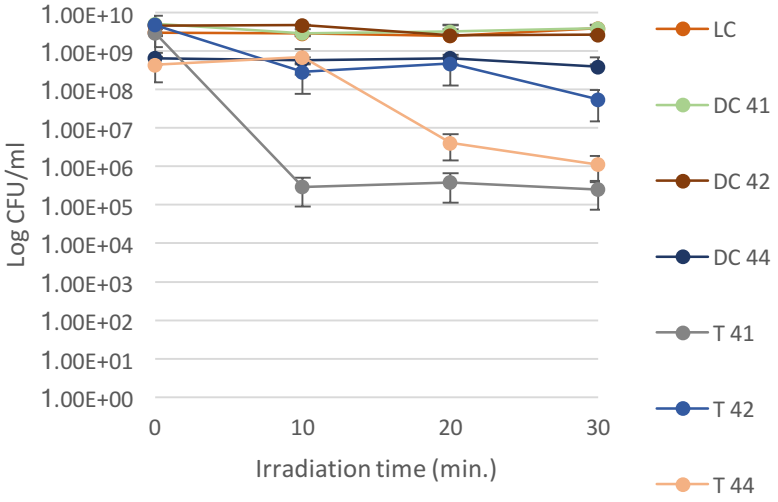

b) 2HPcs

Figure 5.11: Photodynamic inactivation of *S. aureus* in the presence of 20 µM of a) ZnPcs and b) 2HPcs under white light (150 mW/cm^2) for 0, 10, 20, 30 min. Each value represents the average of three independent assays. LC – Light control; DC – Dark control; T – Test. Error bars indicate the standard deviation. Lines just combine the points. Small bars are overlapped by the symbols.

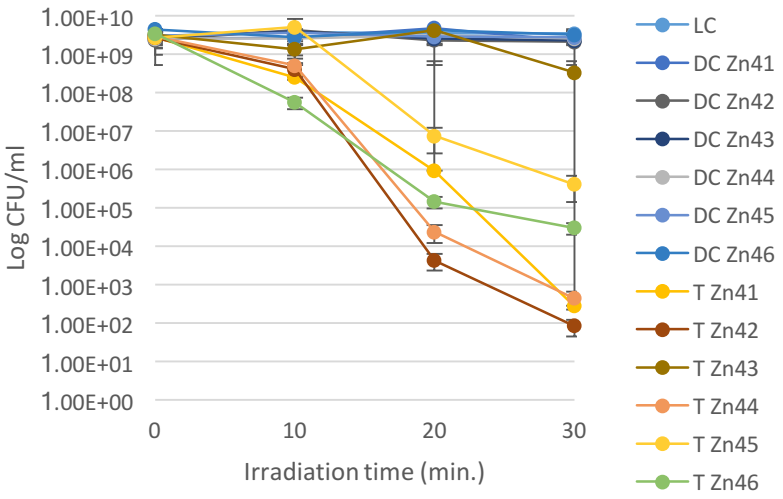

a) ZnPcs

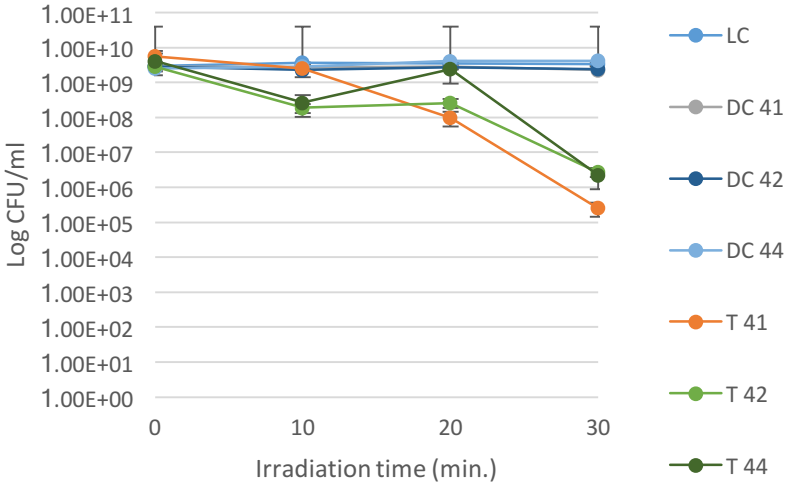

b) 2HPcs

Figure 5.12: Photodynamic inactivation of *S. aureus* in the presence of 20 μM of a) ZnPcs and b) 2HPcs under red light (150 mW/cm^2) for 0, 10, 20, 30 min. Each value represents the average of three independent assays. LC – Light control; DC – Dark control; T – Test. Error bars indicate the standard deviation. Lines just combine the points. Small bars are overlapped by the symbols.

In experiments with white light (Figure 5.13), **Zn41(PVP)**, **Zn42(PVP)**, **Zn44(PVP)** and **Zn46(PVP)** caused 9.5, 9.5, 5.9 and 7.9 log reductions, respectively. Pcs **41(PVP)**, **42(PVP)**, **44(PVP)**, **Zn43(PVP)** and **Zn45(PVP)** showed lower

efficiency than the former, reducing the concentration of viable cells by 0.5, 0.4, 3.0, 3.2 and 5.6 log, respectively. **Zn41(PVP)** showed significant differences between controls and test group considering a p value < 0.05.

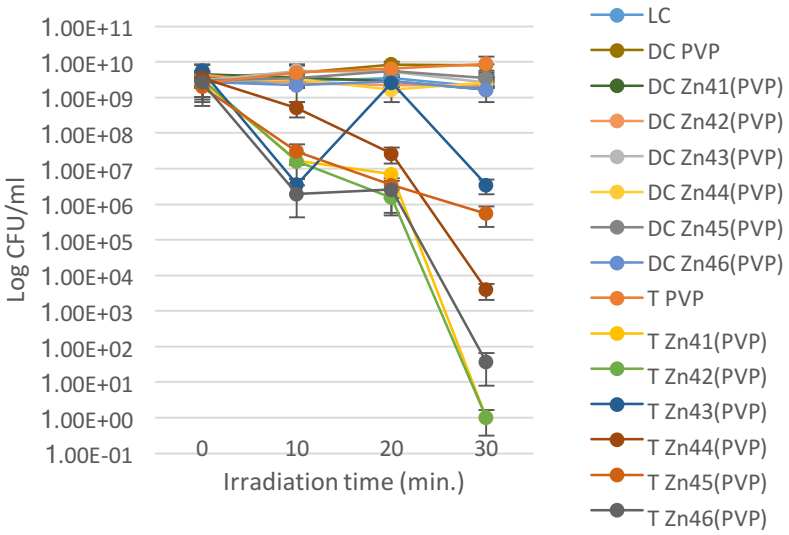

a) ZnPcs(PVP)

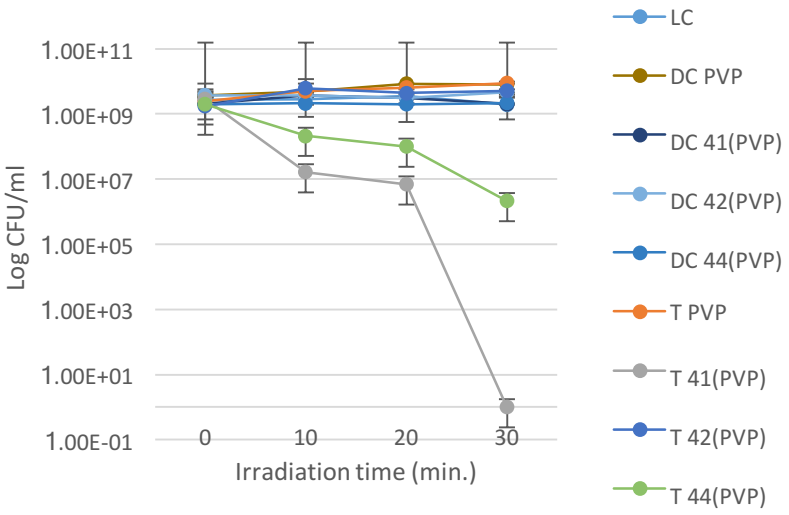

b) 2HPcs(PVP)

Figure 5.13: Photodynamic inactivation of *S. aureus* in the presence of 20 µM of a) ZnPcs(PVP) and b) 2HPcs(PVP) under white light (150 mW/cm^2) for 0, 10, 20, 30 min. Each value represents the average of three independent assays. LC – Light control; DC – Dark control; T – Test. Error bars indicate the standard deviation. Lines just combine the points. Small bars are overlapped by the symbols.

Upon irradiation with red light (Figure 5.14), **Zn41(PVP)**, **Zn42(PVP)**, **Zn44(PVP)** were also the most effective causing significant inactivation of *S. aureus* (9.4, 9.0, 7.9 and 7.1 log reductions, respectively). Pc–SA conjugates **41(PVP)**, **42(PVP)**, **44(PVP)**, **Zn43(PVP)** and **Zn45(PVP)** caused log reduction of 5.3, 3.0, 4.3, 4.3, 3.8 and 4.3, respectively. Significant differences between controls and test group were observed for **41(PVP)** and **44(PVP)**, and for all Zn encapsulated Pc–SA conjugates.

PVP (Pc unloaded control), similarly to what was obtained for E. coli, caused a negligible effect under either white or red light.

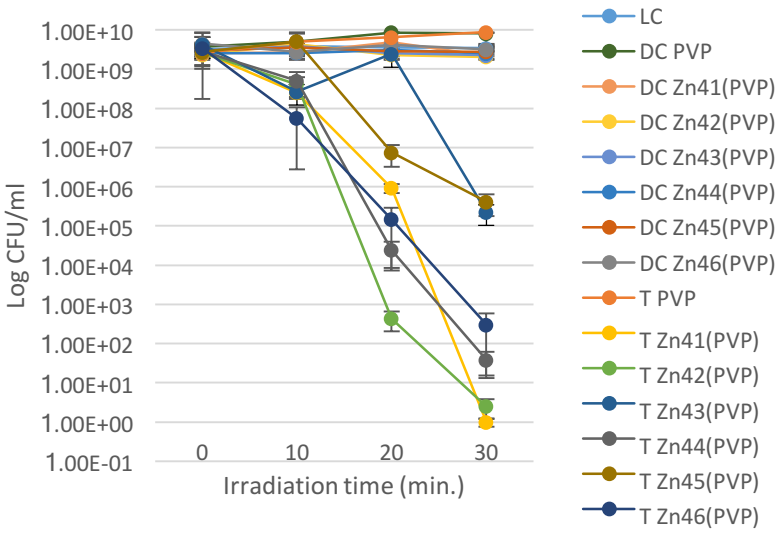

a) ZnPcs(PVP)

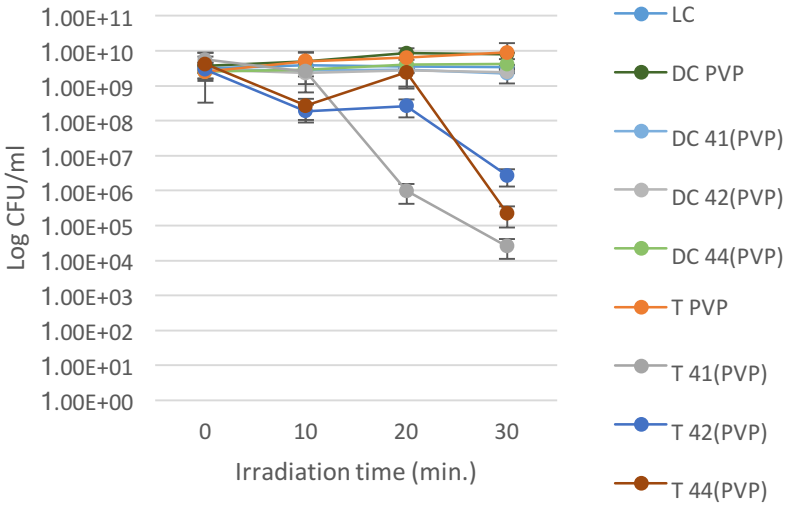

b) 2HPcs(PVP)

Figure 5.14: Photodynamic inactivation of *S. aureus* in the presence of 20 µM of a) ZnPcs(PVP) and b) 2HPcs(PVP) under red light (150 mW/cm^2) for 0, 10, 20, 30 min. Each value represents the average of three independent assays. LC – Light control; DC – Dark control; T – Test. Error bars indicate the standard deviation. Lines just combine the points. Small bars are overlapped by the symbols.

5.3 Discussion

Pcs have emerged as reliable compounds to be used as PS for the inactivation of pathogenic microorganisms in the clinical context due to their interesting photophysical properties, namely the absorbance of light in the red region of the electromagnetic spectrum, the photostability and high singlet oxygen generation yield. This justifies the effort to study new possible modulations of the Pc core with specific groups, like SAs, in order to further enhance their performance for photodynamic antimicrobial therapeutic applications.

In this work, Pc-SA conjugates were tested as PSs in the photodynamic inactivation of *E. coli* and *S. aureus*. In addition, differences in the photosensitization efficiency related with the encapsulation in a drug delivery vehicle (PVP) were also assessed.

The compounds exhibited four or eight peripheral substituents units which makes them different in structure and in physico-chemical properties, namely their solubility in different media. The stability, photostability and the singlet oxygen generation for each conjugate was evaluated.

In the literature it is possible to find several examples of modulation of Pcs such as by sulfonation,[267–269] conjugation with chondroitin sulfate,[270] with cationic groups,[148,271,272] glycosylation,[273,274] or conjugation with peptides.[275,276]

The encapsulation of the synthesized Pcs in the drug delivery vehicle -PVP-, intended to improve the solubility of the Pcs in aqueous media, was a successful strategy since, in addition to an improvement, differences in singlet oxygen generation was observed: the DPBF decay increased from 0.9-6.2% in free-PVP compounds to 58.6-91.0% with Pc(PVP). These results are due to the accommodation of the Pcs within polymer micelles in the monomeric state, confirming that the encapsulation in PVP strongly improves the solubility of these Pcs in aqueous media. This effect had already been observed by Liang *et al.*[169] that reported the preparation of a multifunctional delivery vehicle, which involved a PS - ZnPc - and a targeting agent (folic acid) encapsulated within PVP micelles and which were used as PSs in *in vitro* and *in vivo* studies. In addition, the interaction of PVP with derivatives of chlorin e6 bearing one α-amino acids or 6-aminohexanoic acid as substituent was also demonstrated, confirming PVP an interesting useful drug carrier to be used in PDT and consequently in PDI.[153]

Furthermore, as observed in the singlet oxygen generation studies, this monomerization largely enhanced singlet oxygen production, as was already described by Lian and Coll.[169] This feature highlights the improvement that PVP encapsulation brings to the photosensitization process, in particular with Pcs with low solubility in aqueous media are used. Singlet oxygen generation by Pc(PVP) in aqueous medium was interestingly high, with percentages of DPBF oxidation similar to the ones obtained for the Pcs in DMF.

In addition, the procedure for the encapsulation is simple enough to be done overnight making this method more practical and less expensive than others, such as silica or gold nanoparticles. On the other hand, the differences between the values of oxygen generation of the Pcs and the encapsulated compounds can be somewhat underestimated because of the presence of DMSO, a well-known quencher, in the measurements without PVP.[277]

After assessing the photophysical properties of the new Pc–SA conjugates, *in vitro* assays were performed in order to appraise their potential as PSs for the inactivation of *E. coli* and *S. aureus*. In an overall analysis, none of the compounds showed significant toxicity in the absence of light, as inferred from low log reduction in the dark controls. According to the photosensitization efficiency, two groups of Pc–SA conjugates were defined: Pcs **Zn41**, **Zn42**, **Zn44** and **Zn46** showed high potential to be used as antimicrobial PS under white and red light in both bacteria under study (inactivation factor > 2.0 for *E. coli* and 5.0 for *S. aureus*) whereas **41**, **42**, **Zn43**, **44** and **Zn45** caused very small or insignificant inactivation of either bacteria.

Pcs **Zn41**, **Zn42**, **Zn44** and **Zn46** are zinc Pcs, a group that is very well documented in the literature as particularly suitable for photodynamic inactivation applications due to the presence of the zinc atom enhancing the generation of singlet oxygen.[2,40] On the other hand, simpler structures with smaller chains and less variety of atoms seemed to show greater photosensitization capacity. Pcs **41**, **42** and **44** are metal-free Pcs known to cause milder photosensitization effects. In fact, when coordinated with diamagnetic ions like Zn and Al, Pcs have higher singlet oxygen generation than with paramagnetic ions. In association with the fact that aggregation follows the order Cu > H > Fe > VO > Zn > Co > Al, in which AlPcs were found to be almost in a monomeric form,[40] Pcs coordinated with Zn and Al are firstly consider to be evaluated as PSs.

Pcs **Zn43** and **Zn45** have "atypical" SAs. In particular, **Zn45** has a large alkyl group that reduces water solubility, which can influence the photodynamic process in physiological conditions. For this PS in particular, a lipoic drug delivery vehicle could have been more adequate.[278]

After one preliminary assay at 10 μM in, three independent assays, a 20 μM assay of each PS, corresponding to the concentration used in previous works,[148,279] were conducted.

The group of the best-performing Pc–SA conjugates showed a similar effect on both bacterial models. *E. coli* is a Gram-negative, hence less susceptible to photosensitization than Gram-positive bacteria in general. This limitation is usually overcome by using cationic PS that more easily interact with the negatively charged cell wall.[279] Yet, in this work it was possible to achieve viability reductions of 2-4 logs with the neutral Pcs **Zn41**, **Zn42**, **Zn44** and **Zn46** and the corresponding encapsulated Pc–SA conjugates, under white or red light, with the exception of **Zn41(PVP)** that was only effective with white light. Although complete inactivation was not attained, some of these molecules (**42**, **Zn41**, **Zn42**, **Zn46**, **Zn41(PVP)**, **Zn42(PVP)**, **Zn44(PVP)** and **Zn46(PVP)**) already cause a reduction of > 3 log in the concentration of viable cells, thus meeting the ASM minimum requirement for a new antimicrobial approach.[280] These are the promising Pcs that could be used as the base for subsequent synthetic modifications in order to improve photosensitization of Gram-negative bacteria. Moreover, comparing the PDI efficiency obtained under the two light conditions, there is no evidence that photodynamic inactivation efficiency was improved under red light. In fact, under red light, the photodynamic inactivation of bioluminescent *E. coli* in the presence of 20 μM **41(PVP)**, **44(PVP)** and **Zn43(PVP)** was insignificant.

When tested against *S. aureus*, Pcs **Zn41**, **Zn42**, **Zn44** and **Zn46** and encapsulated Pc–SA conjugates **Zn41(PVP)**, **Zn42(PVP)**, **Zn44(PVP)** and **Zn46(PVP)** were also the most effective, in parallel with the results of the PDI tests with *E. coli*. As expected, being a Gram-positive, *S. aureus* was more susceptible to photosensitization than the bioluminescent *E. coli* and inactivation factors of 6-9 logs were obtained. These results point out Pc–SA conjugates as compounds with high potentiality to be used as PSs of Gram-positive bacteria, which are in line with the results obtained with other Pc bearing other moieties in the photodynamic inactivation of *S. aureus*, and other Gram-positive bacteria at equivalent PS concentrations.[281–285]

Looking closely at the PSs structures under study, a variety of SA moieties, from less complex SAs like *N*,*N*-diethylsulfonamide (compounds **41**, **Zn41** and **Zn46**) or *N*-isopropylsulfonamide (**42** and **Zn42**) to more complex structures like dodecylsulfonamide (**Zn45**), methoxylsulfonamide (**44** and **Zn44**) and thiazol-2-ylsulfonamide (**Zn43**) were tested. The structure of the molecule is an important determinant of the photosensitization efficiency. The structure of the SA can not only affect the specificity for the enzyme DHPS in the folic acid pathway, but can also have an influence in the affinity towards other important components in the cell membrane like polysaccharides, lipids and transport proteins, that will ultimately determine the efficiency of binding of PS molecules to the cell outer structures and the rate of translocation to the intracellular compartment. Pc–SA conjugates containing 'simple' SA structures such as *N*,*N*-diethylsulfonamide or *N*-isopropylsulfonamide seemed a better selection to be used as PSs in the PDI of *E. coli* and *S. aureus*.

5.4 Conclusions

This work demonstrates that Pc–SA conjugates are promising PS for the inactivation of microorganisms. The efficient photosensitization of *E. coli* and *S. aureus* as Gram-negative and Gram-positive bacterial models was demonstrated. Different SA moieties linked to metal-free and ZnPcs were tested. A comparative analysis of the performance of the free and the PVP-encapsulated forms of Pc-SA conjugates was also established. The performance was highly variable between molecules with or without metal and with different SA moieties. Pcs **Zn41**, **Zn42**, **Zn44** and **Zn46** stand out as particularly promising PSs. In addition, PVP monomerization effect enhanced singlet oxygen production and consequently efficiency of inactivation.

The results of this work confirm the potential of Pc derivatives for microbial photodynamic inactivation of Gram-negative and Gram-positive bacteria. Furthermore, it opens a new window for the study of the utilization of Pc-SA conjugates as PSs in a additive effect of the Pc PS properties and biocidal properties of SAs. This additive effect is seen as a way of enhancing PS selectivity. SAs as well-known antimicrobials have the ability to be taken up by bacteria and outer membranes and inhibit DHPS enzyme in the periplasm or cytosol.[266] The binding of this specific type of molecules to the Pc (PS) result in an enhancement of selectivity of these PSs to the target.[286–288]

Taking into consideration the promising results obtained with the tested Pc-SA conjugates, it may be interesting to explore different SA structures in the perspective of enhance antimicrobial effects. Thus, DHPS enzymatic studies by computational simulations technics or in *in vitro* assays can be performed. Biochemical properties of these compounds are an important point to be assessed in the future, by understanding to which cell membrane components these compounds are more likely to attach to.

On the other hand, Pc properties can also be designed. For example, a meticulous comparison between the PDI results obtained in this work, in the same comparable conditions, by using equivalent Pc-SA conjugates but with cationic moieties can be done. Likewise, different drug delivering vehicles can be tested and the susceptibility of other bacterial pathogens needs to be explored.

The results of this work strongly motivates serious attention to Pc-SA conjugates as PS as a new therapeutic approach against bacterial infections and are described in an article that will be submitted for publication.

Chapter 6 Major findings and further work

Photodynamic therapy is a powerful technique with wide range of applications in medicine. Photodynamic inactivation of microorganisms, in particular, it has been proved to be a reliable method to substitute or complement the effect of antibiotics that have become ineffective on the treatment of several multidrug-resistant microorganisms.

PDT efficiency is influenced by different parameters, namely the intensity and wavelength of the light used, the ability of the PS to produce singlet oxygen, and affinity towards target cells or tissues. To determine the effect of all this factors in the outcome of the photosensitization process, different chemical, photochemical, photobiological, photophysical and biological studies have been developed and highly interdisciplinary approaches have been followed. However, the type of PS is still a crucial factor of the success of photodynamic inactivation protocols.

In this work, the main effort was put in the achievement of a more selective and specific PS with optimized photobiological characteristics. We intended to obtain Pc–SA conjugates, which could act as antimicrobial and antitumoral PSs. This increased efficiency would be achieved not only by the excellent ability of Pcs to produce singlet oxygen and to absorb at a wavelength within the optical window CA in tumor cells and DHPS in microorganisms that produce folic acid.

The direct functionalization of Pcs is difficult and leads to the formation of complex mixtures. So, the synthesis of Pcs bearing substituents in well-defined positions requires the use of adequately substituted precursors, such as Phts. In this work was implemented that approach. The synthesis of mono substituted *N*-acyl SAs involved the use of the sulfo-click reaction but this transformation turned out to be quite demanding. After testing various experimental conditions, it was possible to obtain a Pht– *N*-acyl-SA conjugate. However, with this method we were not able to obtain the corresponding Pc–*N*-acyl-SA conjugate as intended. Additionally, new Pcs with ethynyl groups were produced. This new acetylene containing compounds are versatile substrates for further structural modifications. In fact, in collaboration with Brazilian researchers, we are studying the possibility of coupling ethynyl Pcs to AZT derivatives. The resulting compounds may be useful in HIV/AIDS treatment and to be used as antitumoral drugs.

Following the sulfo-click reactions discussed in chapter 2, the possibilities of affording Pc-SA conjugates were explored. Chapter 3 reports on the development of new Pc–SA conjugates.

Some of the conjugates obtained in this study were used for biological evaluation as PSs for the photodynamic inactivation of bacteria and tumor cells. It demonstrated for the first time the additive effect of the photosensitizing properties of the Pcs and biocidal and antitumoral properties of SAs (chapters 4 and 5).

This work allowed us to highlight, for the first time, the potential of Pc-SA conjugates as PSs in PDT. In addition, the capacity of these compounds to inactivate the enzyme CA was also studied. Besides, the capacity of the Pc-SA conjugates to be used in the PDI of Gram-positive and Gram-negative bacteria was demonstrated for the first time. Furthermore, PVP-encapsulated forms of Pc-SA conjugates were also tested and a comparative analysis between these compounds and the corresponding PVP-free derivatives were performed.

From this doctoral work, three articles will be produced for publication. A review article on new developments of the synthetic strategies to afford SAs is nearly ready. Another manuscript on the synthesis of Pc-SA conjugates and PDI studies has been already submitted. Finally, an article with the results obtained in the PDT of HSC3 oral squamous cell carcinoma and HaCaT 'normal' keratinocytes and on the CA enzymatic assays in collaboration with Doctor Jon Golding and Doctor Etelvina Figueira will be written.

This work is well tuned with the future challenges expected for medicine. One of the most challenging diseases is cancer. PDT is a reliable and powerful approach to treat cancer. Pc-SA conjugates contribute to the pursuit for better PSs with the most selective and enhanced properties. This work represents an initial step but a long way still has to be covered before the results of can be transposed to clinical applications. However, the impressive build-up of bacterial resistance to antibiotics, that just recently were still effective, sheds a new perspective to innovative tools to control infections. PDI stands out as one of the most promising alternatives to traditional antimicrobial chemotherapy and with this work, Pc-SA conjugates are unequivocally confirmed as promising PSs for PDI.

Chapter 7 Experimental section

7.1 General information

The organic solvents used in this work were dried according to standard methods by distillation over drying agents and stored under nitrogen. All commercially available reagents were used as acquired. The progress of reactions was followed by TLC performed on silica gel-coated plastic sheets (Merck). TLC plates were visualized under UV light (λ=254 nm). Column chromatography was performed using silica gel (Merck, 35-70 mesh). Deuterated solvents such as $CDCl_3$ and DMSO-d_6 were used for ^1H and ^{13}C NMR spectra.

^1H and ^{13}C NMR spectra were acquired on Bruker DRX AC 300 or 500 instruments $CDCl_3$ and DMSO-d_6 solutions. The frequencies used were 300.13 and 500.13 MHz for ^1H and 75.47 and 125.77 MHz for ^{13}C. Chemical shifts are reported as δ-values in part per million (ppm) in relation to tetramehylsilane. Coupling constants (*J*) are in Hz.

Mass spectra were obtained using Q-TOF (QTOF 2, Micromass, Manchester, UK), MALDI-TOF-TOF Applied Biosystems MDS Sciex 4800 and ultrafleXtreme mass spectrometer (Bruker, Bremen, Germany) controlled by Compass for flex Series 1.4, using chloroform as solvent and with DHB matrix. The mass spectra data are expressed in terms of the ratio of *m/z*.

The UV-Vis spectra (steady-state absorption spectra) were recorded on a spectrophotometer UV-2501 PC, Shimadzu, using glass or quartz cell of 1 cm. Steady-state emission spectra were recorded with a Fluoromax- 3-spectrometer (HORIBA Jobin Yvon).

HSC3 oral squamous carcinoma cells were purchased from ATCC and HaCaT 'normal' keratinocytes cells were a gift of Erik Walbeehm at Erasmus Medical Centre, Rotterdam.

7.2 Synthesis

7.2.1 4-(4-chlorosulfonylphenoxy)phthalonitrile (2)

4-Phenoxyphthalonitrile **1** (1.65 g, 5.29 mmol, 1 eq.) was added to chlorosulfonic acid (2.49 ml, 37.45 mmol, 5 eq.) cooled in an ice bath. The reaction

mixture was stirred for 15 minutes at a temperature between 5 and 10 ºC and then the temperature was allowed to rise to room temperature for 15 minutes. After 30 minutes, thionyl chloride (1.08 ml, 14.9 mmol, 2 eq.) was added and the reaction was left for more 30 minutes at the same temperature. Then, the reaction mixture was poured onto ice (300 g) and the solid formed was filtered and washed with cold water. The compound was dried under vacuum and used in the following reactions without further purification.

7.2.2 4-(4-(diethylaminosulfonyl)phenoxy)phthalonitrile (9)

Pht **2** (1.00 g, 3.13 mmol, 1 eq.) was dissolved in acetonitrile (5 ml) and the solution was cooled to 0 °C. Diethylamine (0.69 ml, 9.41 mmol, 3 eq.) was added slowly to the reaction mixture. The reaction mixture was then stirred at room temperature for 2 hours and poured into ice (~ 200 g). The resulting solid was filtered off and crystallized from CH_2Cl_2/Hexane and drying under vacuum at 60 ºC.

yield: 0.870 g white powder (78.0%). ^{1}H NMR (300 MHz, $CDCl_3$): (ppm) = δ 1.18 (t, *J* = 7.1 Hz, 6 H), 3.29 (q, *J* = 7.1 Hz, 4 H), 7.14 – 7.21 (m, 2 H), 7.31 (dd, *J* = 2.4, 8.7 Hz, 1 H), 7.38 (d, *J* = 2.4 Hz, 1 H), 7.80 (d, *J* = 8.7 Hz, 1 H), 9.91 (m, 2H). ^{13}C NMR (75 MHz, $CDCl_3$) δ 14.26, 42.19, 110.35, 114.66, 115.05, 118.02, 120.38, 122.41, 122.60, 129.85, 135.71, 138.09, 156.97, 160.17. ESI-MS: 355.3 ($[M]^+$).

7.2.3 4-acetylbenzenesulfonyl azide (11)

A solution of sodium azide (0.019 g, 0.029 mmol, 1.5 eq.) in water was added drop-wise to a solution of acetylbenzenesulfonyl chloride **10** (0.054 g, 0.024 mmol, 1 eq.) in acetone. The mixture was stirred during 2 hours under an inert atmosphere. During this period, the reaction was kept below 0 ºC using an ice-salt bath. After that time the mixture was extracted with dichloromethane and the organic layer was dried over $NaSO_4$. After filtration of the $NaSO_4$, the solution was evaporated under reduced pressure at low temperature to prevent decomposition. The white powder obtained was dried under vacuum.

yield: 0.039 g white powder (69.7 %). ^{1}H NMR (300 MHz, $CDCl_3$): δ (ppm) = 2.69 (s, 3 H), 8.05–8.09 (m, 2 H), 8.15–8.19 (m, 2 H). ^{13}C NMR (75 MHz, $CDCl_3$): δ (ppm) = 26.95, 127.85, 129.38, 141.52, 141.94, 195.26. ESI-MS: 219.3 ($[M+H]^+$).

7.2.4 4-(3-ethynylphenoxy)phthalonitrile (13)

A mixture of 4-nitrophthalonitrile (0.50 g, 2.89 mmol, 1 eq.), 3-ethynylphenol (0.38 ml, 0.41 g, 3.47 mmol, 1.2 eq.) and potassium carbonate (0.48 g, 3.47 mmol, 1.2 eq.) in 5 ml of dry DMF was stirred at room temperature overnight. The desired product was precipitated in warm water, and the solid obtained was filtered and washed with several additions of water and hexane. The product was purified by chromatography on a silica gel column using dichloromethane as eluent and recrystallized from CH_2Cl_2/hexane. Product **13** was dried in a vacuum pump during several hours at 60 ºC and stored at 55 ºC to eliminate residual water.

yield: 0.055 g white powder (79.0 %). ^{1}H NMR (300 MHz, $CDCl_3$): δ (ppm) = 4.34 (s, 1 H), 7.24–7.33 (m, 2 H), 7.40–7.45 (m, 2 H), 7.86 (d, *J* = 2.6, 1 H), 8.12 (d, *J* = 8.8, 1 H). ESI-MS: 245.4 ($[M + H]^+$).

7.2.5 Ethynyl-phthalocyanines

The 4-(3-ethynylphenoxy)phthalonitrile (**13**) (0.20 g, 0.81 mmol, 1 eq.) and 4-*tert*-butylphthalonitrile (0.754 g, 4.09 mmol, 5 eq.) in DMAE (5 ml) was maintained overnight at reflux (140 ºC) under a nitrogen atmosphere, in the presence of zinc acetate (0.30 g, 1.64 mmol, 2 eq.). Then, the mixture was precipitated in water/methanol (1:1) and the resulting crude was washed several times with the same solvent mixture. The various Pcs formed in this statistical condensation were separated on a silica gel column using hexane/1,4-dioxane (4:1) as eluent. Finally, the Pc fractions were dried under vacuum atmosphere during 2 h at 60 ºC.

Mono-ethynyl *t*BuZn Phthalocyanine (14)

yield: 0.190 g blue-greenish powder (27.5 %). ^{1}H NMR (300 MHz, $CDCl_3$): δ (ppm) = 4.34 (s, 1 H), 7.93–7.37 (m, 8 H), 9.30 (m, 8 H). MALDI-MS: 860.2 (M^+). UV-Vis: 343 nm (ε = 120 000), 679 nm (ε = 4 500 000). Fluorescence quantum yield: Φ = 0.04.

Di-ethynyl *t*BuZn Phthalocyanine (15)

yield: 0.071 g blue-greenish powder (10.3 %). ^{1}H NMR (300 MHz, $CDCl_3$): δ (ppm) = 4.34 (s, 1 H), 4.37 (s, 1 H), 7.81–7.44 (m, 12 H), 9.33–8.82 (m, 8 H). MALDI-MS: 920.2 (M^+). UV-Vis: 348 nm (ε = 120 000), 678 nm (ε = 5 100 000). Fluorescence quantum yield: Φ = 0.07.

Di-ethynyl *t*BuZn Phthalocyanine (16)

yield: 0.097 g blue-greenish powder (14.1 %). ^{1}H NMR (300 MHz, $CDCl_3$): δ (ppm) = 4.34 (s, 1 H), 4.37 (s, 1 H), 7.80–7.44 (m, 12 H), 9.31–8.80 (m, 8 H). MALDI-MS: 920.2 (M^+). UV-Vis: 3453 nm (ε = 120 000), 679 nm (ε = 5 900 000). Fluorescence quantum yield: Φ = 0.09.

7.2.6 4-[3-(4-acetamidophenyl)sulfonylamino-2-carboxylmethyl)phenoxy]phthalonitrile (17)

In a boiling flash with a magnetic stir bar copper(I) cyanide (0.08 mg, 0.01 mmol, catalytic concentration) and compound **13** (0.367 g, 15.2 mmol, 1 eq.) was added in the presence of distilled water and 4-acetamidobenzenesulfonyl azide (0.085 g, 15.2 mmol, 1 eq.) was added at room temperature.

To this stirred mixture, triethylamine (1,647 ml, 152 mmol, 10 eq.) was slowly added *via* syringe over one min at room temperature. The mixture was then stirred open to air for 4 hours at room temperature. The reaction was quenched by addition of a saturated aqueous ammonium chloride solution. Methanol was added, and then the mixture was stirred for an additional 20 min at the same temperature. The resulting mixture was filtered through a Celite pad, and the pad was washed with methanol (5 × 2 ml). The filtrate was concentrated to half volume using a rotary evaporator, and then the resulting solid was collected by suction filtration with aid of distillated water. The solid was washed with a pre-cooled (0 ºC) mixture of diethyl ether and isopropyl alcohol followed by diethyl ether. After evaporation the light yellowish solid was dissolved in boiling methanol and crystallized upon storage in −4 ºC refrigerator for 3 days. The crystalline product was collect by suction filtration and was washed with pre-cooled (0 ºC) methanol. Then the white solid was dried under vacuum at room temperature.

yield: 0.192 mg white powder (52.4%). ^{1}H NMR (300 MHz, $CDCl_3$): δ (ppm) = 2.09 (s, 3 H), 3.60 (m, 2 H), 6.96 (s,1 H), 7.03–7.12 (m, 2 H), 7.32 (dd, *J* = 8.8, 2.5 Hz, 1 H), 7.40 (t, *J* = 7.9 Hz, 1 H), 7.85 – 7.72 (m, 5 H), 8.09 (d, *J* = 8.7 Hz, 1 H), 10.39 (s, 1 H), 12.24 (s, 1 H).

7.2.7 *N*-((4-acetamidophenyl)sulfonyl)-2-phenylacetamide (22)

Similar to compound **17**, a flash equipped with a magnetic stir bar was charged with copper(I) cyanide (0.08 mg, 0.01 mmol, catalytic concentration) and 4-acetamidobenenesulfonyl azide (0.240 g, 1 mmol, 1 eq.). Distilled water was added to the flash, and then phenylacetylene (0.102 g, 1 mmol, 1 eq.) was added via syringe at room temperature.

To this stirred mixture, triethylamine (0.167 ml, 1.2 mmol, 10 eq.) was slowly added *via* syringe over one min at room temperature. The mixture was then stirred open to air for 4 hours at room temperature. The reaction was quenched by addition of a saturated aqueous ammonium chloride solution. Methanol was added, and then the mixture was stirred for an additional 20 min at the same temperature. The resulting mixture was filtered through a Celite pad, and the pad was washed with methanol (5 × 2 ml). The filtrate was concentrated to half volume using a rotary evaporator, and then the resulting solid was collected by suction filtration with aid of distillated water. The solid was washed with a pre-cooled (0 ºC) mixture of diethyl ether and isopropyl alcohol followed by diethyl ether. After evaporation the light yellowish solid was dissolved in boiling methanol and crystallized upon storage in −4 ºC refrigerator for 3 days. The crystalline product was collect by suction filtration and was washed with pre-cooled (0 ºC) methanol. Then the white solid was dried under vacuum at room temperature.

yield: 0.203 mg white powder (64.5%). ^{1}H NMR (300 MHz, $CDCl_3$): δ (ppm) = 2.09 (s, 3 H), 3.53 (m, 2 H), 7.16–7.12 (m,2 H), 7.20–7.32 (m, 3 H), 7.79 (q, 4 H), 10.39 (s, 1 H), 12.24 (s, 1 H).

7.2.8 4,5-bis(4-(isopropylaminosulfonyl)phenoxy)phthalonitrile (26)

Pht **26** was obtained by the reaction of the compound 4,5-bis(4-chlorosulfonylphenoxy)phthalonitrile **24** (1.54 g, 3.02 mmol, 1 eq.) with slowly added isopropylamine (1.49 ml, 18.12 mmol, 6 eq.) in acetonitrile. The mixture

was stirred for 1 hour at room temperature under nitrogen atmosphere. The desired product was obtained after filtration of the solid formed in water and recrystallization from CH_2Cl_2/hexane.

yield: 0.370 g white powder (23.0%). ^{1}H NMR (300 MHz, $CDCl_3$) δ 7.94–7.89 (m, 4 H), 7.44 (s, 2 H), 7.08–7.02 (m, 4 H), 3.57–3.46 (m, 2 H), 1.12 (d, *J* = 6.5 Hz, 2 H) ^{13}C NMR (126 MHz, $CDCl_3$) δ 23.89, 46.34, 112.77, 114.23, 118.65, 125.14, 129.73, 138.35, 150.42, 157.58. ESI-MS: 555.1 ($[M+H]^+$). mp: 117-123 ºC.

7.2.9 4,5-bis(4-(thiazol-2-ylaminosulfonyl)phenoxy)phthalonitrile (27)

Compound **27** was obtained by reaction of the compound 4,5-bis(4-chlorosulfonylphenoxy)phthalonitrile **2** (1.00 g, 1.96 mmol, 1 eq.) with 2-aminothiazole (0.196 g, 1.96 mmol, 1 eq.) in acetonitrile in the presence of slowly added 4 eq. of triethylamine. The mixture was stirred for 2.5 hours at room temperature under nitrogen atmosphere. The desired product was purified by chromatography over a silica gel column using a mixture of CH_2Cl_2/hexane (3:1) and crystallization from CH_2Cl_2/hexane.

yield: 0.200 g yellow powder (16.2%). ^{1}H NMR (300 MHz, DMSO) δ 7.07 (d, *J* = 5.2 Hz, 2 H), 7.33 (d, *J* = 7.9 Hz, 4 H), 7.56 (dd, *J* = 1.3, 7.9 Hz, 4 H), 7.75 (d, *J* = 5.2 Hz, 2 H), 8.49 (s, 2H). ESI-MS: 554.6 ($[M]^+$). mp: 250-253 ºC.

7.2.10 4-(benzylsulfanyl)phthalonitrile (33)

4-Nitrophthalonitrile (0.100 g, 5.77 mmol, 1 eq.) and phenylmethanethiol (0.08 g, 6.93 mmol, 1.2 eq.) were reacted at room temperature in DMF and in the presence of cesium carbonate (0.094 g, 2.88 mmol, 0.5 eq.). When 4-nitrophthlonitrile was totally consumed, the reaction was stopped with cold water. The resulting solid was filtered and washed with cold water and hexane. The solid obtained was dried at room temperature in a desiccator.

yield: 0.124 g white powder (86.1%). ^{1}H NMR (300 MHz, DMSO) δ 4.25 (s, 2 H), 7.32–7.37 (m, 4 H), 7.49 (dd, *J* = 8.4, 1.9 Hz, 1 H), 7.58 (d, *J* = 1.8 Hz, 1 H), 7.61 (d, *J* = 8.4 Hz, 1H). ESI-MS: 251.1 $(M+H]^+$).

7.2.11 {2,3,9,10,16,17,23,24-[Octakis(4-isopropylaminosulfonyl)phenoxy]phthalocyaninato}magnesium(II) (Mg42)

Magnesium turnings (9.27 mg) were added to pentan-1-ol (0.5 ml) and the suspension was heated to 150 °C (reflux) and maintained at that temperature until the complete formation of the alkoxide (overnight). Octan-1-ol (1 ml) was added to the suspension, followed by Pht **26** (0.100 g, 0.189 mmol). The reaction mixture was stirred at 160 °C overnight and, after cooling to room temperature, it was poured onto a 5:1 methanol/water mixture (20 ml). The resulting precipitate was isolated by filtration and washed several times with methanol.

yield: 0.087 g blue powder (82.0%). ^{1}H NMR (300 MHz, DMSO): δ 1.11 (d, *J* = 6.5 Hz, 48 H), 3.44-3.55 (m, 16 H), 7.02 (d, *J* = 8.8 Hz, 16 H), 7.59 (d, *J* = 9.7 Hz, 8 H), 7.87 (d, *J* = 8.8 Hz, 16 H). MALDI: 2242.5 ($[M]^+$), 2265.5 ($[M+Na]^+$). mp: > 300 ºC.

7.2.12 {2,3,9,10,16,17,23,24-[Octakis(4-thiazol-2-ylaminosulfonyl)phenoxy]phthalocyaninato}magnesium(II) (Mg43)

Magnesium turnings (9.27 mg) were added to pentan-1-ol (0.5 ml) and the suspension was heated to 150 °C (reflux) and maintained at that temperature until the complete formation of the alkoxide (overnight). Octan-1-ol (1 ml) was added to the suspension, followed by Pht **27** (0.100 g, 0.157 mmol). The reaction mixture was stirred at 160°C overnight and, after cooling to room temperature, it was poured onto a 5:1 methanol/water mixture (20 ml). The resulting precipitate was isolated by filtration and washed several times with methanol.

yield: 0.078 g blue powder (78.3%). ^{1}H NMR (500 MHz, $CDCl_3$): δ 6.89-7.11 (m, 24 H), 7.33-7.55 (m, 16 H), 7.56-7.86 (m, 16 H). MALDI: 2557.1 ($[M]^+$); mp: > 300 ºC.

7.2.13 {2,9(10),16(17),23(24)-[Tetrakis(4-diethylaminosulfonyl)phenoxy]phthalocyaninato}magnesium(II) (Mg46)

Magnesium turnings (9.27 mg) were added to pentan-1-ol (0.5 ml) and the suspension was heated to 150 °C (reflux) and maintained at that temperature until the complete formation of the alkoxide (overnight). Octan-1-ol (1 ml) was added to the suspension, followed by Pht **9** (100 mg, 0.281 mmol). The reaction mixture was stirred at 160 °C overnight and, after cooling to room temperature, it was poured onto a 5:1 methanol/water mixture (20 ml). The resulting precipitate was isolated by filtration and washed several times with methanol.

yield: 0.0874 g blue powder (86.3%). ^{1}H-NMR (500 MHz, $CDCl_3$): δ 1.13-1.19 (m, 24 H), 3.21-3.30 (m, 16 H), 7.11-7.20 (m, 4 H), 7.45-7.98 (m, 24 H). MALDI: 1444.4 ($[M]^+$) mp: > 300 ºC.

7.2.14 Metallation of phthalocyanines with Zn^{2+}: general procedure

The MgPc (**Mg42**, **Mg43** or **Mg46**) were dissolved in dry THF (20 ml) in a 50 ml three flask equipped with a water condenser. Trifluoroacetic acid (2 ml) was added and the mixture was heated at 50 ºC for 3 hours. The removal of the coordinated metal cation was monitored by UV-Vis spectroscopy and TLC analysis. The reaction mixture was cooled to room temperature and water (ca. 10 ml) was added until a precipitate was formed. Methanol (2 ml) was added leading to further precipitation. Each metal-free Pc **12**, **13** and **16** were then collected by filtration. After re-dissolving in a minimal amount of DMF, the solution was transferred to a sealed tube and 2.5 eq. of zinc acetate was added. The mixture was left overnight at 150 ºC. The metallation was confirmed by UV-Vis analysis. The reaction mixture was cooled to room temperature and water (ca. 10 ml) was

added until a precipitate was formed. Methanol/water 5:1 (2 ml) was added and the product was extract with dichloromethane/methanol. After drying with anhydrous sodium sulfate the ZnPc (**Zn42**, **Zn43** and **Zn46**) was crystalized from dichloromethane/hexane and the crystals were dried in vacuum.

7.2.15 {9,10,16,17,23,24-[hexafluoro-2,3-bis(4-diethylaminosulfonyl)phenoxy]phthalocyaninato}zinc(II) (Zn49)

4,5-Difluorophthalonitrile (0.214 g, 12.7 mmol, 6 eq.) and Pht **25** (0.051 g, 2.8 mmol, 1 eq.) were reacted in a statistical condensation in chloronaphthalene and in the presence of $Zn(AcO)_2$ (0.088 g, 4,80 mmol, 2.2 eq.) overnight. The reaction was stopped by precipitation with methanol/H_2O (1:1) and the solid obtained was filtered and washed with methanol. After purification by chromatography over a silica gel column using a mixture of THF/hexane (6:1) and crystallization in THF/hexane the desired product was obtained.

yield: 25.2% blue powder. ^{1}H-NMR (300 MHz, $CDCl_3$): δ 1.15 (t, *J* = 7.1 Hz, 1 H), 3.24 (q, *J* = 7.1 Hz, 1 H), 6.99–7.06 (m, 1 H), 7.36–7.61 (m, 1 H), 7.83–7.76 (m, 1 H). MALDI: 1163.4 ($[M+Na]^+$); mp: > 300 ºC.

7.3 Encapsulation of phthalocyanines in polyvinylpyrrolidone micelles

1 mM of stock solutions of Pc **41**–**44**, **46** and **Zn41–Zn46** in dichloromethane were prepared and 0.5 ml of these solutions were placed in sample ports with 100 mg of PVP (40 kDa). As a control, one of the sample ports was prepared in the same way as the others but containing only PVP. The resulting solutions were evaporated in N_2 until oil formation. The sample ports were left at 55 ºC overnight. The resulting polymers were dissolved in 1 ml of distilled water and solubilized using ultra-sounds.

7.4 Photophysics and photochemistry

7.4.1 Solubility

The solubility of Pc–SA conjugates and the respective Pc–SA conjugates encapsulated in PVP micelles in DMSO and PBS was assessed by UV–Vis spectroscopy. Concentrations between 0.625 and 25 μmol/L obtained by the addition of aliquots of each Pc–SA conjugate, were analyzed. The intensity of the Q-band versus conjugate concentration was plotted in a graphic for linear regression to check the compliance of the Beer–Lambert law.

7.4.2 Photostability

The photobleaching rates of Pc–SA conjugates and the respective Pc–SA conjugates encapsulated in PVP micelles were determined by irradiating 2 ml of a diluted solution of each Pc–SA conjugate in PBS under the same conditions used in the biological assays (150 mW/cm^2). During irradiation, the solutions were magnetically stirred and kept at room temperature. The concentration of the Pc–SA conjugates was quantified by visible absorption spectroscopy at regular time intervals. UV–Vis spectroscopy was used to determine the intensity of the Q-band at different intervals of time and the photostability (%) was expressed as $I_t / I_0 * 100$ (I_t = intensity of the band at given time of irradiation, I_0 = intensity of the band before irradiation). Similar assays were performed in the dark to account for the effect of aggregation as a source of light-independent decay.

7.4.3 Singlet oxygen generation

The ability of each Pc–SA conjugates and PVP-encapsulated Pc–SA conjugates to generate singlet oxygen was qualitatively evaluated following the photooxidation of DPBF, a singlet oxygen quencher.[72] Stock solutions of each PS at 0.5 mmol/L in DMF and a stock solution of DPBF at 50 mmol/L in DMF / H_2O (9:1) were prepared. The reaction mixtures of DPBF and each Pc–SA conjugate were irradiated, with white light filtered through a cut-off filter for wavelengths < 550 nm, at a fluence rate of 9.0 mW/cm^2. The absorption decay of DPBF at 415 nm was measured at irradiation intervals of 1 min, during 7 min. The percentage of the DPBF absorption decay,

proportional to the production of $^1O_2$, was assessed by the difference between the initial absorbance and the absorbance of DPBF after a given period of irradiation.

7.5 Photodynamic inactivation

A recombinant bioluminescent strain of *Escherichia coli* was used as a model for Gram-negative bacteria.[289] Before each photodynamic inactivation assay, one isolated colony from a culture growing on tryptic soy agar (TSA, Merck) amended with the antibiotics ampicillin (100 mg/ml) and chloramphenicol (25 mg/ml) was aseptically inoculated on tryptic soy broth (TSB) with both antibiotics and grown overnight at 26 °C under stirring (130 rpm). An aliquot of this primary culture was sub-cultured in TSB with antibiotics (ampicillin and chloramphenicol), grown overnight under stirring (130 rpm) at 26 °C and used to prepare the cell suspensions for the PDI assays.

To confirm the correlation between the bioluminescent signal (in relative light units, RLU) of *E. coli* and the concentration of CFU, two independent assays were carried out. An overnight culture (~10^7 CFU/ml) of bioluminescent *E. coli* was serially diluted (10^1 to 10^7) in PBS. Light emission of the non-diluted and diluted aliquots was read on a luminometer (Turner Designs – 20 / 20). Viable counts were determined by pour-plating 2 replicates of each dilution in TSA medium. After 24 h of incubation at 37 °C, the number of colonies was counted in the most convenient dilution series. Three independent assays were conducted.

Staphylococcus aureus was used as a model for Gram-positive bacteria.[290–292] Stock cultures in TSA, Merck, were kept at 4 ºC. Fresh cultures were prepared before each assay by inoculating an isolated colony in 30 ml of TSB, Merck. The cultures were incubated for 24 hours at 37 ºC under stirring (130 rpm). An aliquot of this primary culture was sub-cultured in TSB, grown overnight under stirring (130 rpm) at 37 °C to obtain fresh cultures for the PDI assays.

Fresh liquid cultures were 10-fold diluted in PBS and allowed to stabilize under stirring for 10 minutes, at room temperature. Aliquots of 0.1 ml were distributed into 1 ml vials and added of convenient volumes of DMSO stock-solutions of the Pc–SA conjugates or aqueous suspensions of PVP-encapsulated conjugates, to achieve final concentrations of 20 μM of Pcs. One sole preliminary assay was conducted with *E. coli* at the concentration of 10 μM. The experiments with PS concentrations of 20 μM were conducted in 3 independent assays. After adding the PS, the suspensions were pre-

incubated in the dark, at 37 ºC, for 30 min for adsorption of the PS to the cells and further irradiated with white light (400–800 nm) or red light (620–750 nm) delivered by an illumination system LC-122 LumaCare equipped with a halogen/quartz 250 W lamp coupled to two different interchangeable optic fiber probes (400–800 nm and 620–750 nm). The fluence rate was set to 150 mW/cm^2 and confirmed with an energy meter Coherent FieldMaxII-Top combined with a Coherent PowerSensPS19Q energy sensor. Irradiation was conducted for 180 minutes for bioluminescent strain *E. coli* and for 30 minutes for *S. aureus*. Aliquots were periodically retrieved for measurement of bioluminescence, in the case of *E. coli*, or to determine the concentration of viable cells by colony counting, in the case of *S. aureus*. Bioluminescence was measurement in triplicate aliquots in a luminometer (TD-20/20 Luminometer; Turner Designs, Inc.). To determine the concentration of viable cells, the suspension of *S. aureus* was serially diluted in PBS and triplicates of the convenient dilutions were pour-plated in TSA. The cultures were incubated at 37 ºC for 24 h. Colonies were counted in the replicates of the most suitable dilution and the concentration of viable cells was expressed as CFU/ml. Light (without PS) and dark (protected from light) controls were included in all experiments.

7.5.1 Statistical analysis

Statistical analysis was performed with SPSS package (SPSS 24.0 SPSS Inc.). Normal distribution was verified by the Kolmogorov–Smirnov test. The significance of irradiation time and type of PS on bacterial inactivation between controls (light control - without PS and dark control - protected from light) and the test groups in which the bacteria was irradiate with the proper light in the presence of the PS was assessed by non-parametric univariate analysis of variance (non-parametric ANOVA) model with the Kruskal-Wallis test. A value of $p < 0.05$ was considered significant.

7.5.2 Cell cultures

HSC3 and HaCaT cells were maintained as monolayers in 25 mM glucose DMEM supplemented with 100 µU/ml penicillin, 100 µU/ml streptomycin (1% penicillin/streptomycin) and 10% heat-inactivated fetal bovine serum, in a humidified 5% CO_2 atmosphere at 37 ºC. For experiments, cells were grown in 24-well tissue culture plates in triplicate in 500 µL 5 mM glucose DMEM supplemented with 1%

pen/strep and 10% heat-inactivated fetal bovine serum at a density of 1 x 10^5 cells per well and allowed to attach for 24 h to attain ~100% confluence.

7.5.3 PS loading and PDT treatment

All manipulations prior to PDT were performed under subdued lighting. Before irradiation, the medium containing serum was replaced with 500 μL serum-free medium containing the 3 μM, 10 μM and 15 μM respectively of each PS and cells were incubated in the dark at 37 ºC and 5% CO_2 for 2 h. Cells were then washed three times with PBS and covered with phenol red-free DMEM. Test samples were immediately exposed to 10 J/cm^2 halogen white light (from a 500 W bulb) for 5 min and 15 sec, heat filtered through 5 cm of water in a T175 flask (Nunc 156502) (or maintained in the dark, for dark cytotoxicity experiments). A negative control with PVP and three positive controls with Foscan (kindly provided by Dr. Alexandre McRobert, UCL, London), at the same concentrations used for the PS under study, were also used. Samples were then left in a culture incubator overnight in the dark, and then assayed for viability.

7.5.4 Cell viability analysis

Cell viability was assessed by MTS assay as described in the technical bulletin. 20,000 cells/well were incubate for 2 hours with 50 μL of each PS in serum-free DMEM. Then, the adhesive cells were washed three times with warm PBS and the medium was changed to 100 μL of DMEM + Serum. Each well was irradiated with white light (10 J/cm^2) for 5 minutes and 15 seconds. Dark toxicity wells were lived away from light. Finally, 20 μL of pre-warmed CellTiter MTS was added and the cells were incubated for 4 hours. The absorbance was read at 492 nm.

7.5.5 PS uptake

The uptake of the PSs in the total cell population was determined by fluorescence spectroscopy as described previously.[226] 10 μM PS in serum-free DMEM were incubated for 1 to 4 h and cells were washed three times with warm Hank's salt (HBSS). Then, cells were incubated with DMSO:PBS (1:9) and shaken for 10 min (tyrosinase cells from 3x control wells in 100 μL TE for haemocytometer). In a different plate, a 10-fold dilution series of each PS in 250 μL DMSO:PBS (1:9) was prepared,

starting at 10 μM (10^{-5} M). PS in the supernatant was assayed by measuring the fluorescence using a FLUOstar Optima plate reader (λ_{ex} = 355 nm, λ_{em} = 680 nm).

7.6 Carbonic anhydrase activity

Swine blood was collected with 10% (v/v) anticoagulant (0.1 M Tris buffer with 3.8% sodium citrate). Total non-coagulated blood was centrifuged twice at 3500 rpm for 10 min. Plasma was removed and the pellet was resuspended in Tris HCl (0.1 M) and vortexed. The suspension was frozen (-80 ºC) and thawed (37 ºC) three times in order to disrupt red cell membranes. Lyses were confirmed under a microscope for > 90% of the cells. A biuret assay was conducted to assess the total protein in the lysate that was further stored at -20 ºC.

An adaptation of the method developed by Moreira *et al.* was used for the determination of CA activity.[293] Aliquots of 20 μL of lysate 1:200 diluted in Tris HCl buffer (pH 8.3) were transferred to microplate wells, with 80 μL TRIS buffer (0.1 M) containing 20 ppm bromothymol blue, and 7.5 μL of each Pc–SA conjugate or PVP-encapsulated Pc–SA conjugate (15 μM). 200 μL of CO_2 saturated distilled H_2O (obtained by bubbling CO_2 gas in distilled H_2O for 10 min, and considered saturated when pH < 3.5) was added to each sample. A standard control (without Pc–SA conjugate or PVP-encapsulated Pc–SA conjugate) was included. Bromothymol blue conversion to yellow, indicating CO_2 was converted to bicarbonate + protons, was immediately measured at 436 nm on a microplate reader (Multiskan GO, VWR) during 20 min in eight independent assays. All samples and reagents were kept and mixed at 4 ºC.

References

1 T. Dai, Y.-Y. Huang and M. R. Hamblin, *Photodiagnosis Photodyn. Ther.*, 2009, **6**, 170–188.

2 E. Ben-Hur and W.-S. Chan, in *The Porphyrin Handbook*, eds. K. Kadish, K. M. Smith and R. Guilard, Academic Press, New York, vol. 19.

3 K. Kadish, K. M. Smith and R. Guilard, in *The Porphyrin Handbook*, Academic Press, New York, 2003, vol. 17.

4 A. Bermingham and J. P. Derrick, *BioEssays*, 2002, **24**, 637–648.

5 J. H. Zagal, F. Bedioui and J. P. Dodelet, *N4-Macrocyclic Metal Complexes*, Springer, 2006.

6 T. Goslinski, T. Osmalek, K. Konopka, M. Wierzchowski, P. Fita and J. Mielcarek, *Polyhedron*, 2011, **30**, 1538–1546.

7 L. F. Lindoy, *The Chemistry of Macrocyclic Ligand Complexes*, Cambridge University Press, Cambridge, 1963.

8 F. H. Moser and A. L. Thomas, *Phthalocyanine Compounds*, Reinhold Publishing Company, 1963.

9 V. N. Nemykin, E. A. Lukyanets, V. N. Nemykina and E. A. Lukyanets, *Arkivoc*, 2010, **2010**, 136–208.

10 M. S. Rodríguez-Morgade, G. de la Torre and T. Torres, in *The Porphyrin Handbook*, eds. K. Kadish, K. M. Smith and R. Guilard, Academic Press, New York, 2003, vol. 15.

11 D. K. MacFarland, C. M. Hardin and M. J. Lowe, *J. Chem. Educ.*, 2000, **77**, 1484.

12 C. G. Claessens, U. Hahn and T. Torres, *Chem. Rec.*, 2008, **8**, 75–97.

13 G. de la Torre, P. Vázquez, F. Agulló-López and T. Torres, *Chem. Rev.*, 2004, **104**, 3723–3750.

14 A. R. M. M. Soares, J. P. C. Tomé, M. G. P. M. S. P. M. S. Neves, A. C. Tomé, J. A. S. J. A. S. Cavaleiro, T. T. Torres, J. P. C. Tom??, M. G. P. M. S. P. M. S. Neves, A. C. Tom??, J. A. S. J. A. S. Cavaleiro and T. T. Torres, *Carbohydr. Res.*, 2009, **344**, 507–510.

15 S. L. Manoto, P. R. Sekhejane, N. N. Houreld and H. Abrahamse, *Photodiagnosis Photodyn. Ther.*, 2012, **9**, 52–59.

16 T. Stuchinskaya, M. Moreno, M. J. Cook, D. R. Edwards and D. A. Russell, *Photochem. Photobiol. Sci.*, 2011, **10**, 822.

17 M.-R. R. Ke, S.-L. L. Yeung, W.-P. P. Fong, D. K. P. P. Ng and P.-C. C. Lo, *Chem. - A Eur. J.*, 2012, **18**, 4225–4233.

18 T. Maisch, *Photochem. Photobiol. Sci.*, 2015, **14**, 1518–1526.

19 I. M. Belousova, I. M. Kislyakov, T. D. Muraviova, A. M. Starodubtsev, T. K. Kris'ko, E. A. Selivanov, N. P. Sivakova, I. S. Golovanova, S. D. Volkova, A. A. Shtro and V. V. Zarubaev, *Photodiagnosis Photodyn. Ther.*, 2014, **11**, 165–170.

20 M. G. Alvarez, M. N. Montes de Oca, M. E. Milanesio, C. S. Ortiz and E. N. Durantini, *Photodiagnosis Photodyn. Ther.*, 2014, **11**, 148–155.

21 N. Sekkat, H. Van Den Bergh, T. Nyokong and N. Lange, *Molecules*, 2012, **17**, 98–144.

22 M. Overhaus, J. Heckenkamp, S. Kossodo, D. Leszczynski and G. M. LaMuraglia, *Circ. Res.*, 2000, **86**, 334–340.

23 V. N. Borshch, E. R. Andreeva, S. G. Kuz'min and I. N. Vozovikov, *Russ. J. Gen. Chem.*, 2012, **82**, 554–563.

24 J. Heckenkamp, D. Leszczynski, J. Schiereck, J. Kung and G. M. LaMuraglia, *Arterioscler. Thromb. Vasc. Biol.*, 1999, **19**, 2154–2161.

25 J. F. Lovell and P.-C. Lo, *Theranostics*, 2012, **2**, 815–816.

26 G. P. Amaral, G. O. Puntel, C. L. Dalla Corte, F. Dobrachinski, R. P. Barcelos, L. L. Bastos, D. S. Ávila, J. B. T. Rocha, E. O. Da Silva, R. L. Puntel and F. A. A. Soares, *Toxicol. Vitr.*, 2012, **26**, 125–132.

27 N. Cauchon, E. Turcotte, R. Lecomte, H. M. Hassessian, J. E. van Lier, H. M. Hasséssian and J. E. van Lier, *Photochem. Photobiol. Sci.*, 2012, **11**, 364.

28 E. R. Ranyuk, N. Cauchon, H. Ali, R. Lecomte, B. Guerin and J. E. van Lier, *Bioorg. Med. Chem. Lett.*, 2011, **21**, 7470–7473.

29 M. Ethirajan, Y. Chen, P. Joshi, R. K. Pandey, S. K. Pushpan, S. Venkatraman, V. G. Anand, J. Sankar, D. Parmeswaran, S. Ganesan, T. K. Chandrashekar, A. Porfirinas, T. Fotodin, E. D. Sternberg, D. Dolphin, C. Brickner, H. Zheng, A. E. O'Connor, W. M. Gallagher, A. T. Byrne, R. R. Allison, C. H. Sibata, M. Ethirajan, Y. Chen, P. Joshi, R. K. Pandey, E. Zenkevich, E. Sagun, V. Knyukshto, A. Shulga, A. Mironov, O. Efremova, R. Bonnett, S. P. Songca and M. Kassem, *Chem. Soc. Rev.*, 2011, **40**, 340–362.

30 M. Nicastro, L. Tonucci, N. d'Alessandro, M. Bressan, L. K. Dragani and A. Morvillo, *Inorg. Chem. Commun.*, 2007, **10**, 1304–1306.

31 F. I. Bohrer, C. N. Colesniuc, J. Park, M. E. Ruidiaz, I. K. Schuller, A. C. Kummel and W. C. Trogler, *J. Am. Chem. Soc.*, 2009, **131**, 478–485.

32 I. Chambrier, M. J. Cook, P. T. Wood, M. J. Cook and P. T. Wood, *Chem. Commun.*, 2000, 2133–2134.

33 S. Pochekaylov, S. Nešpůrek, J. Rakušan, M. Kańskov and M. Karásková, *Mol. Cryst. Liq. Cryst.*, 2007, **468**, 23–31.

34 M. Calvete, G. Y. Yang and M. Hanack, *Synth. Met.*, 2004, **141**, 231–243.

35 M. Hanack, D. Dini, M. Barthel and S. Vagin, *Chem. Rec.*, 2002, **2**, 129–148.

36 M. A. Díaz-García, *J. Porphyr. Phthalocyanines*, 2009, **13**, 652–667.

37 N. B. McKeown, in *The Porphyrin Handbook*, eds. K. Kadish, K. M. Smith and R. Guilard, Academic Press, New York, 2003, vol. 15.

38 N. B. McKeown, *Phthalocyanine Materials: Synthesis, Structure and Function*, Cambridge University Press, Cambridge, U.K. ; New York, 1998.

39 L. R. Milgrom, *The colours of life: an introduction to the chemistry of porphyrins and related compounds*, Oxford University Press, Oxford; New York, 1997.

40 C. C. Leznoff and A. B. P. Lever, *Phthalocyanines: properties and applications*, VCH Publishers, New York, 1989, vol. 1.

41 A. Tomé, *Introdução à Nomenclatura dos Compostos Orgânicos*, Escolar Editora, Lisboa, 2ª edição., 2010.

42 J. R. Lakowicz, *Principles of fluorescence spectroscopy*, Springer, New York, N.Y., 2006.

43 M. Fadel, K. Kassab and D. Abdel Fadeel, *Lasers Med. Sci.*, 2010, **25**, 283–292.

44 K. Maduray, A. Karsten, B. Odhav and T. Nyokong, *J. Photochem. Photobiol. B Biol.*, 2011, **103**, 98–104.

45 H.-J. J. Lim and C.-H. H. Oh, *Photodiagnosis Photodyn. Ther.*, 2011, **8**, 337–342.

46 H. Tappeiner, .

47 H. Isago, *Optical Spectra of Phthalocyanines and Related Compounds*, Springer, New York, NY, 2015 editi., 2015.

48 Y. Rio, M. Salomé Rodríguez-Morgade and T. Torres, *Org. Biomol. Chem.*, 2008, **6**, 1877.

49 J. Mack and M. J. Stillman, in *The Porphyrin Handbook*, eds. K. Kadish, K. M. Smith and R. Guilard, Academic Press, New York, 2003, vol. 16.

50 W. M. Sharman and J. E. Van Lier, in *The Porphyrin Handbook*, eds. K. Kadish, K. M. Smith and R. Guilard, Academic Press, New York, 2003, vol. 15.

51 B. Turanli-Yildiz, T. T. Sezgin, Z. P. Akar, C. Uslan, B. Ş. S. Sesalan, A. Gül, Z. P. Cakar, C. Uslan, B. Ş. S. Sesalan, A. Gul, Z. P. Akar, C. Uslan, B. Ş. S. Sesalan and A. Gül, *Synth. Met.*, 2011, **161**, 1720–1724.

52 C. Uslan and B. Şebnem Sesalan, *Dye. Pigment.*, 2012, **94**, 127–135.

53 H. Yaku, T. Murashima, D. Miyoshi and N. Sugimoto, *Chem. Commun.*, 2010, **46**, 5740.

54 B. E. Logan, B. Hamelers, R. Rozendal, U. Schröder, J. Keller, S. Freguia, P. Aelterman, W. Verstraete and K. Rabaey, *Environ. Sci. Technol.*, 2006, 40, 5181–5192.

55 F. Zhao, F. Harnisch, U. Schröder, F. Scholz, P. Bogdanoff and I. Herrmann, *Electrochem. commun.*, 2005, **7**, 1405–1410.

56 Y. Yuan, B. Zhao, Y. Jeon, S. Zhong, S. Zhou and S. Kim, *Bioresour. Technol.*, 2011, **102**, 5849–5854.

57 J. Ahmed, Y. Yuan, L. Zhou and S. Kim, *J. Power Sources*, 2012, **208**, 170–175.

58 Y. Yuan, J. Ahmed and S. Kim, *J. Power Sources*, 2011, **196**, 1103–1106.

59 J. Manono, P. A. Marzilli and L. G. Marzilli, *Inorg. Chem.*, 2009, **48**, 5636–5647.

60 A. J. F. N. Sobral, S. Eléouet, N. Rousset, A. M. d'A. R. Gonsalves, O. Le Meur, L. Bourré and T. Patrice, *J. Porphyr. Phthalocyanines*, 2002, **6**, 456.

61 E. F. A. Carvalho, M. J. F. Calvete, J. A. S. Cavaleiro, D. Dini, M. Meneghetti and A. C. Tomé, *Inorganica Chim. Acta*, 2010, **363**, 3945–3950.

62 E. F. A. Carvalho, M. J. F. Calvete, A. C. Tomé and J. A. S. Cavaleiro, *Tetrahedron Lett.*, 2009, **50**, 6882–6885.

63 P. S. Gandhi, P. L. Gaikwad, D. M. Jagdale and V. J. Kadam, *Am. J. PharmTech Res.*, 2012, **2**, 83–103.

64 B. D. Fahlman, *Materials Chemistry*, Springer, 2011.

65 H. C. Kolb, M. G. Finn and K. B. Sharpless, *Angew. Chemie - Int. Ed.*, 2001, **40**, 2004–2021.

66 J. Lahann, *Click Chemistry for Biotechnology and Materials Science*, 2009.

67 M. P. Cassidy, J. Raushel and V. V. Fokin, *Angew. Chemie - Int. Ed.*, 2006, **45**, 3154–3157.

68 S. H. Cho, E. J. Yoo, I. Bae and S. Chang, *J. Am. Chem. Soc.*, 2005, **127**, 16046–16047.

69 S. H. Cho and S. Chang, *Angew. Chemie - Int. Ed.*, 2007, **46**, 1897–1900.

70 I. Bae, H. Han and S. Chang, *J. Am. Chem. Soc.*, 2005, **127**, 2038–2039.

71 V. D. Bock, H. Hiemstra and J. H. van Maarseveen, *European J. Org. Chem.*, 2006, **2006**, 51–68.

72 C. Barner-Kowollik and A. J. Inglis, *Macromol. Chem. Phys.*, 2009, **210**, 987–992.

73 J. C. Morris, J. Chiche, C. Grellier, M. Lopez, L. F. Bornaghi, A. Maresca, C. T. Supuran, J. Pouysségur and S.-A. Poulsen, *J. Med. Chem.*, 2011, **54**, 6905–6918.

74 T. Owa, H. Yoshino, T. Okauchi, T. Okabe, Y. Ozawa, N. Hata Sugi, K. Yoshimatsu, T. Nagasu, N. Koyanagi and K. Kitoh, *Bioorg. Med. Chem. Lett.*, 2002, **12**, 2097–2100.

75 S. H. Cho, E. J. Yoo, I. Bae and S. Chang, 2005, **127**, 16046–16047.

76 C. M. Cassidy, R. F. Donnelly, J. S. Elborn, N. D. Magee and M. M. Tunney, *J. Photochem. Photobiol. B Biol.*, 2012, **106**, 95–100.

77 N. E. Galanin, E. V. Kudrik and G. P. Shaposhnikov, *Russ. J. Org. Chem.*, 2006, **42**, 603–606.

78 J. Boudon, J. Paris, Y. Bernhard, E. Popova, R. A. Decréau and N. Millot, *Chem. Commun.*, 2013, **49**, 7394–7396.

79 P. M. Anbarasan, K. Vasudevan, P. Senthil Kumar, A. Prakasam, M. Geetha and K. Lalithambigai, *Bull. Mater. Sci.*, 2012, **35**, 265–275.

80 P. Tau and T. Nyokong, *Polyhedron*, 2006, **25**, 1802–1810.

81 D. K. Modibane and T. Nyokong, *Polyhedron*, 2008, **27**, 1102–1110.

82 X.-F. F. Zhang, Y. Wang and L. Niu, *J. Photochem. Photobiol. A Chem.*, 2010, **209**, 232–237.

83 L. De Luca and G. Giacomelli, *J. Org. Chem.*, 2008, **73**, 3967–3969.

84 G. Blotny, *Tetrahedron Lett.*, 2003, **44**, 1499–1501.

85 A. Aggarwal, S. Singh, Y. Zhang, M. Anthes, D. Samaroo, R. Gao and C. M. Drain, *Tetrahedron Lett.*, 2011, **52**, 5456–5459.

86 T. Govindaraju, P. Jonkheijm, L. Gogolin, H. Schroeder, C. F. W. Becker, C. M.

Niemeyer and H. Waldmann, *Chem. Commun.*, 2008, 3723.

87 S. H. Cho, S. J. Hwang and S. Chang, in *Organic Syntheses*, John Wiley & Sons, Inc., 2003.

88 D. de Souza, D. O. C. Mariano, F. Nedel, E. Schultze, V. F. Campos, F. Seixas, R. S. da Silva, T. S. Munchen, V. Ilha, L. Dornelles, A. L. Braga, J. B. T. Rocha, T. Collares and O. E. D. Rodrigues, *J. Med. Chem.*, 2015, **58**, 3329–3339.

89 V. J. Morris, A. R. Kirby and A. P. Gunning, *Atomic Force Microscopy for Biologists*, Imperial College Press, London, 2009.

90 T. Owa, H. Yoshino, T. Okauchi, K. Yoshimatsu, Y. Ozawa, N. H. Sugi, T. Nagasu, N. Koyanagi and K. Kitoh, *J. Med. Chem.*, 1999, **42**, 3789–3799.

91 A. Scozzafava, T. Owa, A. Mastrolorenzo and C. T. Supuran, *Curr. Med. Chem.*, 2003, **10**, 925–953.

92 G. E. Shambaugh, *Arch. Otolaryngol.*, 1966, **83**, 1–2.

93 C. Jeśman, A. Młudzik and M. Cybulska, *Pol. Merkur. Lekarski*, 2011, **30**, 320–2.

94 R. Cremlyn, F. Swinbourne, P. Fitzgerald, N. Godfrey, P. Hedges, J. Lapthorne and C. Mizon, *Indian J. Chem. Sect. B-Organic Chem. Incl. Med. Chem.*, 1984, **23**, 962–968.

95 R. J. Cremlyn, *Cholosulfonic Acid - A versatile reagent*, Royal Society of Chemsitry, Cambridge, 2002.

96 S. Tan, Y. Yang, Z. Luo, S. Zhao, D. Huang, J. Zhang, L. Dong and G. Wang, *Chem. Pap.*, 2011, **65**, 510–518.

97 S. Fujita, 1982, **1982**, 423–424.

98 Y. Huang, F. Bennett, V. Verma, F. George Njoroge and M. MacCoss, *Tetrahedron Lett.*, 2012, **53**, 3203–3205.

99 B. R. Rosen, J. C. Ruble, T. J. Beauchamp and A. Navarro, *Org. Lett.*, 2011, **13**, 2564–2567.

100 J. Yin and S. L. Buchwald, *J. Am. Chem. Soc.*, 2002, **124**, 6043–6048.

101 J. Yin and S. L. Buchwald, *Org. Lett.*, 2000, **2**, 1101–1104.

102 J. Baffoe, M. Y. Hoe and B. B. Touré, *Org. Lett.*, 2010, **12**, 1532–1535.

103 H. He and Y.-J. Wu, *Tetrahedron Lett.*, 2003, **44**, 3385–3386.

104 W. Deng, L. Liu, C. Zhang, M. Liu and Q.-X. Guo, *Tetrahedron Lett.*, 2005, **46**, 7295–7298.

105 E. Flegeau, J. Harrison and M. Willis, *Synlett*, 2015, **27**, 101–105.

106 Z. Yang, B. Zhou and J. Xu, *Synth.*, 2014, **46**, 225–229.

107 Z. Yang, B. Zhou and J. Xu, 2014, **46**, 225–229.

108 M. Zhu, K. Fujita and R. Yamaguchi, *Org. Lett.*, 2010, **12**, 1336–1339.

109 B. Xiao, T.-J. Gong, J. Xu, Z.-J. Liu and L. Liu, *J. Am. Chem. Soc.*, 2011, **133**, 1466–1474.

110 B. Kalita, A. A. Lamar and K. M. Nicholas, *Chem. Commun.*, 2008, 4291–4293.

111 J. García Ruano, A. Parra, F. Yuste and V. Mastranzo, *Synthesis (Stuttg).*, 2008, **2008**, 311–319.

112 H. Abdellaoui, X. Chen and J. Xu, *Synth.*, 2017, **49**, 2250–2256.

113 D. K. H. Ho, L. Chan, A. Hooper and P. E. Brennan, *Tetrahedron Lett.*, 2011, **52**, 820–823.

114 X. Tang, L. Huang, C. Qi, X. Wu, W. Wu and H. Jiang, *Chem. Commun.*, 2013, **49**, 6102.

115 K. Czifrák and L. Somsák, *Carbohydr. Res.*, 2009, **344**, 269–277.

116 E. D. Goddard-Borger and R. V Stick, *Org. Lett.*, 2007, **9**, 3797–3800.

117 A. J. Brouwer and R. M. J. Liskamp, *Synlett*, 2011, **15**, 2228–2230.

118 P. R. Martins, W. D. Popolim, L. A. F. Nagato, E. Takemoto, K. Araki, H. E. Toma, L. Angnes and M. D. V. C. Penteado, *Food Chem.*, 2011, **127**, 249–255.

119 B. Das, M. Krishnaiah and K. Venkateswarlu, *Tetrahedron Lett.*, 2006, **47**, 6027–6029.

120 C. A. Olsen, H. Franzyk and J. W. Jaroszewski, *Synthesis (Stuttg).*, 2005, **16**, 2631–2653.

121 M. Packiarajan, H. Coate, M. Desai, H. N. Jimenez, E. J. Reinhard, V. J. Jubian, M. R. Marzabadi, G. Chandrasena, T. C. Wolinski, M. W. Walker and K. Andersen, *Bioorg. Med. Chem. Lett.*, 2011, **21**, 6500–6504.

122 S. Shekhar, T. B. Dunn, B. J. Kotecki, D. K. Montavon and S. C. Cullen, *J. Org. Chem.*, 2011, **76**, 4552–4563.

123 A. J. A. Watson, A. C. Maxwell and J. M. J. Williams, *J. Org. Chem.*, 2011, **76**, 2328–2331.

124 G. Burton, P. Cao, G. Li and R. Rivero, *Org. Lett.*, 2003, **5**, 4373–4376.

125 D. W. Old, J. P. Wolfe and S. L. Buchwald, *J. Am. Chem. Soc.*, 1998, **120**, 9722–9723.

126 K. Dong, X. Fang, R. Jackstell and M. Beller, *Chem. Commun.*, 2015, **51**, 5059–5062.

127 K. Sumi, Y. Inoue, M. Nishio, Y. Naito, T. Hosoya, M. Suzuki and H. Hidaka, *Bioorg. Med. Chem. Lett.*, 2014, **24**, 831–834.

128 M. Kumar, B. Narasimhan, P. Kumar, K. Ramasamy, V. Mani, R. K. Mishra and A. B. A. Majeed, *Arab. J. Chem.*, 2014, **7**, 436–447.

129 M. Ceruso, S. Antel, D. Vullo, A. Scozzafava and C. T. Supuran, *Bioorg. Med. Chem.*, 2014, **22**, 6768–6775.

130 J. Pan, J. Li, R. Huang, X. Zhang, H. Shen, Y. Xiong and X. Zhu, *Synthesis (Stuttg).*, 2015, **47**, 1101–1108.

131 B. L. Wilkinson, L. F. Bornaghi, T. A. Houston, A. Innocente, C. T. Supuran and S. A. Poulsen, *J. Med. Chem.*, 2006, **49**, 6539–6548.

132 N. Taniguchi, *European J. Org. Chem.*, 2010, **2010**, 2670–2673.

133 X. Huang, J. Wang, Z. Ni, S. Wang and Y. Pan, *Chem. Commun.*, 2014, **50**, 4582–4584.

134 K. D. Modibane, 2009, 1–308.

135 A. Publication, *Org. Synth.*, 1998, **75**, 161.

136 J. Trujillo, E. Arnold, S. Kortum and R. Robinson, *Synlett*, 2015, **26**, 1764–1768.

137 K. Bahrami, M. M. Khodaei and M. Soheilizad, *Tetrahedron Lett.*, 2010, **51**, 4843–4846.

138 K. Bahrami, M. M. Khodaei and M. Soheilizad, *Synlett*, 2009, **2009**, 2773–2776.

139 K. Bahrami, M. M. Khodaei and M. Soheilizad, *J. Org. Chem.*, 2009, **74**, 9287–9291.

140 K. Bahrami, M. M. Khodaei and J. Abbasi, *Tetrahedron*, 2012, **68**, 5095–5101.

141 P. Ma, Z. Bai, Y. Gao, Q. Wang, J. Kan, Y. Bian and J. Jiang, *Soft Matter*, 2011, **7**, 3417–3422.

142 Z. Bai, Y. Gao, P. Zhu, Y. Bian and J. Jiang, *Inorg. Chem.*, 2010, **49**, 9005–9011.

143 W. O. Siegl, *J. Heterocycl. Chem.*, 1981, **18**, 1613–1618.

144 S. Lee, K. Fukuda and J. Anzai, *Mater. Sci. Eng. C*, 1998, **6**, 41–45.

145 S. Gürsoy, A. Cihan, M. B. Koçak and O. Bekaroğlu, *Monatshefte für Chemie / Chem. Mon.*, 2001, **132**, 813–819.

146 Y. Arslanoğlu and E. Hamuryudan, *Dye. Pigment.*, 2007, **75**, 150–155.

147 Y. Arslanoğlu, E. Hayran and E. Hamuryudan, *Dye. Pigment.*, 2013, **97**, 340–

346.

148 J. B. Pereira, E. F. A. Carvalho, M. A. F. Faustino, R. Fernandes, M. G. P. M. S. Neves, J. A. S. J. A. S. Cavaleiro, N. C. M. Gomes, Â. Cunha, A. Almeida and J. P. C. Tomé, *Photochem. Photobiol.*, 2012, **88**, 537–547.

149 M. C. Gomes, S. M. Woranovicz-Barreira, M. A. F. Faustino, R. Fernandes, M. G. P. M. S. Neves, A. C. Tomé, N. C. M. Gomes, A. Almeida, J. Cavaleiro, Â. Cunha and J. P. C. Tomé, *Photochem. Photobiol. Sci.*, 2011, **10**, 1735–1743.

150 S. Silva, P. M. R. Pereira, P. Silva, F. Paz, A. Almeida, M. A. F. Faustino, J. A. S. Cavaleiro and J. P. C. Tomé, *Chem. Commun.*, 2012, **48**, 3608–3610.

151 D. C. S. Costa, M. C. Gomes, M. A. F. Faustino, M. G. P. M. S. Neves, A. Cunha, J. A. S. Cavaleiro, A. Almeida and J. P. C. Tomé, *Photochem. Photobiol. Sci. Off. J. Eur. Photochem. Assoc. Eur. Soc. Photobiol.*, 2012, **11**, 1905–1913.

152 M. C. Gomes, S. Silva, M. A. F. Faustino, M. G. P. M. S. Neves, A. Almeida, J. A. S. Cavaleiro, J. P. C. Tomé and Â. Cunha, *Photochem. Photobiol. Sci. Off. J. Eur. Photochem. Assoc. Eur. Soc. Photobiol.*, 2013, **12**, 262–271.

153 M. Hädener, I. Gjuroski, J. Furrer and M. Vermathen, *J. Phys. Chem. B*, 2015, **119**, 12117–12128.

154 H. A. Isakau, M. V. Parkhats, V. N. Knyukshto, B. M. Dzhagarov, E. P. Petrov and P. T. Petrov, *J. Photochem. Photobiol. B Biol.*, 2008, **92**, 165–174.

155 M. V. Parkhats, V. A. Galievsky, A. S. Stashevsky, T. V. Trukhacheva and B. M. Dzhagarov, *Opt. Spectrosc.*, 2009, **107**, 974–980.

156 P. Gaudillat, F. Jurin, B. Lakard, C. Buron, J. M. Suisse and M. Bouvet, *Sensors (Switzerland)*, 2014, **14**, 13476–13495.

157 E. Fagadar-Cosma, E. Tarabukina, N. Zakharova, M. Birdeanu, B. Taranu, A. Palade, I. Creanga, A. Lascu and G. Fagadar-Cosma, *Polym. Int.*, 2016, **65**, 200–209.

158 A. G. Bobylev, Y. V. Shatalin, I. M. Vikhlyantsev, L. G. Bobyleva, S. V. Gudkov, Z. A. Podlubnaya, I. V. Shatalin, I. M. Vikhliantsev, L. G. Bobyleva, S. V. Gudkov and Z. A. Podlubnaia, *Biophysics (Oxf).*, 2014, **59**, 685–688.

159 O. O. Udartseva, A. V. Lobanov, E. R. Andreeva, G. S. Dmitrieva, M. Y. Mel'nikov and L. B. Buravkova, *Biophysics (Oxf).*, 2014, **59**, 854–860.

160 R. M. Ion, R. C. Fierascu, M. Neagu, C. Constantin and C. Stavaru, *Sci. Adv. Mater.*, 2010, **2**, 223–229.

161 T. J. Dougherty, C. J. Gomer, B. W. Henderson, G. Jori, D. Kessel, M. Korbelik, J. Moan and Q. Peng, *J. Natl. Cancer Inst.*, 1998, **90**, 889–905.

162 R. Bonnett, *Chem. Soc. Rev.*, 1995, **24**, 19.

163 C. M. Allen, W. M. Sharman and J. E. Van Lier, *J. Pept. Res.*, 2001, **5**, 161–169.

164 E. Ben-Hur and I. Rosenthal, *Int. J. Radiat. Biol. Relat. Stud. Phys. Chem. Med.*, 1985, **47**, 145–147.

165 P. Agostinis, K. Berg, K. A. Cengel, T. H. Foster, A. W. Girotti, S. O. Gollnick, S. M. Hahn, M. R. Hamblin, A. Juzeniene, D. Kessel, M. Korbelik, J. Moan, P. Mroz, D. Nowis, J. Piette, B. C. Wilson and J. Golab, *CA. Cancer J. Clin.*, 2011, **61**, 250–281.

166 R. K. Pandey, *J. Porphyr. Phthalocyanines*, 2000, **4**, 368–373.

167 S.-I. Ogura, Y. Hagiya, K. Tabata, T. Kamachi and I. Okura, 2012, **12**, 176–184.

168 S. Yano, S. Hirohara, M. Obata, Y. Hagiya, S. ichiro Ogura, A. Ikeda, H. Kataoka, M. Tanaka and T. Joh, *J. Photochem. Photobiol. C Photochem. Rev.*, 2011, **12**, 46–67.

169 R. Liang, L. Ma, L. Zhang, C. Li, W. Liu, M. Wei, D. Yan, D. G. Evans and X. Duan, *Chem. Commun.*, 2014, **50**, 14983–14986.

170 A. G. Bobylev, I. V. Shatalin, I. M. Vikhliantsev, L. G. Bobyleva, S. V. Gudkov and Z. A. Podlubnaia, *Biofizika*, 2014, **59**, 843–847.

171 R. Ackroyd, C. Kelty, N. Brown and M. Reed, *Photochem. Photobiol.*, 2001, **74**, 656–669.

172 M. D. Daniell and J. S. Hill, *Aust. N. Z. J. Surg.*, 1991, **61**, 340–348.

173 R. L. Edelson, *Sci. Am.*, 1988, **259**, 68–75.

174 J. D. Spikes, in *Primary Photo-Processes in Biology and Medicine*, eds. R. V. Bensasson, G. Jori, E. J. Land and T. G. Truscott, Springer US, 1985, pp. 209–227.

175 Z. Huang, *Technol. Cancer Res. Treat.*, 2005, **4**, 283–93.

176 O. Raab, 1900, **39**, 524–546.

177 F. Meyer-Betz, *Dtsch. Arch. Klin. Med. (in Ger.*, 1913, **112**, 476–503.

178 T. J. Dougherty, J. E. Kaufman, A. Goldfarb, K. R. Weishaupt, D. Boyle and A. Mittleman, 1978, **38**, 2628–2635.

179 R. R. Allison, G. H. Downie, R. Cuenca, X. H. Hu, C. J. H. Childs and C. H. Sibata, *Photodiagnosis Photodyn. Ther.*, 2004, **1**, 27–42.

180 B. W. Henderson and T. J. Dougherty, *Photochem. Photobiol.*, 1992, **55**, 145–157.

181 E. S. for Photobiology, H. Kostron, C. J. Gomer, T. G. Sutedja, N. Brasseur, T. Hasan, C. Fritsch, D.-P. Hader and P. Jori, *Photodynamic Therapy*, Royal Society of Chemistry, Cambridge; Secaucus, 2003.

182 M. R. Hamblin, *Advances in Photodynamic Therapy: Basic, Translational and Clinical*, Artech House, Boston, Mass, 1 edition., 2008.

183 Y. Takeuchi, K. Ichikawa, S. Yonezawa, K. Kurohane, T. Koishi, M. Nango, Y. Namba and N. Oku, *J. Control. Release*, 2004, **97**, 231–240.

184 R. Bonnett, *Chemical Aspects of Photodynamic Therapy*, CRC Press, 1st edn., 2000.

185 E. D. Baron, M. Lam, Y. Lee, M. Deng, A. H. Hsia, K. A. Morrissey, C. Yan, K. Azzizudin, N. L. Oleinick, T. S. McCormick and K. D. Cooper, *Adv. Hematol.*, 2010, **2010**, 1–8.

186 L. B. Josefsen and R. W. Boyle, *Br. J. Pharmacol.*, 2008, **154**, 1–3.

187 G. de la Torre, C. G. Claessens and T. Torres, *Chem. Commun.*, 2007, 2000–2015.

188 L. Howe and J. Z. Zhang, *J. Phys. Chem. A*, 1997, **101**, 3207–3213.

189 J. Kopeček, P. Kopečková, T. Minko, Z.-R. Lu and C. M. Peterson, *J. Control. Release*, 2001, **74**, 147–158.

190 R. Ideta, F. Tasaka, W.-D. Jang, N. Nishiyama, G.-D. Zhang, A. Harada, Y. Yanagi, Y. Tamaki, T. Aida and K. Kataoka, *Nano Lett.*, 2005, **5**, 2426–2431.

191 W.-D. Jang, Y. Nakagishi, N. Nishiyama, S. Kawauchi, Y. Morimoto, M. Kikuchi and K. Kataoka, *J. Control. Release*, 2006, **113**, 73–79.

192 A. Vargas, B. Pegaz, E. Debefve, Y. Konan-Kouakou, N. Lange, J.-P. Ballini, H. van den Bergh, R. Gurny and F. Delie, *Int. J. Pharm.*, 2004, **286**, 131–145.

193 G. Canti, A. De Simone and M. Korbelik, *Photochem. Photobiol. Sci.*, 2002, **1**, 79–80.

194 B. P. Shumaker and F. W. Hetzel, *Photochem. Photobiol.*, 1987, **46**, 899–901.

195 L. M. O. Lourenço, P. M. R. Pereira, E. Maciel, M. Válega, F. M. J. Domingues, M. R. M. Domingues, M. G. P. M. S. Neves, J. A. S. Cavaleiro, R. Fernandes and J. P. C. Tomé, *Chem. Commun. (Camb).*, 2014, **50**, 1–4.

196 N. Venkatramaiah, P. M. R. Pereira, F. A. Almeida Paz, C. A. F. Ribeiro, R.

Fernandes and J. P. C. Tome, *Chem. Commun.*, 2015, **51**, 15550–15553.

197 P. M. R. Pereira, S. Silva, J. A. S. Cavaleiro, C. A. F. Ribeiro, J. P. C. Tomé and R. Fernandes, *PLoS One*, 2014, **9**, 22–30.

198 A. R. M. Soares, M. G. P. M. S. Neves, A. C. Tomé, M. C. Iglesias-de la Cruz, A. Zamarrón, E. Carrasco, S. González, J. A. S. Cavaleiro, T. Torres, D. M. Guldi and A. Juarranz, *Chem. Res. Toxicol.*, 2012, **25**, 940–951.

199 M. Korbelik, R. Madiyalakan, T. Woo and A. Haddadi, *Photochem. Photobiol.*, 2012, **88**, 188–193.

200 K. Fukuoka, J. Usuda, Y. Iwamoto, H. Fukumoto, T. Nakamura, T. Yoneda, N. Narita, N. Saijo and K. Nishio, *Invest New Drugs*, 2001, **19**, 219–227.

201 S. Huang, P. J. Connolly, R. Lin, S. Emanuel and S. A. Middleton, *Bioorganic Med. Chem. Lett.*, 2006, **16**, 3639–3641.

202 W. R. Chegwidden and I. M. Spencer, *Inflammopharmacology*, 1995, **3**, 231–239.

203 C. T. Supuran, *Future Med. Chem.*, 2011, **3**, 1165–1180.

204 M. Hilvo, M. Tolvanen, A. Clark, B. Shen, G. N. Shah, A. Waheed, P. Halmi, M. Hänninen, J. M. Hämäläinen, M. Vihinen, W. S. Sly and S. Parkkila, *Biochem. J.*, 2005, **392**, 83–92.

205 S. Lindskog and D. N. Silverman, in *The Carbonic Anhydrases*, eds. P. D. W. R. Chegwidden, N. D. Carter and Y. H. Edwards, Birkhäuser Basel, 2000, pp. 175–195.

206 A. Di Fiore, S. M. Monti, M. Hilvo, S. Parkkila, V. Romano, A. Scaloni, C. Pedone, A. Scozzafava, C. T. Supuran and G. De Simone, *Proteins*, 2009, **74**, 164–175.

207 C. T. Supuran, F. Briganti, S. Tilli, W. R. Chegwidden and A. Scozzafava, *Bioorg Med Chem*, 2001, **9**, 703–714.

208 W. S. Sly and P. Y. Hu, *Annu. Rev. Biochem.*, 1995, **64**, 375–401.

209 C. T. Supuran, *Nat. Rev. Drug Discov.*, 2008, **7**, 168–181.

210 S. Del Prete, D. Vullo, V. De Luca, V. Carginale, S. M. Osman, Z. Alothman, C. T. Supuran and C. Capasso, *Bioorganic Med. Chem. Lett.*, 2016, **26**, 1941–1946.

211 S. Del Prete, D. Vullo, P. Di Fonzo, S. M. Osman, Z. AlOthman, W. A. Donald, C. T. Supuran and C. Capasso, 2017, **27**, 490–495.

212 A. M. Alafeefy, M. Ceruso, A.-M. M. S. Al-Tamimi, S. Del Prete, C. Capasso, C.

T. Supuran, S. Del Prete, C. Capasso and C. T. Supuran, *Bioorganic Med. Chem.*, 2014, **22**, 5133–5140.

213 D. Vullo, S. Del Prete, G. M. Fisher, K. T. Andrews, S.-A. A. Poulsen, C. Capasso and C. T. Supuran, *Bioorganic Med. Chem.*, 2015, **23**, 526–531.

214 D. Vullo, V. De Luca, S. Del Prete, V. Carginale, A. Scozzafava, C. Capasso and C. T. Supuran, *Bioorganic Med. Chem.*, 2015, **23**, 1728–1734.

215 D. Vullo, A. Bhatt, B. P. Mahon, R. McKenna and C. T. Supuran, *Bioorganic Med. Chem. Lett.*, 2016, **26**, 401–405.

216 D. Vullo, S. Del Prete, C. Capasso and C. T. Supuran, *Bioorganic Med. Chem. Lett.*, 2016, **26**, 1381–1385.

217 D. Vullo, V. De Luca, A. Scozzafava, V. Carginale, M. Rossi, C. T. Supuran and C. Capasso, *Bioorg. Med. Chem.*, 2013, **21**, 1534–1538.

218 D. Vullo, V. De Luca, A. Scozzafava, V. Carginale, M. Rossi, C. T. Supuran and C. Capasso, *Bioorganic Med. Chem.*, 2013, **21**, 4521–4525.

219 K. K. Sethi, S. M. Verma, M. Tanç, G. Purper, G. Calafato, F. Carta and C. T. Supuran, *Bioorganic Med. Chem.*, 2014, **22**, 1586–1595.

220 L. E. Riafrecha, O. M. Rodríguez, D. Vullo, C. T. Supuran and P. A. Colinas, *Bioorganic Med. Chem.*, 2014, **22**, 5308–5314.

221 D. A. Ibrahim, D. S. Lasheen, M. Y. Zaky, A. W. Ibrahim, D. Vullo, M. Ceruso, C. T. Supuran and D. A. Abou El Ella, *Bioorg. Med. Chem.*, 2015, **23**, 4989–4999.

222 M. M. Ghorab, M. S. Alsaid, M. Ceruso, Y. M. Nissan and C. T. Supuran, *Bioorganic Med. Chem.*, 2014, **22**, 3684–3695.

223 E. Barresi, S. Salerno, A. M. Marini, S. Taliani, C. La Motta, F. Simorini, F. Da Settimo, D. Vullo and C. T. Supuran, *Bioorganic Med. Chem.*, 2016, **24**, 921–927.

224 H. S. Jung, J. Han, H. Shi, S. Koo, H. Singh, H. J. Kim, J. L. Sessler, J. Y. Lee, J. H. Kim and J. S. Kim, *J. Am. Chem. Soc.*, 2017, **139**, 7595–7602.

225 V. Dudutienė, A. Zubrienė, A. Smirnov, D. D. Timm, J. Smirnovienė, J. Kazokaitė, V. Michailovienė, A. Zakšauskas, E. Manakova, S. Gražulis and D. Matulis, *ChemMedChem*, 2015, **10**, 662–687.

226 S. G. Kimani, T. A. Shmigol, S. Hammond, J. B. Phillips, J. I. Bruce, A. J. MacRobert, M. V. Malakhov and J. P. Golding, *Photochem. Photobiol.*, 2013,

89, 139–149.

227 C. S. Vinagreiro, N. P. F. Gonçalves, M. J. F. Calvete, F. A. Schaberle, L. G. Arnaut and M. M. Pereira, *J. Fluor. Chem.*, 2015, **180**, 161–167.

228 C. J. P. Monteiro, M. M. Pereira, S. M. A. Pinto, A. V. C. Simões, G. F. F. Sá, L. G. Arnaut, S. J. Formosinho, S. Simões and M. F. Wyatt, *Tetrahedron*, 2008, **64**, 5132–5138.

229 J. Bhaumik, R. Weissleder and J. R. McCarthy, *J. Org. Chem.*, 2009, **74**, 5894–5901.

230 O. Sköld, *Drug Resist. Updat.*, 2000, **3**, 155–160.

231 R. Karaman, *Commonly used drugs - Uses, Side Effects, Bioavailability and Approaches to Improve It*, Nova Science Pub Inc, Hauppauge, NY, 2015.

232 P. Klahn and M. Brönstrup, *Curr. Top. Microbiol. Immunol.*, 2016, **398**, 365–417.

233 S. Bag, R. Tulsan, A. Sood, H. Cho, H. Redjeb, W. Zhou, H. LeVine III, B. Török and M. Török, *Bioorg. Med. Chem. Lett.*, 2015, **25**, 626–630.

234 B. C. A. Gassani, R. M. Rezende, P. Paiva-Lima, D. L. Ferreira-Alves, W. G. P. dos Reis, Y. S. Bakhle and J. N. de Francischi, *Pharmacol. Res.*, 2010, **62**, 439–443.

235 C.-H. Fabritius, U. Pesonen, J. Messinger, R. Horvath, H. Salo, M. Gałęzowski, M. Galek, K. Stefańska, J. Szeremeta-Spisak, M. Olszak-Płachta, A. Buda, J. Adamczyk, M. Król, P. Prusis, M. Sieprawska-Lupa, M. Mikulski, K. Kuokkanen, H. Chapman, R. Obuchowicz, T. Korjamo, N. Jalava and M. Nowak, *Bioorganic Med. Chem. Lett.*, 2016, **26**, 2610–2615.

236 K. N. De Oliveira, P. Costa, J. R. Santin, L. Mazzambani, C. Bürger, C. Mora, R. J. Nunes and M. M. De Souza, *Bioorganic Med. Chem.*, 2011, **19**, 4295–4306.

237 Z. Chen, Z.-C. Wang, X.-Q. Yan, P.-F. Wang, X.-Y. Lu, L.-W. Chen, H.-L. Zhu and H.-W. Zhang, *Bioorg. Med. Chem. Lett.*, 2015, **25**, 1947–1951.

238 M. Barone, A. C. E. Graziano, A. Marrazzo, P. Gemmellaro, A. Santagati and V. Cardile, *Mol. Divers.*, 2013, **17**, 445–458.

239 F. A. Abulwerdi, C. Liao, A. S. Mady, J. Gavin, C. Shen, T. Cierpicki, J. A. Stuckey, H. D. H. Showalter and Z. Nikolovska-Coleska, *J. Med. Chem.*, 2014, **57**, 4111–4133.

240 H.-Y. Y. Lee, A.-C. C. Tsai, M.-C. C. Chen, P.-J. J. Shen, Y.-C. C. Cheng, C.-C.

C. Kuo, S.-L. L. Pan, Y.-M. M. Liu, J.-F. F. Liu, T.-K. K. Yeh, J.-C. C. Wang, C.-Y. Y. Chang, J.-Y. Y. Chang and J.-P. P. Liou, *J. Med. Chem.*, 2014, **57**, 4009–4022.

241 G. Nasr, E. Petit, C. T. Supuran, J. Y. Winum and M. Barboiu, *Bioorganic Med. Chem. Lett.*, 2009, **19**, 6014–6017.

242 C. T. Supuran, *Expert Opin. Investig. Drugs*, 2003, **12**, 283–287.

243 P. M. Scola, A. X. Wang, A. C. Good, L.-Q. Sun, K. D. Combrink, J. A. Campbell, J. Chen, Y. Tu, N. Sin, B. L. Venables, S.-Y. Sit, Y. Chen, A. Cocuzza, D. M. Bilder, S. D'Andrea, B. Zheng, P. Hewawasam, M. Ding, J. Thuring, J. Li, D. Hernandez, F. Yu, P. Falk, G. Zhai, A. K. Sheaffer, C. Chen, M. S. Lee, D. Barry, J. O. Knipe, W. Li, Y.-H. Han, S. Jenkins, C. Gesenberg, Q. Gao, M. W. Sinz, K. S. Santone, T. Zvyaga, R. Rajamani, H. E. Klei, R. J. Colonno, D. M. Grasela, E. Hughes, C. Chien, S. Adams, P. C. Levesque, D. Li, J. Zhu, N. A. Meanwell and F. McPhee, *J. Med. Chem.*, 2014, **57**, 1708–1729.

244 M. Kołaczkowski, M. Marcinkowska, A. Bucki, M. Pawłowski, K. Mitka, J. Jaśkowska, P. Kowalski, G. Kazek, A. Siwek, A. Wasik, A. Wesołowska, P. Mierzejewski and P. Bienkowski, *J. Med. Chem.*, 2014, **57**, 4543–4557.

245 C. A. Hernberg, *Acta Endocrinol. (Copenh).*, 1956, **23**, 281–288.

246 G. De Simone, A. Di Fiore, C. Capasso and C. T. Supuran, *Bioorganic Med. Chem. Lett.*, 2015, **25**, 1385–1389.

247 L. Syrjänen, M. Kuuslahti, M. Tolvanen, D. Vullo, S. Parkkila and C. T. Supuran, *Bioorganic Med. Chem.*, 2015, **23**, 2303–2309.

248 K. Yamashita, Y. Yoshioka, H. Pan, M. Taira, T. Ogura, T. Nagano, M. Aoyama, K. Nagano, Y. Abe, H. Kamada, S. I. Tsunoda, H. Aoshima, H. Nabeshi, T. Yoshikawa and Y. Tsutsumi, *Pharmazie*, 2013, **68**, 54–57.

249 H. Tappeiner, 1904, **80**, 427–487.

250 M. R. Hamblin, D. A. O'Donnell, N. Murthy, C. H. Contag and T. Hasan, *Photochem. Photobiol.*, 2002, **75**, 51–57.

251 K. P. Francis, J. Yu, C. Bellinger-Kawahara, D. Joh, M. J. Hawkinson, G. Xiao, T. F. Purchio, M. G. Caparon, M. Lipsitch and P. R. Contag, *Infect. Immun.*, 2001, **69**, 3350–3358.

252 M. R. Hamblin and T. Hasan, *Photochem. Photobiol. Sci.*, 2004, **3**, 436–450.

253 E. A. Meighen, *FASEB J. Off. Publ. Fed. Am. Soc. Exp. Biol.*, 1993, **7**, 1016–

1022.

254 E. A. Meighen, *Microbiol. Rev.*, 1991, **55**, 123–142.

255 T. N. Demidova, F. Gad, T. Zahra, K. P. Francis and M. R. Hamblin, *J. Photochem. Photobiol. B.*, 2005, **81**, 15–25.

256 M. S. Baptista and M. Wainwright, *Brazilian J. Med. Biol. Res.*, 2011, **44**, 1–10.

257 H. Nikaido, *Microbiol. Mol. Biol. Rev. MMBR*, 2003, **67**, 593–656.

258 H. Nikaido, M. Vaara and N. Public, *Microbiol. Rev.*, 1985, **49**, 1–32.

259 M. Vaara, *Microbiol. Rev.*, 1992, **56**, 395–411.

260 J. G. Black and L. J. Black, *Microbiology principles and explorations: international student version*, J. Wiley & Sons, Hoboken, NJ, 7th edn., 2008.

261 E. Alves, L. Costa, C. M. Carvalho, J. P. Tomé, M. A. Faustino, M. G. Neves, A. C. Tomé, J. A. Cavaleiro, A. Cunh and A. Almeida, *BMC Microbiol.*, 2009, **9**, 1–13.

262 A. Tavares, C. M. B. Carvalho, M. A. Faustino, M. G. P. M. S. Neves, J. P. C. Tome, A. C. Tome, J. A. S. J. A. S. Cavaleiro, A. Cunha, N. C. M. Gomes, E. Alves, A. Almeida, J. P. C. Tomé, A. C. Tomé, J. A. S. J. A. S. Cavaleiro, Â. Cunha, N. C. M. Gomes, E. Alves and A. Almeida, *Mar. Drugs*, 2010, **8**, 91–105.

263 L. Costa, J. P. C. Tomé, M. G. P. M. S. P. M. S. Neves, A. C. Tomé, J. A. S. J. A. S. Cavaleiro, M. A. F. F. Faustino, Â. Cunha, N. C. M. M. Gomes, A. Almeida, J. P. C. Tome, M. G. P. M. S. P. M. S. Neves, A. C. Tome, J. A. S. J. A. S. Cavaleiro, M. A. F. F. Faustino, A. Cunha, N. C. M. M. Gomes and A. Almeida, *Antiviral Res.*, 2011, **91**, 278–282.

264 M. Soncin, C. Fabris, A. Busetti, D. Dei, D. Nistri, G. Roncucci and G. Jori, *Photochem. Photobiol. Sci.*, 2002, **1**, 815–819.

265 P. Huovinen, L. Sundström, G. Swedberg, O. Sköld, L. Sundstrom, G. Swedberg and O. Skold, *Antimicrob. Agents Chemother.*, 1995, **39**, 279–289.

266 A. Achari, D. O. Somers, J. N. Champness, P. K. Bryant, J. Rosemond and D. K. Stammers, *Nat. Struct. Biol.*, 1997, **4**, 490–497.

267 H. Ali, R. Langlois, J. R. Wagner, N. Brasseur, B. Paquette and J. E. VAN Lier, *Photochem. Photobiol.*, 1988, **47**, 713–717.

268 S. M. Bishop, B. J. Khoo, A. J. MacRobert, M. S. C. Simpson, D. Phillips and A. Beeby, *J. Chromatogr. A*, 1993, **646**, 345–350.

269 R. Cubeddu, A. Pifferi, P. Taroni, A. Torricelli, G. Valentini, D. Comelli, C.

D'Andrea, V. Angelini and G. Canti, *Photochem. Photobiol.*, 2000, **72**, 690–695.

270 S. Baek and K. Na, *J. Porphyr. Phthalocyanines*, 2013, **17**, 125–134.

271 D. Çakır, V. Çakır, Z. Bıyıklıoğlu, M. Durmuş and H. Kantekin, *J. Organomet. Chem.*, 2013, **745–746**, 423–431.

272 L. M. O. Lourenço, A. Sousa, M. C. Gomes, M. A. F. Faustino, A. Almeida, A. M. S. Silva, M. G. P. M. S. Neves, J. A. S. Cavaleiro, A. Cunha and J. P. C. Tomé, *Photochem. Photobiol. Sci.*, 2015, **14**, 1853–1863.

273 L. M. O. Lourenço, M. G. P. M. S. Neves, J. A. S. Cavaleiro and J. P. C. Tomé, *Tetrahedron*, 2014, **70**, 2681–2698.

274 L. M. O. Lourenço, P. M. R. Pereira, E. Maciel, M. Válega, F. M. J. Domingues, M. R. M. Domingues, M. G. P. M. S. Neves, J. A. S. Cavaleiro, R. Fernandes and J. P. C. Tomé, *Chem. Commun.*, 2014, **50**, 8363–8366.

275 O. B.G., F. K.R., H. X., S. I., S.-J. S.D., V. D.G.H., B. G. Ongarora, K. R. Fontenot, X. Hu, I. Sehgal, S. D. Satyanarayana-Jois, M. G. H. Vicente and D. G. H. Vicente, *J. Med. Chem.*, 2012, **55**, 3725–3738.

276 E. Ranyuk, N. Cauchon, K. Klarskov, B. Guérin and J. E. van Lier, *J. Med. Chem.*, 2013, **56**, 1520–1534.

277 F. Mitzel, S. FitzGerald, A. Beeby and R. Faust, *European J. Org. Chem.*, 2004, **2004**, 1136–1142.

278 M. S. T. Rocha, C. M. Lucci, J. P. F. Longo, P. D. Galera, A. R. Simioni, Z. G. M. Lacava, A. C. Tedesco and R. B. Azevedo, *J. Biomed. Nanotechnol.*, 2012, **8**, 251–257.

279 D. M. G. C. Rocha, N. Venkatramaiah, M. C. Gomes, A. Almeida, M. A. F. Faustino, F. A. Almeida Paz, A. Cunha, J. P. C. Tomé, F. A. A. Paz, Â. Cunha, J. P. C. Tomé, F. A. Almeida Paz, A. Cunha and J. P. C. Tomé, *Photochem. Photobiol. Sci.*, 2015, **14**, 1872–1879.

280 F. Cieplik, L. Tabenski, W. Buchalla and T. Maisch, *Front. Microbiol.*, 2014, **12**, 1–17.

281 M. A. Griffiths, B. W. Wren and M. Wilson, *J. Antimicrob. Chemother.*, 1997, **40**, 873–876.

282 A. Minnock, D. I. Vernon, J. Schofield, J. Griffiths, J. H. Parish and S. T. B. Brown, *J. Photochem. Photobiol. B Biol.*, 1996, **32**, 159–164.

283 F. Gabor, G. Csik and G. Ronto, *Med. Sci. Monit.*, 1997, **3**, BR294-BR298.

284 N. Masilela, E. Antunes and T. Nyokong, *J. Porphyr. Phthalocyanines*, 2013, **17**, 417–430.

285 G. C. Taşkin, M. Durmuş, F. Yüksel, V. Mantareva, V. Kussovski, I. Angelov and D. Atilla, *J. Photochem. Photobiol. A Chem.*, 2015, **306**, 31–40.

286 C. Zarfl, M. Matthies and J. Klasmeier, *Chemosphere*, 2008, **70**, 753–760.

287 D. Büttner and H. Bütlner, *Chemotherapy*, 1980, **26**, 153–163.

288 I. H. Lo and W. L. Hayton, *J. Pharmacokinet. Biopharm.*, 1981, **9**, 443–459.

289 E. Alves, L. Costa, Â. Cunha, M. A. F. Faustino, M. G. P. M. S. Neves and A. Almeida, *Appl. Microbiol. Biotechnol.*, 2011, **92**, 1115–1128.

290 N. Tortik, A. Spaeth and K. Plaetzer, *Photochem. Photobiol. Sci.*, 2014, **13**, 1402–1409.

291 Y. Arenas, S. Monro, G. Shi, A. Mandel, S. McFarland and L. Lilge, *Photodiagnosis Photodyn. Ther.*, 2013, **10**, 615–625.

292 N. Masilela, P. Kleyi, Z. Tshentu, G. Priniotakis, P. Westbroek and T. Nyokong, *Dye. Pigment.*, 2013, **96**, 500–508.

293 A. Moreira, E. Figueira, A. M. V. M. Soares and R. Freitas, *Sci. Total Environ.*, 2016, **545**–**546**, 569–581.